

Surface Engineering of Upconversion Nanoparticles for Bioassays



Dissertation zur Erlangung des Doktorgrades der
Naturwissenschaften (Dr. rer. nat.) der Fakultät
Chemie und Pharmazie der Universität Regensburg

vorgelegt von

Sandy Franziska Himmelstoß

aus Walderbach (Landkreis Cham)

im Jahr 2019

Surface Engineering of Upconversion Nanoparticles for Bioassays



Dissertation zur Erlangung des Doktorgrades der
Naturwissenschaften (Dr. rer. nat.) der Fakultät
Chemie und Pharmazie der Universität Regensburg

vorgelegt von

Sandy Franziska Himmelstoß

aus Walderbach (Landkreis Cham)

im Jahr 2019

Die vorgelegte Doktorarbeit entstand in der Zeit von November 2015 bis Juni 2019 am Institut für Analytische Chemie, Chemo- und Biosensorik an der Universität Regensburg.

Die Arbeit wurde angeleitet von Dr. Thomas Hirsch und Prof. Dr. Antje J. Bäumner.

Promotionsgesuch eingereicht am: 06. Juni 2019

Prüfungsausschuss

Vorsitzender: Prof. Dr. Frank-Michael Matysik

Erstgutachterin: Prof. Dr. Antje J. Bäumner

Zweitgutachter: Prof. Dr. Hubert Motschmann

Drittprüfer: Prof. Dr. Reinhard Rachel

Table of Contents

STRUCTURE OF THE THESIS	1
GERMAN SUMMARY.....	3
DECLARATION OF CONTRIBUTIONS.....	5
CHAPTER 1	7
A critical comparison of lanthanide based upconversion nanoparticles to fluorescent proteins, semiconductor quantum dots, and carbon dots for use in optical sensing and imaging	
1.1 Introduction.....	8
1.2 Optical properties	10
1.2.1 Origin of photoluminescence.....	10
1.2.2 Shape of the emission spectra.....	12
1.2.3 Extinction coefficient, quantum yield and brightness	13
1.2.4 Lifetime	14
1.2.5 Photostability.....	15
1.3 Chemical and physical properties	17
1.3.1 Synthesis.....	17
1.3.2 Core/shell and multimodal nanosystems.....	20
1.3.3 Commercial availability	21
1.3.4 Surface functionalization and labeling.....	21
1.3.5 Colloidal stability	25
1.3.6 Chemical stability.....	27
1.3.7 Biocompatibility, biodistribution and toxicity	28
1.4 Bioanalytical applications.....	31
1.4.1 Sensing.....	31
1.4.2 Imaging.....	33
1.5 Conclusion and perspective	37
1.6 References.....	39
CHAPTER 2	53
Motivation and aim of the work	

CHAPTER 3.....	55
Long-term colloidal and chemical stability in aqueous media of NaYF₄-type upconversion nanoparticles modified by ligand-exchange	
3.1 Introduction	56
3.2 Materials and methods.....	58
3.2.1 Chemicals	58
3.2.2 Characterization and measurement methods	58
3.2.3 Surface modification of upconversion nanoparticles <i>via</i> NOBF ₄	59
3.2.4 Surface modification of upconversion nanoparticles <i>via</i> HCl	59
3.2.5 Time-dependent colloidal stability study and the influence of different solution systems	59
3.3 Results and discussion.....	60
3.3.1 Synthesis and design of hydrophilic upconversion nanoparticles	60
3.3.2 Surface coverage by using small ligands or polymers	63
3.3.3 Colloidal stability of hydrophilic upconversion nanoparticles	64
3.3.4 Long-term stability of aqueous dispersion of upconversion nanoparticles	66
3.3.5 Stabilization of highly diluted aqueous upconversion nanoparticle dispersions.....	68
3.4 Conclusion.....	70
3.5 References	71
3.6 Supporting information.....	74
3.6.1 Synthesis and characterization of upconversion nanoparticles	74
3.6.2 Determination of the phonon energy	75
3.6.3 Calculation of the absorption cross-section of Yb ³⁺	76
3.6.4 Lifetime	77
3.6.5 Thermogravimetric analysis to determine the number of ligands attached to the surface of the nanoparticles.....	78
3.6.6 Determination of the required amount of water molecules for the ligand removal <i>via</i> NOBF ₄	80
3.6.7 FT-IR measurements of the cyclohexane and DMF phase after ligand removal <i>via</i> NOBF ₄	82
3.6.8 Dynamic light scattering before and after ligand removal <i>via</i> NOBF ₄	83
3.6.9 Surface modification <i>via</i> HCl assisted ligand removal	84
3.6.10 Calculations of the distance between single ligands.....	86
3.6.11 Overview of the pK _a values of the surface ligands.....	87
3.6.12 Dynamic light scattering and surface charge of water dispersible UCNPs	88
3.6.13 Luminescence spectra of water dispersible UCNPs	88
3.6.14 Determination of number of unit cells and total amount of F ⁻ ions within a 28 nm-sized upconversion nanoparticle	89

3.6.15 Disintegration of diluted upconversion nanoparticles	90
3.6.16 Overview of the mass concentration range of upconversion nanoparticles used for (bio)analytical application.....	93
3.6.17 Analysis of the chemical and colloidal stability of hydrophilic UCNPs.....	94
3.6.18 Influence of the dispersion media on the stability of UCNPs.....	104
3.6.19 Crosslinking of upconversion nanoparticles by dissolved Ln ³⁺	107
3.6.20 Lattice constant of upconversion nanoparticles	108
3.6.21 References	109
CHAPTER 4.....	111
980 nm and 808 nm excitable upconversion nanoparticles for the detection of enzyme related reactions	
4.1 Introduction.....	112
4.2 Experimental Section	113
4.2.1 Materials.....	113
4.2.2 Characterization methods.....	113
4.2.3 Synthesis of β-NaYF ₄ nanoparticles doped with lanthanide ions	113
4.2.4 Synthesis of α-NaYF ₄ nanoparticles	114
4.2.5 Synthesis of β-phase core/shell upconversion nanoparticles	114
4.2.6 Surface modification of upconversion nanoparticles	114
4.3 Results and discussion.....	116
4.3.1 Characterization of upconversion nanoparticles.....	116
4.3.2 Optical properties of 980 nm and 808 nm excitable upconversion nanoparticles.....	117
4.3.3 Inner filter effect of 980 nm and 808 nm excitable upconversion nanoparticles.....	118
4.4 Conclusion	119
4.5 References.....	120
CHAPTER 5.....	121
Luminescence-based self-referenced enzymatic L-lactate sensing by tandem-sensitized NIR to UV NaYF₄(Yb,Tm) upconversion nanoparticles	
5.1 Introduction.....	123
5.2 Methods and materials	127
5.2.1 Materials.....	127
5.2.2 Characterization methods.....	127
5.2.3 Synthesis of hexagonal β-NaYF ₄ (Yb,Tm) nanoparticles	128
5.2.4 Synthesis of α-NaYF ₄ and α-NaYF ₄ (Yb, Nd).....	128
5.2.5 Core-shell synthesis of β-NaYF ₄ (Yb, Tm)@NaYF ₄ and β NaYF ₄ (Yb, Tm)@NaYF ₄ (Yb, Nd).....	128
5.2.6 Surface modification with poly(acrylic acid)	129

5.2.7	L-lactate assay.....	129
5.2.8	Preparation of a sensor film.....	129
5.2.9	Immobilization of L-lactate dehydrogenase on a polyacrylamide sensor film	130
5.2.10	Activity of L-lactate dehydrogenase on the enzyme film	130
5.2.11	Online measurement of L-lactate	130
5.3	Results and discussion.....	132
5.3.1	Synthesis and surface modification of hydrophobic upconversion nanoparticles with tandem sensitization.....	132
5.3.2	Optical properties of upconversion nanoparticles with and without tandem sensitization	134
5.3.3	Determination of L-lactate	138
5.3.4	Online monitoring of L-lactate	140
5.4	Conclusion.....	147
5.5	References	148
CHAPTER 6	153
	Conclusion and future perspectives	
6.1	Nanomaterials in bioassays	153
6.2	Surface-engineering of upconversion nanoparticles	154
6.2.1	Particle size and the choice of the surface modification strategy	155
6.2.2	Chemical stability of upconversion nanoparticles	157
6.2.3	Influence of the dispersion media on the stability of upconversion nanoparticles.....	158
6.2.4	Surface functionalization for analytical applications	159
6.3	Future perspectives of upconversion nanoparticles.....	160
6.4	References	163
	CURRICULUM VITAE	165
	LIST OF PUBLICATIONS.....	167
	CONFERENCE CONTRIBUTIONS	169
	DANKSAGUNG	171
	EIDESSTATTLICHE ERKLÄRUNG	173

STRUCTURE OF THE THESIS

This doctoral thesis investigates the impact of the surface chemistry of upconversion nanoparticles (UCNPs) in terms of chemical and colloidal stability, as well as the luminescence properties with the emphasis on the design of particles to be used in bioanalytical assays. The chapters represent published manuscripts or manuscripts submitted for peer reviewing or intended to be submitted in the near future.

Chapter 1 has been published as a topical review in the IOP journal *Methods and Applications of Fluorescence* (Impact Factor: 2.2) in the special issue on “Upconversion Methods, Applications and Materials”. Thereby, UCNPs are introduced by a critical comparison to other prominent luminescent probes including semiconductor quantum dots, carbon dots and, fluorescent proteins. The comparison focuses on three main categories: a) the optical properties including quantum yield, lifetime and the origin of the luminescence b) the chemical and physical properties including the synthesis, surface modification and stability of the systems and c) the application in bioimaging and biosensing.

Chapter 2 summarizes the motivation and aim of this work to obtain nanoparticles suitable for bioanalytical assays. One focus was to get a better understanding of the chemical and colloidal stability properties of upconversion nanoparticles with different surface architectures. The second part of the thesis focuses on the realization of a sensing concept under the usage of upconversion nanoparticles for self-referenced continuous online monitoring of an analyte in a complex media.

Chapter 3 has been submitted for publication to the Wiley journal *Particle and Particle Systems Characterization* (Impact Factor: 4.4, accepted July 2019) and describes the influence of the surface modification of UCNPs and their resulting colloidal and chemical stability. The particles are modified *via* a two-step ligand exchange whereas the oleic acid is removed from the surface of the nanoparticles *via* the addition of NOBF_4 . The bare UCNPs are stabilized by the addition of a desired ligand. A set of five different capping agents consisting of small molecules and polymers with different coordination groups and different charges at neutral pH are investigated in detail. As stock solution all types of particles exhibit excellent colloidal stability. However, under non-steady conditions, especially in low concentrations as present in single particle imaging or in flow conditions, the particles start to disintegrate after a short time. This is a consequence of incomplete surface coverage which is achieved by the ligand exchange method. Thereby the nature of the surface modification has only a minor influence.

In **Chapter 4** (published as peer reviewed proceedings to a talk presented at the conference “Nanoscale Imaging, Sensing, and Actuation for Biomedical Applications XIV” at SPIE Bios in San Francisco, California in 2017) efficient UCNPs were designed to use them as luminescent reporters in bioanalytical applications. Upconversion nanoparticles from the type $\text{NaYF}_4:\text{Yb,Tm}$ show several

emission bands when excited with a 980 nm continuous wave (CW) laser module. Thereby especially the emissions at 345 nm, 360 nm (UV), 450 nm, and 470 nm (blue) are of huge interest for bioanalytical application as those bands show a spectral overlap with the common enzymatic factor pairs NAD^+/NADH and FAD/FADH_2 .

Chapter 5 is prepared for submission to *ACS Sensors* (Impact factor 5.7). Here the surface engineering aspects in terms of the core/shell particle growth to tune the excitation wavelength *via* additional Nd^{3+} sensitization as well as the surface functionalization with a polymer (here poly(acrylic acid)) have been investigated in detail. Such UCNPs embedded in an enzyme-modified gel have been used for the design of a biosensor for L-lactate. The sensing principle is based on the enzymatic turnover of L-lactate *via* lactate dehydrogenase. Thereby the co-factor NAD^+ is transferred to NADH which affects the monitored emission of the UCNPs. In this chapter both 980 nm and 808 nm excitable nanoparticles are analysed in regard to their usability of this bioassay. In cuvette applications, both systems show similar results. However, in the course of the online measurement of L-lactate by the 808 nm excitable nanoparticles a lower limit of detection for L-lactate and higher stability of the hydrogel can be obtained.

Chapter 6 reflects the state of the art of UCNPs for bioanalytical applications. Moreover, the results from this thesis are critically evaluated and future perspectives for UCNPs are envisioned.

GERMAN SUMMARY

Die hier vorliegende Doktorarbeit untersucht den Einfluss der Oberflächenchemie von Photonen aufkonvertierenden Nanopartikeln (UCNPs) hinsichtlich der chemischen und kolloidalen Stabilität, sowie die Möglichkeiten über gezielte Partikelarchitektur die Lumineszenzeigenschaften dieser Nanomaterialien derart zu verbessern, dass eine Anwendung in der Bioanalytik ermöglicht wird. Die einzelnen Kapitel sind dabei als (publizierte) Manuskript-Entwürfe zu betrachten.

Kapitel 1 wurde als Review-Artikel in der Sonderausgabe über aufkonvertierende Methoden, Anwendung und Materialien im Journal „Methods and Applications of Fluorescence“ (Impact Factor: 2.2) publiziert. Hier werden UCNPs durch einen kritischen Vergleich mit anderen bekannten Lumineszenzsonden, einschließlich Halbleiterquantenpunkten, C-dots und fluoreszierenden Proteinen, vorgestellt. Der Vergleich konzentriert sich hierbei auf drei Hauptaspekte: a) die optischen Eigenschaften einschließlich Quantenausbeute, Lebensdauer und Ursprung der Lumineszenz b) die chemischen und physikalischen Eigenschaften einschließlich Synthese, Oberflächenmodifikation und Stabilität der Systeme und c) die Anwendung der Materialien in der (Bio)-Sensorik und für die biologischen Bildgebung.

Kapitel 2 fasst die Motivation und das Ziel der Arbeit zusammen. Dabei steht zunächst die systematische Untersuchung der chemischen und kolloidalen Stabilität der Nanoteilchen mit unterschiedlicher Oberflächenchemie im Vordergrund. Im zweiten Teil der Arbeit wird ein Sensorkonzept unter Verwendung von UCNPs für das selbstreferenzierte kontinuierliche Messen eines Analyten in einem komplexen Medium realisiert.

Kapitel 3 wurde beim Wiley Journal „Particles and Particle System Characterization“ (Impact Faktor 4.4) zur Begutachtung eingereicht (akzeptiert Juli 2019). Das Hauptaugenmerk in diesem Teil der Arbeit liegt auf der Untersuchung des Einflusses der Oberflächenmodifikation von UCNPs und den daraus resultierenden Folgen für die kolloidale und chemische Stabilität. Dabei werden die Partikel über einen zweistufigen Ligandenaustausch modifiziert, wobei der ursprüngliche Ligand - Ölsäure - durch Zugabe von NOBF_4 von der Oberfläche der Nanoteilchen entfernt wird. Die unmodifizierten UCNPs werden schließlich durch Zugabe eines gewünschten Liganden stabilisiert. Dabei wird ein Ensemble von fünf verschiedenen Liganden, bestehend aus kleinen Molekülen und Polymeren, mit unterschiedlichen Koordinationsgruppen und unterschiedlichen Ladungen bei neutralem pH-Wert, im Detail untersucht. In hoch konzentrierten Dispersionen weisen alle Systeme hervorragende Kolloidstabilität auf. Unter nicht-Gleichgewichtssituationen, insbesondere in geringen Konzentrationen, wie sie bei der Einzelpartikelbildung oder unter Strömungsbedingungen vorliegen, beginnen die Partikel sich jedoch nach kurzer Zeit aufzulösen. Dies ist eine Folge einer unvollständigen Oberflächenbedeckung, die durch das Ligandenaustauschverfahren erreicht wird. Die Art der Oberflächenmodifikation hat dabei nur einen geringen Einfluss.

Der Fokus in **Kapitel 4** (publiziert als begutachteter Konferenzbeitrag zu einem Vortrag der Reihe „Nanodimensionale Bildgebung und Sensorik für biomedizinische Anwendungen“ während der SPIE Photonics West in San Francisco, USA, 2017) liegt auf der Entwicklung von effizienten UCNPs zur Verwendung als Lumineszenzreporter in bioanalytischen Anwendungen. Aufkonvertierende Nanoteilchen vom Typus $\text{NaYF}_4:\text{Yb},\text{Tm}$ zeigen bei Anregung mit einem 980 nm Diodenlaser (CW) mehrere Emissionsbanden. Dabei sind insbesondere die Emissionen bei 345 und 360 nm (UV), sowie diejenige im blauen Bereich (450 und 470 nm) für die Bioanalytik von großem Interesse, da diese Banden eine spektrale Überlappung mit den Absorbanzen wichtiger enzymatischer Co-Faktoren ($\text{NAD}^+ / \text{NADH}$ und $\text{FAD} / \text{FADH}_2$) aufweisen und so zur Beobachtung enzymatischer Reaktionen benutzt werden können.

Kapitel 5 steht kurz vor der Einreichung im analytischen Journal „ACS – Sensors“ (Impact Faktor 5.7). Es beschreibt die Aspekte hinsichtlich des Kern-Hülle-Wachstums bei UCNPs zur Verschiebung der Anregungswellenlänge von 980 auf 808 nm infolge zusätzlicher Nd^{3+} -Dotierung. Diese mit Polyacrylsäure funktionalisierten Partikel werden schließlich in ein Gel eingebettet und für die Detektion von L-Laktat verwendet. Der Sensor basiert dabei auf dem enzymatischen Umsatz von L-Laktat über Laktatdehydrogenase. Dadurch wird der Co-Faktor NAD^+ zu NADH reduziert, und dadurch die Emission der UCNPs über Reabsorptionseffekte beeinflusst. Hier werden zwei Systeme identischer, monodisperser, phasenreiner Nanopartikel, die entweder bei 980 oder 808 nm anregbar sind, auf ihre Verwendbarkeit für diesen Bioassay untersucht. In Küvettenanwendungen zeigen beide Systeme ähnliche Ergebnisse. Bei der Online-Messung von L-Laktat liefern Partikel anregbar mit 808 nm ein geringeres Detektionslimit sowie eine bessere Stabilität.

Kapitel 6 spiegelt den Stand der Technik zur Verwendung von UCNPs für bionalytische Anwendungen wider. Dabei werden auch die Ergebnisse dieser Arbeit kritisch bewertet und zukünftige Perspektiven von UCNPs vorgestellt.

DECLARATION OF CONTRIBUTIONS

Most of the experimental and theoretical work presented in this thesis was carried out solely by the author. However, some of the results were obtained together with other researchers. In accordance with § 8 Abs. 1 Satz 2 Punkt 7 of the “Ordnung zum Erwerb des akademischen Grades eines Doktors der Naturwissenschaften (Dr. rer. nat.) an der Universität Regensburg vom 18. Juni 2009“, this section gives information about these collaborations.

Chapter 1: A critical comparison of lanthanide based upconversion nanoparticles to fluorescent proteins, semiconductor quantum dots, and carbon dots for use in optical sensing and imaging

This chapter has been published as a review article. The literature survey was performed by the author. The concept and structure of the manuscript was planned with Thomas Hirsch. The author wrote the manuscript. Thomas Hirsch revised the manuscript and is corresponding author.

Chapter 3: Long-term colloidal and chemical stability in aqueous media of NaYF₄-type upconversion nanoparticles modified by ligand-exchange

This chapter has been submitted for publication to the journal *Particle and Particle Systems Characterization* (accepted July 2019). All measurements and synthesis steps were carried out by the author. The initial particles NaYF₄(Yb,Er)@OA were prepared during the master's study of the author. The manuscript was written by the author. The article was revised by Thomas Hirsch, who is corresponding author.

Chapter 4: 980 nm and 808 nm excitable upconversion nanoparticles for the detection of enzyme related reactions

Susanne Märkl synthesized the upconversion nanoparticles supervised by the author. All other experiments were carried out by the author. Surface chemistry of the nanoparticles was discussed with Verena Muhr and Markus Buchner. The shift of the excitation wavelength was discussed with Lisa Marie Wiesholler. Lisa Marie Wiesholler contributed to XRD measurements. The author wrote the manuscript. The article was revised by Thomas Hirsch and Antje J. Baeumner. Thomas Hirsch is corresponding authors.

Chapter 5: Luminescence-based self-referenced enzymatic L-lactate sensing by tandem-sensitized NIR to UV NaYF₄(Yb,Tm) upconversion nanoparticles

This chapter is prepared for submission to *ACS Sensors*. Susanne Märkl synthesized the upconversion nanoparticles and measured the dose-response curve for L-lactate (in the cuvette) under 980 nm excitation. The synthesis and the measurement were supervised by the author. Lisa Marie Wiesholler contributed to XRD and Nd³⁺ absorption measurements. The shift of the excitation wavelength was discussed with Lisa Marie Wiesholler. Results were discussed with Thomas Hirsch, Axel Dürkop and

Antje J. Baeumner. The author wrote the manuscript and revision was carried out by Thomas Hirsch and Antje J. Baeumner. Thomas Hirsch will be the corresponding author.

CHAPTER 1

A critical comparison of lanthanide based upconversion nanoparticles to fluorescent proteins, semiconductor quantum dots, and carbon dots for use in optical sensing and imaging

The right choice of a fluorescent probe is essential for successful luminescence imaging and sensing and especially concerning in vivo and in vitro applications, the development of new classes have gained more and more attention in the last years. One of the most promising class are upconversion nanoparticles (UCNPs)-inorganic nanocrystals capable to convert near-infrared light in high energy radiation.

In this review we will compare UCNPs with other fluorescent probes in terms of (a) the optical properties of the probes, such as their brightness, photostability and excitation wavelength; (b) their chemical properties such as the dispersibility, stability under experimental or physiological conditions, availability of chemical modification strategies for labeling; and (c) the potential toxicity and biocompatibility of the probe.

Thereby we want to provide a better understanding of the advantages and drawbacks of UCNPs and address future challenges in the design of the nanocrystals.

This chapter has been published:

Sandy F. Himmelstoß, Thomas Hirsch. *Methods and Applications in Fluorescence*, 2019, 7, 0022002.

Author contributions:

The literature survey was performed by the SFH. The concept and structure of the manuscript was planned with TH. SFH wrote the manuscript. TH revised the manuscript and is corresponding author.

1.1 Introduction

Upconversion Nanoparticles (UCNPs), *e.g.* consisting of a NaYF_4 host lattice, doped with lanthanide ions classified as sensitizer (*e.g.* Yb^{3+}) and activator (*e.g.* Er^{3+} , Tm^{3+} or Ho^{3+}), represent a special class of probes. In contrast to most other fluorescent probes, these probes exhibit anti-Stokes emissions upon excitation. The architecture of the UCNPs enables the absorption of light in the near-infrared (NIR) by the sensitizer ion. Within the crystal, the energy is transferred sequentially to an activator ion, which leads to emissions of shorter wavelength than the excitation wavelength [1]. The upconversion luminescence of lanthanide doped nanocrystals attractively does not suffer from photobleaching or intermittence, but it is limited in its efficiency. In the past, the improvement of the particles' synthesis [2] and surface modifications [3] as well as the understanding [4] and enhancement of the upconversion process [5] was in the focus of research. Based on those efforts, UCNPs have established as an alternative to fluorescent probes like quantum dots (QDs), carbon dots (C-Dots) and fluorescent proteins (FPs) (Figure 1.1).

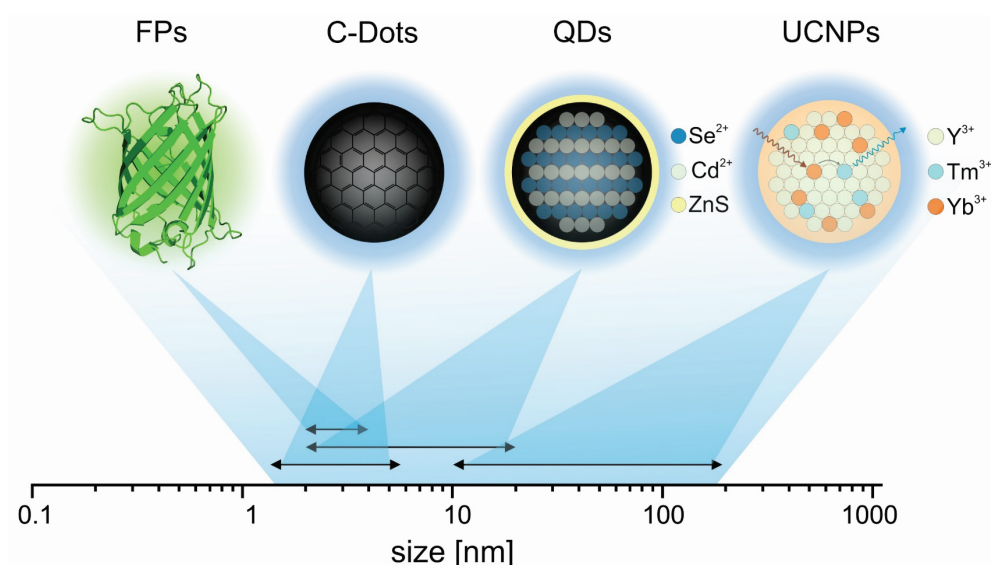


Figure 1.1 | Overview of luminescent probes of upconversion nanoparticles (UCNPs), carbon dots (C-Dots), semiconductor quantum dots (QDs) and fluorescent proteins (FPs) compared in this review.

Fluorescent proteins are complex three-dimensional polypeptide structures with a molecular weight in the range of 25 kDa [6]. In general, those naturally obtained probes (*e.g.* from jellyfish) have a rigid barrel-like structure, consisting of typically eleven β -sheets [7], where the chromophore is located. The chromophore itself is formed by a tyrosine-glycine dipeptide linked *via* a double bond. The luminescence properties are characterized by narrow excitation spectra. The small Stokes-shift together with low photostability are main shortcomings [8]. Quantum dots are semiconductor materials with atoms from groups II–VI, III–V, or IV–VI of the periodic table, with most prominent candidates such as CdSe, ZnS, InP or PbSe [9], offering size-dependent absorption and emission in the visible and NIR regions, with high quantum yield, large photon absorption cross-sections and outstanding photostability [9]. The exceptional variations in narrow emissions render this class of luminescent probes most suitable for multiplexing. However, the presence of heavy metal ions in QDs and its toxicity is a matter of considerable discussion for biomedical applications [10].

Zero-dimensional carbon nanomaterials, including amorphous spherical particles of sp^2/sp^3 -hybridized carbon atoms, as well as so-called graphene quantum dots, which comprise of usually less than 10 carbon layers consisting of a graphene lattice [11] are a rather new class of materials, first discovered in 2004 [12]. The starting products such as saccharides or citric acid are abundant, inexpensive and show good biocompatibility and low cytotoxicity [13]. The surface of these particles is often covered with carboxyl or amine moieties, which lead to high colloidal stability in aqueous media. Additional surface passivation and functionalization will tune the optical properties of such systems. Consequently, these probes have become a rising star for biosensing and imaging applications [13]. The tremendous efforts in development of luminescent probes in the last years are also driven by the fast progress of high-resolution techniques in microscopy like stimulated emission depletion (STED) [14], STORM (Stochastic Optical Reconstruction Microscopy) [15] and (F)PALM (Fluorescence Photo-Activated Localization Microscopy) [16], and by an increased demand for chemical and biological sensors in many areas of life, including health care, food safety, production processes, environmental monitoring or life science [17]. Therefore, it is not surprising that the classes of fluorescent probes compared in this review are widely used for those applications as reflected by a Web-of-Science survey (Figure 1.2).

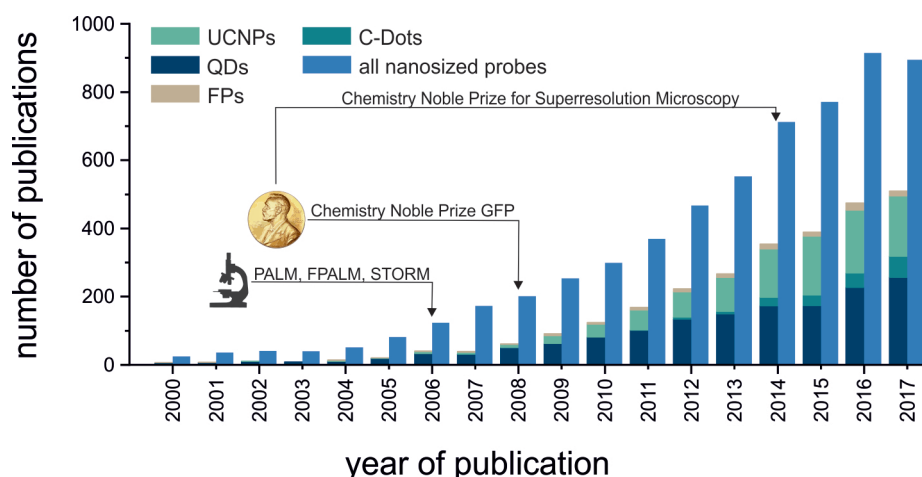


Figure 1.2| Web-of-Science survey for publications for nano-sized luminescent probes used in sensing or imaging applications as well as the fraction dealing with either upconversion nanoparticles (UCNPs), quantum dots (QDs), carbon dots (C-Dots) or fluorescent proteins (FPs).

In 2017, 57% of all publications, dealing with nano-sized luminescent sensing and imaging applications are using one of these probes, whereas QDs (50%) and UCNPs (35%) are the ones, which attracted the highest interest. Due to the short history of C-Dots, their impact is still not so huge, but with an increase of 350% in the number of publications over the last five years, it is expected that this class will get more and more important. All four types of probes discussed have been extensively reviewed in term of synthesis, chemistry, luminescence as well as their potential applications. For more detailed information the reader is referred to these numerous excellent reviews for UCNPs [18–22], C-Dots [13, 23, 24], FPs [25–28], or QDs [29–32]. In this review, these probes will be compared to each other in order to identify their benefits and limits in regard to their usability for bioanalytical sensing and imaging. Some of these probes have also been studied for deep tissue bioimaging, due to the emissions in the second biological window (1000–1350 nm). The state of the art and the challenges in the design of nanoprobe for bioimaging in the NIR has been reviewed in detail elsewhere and will not be covered by this review [33–35].

1.2 Optical properties

1.2.1 Origin of photoluminescence

The comparison of the origin of photoluminescence of UCNPs to other fluorescent probes reveals two different principles (Figure 1.3). Fluorescent proteins, carbon and quantum dots are representatives for the Stokes-shifted excitation-emission characteristics, where high-energy radiation is transferred into low energy emission. Upconversion nanoparticles on the other side, transform low energy excitation in high-energy radiation. In the following, the origin of photoluminescence of all systems will be briefly explained.

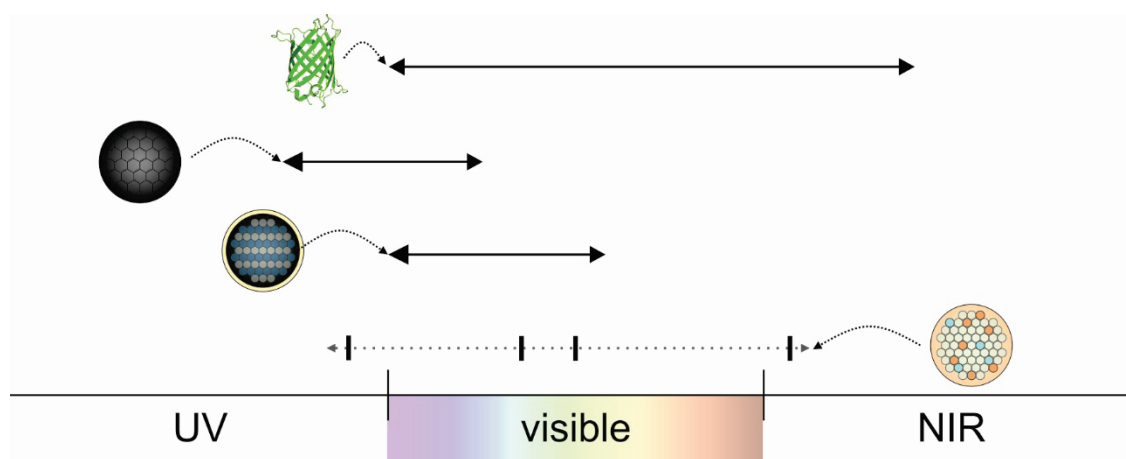


Figure 1.3 | Comparison of typical excitation wavelengths (symbolized by the symbol of the probe in the order fluorescent proteins, carbon dots, quantum dots, and upconversion nanoparticles from top to the bottom). The typical emission ranges are symbolized by black arrows. In case of UCNPs, low energy excitation is converted to high energy (anti-Stokes shift) radiation with most prominent distinct emission wavelengths indicated by black ticks.

The luminescence of the FPs is generated by a classical fluorophore, thereby the same model as it is used for organic dyes is valid. The ternary structure of the proteins is building up a barrel structure in which the chromophore is located. In all natural occurring FPs the chromophore is consisting of a 4-(p-hydroxybenzylidene)-5-imidazolinone structure [36]. By irradiation of this molecule, π -electrons are transferred from the electronic ground state to an excited state. The transition back to the ground state is accompanied by the emission of photons (Figure 1.4 A). In contrast to this, the photoluminescence of QDs is based on the properties of semiconductors like CdS, CdSe or ZnS. Such materials are characterized by an electronic structure, consisting of a valence band and a conduction band [9]. The absorption of a photon, promotes an electron from the valence band to the conduction band, leaving behind a hole [37]. Both, the hole and the electron have opposite charges and can bind to each other, generating a hydrogen-like quasi particle called exciton [38]. Those excitons can be classified by their size, the Bohr radius a_B . In the case of QDs, the size of the particles is smaller than this Bohr radius, resulting in the quantum confinement of the excitons. When excitons are confined in a quantum dot, discrete energy states appear in its energy structure as depicted in Figure 1.4 B. Thereby the number and energy of those states depend on the size of the nanoparticles, affecting the absorption and emission of the material. The transition of the electron back to the valence band (called recombination) cleaves this binding and light of the exciton's energy is emitted.

A critical comparison of lanthanide based upconversion nanoparticles to fluorescent proteins, semiconductor quantum dots, and carbon dots for use in optical sensing and imaging

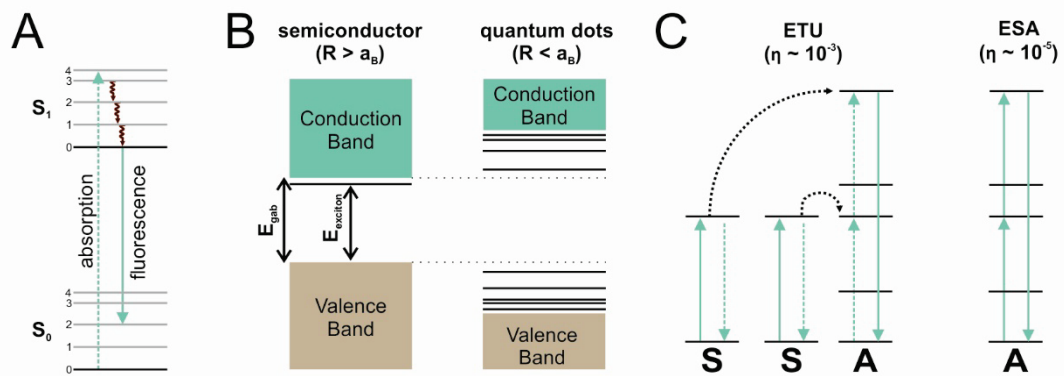


Figure 1.4 | Scheme of the origin of photoluminescence for fluorescent proteins (A), quantum dots (B) and upconversion nanoparticles (C). (A) Jablonski-diagram including vibrating levels (grey horizontal lines), the absorption of light (dashed arrow), non-radiative transitions (red arrows) and fluorescence (solid arrow) (B) Comparison of the distribution of the energy levels of semiconductors and semiconductor quantum dots, each with a radius R . In the case that R is smaller than the Bohr radius a_B , discrete levels are formed between the energy gap. (C) Energy schemes for different two-photon upconversion processes with their probability η . Transitions between energy levels are indicated by vertical and curved arrows. S refers to the energy levels of the sensitizer ions, A to such of the activator ion. Horizontal lines reflect energy levels.

The origin of the photoluminescence of C-Dots is still a matter of debating. Carbon dots, mainly consisting of sp^2 -hybridized atoms, show a strong absorption in the ultraviolet (UV) [39]. Beside this, also surface passivation and doping by hetero atoms can attribute to the optical properties, shifting the absorption into the visible range, generating broad non-Gaussian absorption peaks with its maximum between 250 and 360 nm [40]. However, the detailed nature of photoluminescence of this nanomaterial is still under investigation [13]. Beside the quantum confinement effects several other contributions from surface defects, surface passivation and functional groups attached to the C-Dots have been allocated with the origin of their luminescence.

The anti-Stokes emission of UCNPs rises significant interest for bioanalytical applications. Due to excitation at longer wavelength, almost no autofluorescence of biological compounds is triggered, preventing strong background luminescence. Excitation at low energy can also be achieved by a two-photon process, but this mechanism suffers from very low absorption and needs high intensities. In contrast, upconversion is a sequential absorption of photons. Several mechanisms are reported to explain the nature of the upconversion luminescence, whereas the excited state absorption (ESA) and energy transfer upconversion (ETU) (Figure 1.4 C) are the ones with the highest probability [41–43]. Thereby ESA is based on the sequential uptake of at least two photons by one ion, whereas in the ETU the presence of two components – sensitizer and activator ions – is essential [21]. The process starts with the absorption of NIR photons *via* the sensitizer ions. Therefore, most upconversion lanthanide materials are co-doped with Yb^{3+} , which has an absorption maximum at 975 nm [44, 45]. Due to the close proximity of sensitizer ions and activator ions an energy transfer can occur, and an excited state is populated. Ideal candidates for efficient upconversion are thereby lanthanide ions such as Pr^{3+} , Nd^{3+} , Er^{3+} , Tm^{3+} or Ho^{3+} [46] as they have several 4f excited states with long lifetime, which can be further excited by another energy transfer process.

1.2.2 Shape of the emission spectra

The classical and widely used green fluorescent proteins (GFPs) found in a jellyfish have two absorption maxima at 395 and 475 nm and an emission maximum of 510 nm [47]. Nowadays, there is a wide choice of fluorescent proteins available, which can be divided in different classes (e.g. blue, green, red, and far red) covering the visible range of the spectra and tailing into the NIR. This variety is based on the different chromophores, which can be formed within the β -barrel structure of the protein. As seen in Figure 1.5, small changes of its molecular structure, extending the π -system, shifts absorption and emission to longer wavelengths [48, 49].

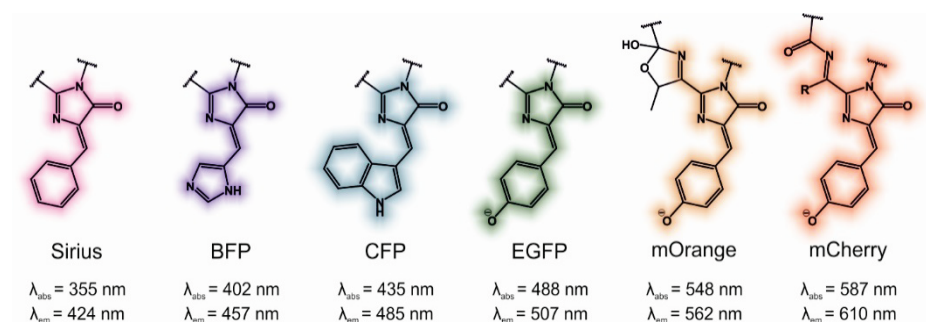


Figure 1.5| Chemical structures of chromophores used in fluorescent proteins with increasing emission maxima.

In all examples, the Stokes-shift is only between 20 and 50 nm and the spectra show an asymmetric broad emission band shape with a Full Width Half Maximum (FWHM) of around 40 - 60 nm [50], as illustrated in Figure 1.6. Beside the classical FPs derived from the GFP, nowadays alternative systems like flavin mononucleotide binding fluorescent proteins (FbFPs) are known [51]. In contrast to commonly known FPs, those systems can form their chromophore under anaerobic (O_2 free) conditions [52].

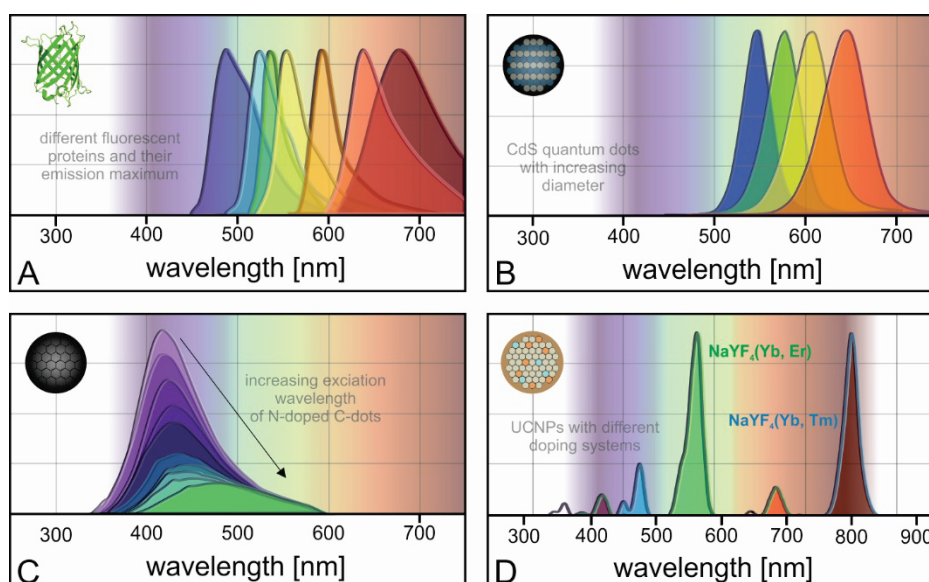


Figure 1.6| Typical emission spectra of each class of luminescent probes. (A) Different fluorescent proteins emitting between 450 and 800 nm. (B) Emission spectra of quantum dots with variation of the size between 2.9 and 3.8 nm. (C) N-doped carbon dots show an excitation wavelength dependent variation of luminescence. (D) Upconversion nanoparticles with different doping systems exhibit emissions peaking at different wavelengths.

The emission maxima of QDs can be tuned by the composition of the nanomaterials [53] and by variation of the particle size [54]. Figure 1.6 B shows the redshift of the emission maximum from 550 to 660 nm when the diameter of a CdS QDs is stepwise increased from 2.9 to 3.8 nm [8]. In another example, QDs consisting of ZnS with diameters between 6.0 and 17.0 nm cover an emission range between 258 and 441 nm [53]. Compared to FPs, the width of the peaks is generally slightly narrower (20 - 50 nm) for an emission maximum in the visible [9], *e.g.* CdSe QDs, with an emission peaking at 535 nm, show a FWHM of ~23 nm [55]. In contrast QDs emitting in the NIR show much broader peaks with FWHM in the range of 50 - 100 nm [8], as it is the case for PbS QDs (~90 nm FWHM) with an emission maximum at 775 nm [56]. Analogous to the size dependent emission of QDs, the same phenomenon can be observed for C-Dots, which also give evidence that the quantum confinement effects significantly contribute to the origin of their photoluminescence. Additionally, and exclusively for the probes compared here, the emission of C-Dots is excitation wavelength dependent. This is a consequence of the broad absorption bands, which can be assigned to different excitation pathways, leading to different emission properties. As seen in Figure 1.6 C, N-doped C-Dots are redshifted with increasing the excitation wavelength from 310 to 390 nm.

By the shift of the excitation wavelength to lower energies, the less intensive and broader the emission peaks become [57]. The emission bands collected at excitation maximum show a FWHM of around 60 nm and large Stokes-shifts of about 150 nm. Compared to the other probes, the emission spectra of upconversion nanoparticles (Figure 1.6 D) are characterized by several sharp emission bands with typical FWHM values of 10 - 15 nm and an anti-Stokes shift of typically more than 100 nm [58]. The peak wavelengths are fixed by the choice of the activator ion of the nanocrystal, and are independent on the size and concentration of the particles [59]. Tm³⁺ doped particles are characterized by emissions in the blue, whereas Er³⁺ doped UCNPs are identified by a strong emission in the green. The peak ratios can be tuned by the doping ratio or by surface chemistry, preventing non-radiative deactivation of certain excited states [60, 61].

1.2.3 Extinction coefficient, quantum yield and brightness

One of the key parameters for bioanalytical applications are brightness and efficiencies of luminescent probes. Brightness is determined by two parameters: the extinction coefficient at a specific wavelength and the quantum yield (QY), which is usually defined as the ratio between the numbers of emitted photons to the number of photons absorbed by the probe [4]. For FPs, with their similarity to molecular probes, those values can become very high, depending on the chromophore. Molecules emitting in the orange, red or far-red region of the spectra, have rather low quantum yields of around 45% - 10%, whereas higher QYs (~80%) are obtained for proteins with an emission in the range of 475 and 500 nm [62]. For GFPs and their modifications, the QYs are slightly lower (~70%), but they have a high extinction coefficient of ~120,000 M⁻¹·cm⁻¹. Therefore, GFPs are known as the brightest among the compared fluorescent proteins [62].

The QY of semiconductor QDs strongly depends on the composition of the nanocrystals. For example, CdTe/CdSe QDs have a poor efficiency of 13% and an extinction coefficient of 6·10⁵ M⁻¹·cm⁻¹. By changing the composition of the materials to CdSe/ZnS, the quantum yield can be increased to 82% [63]. Usually those particles are modified with an additional (protective) shell or different coatings, which have a significantly higher band gap energy than the core material. For example, the QY of CdSe QDs can be increased from 5% to 50% by the epitaxial growth of a ZnS shell around the core material

[64]. For C-Dots consisting of only carbon, the QY is very low (typically lower 10%) [40], so that further surface passivation and functionalization steps are essential to obtain probes with efficient luminescence [13]. C-Dots with *e.g.* $-\text{COOH}$, $-\text{CN}$, or $-\text{CO}$ moieties reach QYs of $\sim 17\%$, whereas an outstanding QY of 75% was reported for CDs with polyethylene glycol (PEG) modification [65]. Beside this, element-doping is used to increase the QY of the CDs. Co-doping with nitrogen results in a QY of around 16%, whereas a system with additional sulfur even reaches values up to 67% [66].

In terms of QY, UCNPs are not convincing by exceptional good numbers, but a comparison to quantum dots and gold nanorods revealed that they are already of acceptable brightness for bioimaging applications [67]. Enhancing the brightness is still one of the greatest challenges for the UCNPs. On one side Yb^{3+} has a low molar absorption coefficient with a maximum value of $3.39 \pm 0.04 \text{ M}^{-1}\cdot\text{cm}^{-1}$ [68]. Beside this, the quantum yield of the particles is strongly dependent on the power density of the laser module. With increasing power densities, also the QY increases as seen in Figure 1.7. However, in region of low excitation power densities, which are required for *in vivo* diagnostics, the QY is far below 1%. This is mainly a consequence of surface defects, interactions of the surface ions with surface ligands or the type of dispersion media. To gain more interest in UCNPs for medical applications, the quantum yield needs to be improved by core/shell-architectures of the particles, *e.g.* with an inert NaYF_4 shell [69]. For more detailed information on enhancing the upconversion efficiency several reviews on this topic have been published [61, 70–72].

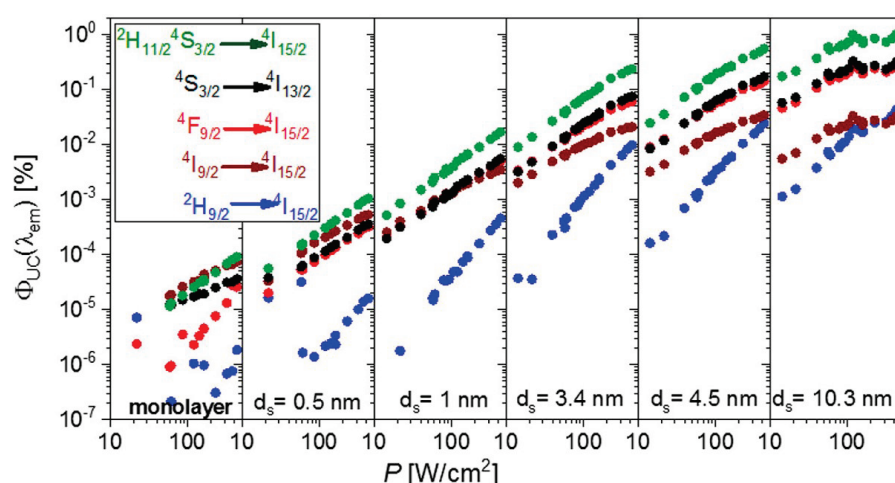


Figure 1.7 | Power density dependency of the quantum yield of $\text{NaGdF}_4(\text{Yb}, \text{Er})$ nanoparticles with a core diameter of $3.7 \pm 0.5 \text{ nm}$ and the influence of different shell thickness on the quantum yield. Adapted with permission from [69]. Copyright 2019 American Chemical Society.

1.2.4 Lifetime

The lifetime reports the time an excited state needs to decay to e^{-1} *via* all possible radiative and non-radiative depopulation pathways. At a constant flux of excitation, a short lifetime is advantageous for the brightness of a probe. On the other hand, changes in the lifetime of a probe can also be attractive in sensing application based on Förster Resonance Energy Transfer (FRET) or in Fluorescence Lifetime Imaging (FLIM). The lifetime of molecular probes is in the range of nanoseconds [73] and thus, also the lifetime of FPs can be found in this range [74]. As an example, the lifetime of mScarlet (red fluorescent protein family) is $\sim 3.9 \text{ ns}$ [75], which is very similar to the one of GFP with $\sim 3 \text{ ns}$ [36]. The decay times of C-Dots are also in the low ns-regime [76, 77]. Usually plain C-Dots, without any

modification, expose the shortest lifetimes. By addition of heteroatoms or by surface modification the values increase. C-Dots obtained from glucose, decay within 2.8 ns. By doping the system with nitrogen and sulfur, the lifetime increases to 3.9 ns [78]. It is reported that the size of heteroatom doped C-Dots has an impact on the lifetime. By increasing the size of N-doped C-Dots from 2 to 10 nm, a decrease of the lifetime from 3.4 to 1.1 ns was observed [57].

Compared to this, QDs obtain longer lifetimes, ranging from 10 - 300 ns, whereas the exact value depends on the composition and surface functionalization of the nanomaterial. Binary II-VI-type QDs show average lifetimes between 1 and 20 ns, whereas much higher lifetimes (100 - 300 ns) are reported for ternary type I-III-VI QDs [54]. Among the described fluorescent probes, UCNPs are characterized by the longest lifetimes in the μ s to ms range. Due to the unique origin of luminescence, every transition state of UCNPs has a different decay time. Hydrophilic PEG-modified nanoparticles consisting of NaGdF₄ co-doped with Yb³⁺ and Er³⁺ ions, ~17 nm diameter, are emitting at 540 and 656 nm. Thereby the emission in the green decays with 74 μ s, whereas at 656 nm the lifetime is 144 μ s. The modification of this system by an inert shell with a thickness of 2.5 nm increases the lifetime further to values of 101 μ s (green) and 207 μ s (red) [79]. This architecture reduces the non-radiative relaxations due to surface defects as well as by the dispersion media [80]. By comparing UCNPs of the same composition but different sizes, a similar trend can be observed. The decay time at 540 nm of NaYF₄(Yb, Er) nanoparticles with sizes between 15.3 and 27.2 nm increases from 69 to 506 μ s [81].

1.2.5 Photostability

For many applications an important parameter is given by the photostability of a luminescent probe. Thereby two phenomena have to be distinguished. Fluorescence intermittency, also called blinking, and photobleaching. The first describes the random switching of a fluorophore between on (bright) and off (dark) states of the fluorophore under continuous excitation. Prominent representatives known for blinking are QDs like CdS [82] or fluorescent proteins [49]. This effect formally seen as a disadvantage has become attractive for super resolution microscopy like STED or STORM [83]. A rather new method is Super resolution Optical Fluctuation Imaging (SOFI), which relies only on quick signal fluctuations [84]. Based on this, Xu *et al.* used three commercially available QDs – QD525, QD625 and QD705 – to obtain a high spatial resolution (~85 nm) of the tubulin in COS-7 cells [85]. On the other side, also the stability against photobleaching is of huge importance, especially if the fluorescent probes should be used for long-term measurements like monitoring of processes in living cells or organisms. Upconversion nanoparticles, QDs, and C-Dots show excellent photostability. Upon illumination of UCNPs with a 980 nm continuous wave (CW) laser source for 400 s, only 4% of the signal gets lost, whereas the luminescence intensity of a dye, *e.g.* 4',6'-diamidino-2-phenylindole decreased to 1% of its initial value [1]. Carbon Dots were irradiated for four hours and only a decrease of the intensity by 4.5% was detected [86]. In the case of fluorescent proteins, often a rapid bleaching is observed [87]. Table 1.1 summarizes the photophysical properties of UCNPs, C-Dots, QDs and FPs.

A critical comparison of lanthanide based upconversion nanoparticles to fluorescent proteins, semiconductor quantum dots, and carbon dots for use in optical sensing and imaging

Table 1.1: Comparison of upconversion nanoparticles [1, 58, 88, 89], carbon dots [39, 40, 76, 86], semiconductor quantum dots [9, 90] and fluorescent proteins [25, 50, 62, 74, 87, 91] concerning their optical properties.

	UCNPs	C-Dots	QDs	FPs
Excitation range	NIR	UV	UV	VIS/UV
Emission range	UV / VIS / NIR (several bands)	VIS (typ. single bands)	VIS/NIR (typ. single bands)	VIS/NIR (typ. single bands)
Emission tuned by	composition ^a doping ratio	excitation wavelength doping ratio surface functionalization	composition size	chromophore
Shape of emission bands	symmetric Gaussian like	asymmetric	symmetric Gaussian like	asymmetric
FWHM	~15 nm	> 80 nm	VIS 20 - 50 nm NIR 50 - 100 nm	35 - 60 nm
Spectral shift	> 100 nm (anti-Stokes)	> 100 nm	< 100 nm	typical 20 - 60 nm
Lifetime	> 100 μ s	< 20 ns	1 - 300 ns	< 5 ns
Two-photon cross section^b	$8 \cdot 10^6$ GM	< 39,000 GM	< 100,000 GM	< 645 GM
Quantum yield	< 5%	< 90%	VIS: 40 - 70%, < 90%, NIR: 20 - 40%, < 80%	average 70 - 80%
Photostability	excellent	excellent	excellent	weak

^a Composition of UCNPs refers to the choice of host lattice and the sensitizer and activator ions.

^b Probability of a probe to absorb two photons at the same time.

1.3 Chemical and physical properties

In the following, the four classes of luminescent probes are compared regarding their synthesis, commercial availability, the colloidal and chemical stability as well as the ability for chemical functionalization. Especially the size and the shape of the resulting nanosystem is important concerning particle transport, adhesion and biodistribution within an organism [92]. Here, UCNPs give the largest flexibility. Beside dimensions ranging from ~10 to more than 100 nm (as seen in Figure 1.1) also variations in shapes like flowers [93], dumbbell [94] or rods with high aspect ratios [95] have been reported.

1.3.1 Synthesis

Synthesis of luminescent nanomaterials can be classified as bottom-up and top-down approaches. In the case of top-down methods, a starting bulk material is broken down to the nano-level, whereas the synthesis starts from small precursor material in bottom-up approaches. Figure 1.8 gives an overview of the most common fabrication techniques for the probes discussed in this review.

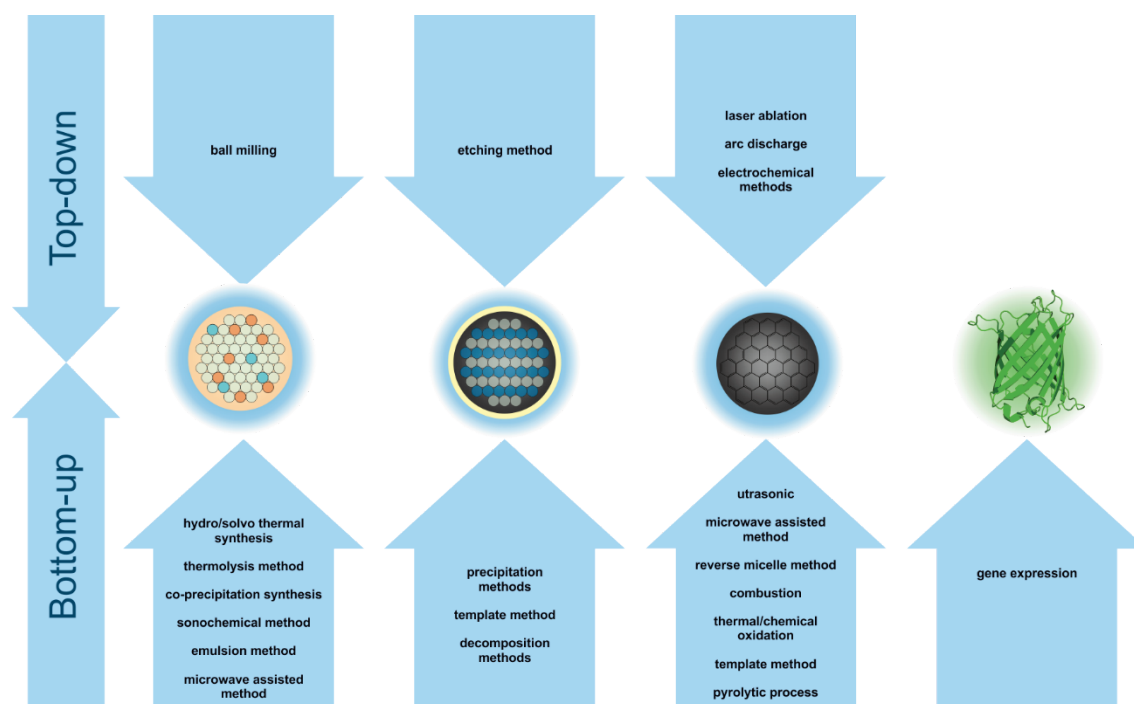


Figure 1.8| Overview of commonly used synthesis strategies (bottom-up and top-down) of the upconversion nanoparticles, semiconductor quantum dots, carbon dots and fluorescent proteins (from left to right).

For FPs, gene expression is the method of choice. Thereby the probe is obtained directly within a chosen cell. This process starts with the introduction of genetically engineered bacterial plasmid or viral vectors into mammalian or other host cells [47]. The basic plasmid vector must have several components including the coding sequence for the FPs, a sequence coding for a bacterial replication origin for the deoxyribonucleic acid (DNA), elements that control the initiation of messenger RNA transcription (promoters) and a gene for co-selection in mammalian cells [96]. In the course of transfection into the cell, one has to distinguish between stable and transient transfection. In the transient transfection, the DNA does not integrate into the chromosome and is only expressed in the

cytoplasm for a short period. In the stable transfection, the plasmid DNA can be incorporated into the genome in a permanent state to form stable (transformed) cell lines [97]. Once the protein is produced, the chromophore needs to be formed. Thereby the polypeptide backbone must undergo several autocatalytic processes. The exact mechanism is still under investigation. For further information the reader is referred to the literature [98] where the crucial steps including folding, cyclisation, oxidation and dehydration are described and different possible mechanisms are discussed and compared to each other. Recent studies [99] showed that the oxidation of the chromophore during the whole maturation process is the rate-limiting step. Depending on the exact chromophore composition and temperature of the environment, this can take a few minutes up to several hours [100].

The synthesis of luminescent nanomaterials including UCNPs, C-Dots and QDs is mostly done by a bottom-up approach, which allows a better control of the size, size-distribution and reproducibility. A milestone for the reproducible preparation of highly luminescent, water-dispersible and monodisperse QDs was the method reported by Murray *et al.* [101]. This approach is based on the pyrolysis of organometallic precursors in a hot coordination solvent and in presence of a stabilizing agent [9]. The particles show a homogenous size-distribution, but low quantum yields. By growing shells, consisting of semiconductor materials (like CdS or ZnS) with a higher band gap, further passivation of the surface increases the quantum yield of QDs [102, 103]. For example, in the core/shell system CdSe/ZnS the QY is improved from 15% to 50% [104]. An alternative method, which uses less toxic precursor material and allows large-scale production of the nanomaterial was reported by Peng *et al.* [105]. Instead of the sensitive and toxic Cd(CH₃)₂, CdO is used as starting material. The obtained QDs (CdSe or CdTe) are highly monodisperse. However, particles obtained by these approaches, are hydrophobic by nature, so that surface modifications are required to render the particles water-dispersible and accessible for bioanalytical applications. For detailed information on synthetic routes to directly obtain hydrophilic QDs the reader is referred to a review on aqueous synthesis of QDs published by Jing *et al.* [106].

In the case of C-Dots the nanoparticles can be obtained by both synthesis routes. Among the top-down methods, arc discharge, electrochemical approaches or laser ablation are common techniques [107]. However, those methods require harsh and long reaction conditions. On the other side, bottom-up methods starting with molecular precursors are promising alternatives [13], as they lead to highly fluorescent and efficient C-Dots. Thereby the synthesis is based on the dehydration of carbohydrates in an aqueous media yielding a hydrophilic product. Those are often catalyzed by acid or basic condition, ultrasound, hydrothermal or microwave assisted techniques [13]. Especially the hydrothermal treatment of the carbon source is one of the most popular techniques as it allows mild conditions [108] suitable for a large variety of different starting materials. At the end of the synthesis most of the educts have been carbonized (depending on the dehydration rate) and the surface of the nanomaterial is decorated with functional groups as already present in the precursor material. Possible carbon sources for the nanoparticles are carbohydrates like glucose, fructose [39], aromatic molecules and polymers [107] with functional groups (*e.g.* hydroxyl, carboxyl or aldehyde). Beside this, it is also possible to obtain nanoparticles doped with heteroatoms, mainly used to increase the quantum efficiency [57]. By hydrothermal treating of citric acid in the presence of ethylenediamine, water-dispersible nitrogen-doped C-Dots with an increased QY of 80% are reported [109].

For the synthesis of UCNPs one of the most popular methods is the thermal decomposition method, firstly reported by Zhang *et al.* [110], due to its efficient pathway to prepare high quality particles of

controlled size and shape. Thereby lanthanide salt precursors (chlorides, acetates or oleates), together with NaOH and NH_4F are dissolved in a mixture of high boiling solvents (1-octadecene and oleic acid or oleylamine) and heated above 300 °C to obtain particles with a pure hexagonal crystal lattice. By changing different parameters like the host material, the ratio of the high boiling solvents, the amount of NaOH or KOH, the pH value, or the reaction time, nanoparticles with different sizes and shapes can be prepared. Liu *et al.* have fabricated particles below 50 nm with distinct shapes from flowers to bamboo-like nanorods, as shown in Figure 1.9 [95]. By substitution of sodium by lithium, rhombus-shaped particles were reported by Rojas-Gutierrez *et al.* [111]. In each case, the particles show a narrow size distribution with a surface coating of oleic acid or oleylamine, so that further surface modifications are necessary for bioanalytical applications.

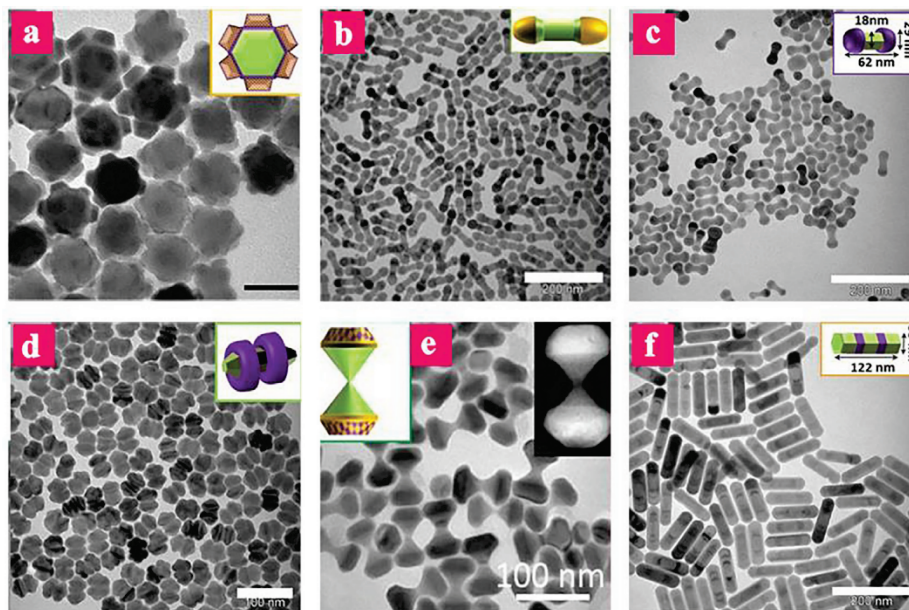


Figure 1.9| TEM image of UCNPs of different shapes like flower (a), round-end dumbbell (b), nano-dumbbells (c), double rings (d), hourglass (e) and bamboo-like nanorods (f). Reprinted from [2] Copyright (2019) with permission from Elsevier.

Another popular fabrication method yielding already in water dispersible particles is the hydro-/solvothermal synthesis at high pressure and temperature [112], *e.g.* reported by Li *et al.* [113]. Here the lanthanide precursors (*e.g.* nitrates or chlorides) and fluoride precursors are mixed with oleic acid/oleylamine, ethanol, surfactants and water to form a three-phase system (liquid, solid and solution phases) which is then placed in an autoclave [2]. Up to now, UCNPs with different sizes, hosts such as NaYbF_4 [114] and morphology were prepared by tuning the reaction conditions. A rather new method is the one-step microwave assisted synthesis of hydrophilic UCNPs as reported by Krishan *et al.* [115]. Thereby lanthanide ions are mixed with a fluoride source (here NH_4F), transferred in a microwave reaction vessel and heated for 3 h at 150 °C. However, the solvothermal as well as the microwave assisted synthesis still suffer from large size distribution and poor colloidal stability of the particles.

1.3.2 Core/shell and multimodal nanosystems

The tremendous progress in the synthesis of nanoparticles can be seen by the trend to design onion-like particle systems comprising of a core surrounded by one or more shells of different composition. Especially for UCNPs this has become very popular [79, 116, 117]. Such complex architectures can be designed to tune the optical properties or to end up with multimodal systems. Of great importance, in terms of brightness of the UCNPs, is the epitaxial growth of an inert shell on the UCNPs to minimize surface quenching [69]. Quite common is a method where the shell is obtained by an Ostwald-ripening process, whereas a sacrificing shell material (*e.g.* cubic NaYF₄) is injected in a boiling mixture of oleic acid, octadecene, and hexagonal lanthanide doped NaYF₄ particles [5, 118]. The small cubic particles get dissolved and grow a homogeneous shell around the core particles. By changing the doping additional sensitization can be realized *via* Nd³⁺ ions absorbing light of 808 nm. Multimodality can be achieved by using of Gd³⁺ for Magnetic Resonance Imaging (MRI) or heavy ions like Lu³⁺ to attenuate more X-rays for Computed Tomography (CT) [93, 119–121]. Magnetic resonance imaging (MRI) has become a powerful tool for clinical diagnostics. The non-invasive method distinguish itself from others by its high tissue penetration and high spatial and temporal resolution. The precondition is the presence of atoms with a net nuclear spin like Gd³⁺, which has seven unpaired electron pairs in its 4f orbital [122]. Under a magnetic field this compound generates an MRI signal with a large magnetic moment and a high relaxation efficiency. Based on this Gd³⁺ is widely used as contrast agent for MR imaging. However, free gadolinium ions are highly toxic so that contrast agents commonly used need to be stabilized by chelating agents. Gd³⁺ can be easily co-doped into upconversion nanoparticles. This can be realized *e.g.* by a core/shell structure [93] or by integrating the lanthanide as dopant into the host matrix [123]. Here antitumor-antibody modified NaGdF₄(Yb, Er) nanoparticles were used for dual imaging of tumors *in vivo*. Thereby the Yb³⁺ and Er³⁺ lead to the green luminescence, whereas the host material itself worked as contrast agent for MRI imaging. With this probe it was possible to visualize and identify even small tumors (1.7 × 1.9 mm).

A common method for the fabrication of Gd-doped C-Dots is the direct pyrolysis of gadopentetic acid (Gd-DTPA) [124] with a carbon source like citric acid (Figure 1.10). The particle surface is functionalized with DTPA-moieties, which are acting as chelating agents for Gd³⁺ [125]. In the case of QDs, not only optical, but also their biological properties are increased by a core/shell structure. In the presence of ZnS the toxicity of QDs is reduced due to limited leakage of the heavy metal ions [126].

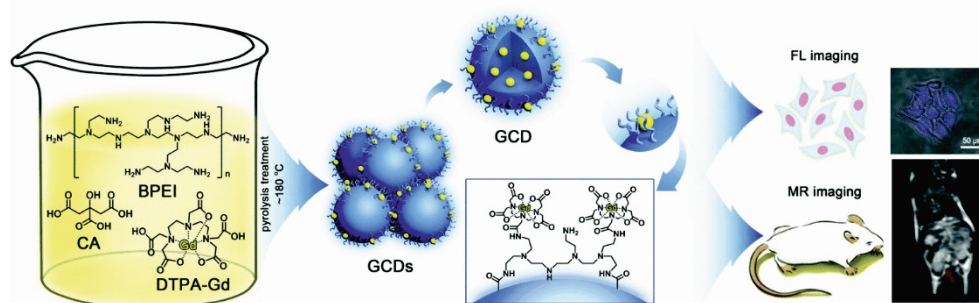


Figure 1.10| Schematic illustration of the synthesis of Gd-doped C-Dots based on the pyrolysis of Gd-DTPA in the presence of citric acid (CA) and branched polyethylenimine (BPEI). The obtained C-Dots have a surface where the Gd³⁺ is stabilized by chelating with DTPA moieties. Reprinted from [125]. Copyright (2019) from Royal Society.

1.3.3 Commercial availability

Fluorescent proteins and QDs are commercially available in a wide range of colors and as labeling kits. Often it is difficult, which FP should be used by cell biologists, as in many cases important information, such as oligomer formation or photostability is not provided [127]. Quantum dots, *e.g.* CdSe, CdTe, InGaP (available from Creative Diagnostics, Evident, Merck, Plasmachem, or ThermoFisher) can already be bought with a large variation of surface modifications, including biotin, streptavidin, proteins or antibodies. For nanomaterials one issue is the difficulty to achieve high batch-to-batch reproducibility in terms of particle size distribution or loading capacities of ligands, which might not be a problem for a research study using only a small amount of these materials, but which is limiting the practical use of those probes in commercial applications. This is also an issue for UCNPs. Companies like ACS Materials distribute 25 nm sized oleate coated particles with different doping systems (*e.g.* Yb/Er, Yb/Tm). However, no detailed information about the doping ratio and size distribution are given. Water dispersible nanoparticles can be purchased either with PEG modifications or SiO₂ coating. C-Dots are still a rather new material which limits their commercial availability. So far only aqueous dispersions are offered without detailed information on the size, quantum yield or exact concentration.

1.3.4 Surface functionalization and labeling

Working with fluorescent probes often requires post-synthesis surface modification and labeling steps. On one side, it follows the demand to improve the properties of the fluorescent probes such as improving water dispersibility, biocompatibility, cellular uptake or to introduce targeting functionalities for biosensing or imaging. On the other side, surface functionalization can be required to tune the luminescence, as it is the case for C-Dots. Therefore, it is of big importance, that well-established libraries of functionalization and labeling techniques are available. Many of these strategies bear the risk of crosslinking, especially when biomolecules are used, and demand to be carefully selected.

Functionalization of fluorescent proteins

Among the four presented probes, the fluorescent proteins are somehow special concerning modification and functionalization. Due to their high number of functional groups, additional solubilization steps can be excluded. Beside this, numerous labeling techniques have been established for proteins which of course can also be used for FPs. Either common conjugation techniques *via* carbodiimide chemistry or thiol crosslinking are favourable to attach FPs to the C- or N- terminus of another protein [128, 129]. However, the proteins are mostly expressed directly in living cells, where such modification steps are avoided due to difficult purification steps. It is more beneficial to directly modify the proteins during their expression in the cell. Therefore, the plasmid vector also contains the information for the surface functionalization, which is linked during expression to the molecules [130]. Those assemblies are called fusions fluorescent protein (fusion FPs) and are widely used for bioimaging (Figure 1.11).

A critical comparison of lanthanide based upconversion nanoparticles to fluorescent proteins, semiconductor quantum dots, and carbon dots for use in optical sensing and imaging

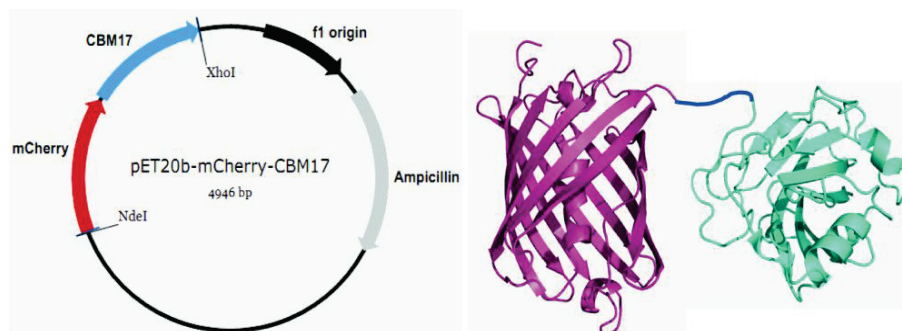


Figure 1.11| Left: Plasmid Vector for the expression of m-Cherry linked to a carbohydrate binding module (CBM17). Right: Molecular structure of the m-Cherry fusion protein. Adapted from [130].

Functionalization of nanoparticles

In contrast to this, the modification of the luminescent nanoparticles, like UCNPs, is much more challenging. To guarantee the stability of the colloidal dispersion, the surface of the particles must have a certain coating, which prevents aggregation. The principles of electrostatic repulsion and steric hinderance are frequently used to fulfil this purpose. In literature for each particle system different surface modification methods are reported. Especially particles obtained *via* synthesis in high boiling solvents are coated with a hydrophobic layer consisting of long chained alkyl moieties. Those particles cannot be dispersed in an aqueous media and surface modification is important to provide them with hydrophilic groups like $-\text{COOH}$, $-\text{NH}_2$, or $-\text{OH}$.

Methods such as ligand oxidation, ligand exchange, ligand removal, amphiphilic polymer coating and encapsulation within an inorganic shell or noble metal layer have been successfully described for UCNPs (Figure 1.12).

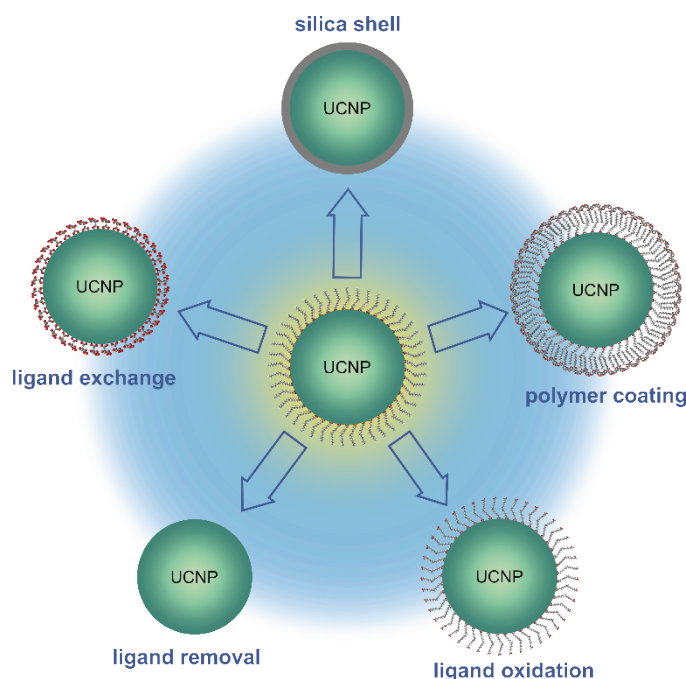


Figure 1.12| Schematic illustration of several strategies known for the modification of UCNPs including ligand oxidation, ligand exchange, ligand removal, polymer coating and coating with a silica shell.

Thereby the ligand oxidation is one of the easiest surface modification techniques, due to the direct transformation of the present hydrophobic ligand. The often-used oleic acid owns one double bond and can be oxidized *via* the Lemieux-von Rudloff method [2]. Thereby –COOH groups are generated on the surface of the particles. Ligand exchange can be performed either in one step or in two steps. If the new surface capping can be added in its acidic form, such as citric acid in case of citrate, the protons can remove the oleate and transfer the particles to the aqueous phase where they will be capped by the new ligand [131]. In the case of a two-step ligand exchange, first the oleate has to be removed from the surface of the particles. This ligand removal can be induced by NOBF_4 [132] or HCl [133]. In the second step a desired ligand such as citric acid, biotin or a polymer like polyallylamine, poly(acrylic acid) or polyethyleneimine [133] is attached to the particle. The two-step ligand exchange is beneficial due to better control of the particle surface in terms of complete removal of the oleate. Much more convenient is the surface functionalization *via* polymer coating. Thereby amphiphilic polymers are attached to the particles surface *via* van der Waals interaction of the hydrophobic part of oleic acid and the polymer. Typical polymers for this approach are phosphatidylcholines [134]. Another interesting approach is to encapsulate UCNPs in nanocarriers such as liposomes, which is promising in drug delivery applications [135]. For more detailed information on the different modification techniques, the reader is referred to reviews published by Sun [2] or Muhr *et al.* [136]. Each of the methods has several benefits, whereas ligand exchange and ligand removal give access to UCNPs with thin organic surface capping advantageous in distance dependent energy transfer. On the other hand, particles with a silica shell or polymer coating are known for an increased stability against disintegration because of better shielding effects.

The surface modification strategies of QDs differ not much to those of the UCNPs, however, beside the demand for colloidal stability, there is also an increased interest for biocompatibility preventing any leaking of toxic heavy metal ions. Another parameter to consider when dealing with QDs, is the size dependency of their optical properties. Therefore, the maximum number of dyes or reporter molecules linked directly to the surface of the nanoparticles is fixed, which limits flexibility in applications dealing with drug delivery, energy transfer and so on. A frequently used method to render QDs water-dispersible is the two-step ligand exchange. Ideal ligands should be bifunctional, with a hydrophilic group (*e.g.* carboxylic) and a metal-capping group. Thiol containing molecules are thereby favoured due to their abundance, high affinity and efficiency [137]. But also, the encapsulation of the QDs within a silica shell or liposomes is a prominent method to render the nanoparticles water dispersible [137].

In case of C-Dots, the surface modification comes with two benefits: On one side, the surface of the particles should become accessible for bioconjugation and render the particles water dispersible. On the other side, the optical properties of C-Dots are often tuned by surface passivation. Beside the attachment of polymers like of PEG [138] or polyvinylpyrrolidone (PVP), the treatment of the particles with HNO_3 (oxidation) or NaBH_4 (reduction) [139] modulates the photoluminescence of the particles.

Bioconjugation of nanoparticles

The attachment of biomolecules to the surface engineered probes can occur either electrostatically or covalently. However, electrostatically bound labels suffer from leakage, which makes covalent binding more attractive. The same has also to be taken into account when a large biomolecule is covalently attached to a surface ligand which is only bound by electrostatic interaction to the particle surface.

The risk of ligand detachment after bioconjugation is often overlooked and according to our knowledge has not been studied in detail so far. At a closer look, a huge variety of different techniques are available for UCNPs, C-Dots and QDs (Figure 1.13).

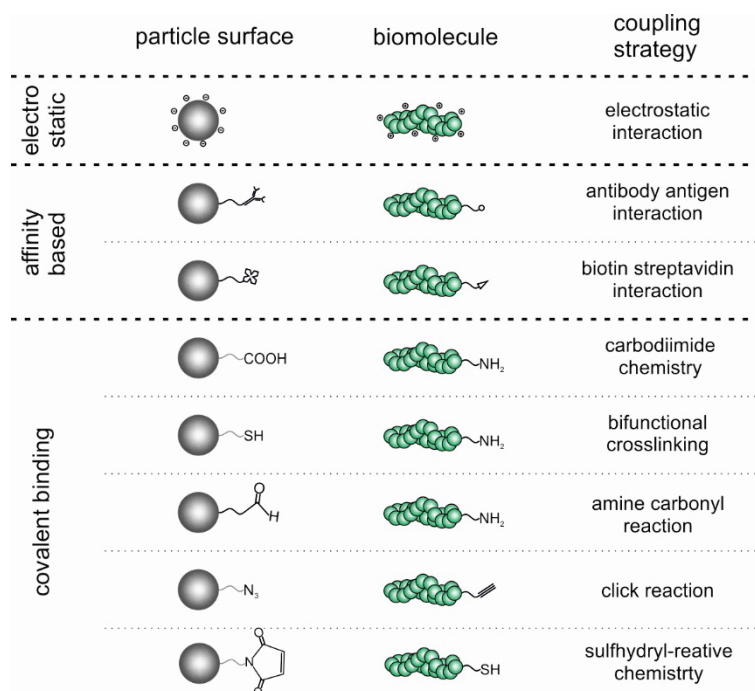


Figure 1.13| Overview of common bioconjugation techniques.

In the presence of carboxylic groups, amines can be attached to the particles *via* carbodiimide activation and vice versa. Han *et al.* show the conjugation of hyaluronate to amine modified UCNPs. This system was able to monitor the transdermal delivery of these particles into the deep skin tissue [119]. Click chemistry is another possibility to attach biomolecules as shown by Horák *et al.* [140]. Based on a Cu(I) catalyzed Huisgen 1,4-dipolar cycloaddition azide modified biomolecules can be attached to alkyne functionalized UCNPs. Thereby the nanoparticles were labeled with trans-activating transcriptional activator peptide (TAT) in order to study their uptake by human cervix carcinoma HeLa cells. Quite similar to UCNPs are the bioconjugation techniques of C-Dots. Cui *et al.* [141] use the intrinsic carboxylic groups of C-Dots, derived from citric acid, for coupling of desoxyribonucleotides by carbodiimide chemistry. These particles can be applied for the detection of Hg^{2+} in a FRET-based system. Due to the high affinity between QDs and thiols groups, biomolecules with such functional groups can be easily attached to the nanoparticles within a ligand exchange process. Based on this, the group of Hildebrandt [142] has reported a strategy for the direct attachment of antibodies to the surface of CdSeTe/ZnS QDs using the endogenous disulfide groups of the biomolecule. Compared to other QD-based immunoassays, this system comprises with the lowest limit of detection (2.5 pM) for the prostate specific antigen (PSA) in serum so far.

1.3.5 Colloidal stability

Even when luminescent probes have been optimized in their optical and chemical properties, it remains still challenging to prevent aggregation or unspecific binding and to maintain colloidal stability in complex biological media. For monitoring cellular compartments, drastic changes of the local pH, concentration and presence of certain ions, or changes in temperature, osmotic pressure and viscosity have to be considered. The eukaryotic secretory pathway and mitochondrial inner membrane space for instance shows a strongly oxidizing environment, whereas endocytic and secretory compartments have acidic pH values [143]. Therefore, the colloidal stability of FPs, C-Dots, QDs and UCNPs is crucial not only in water but also in buffered system or complex biological media. For the description of the stability of nanoparticles different forces acting on a nanoparticle need to be considered: gravity, thermal motion and forces between the particles itself [144]. The larger the radius of nanoparticles, the higher is the mass of the particles. In this case the gravitational forces outrank the Brownian motion and the particles starts to precipitate. In the case of small particles, the Brownian motion is the dominant force (Figure 1.14 A).

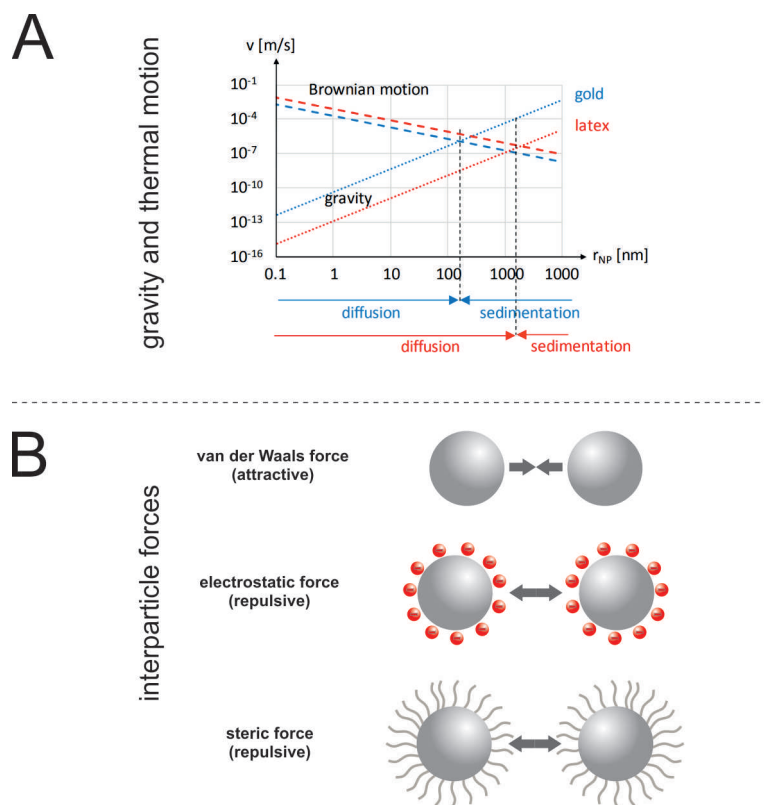


Figure 1.14| Different effects acting on nanoparticles in solution: (A) Sedimentation velocity due to gravity and diffusion velocity for gold and latex spheres of different diameters. Reprinted with permission from [144]. Copyright (2019) American Chemical Society. (B) Scheme of the most important interparticle forces dealing with colloidal stability. Attractive van der Waal forces lead to colloidal unstable systems where electrostatic and steric forces (both repulsive) increase the stability of a dispersion.

However, also interparticle forces can lead to colloidal instability. The most important contributions thereby are van der Waals (vdW), electrostatic and steric interactions (Figure 1.14 B). Nanoparticles are assembled by several atoms or molecules and their individual contribution have to be taken into

account. This problem can be described by London dispersion interactions which are a result of charge fluctuations within an atom associated with the motion of its electrons [145].

For two nanoparticles with the radius R at a distance h , the van der Waals attractive energy is given by Equation 1.1 [145]

$$E_{v.d.W} = -\frac{A_H}{6} \left(\frac{2}{s^2-4} + \frac{2}{s^2} + \ln\left(\frac{s^2-4}{s^2}\right) \right). \quad (\text{Equation 1.1})$$

Where $s = (2R + h)/R$ and A_H is the Hamaker constant, which characterizes the electronic interactions across a medium like water. In the case of two spherical nanoparticles with diameters of the same size which is large compared to their distance ($R \gg h$), the equation can be simplified to Equation 1.2 [145]

$$E_{v.d.W} = -\frac{A_H R}{12h}. \quad (\text{Equation 1.2})$$

For all fluorescent nanoparticles (CdSe QDs: $7 \cdot 10^{-19}$ J [146], C-Dot from cleaved muscovite mica: $0.99 \cdot 10^{-19}$ J [147] and Y_2O_3 upconverting material in bulk phase: $3.0 \cdot 10^{-20}$ J [148]) the constant has similar values. Additional repulsive forces can be of electrostatic or steric nature. The electrostatic interactions are caused by charged species directly to the surface. Thereby a surface charge is formed which is compensated with unequal distribution of counter and co-ions (diffuse double layer). The potential ψ_0 at the surface decreases to a certain value ψ_d , and then decreases further linearly with increasing distance to the surface until it reaches zero in the bulk solution. Therefore, the ζ -potential describes the potential at the shear plane of a colloidal particle moving in an electric field and represents the number of charged groups on the surface of the nanoparticles. By combining all those parameters an overall electrostatic energy of repulsion can be described by Equation 1.3 and Equation 1.4 [145]

$$E_{el.} = \frac{4\pi\epsilon_r\epsilon_0 R^2 \psi_d^2 e^{-kh}}{2R+h} \quad (\text{Equation 1.3})$$

and

$$\frac{1}{\kappa} = \frac{\epsilon_r \epsilon_0 kT}{2n_0 Z^2 e^2}. \quad (\text{Equation 1.4})$$

Thereby ϵ_r is the relative permittivity, ϵ_0 the permittivity of free space, k is the Boltzmann constant, T the absolute temperature, n_0 is the number of ions (of each type) present in the bulk phase. Z is the valency of the ions and e is the electronic charge. The total interaction energy of electronic and vdW interactions are summarized in the Derjaguin Landau Verwey Overbeek (DLVO) theory [145]:

$$E_{total} = E_{el.} + E_{v.d.W} = \frac{4\pi\epsilon_r\epsilon_0 R^2 \psi_d^2 e^{-kh}}{2R+h} - \frac{A_H R}{12h}. \quad (\text{Equation 1.5})$$

A closer look at this reveals that both, the surface (zeta) potential and the electrolyte concentration, are essential for the value of E_{total} and therefore, for the colloidal stability of the nanoparticles. Generally nanoparticle dispersions with a value between $\pm(10 - 20)$ mV show strong repulsion to each other and are classified as stable [149]. But this value also strongly depends on the pH values of the dispersion media. In order to warrant a stable dispersion, the pH needs to be within a certain range to ensure the stabilizing charged groups do not get neutralized by protonation or deprotonation. Too high

or too low pH values lead to a protonation or deprotonation of surface ligands resulting in its detachment. Additionally, to this, the ionic strength needs to be low (ideally $<10^{-2}$ mol·L⁻¹) [145] because it affects the range of the electrostatic interaction. Nevertheless, there are limitations in this theory, for example when it comes to uncharged bulky surface ligands. Here forces like the repulsion due to steric interactions provide colloidal stable nanoparticles. In completion to the measurement of the surface charge, the hydrodynamic diameters obtained by dynamic light scattering gives direct information on the homogeneity of the dispersion as it detects aggregation. By comparing those parameters (ζ -potential and hydrodynamic diameter) a quantitative statement about its stability can be achieved. Up to now, there are only limited systematic studies available discussing the stability of UCNPs, QDs and C-Dots. Many publications report on a high colloidal stability without giving full details of all parameters.

One example for work on colloidal stability of NaYF₄(Yb, Er) modified with citrate, given by Wilhelm *et al.*, reports on a ζ -potential of -25 mV and a hydrodynamic diameter of 24 nm (Pdl of 0.025). By changing the surface modification to poly(acrylic acid), the ζ -potential of the same particles can be increased to -36 mV [60]. However, in the presence of competitive capping ligands like phosphates in the case of UCNPs, limited colloidal stability can be observed. Qiao *et al.* [150] presented a smart technique to bind antibodies to the surface of the UCNPs and to render the particles stable in phosphate buffered saline (PBS). An asymmetric PEG, containing a maleimide group at one end and a diphosphate on the other end, was attached to the surface of the nanoparticles. The maleimide group was then used for bioconjugation whereas the phosphates coordinating the particles surface warrant their stability. Similar surface charges to those of the UCNPs can be obtained for C-Dots fabricated from citric acid. The particles have ζ -potential of -15.5 mV at pH 4 which increases to -28.2 mV by changing the pH-value to 9 [151]. C-Dots synthesized in distilled water under the hydrothermal treatment of N, N-dimethyl-m-phenylenediamine dihydrochloride, poly(sodium 4-styrenesulfonate), and 5-(dimethylaminomethyl)furfuryl alcohol hydrochloride lead to particles with sizes between 10 and 20 nm and a ζ -potential of -16.8 mV [152]. For polyacrylamide modified CdSe QDs, the group of Pu reported [153] a hydrodynamic diameter of 7 nm and a ζ -potential of -5.69 mV (pH 10). Despite this low value, the particles show high colloidal stability due to the steric repulsion of the surface ligands.

1.3.6 Chemical stability

Especially for bio-applications, the chemical stability of the probes is of importance. Among the luminescent probes presented here, FPs are one of the most stable ones. The stability of FPs is not only given by that of the chromophore, as the emission also depends by its interaction with amino acids in the microenvironment. For instance, the yellow fluorescence protein (YFP) has the same chromophore as GFP, but a different composition of the β -barrel, which lead to bathochromic shifts of 20 nm [154]. A denaturation of the proteins can lead to a complete loss of the spectral characteristics of the fluorophore. Common critical factors thereby are pH values, temperature, or the presence of proteases. In each case the FPs have been designed in such ways to provide outstanding stability. For instance, the GFP has an average denaturation temperature (76 °C) far beyond the standard physiological condition [6]. In the case of low protease concentration, none of the known proteases influences FPs. At higher concentrations (~ 43 mg·mL⁻¹) special proteases like bromelain however affect the probes and therefore destroy the emission signal [155]. Unfortunately, QDs are

quite unstable under certain physiological, chemical and environmental conditions [9]. Under acidic conditions for instance CdSe/CdS QDs start to decompose and release Cd²⁺ as shown by Braeckmans *et al.* [156]. Thereby the amount of released Cd²⁺ was measured depending on the pH value of the aqueous media (pH 7.4, 5.5 and 4.5). Within five days ~20% of the QDs-associated Cd²⁺ was released for the lowest pH value. As the QDs will need to cross several pH regions when transferred into a cell line (7.4 in the extracellular medium, 4.5 in lysosomes) such influences need to be considered. Several functionalization strategies involving small molecule ligands, amphiphilic polymers or encapsulation within silica materials have improved the stability of QDs under physiological relevant conditions [9]. Upconversion nanoparticles, especially the ones composed by NaYF₄ host materials seemed to be chemically inert. However, recent studies have shown that high-diluted particle dispersions tend to dissolve in aqueous media at room temperature [157–160]. The amount of fluoride ions measurable in the dispersion media increases in a course of 30 days. Recently this observation was confirmed by the group of Mely [161], reporting on a time-dependent luminescence dissolution of individual polymer-coated UCNPs in water, which can be stopped in the presence of 1 mM fluoride in the solution. In contrast to this, C-Dots are not consisting of heavy metals or other toxic ions and therefore leaking problems can be excluded. Generally, in the literature these materials are described as remarkably chemically stable [162, 163].

1.3.7 Biocompatibility, biodistribution and toxicity

For the goal, to apply such probes in clinical applications, the issues of biocompatibility, toxicity and biodistribution have to be fully investigated. Not surprisingly, a detailed study revealed that the biodistribution not only depends on the particles' size and shape, but also on their surface functionalization including surface charge [164]. Smaller particles remain shorter in an organism compared to bigger ones. Furthermore, for sizes less than 100 nm particles can enter the cells, and when smaller than 40 nm, the nucleus of the cells can be penetrated. These are rules of thumb and exceptions can be found in literature. Betzer *et al.* fabricated gold nanoparticles with 20, 50 and 70 nm and studied their ability to cross the blood-brain barrier. Two hours after incubation, the highest accumulation within the brain was observed for 20 nm-sized particles [165]. The largest accumulation of nanoparticles usually occurs in the blood, liver and spleen, whereas the larger ones normally accumulate in the liver and spleen and the minimum size of the particles to be rapidly cleared *via* renal filtrations is between 8 and 10 nm [166]. Similar size dependent studies for UCNPs and QDs would be helpful. Recently Yu *et al.* [167], analyzed the biodistribution of polyethyleneimine coated UCNPs with a size of 30 nm. Therefore, the particles were injected by three different routes intravenous, intraperitoneal, as well as intragastric and their distribution into the organs of three individual mice was monitored over a course of 30 days. With the lapse of time, the concentration of UCNPs increased in the spleen and slightly in the liver for the intravenous injection. For the intragastric injection, the highest UCNPs concentration was found in the gastrointestinal tract after one hour. After 48 h the concentration decreased and only low concentrations of UCNPs were found in the other major organs like liver spleen and kidney. By using citrate capped UCNPs as reported by Gao *et al.* [168], the particles were preferentially accumulated in the pancreas and the mesentery after 1 h post-injection (intraperitoneal and intravenous). With time, an increased amount of nanoparticles was found in the spleen and liver as dominant mode of clearance for the particles (Figure 1.15).

A critical comparison of lanthanide based upconversion nanoparticles to fluorescent proteins, semiconductor quantum dots, and carbon dots for use in optical sensing and imaging

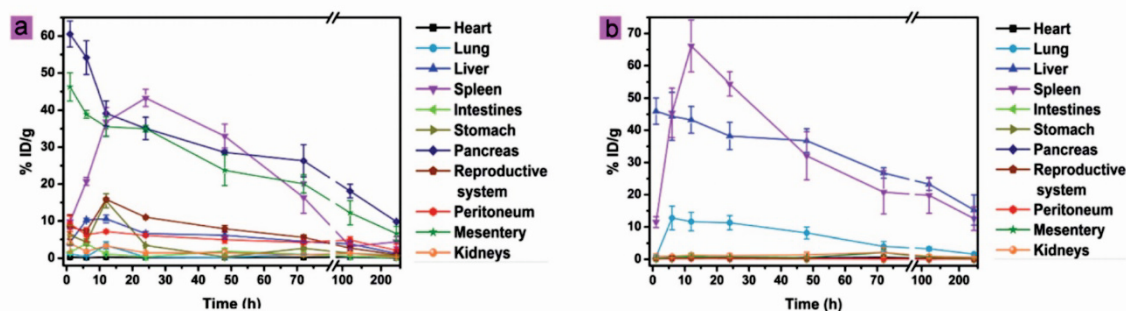


Figure 1.15| Accumulation of Lu^{3+} in the main tissues at various time points after intraperitoneal (IP, a) and intravenous (iv, b) injection of citrate capped UCNPs [168]. Published by The Royal Society of Chemistry.

Based on the long accumulation times of UCNPs within the body, also the toxicity is important. Thereby the influence of UCNPs on a cellular level is strongly depending on the surface coating and the examined cell line as shown by Guller *et al.* [169]. The non-specific uptake and viability of immortalized human epidermal linear keratinocytes after incubation for 24 h with UCNPs of different surface functionalization was very impressive as shown in Figure 1.16. Despite the common believe, that UCNPs are generally non-cytotoxic, UCNPs coated with polyethyleneimine (PEI) were least tolerated by this cell line with only 54% cell viability. However, by incubation of human dermal fibroblasts with the same amount of identical particles a viability of nearly 80% can be detected [169].

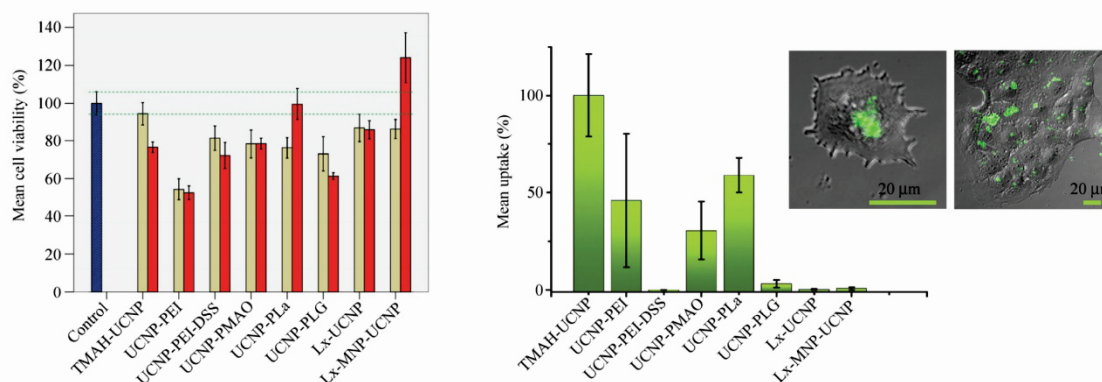


Figure 1.16| Left: Histograms of the viability of human keratinocytes, co-cultured for 24h with UCNPs at concentrations of $65 \mu\text{g}\cdot\text{mL}^{-1}$ and $125 \mu\text{g}\cdot\text{mL}^{-1}$. The control sample viability, shown as blue bar, was set to 100%. Green dashed lines delineate the lower and upper boundaries of 96% for the mean value of the control group. Right: Non-specific cellular uptake of UCNPs by keratinocytes 24 h post incubation. UCNPs were used at a concentration of $125 \mu\text{g}\cdot\text{mL}^{-1}$. Inset: Overlay of bright field and confocal PL images of a single cell. Reprinted by permission from Nature Nano Research, [169], Copyright (2018).

In contrast to this, FPs, are known for their biocompatibility by their nature. However as reported by Ganini *et al.* [170], the expression of FPs in *E. coli* lead to oxidative stress in cells. Closely linked with this is the increase of reactive oxygen species such as the free superoxide $\text{O}_2^{\cdot-}$ and H_2O_2 . Both molecules induce the redox signalling mechanism and lead to a change of the expression of cell regulatory proteins. Those are involved in cell proliferation, cell differentiation and cell death [171].

Carbon dots, in contrast to QDs, are reported to be less toxic. Pristine C-Dots show no cytotoxicity and high biocompatibility [172]. However, surface passivation and oxidation processes lead to

functional groups at the surface of the particles, which may seriously influence the biocompatibility of those particles. Non-toxic and biocompatible compounds like a quinolone derivative or hyaluronic acid can be chosen for the modification of C-Dots [172]. By labeling C-Dots with a signal peptide for localization in cells an enrichment in the nucleus is found. The average viability of cells was decreased to 90% within 24 h after incubation of $0.5 \text{ mg}\cdot\text{mL}^{-1}$ C-Dots [172]. With increasing concentration of the particles to $1.0 \text{ mg}\cdot\text{mL}^{-1}$ and $2.0 \text{ mg}\cdot\text{mL}^{-1}$ the cell viability decreased to 85% and 75% indicating that a higher concentration of C-Dots has a slightly toxic effect.

Many QDs consisting of heavy metal ions like Cd^{2+} , which release within the organism would result in potentially high toxicity [156]. Already 10 nM of CdSe/CdS QDs showed a toxic effect on three different cell lines (primary human umbilical vein endothelial cells (HUVECs), murine neural progenitor cells (C17.2) and rat pheochromocytoma (PC12) cells). Consequently, research was directed towards the development of non-heavy metal based QDs or their encapsulation with protective layers of materials such as ZnS or silica [9]. A MTT-assay shows the influence of Mn^{2+} doped ZnS QDs with concentrations ranging from 7 to $500 \text{ }\mu\text{g}\cdot\text{mL}^{-1}$ on a breast cancer cell line (MCF-10). After incubation for 24 h the cell viability was reduced to only 95% [173].

1.4 Bioanalytical applications

1.4.1 Sensing

Temperature is a key parameter in biology and medicine, especially when acquired with a high spatial resolution or with the ability of being measured inside a tissue. Nanomedicine takes benefit of luminescent probes changing their optical properties with temperature to monitor tumors during photodynamic therapy (PDT), or to control the health of living tissues affected by a cardiovascular disease [174–178]. The measurement of a temperature change is often strongly linked to the electronic structure of the fluorophore. Several lanthanide ions like Nd^{3+} or Er^{3+} are characterized by temperature sensitive 4f transition states and therefore UCNPs are ideal candidates of nanothermometers. For example, the populations of the $^4\text{S}_{3/2}$ and $^2\text{H}_{11/2}$ state of Er^{3+} follows the Boltzmann distribution under steady-state excitation [1] and therefore the transition ($^2\text{H}_{11/2} \rightarrow ^4\text{I}_{15/2}$ and $^4\text{S}_{3/2} \rightarrow ^4\text{I}_{15/2}$) of those are an indicator of the temperature next to the particles. The group of Capobianco reported the first nanothermometer consisting of NaYF_4 co-doped with Yb^{3+} and Er^{3+} . With this, it was possible to detect temperature changes between 25 and 45 °C in solution as well as in biological samples such as HeLa cancer cells [179]. Since then, a lot of work has been done to increase the sensitivity of the UCNPs. In nanothermometry UCNPs suffer from an excitation at 980 nm, where also water is absorbing. In order to decrease the background temperature drift due to the water absorption, core/shell UCNPs consisting of $\text{NaYF}_4(\text{Yb}, \text{Nd})@\text{NaYF}_4(\text{Yb}, \text{Er})$ were designed by Shi *et al.* [180]. These particles were capable to detect temperature changes within NIH-3T3 cells between ~32 and ~42 °C. The maximum relative sensitivity of the nanothermometers based on UCNPs strongly depends on the composition, size and surrounding of the nanoparticles [181, 182]. For $\text{Yb}^{3+}/\text{Er}^{3+}$ co-doped nanomaterials with different host lattices [183] it varies between 0.18% K^{-1} (NaYF_4) and 1.4% K^{-1} (LiNbO_3). In the case of quantum dots an intensity quenching is observed when the temperature is increased. This can be attributed to the existence of trap states or defects associated to the surface of the particles [38]. A hybrid polymer nanostructure, excitable at 808 nm, with encapsulated temperature-independent particles ($\text{NaGdF}_4:\text{Nd}^{3+}$) and temperature-dependent $\text{PbS}/\text{CdS}/\text{ZnS}$ quantum dots allowed sensitive ratiometric thermal sensing [184]. In the case of carbon dots, where the luminescence is strongly influenced by the surface chemistry also a temperature dependency was reported. For instance, nitrogen doped C-Dots, obtained from C_3N_4 and ethanediamine show a temperature dependent bright blue fluorescence [185]. This dependency is attributed to the synergistic effect of abundant oxygen containing functional groups and hydrogen bonds which allows the detection of temperature changes between 20 and 80 °C, with a sensitivity of 0.85 K^{-1} . Fluorescent proteins are mainly used in imaging to study and visualize intercellular processes and they play only a minor role for biosensing applications [74]. Therefore, only sensing systems based on the luminescent nanoparticles will be compared in the following. Luminescence based quantification of an analyte using nanoprobe can be performed in multiple ways. Most prominent are intensity-based read-out strategies relying on the quenching, enhancing or wavelength shifting effects of the emission. A requirement is the spectral overlap of the emission spectra of the probes and the absorption spectra of the analyte or a second label. The excitation energy can be transferred by two mechanism to an analyte molecule: (i) in a radiative way *via* emission and subsequent reabsorption, the so-called inner filter effect, and (ii) in a non-radiative way by an energy transfer which is characterized by a strong distance dependency (Figure 1.17) [53, 186, 187].

A critical comparison of lanthanide based upconversion nanoparticles to fluorescent proteins, semiconductor quantum dots, and carbon dots for use in optical sensing and imaging

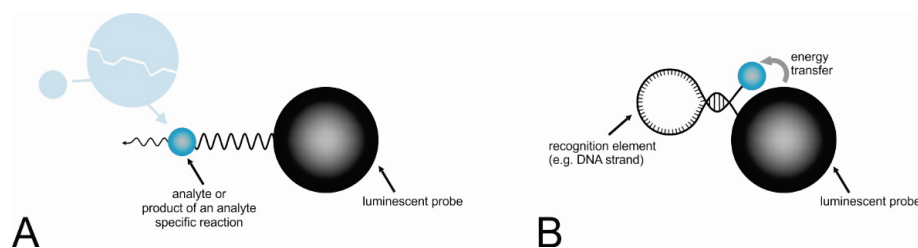


Figure 1.17| Schemes for sensors based on inner filter effect (A) or energy resonance transfer (B).

An intracellular sensor based on energy transfer from polyethylene coated $\text{NaY}_4(\text{Yb}, \text{Er})$ to the pH-sensitive dye pHrodo Red ($\lambda_{\text{ex}} = 520 - 550 \text{ nm}$, $\lambda_{\text{em}} = 590 \text{ nm}$) covalently linked to the particle was reported. This sensor enables the detection of pH changes ranging from 5 to 7 [173]. Here, a dye acts as reporter, which always is accompanied by the risk of photobleaching, and therefore, QDs attached to the surface of UCNP will be a promising alternative. The binding of CdSe/ZnS QDs to $\text{Yb}^{3+}/\text{Er}^{3+}$ doped UCNP was achieved by streptavidin-biotin coupling. The particle assembly was used in a biotin replacement assay allowing the detection of vitamin H with a detection limit of 5 nM [188]. Recently Hu *et al.* [189] presented an aptamer-based sensor for adenosine triphosphate (ATP) using C-Dots in combination with graphene oxide. Thereby the nanoparticles were functionalized using carbodiimide chemistry. In the absence of the biomolecule the aptamer modified C-Dots adsorb on the surface of the graphene oxide by π -stacking, whereas the emission of the C-Dots at 446 nm gets quenched. In the presence of the analyte ATP (LOD = 80 pM), the C-Dots are released, and the luminescence is recovered. A huge variety of sensing principles based on quenching, energy transfer or fluorescence shifting with luminescent nanomaterials have been reported. In Figure 1.18, sensors based on C-Dots, QDs and UCNP are compared in terms of the LODs which were retrieved for most prominent analytes like ions, small molecules, nucleic acids or proteins.

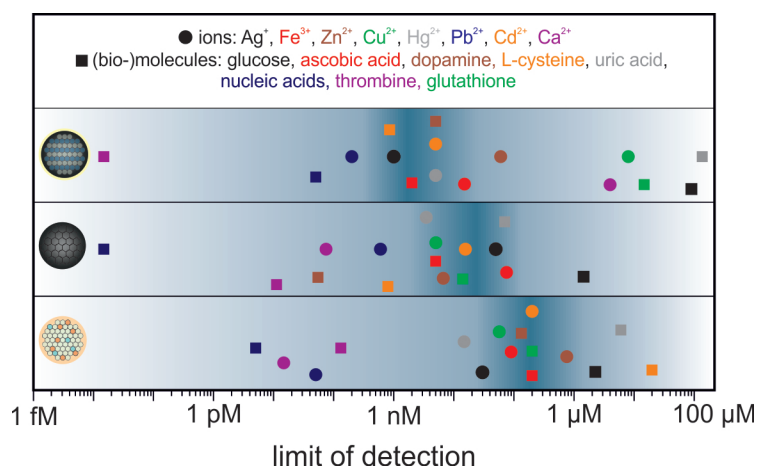


Figure 1.18| Comparison of the limit of detection for ions (circles) or (bio)molecules (squares) of sensors based on UCNP (Ag^+ [190], Fe^{3+} [191], $\text{Zn}^{2+}/\text{Pb}^{2+}$ [192], Cu^{2+} [193], Hg^{2+} [194], Cd^{2+} [195], Ca^{2+} [196], glucose [197], dopamine [198], ascorbic acid [199], L-cysteine [200], uric acid [201], nucleic acid [202], thrombin [203], glutathione [204]), C-Dots (Ag^+ [205], Fe^{3+} [206], Zn^{2+} [207], Cu^{2+} [208], Hg^{2+} [209], Pb^{2+} [210], Cd^{2+} [211], Ca^{2+} [212], glucose [213], dopamine [214], ascorbic acid [215], L-cysteine [216], uric acid [217], nucleic acid [218], thrombin [219], glutathione: [220]) and QDs (Ag^+ [221], Fe^{3+} [222], Zn^{2+} [223], Cu^{2+} [224], Hg^{2+} [225], Pb^{2+} and Cd^{2+} [226], Ca^{2+} [227], glucose [228], dopamine [229], ascorbic acid [230], L-cysteine [231], uric acid [232], nucleic acid [233], thrombin [234], glutathione [235]). The maximum of the color-gradient shows the mean LOD over all analytes for the respective probe.

From Figure 1.18 one can see that in average (symbolized by the color-gradient) QDs are ~100-times and C-Dots about a factor of 10 better in sensitivity compared to UCNPs. According to the fact that the recognition principle for the analytes is almost the same it seems that UCNPs potential for sensing applications is not yet at the same stage as that of QDs and C-Dots.

One might speculate that two reasons are responsible: (a) the weak luminescence and (b) the larger size of UCNPs. The brightness of UCNPs is increasing with their size. Therefore, often much bigger UCNPs (20 to 50 nm in diameter) compared to QDs and C-Dots (both smaller than 10 nm) are used to overcome the weak luminescence. By this also the surface-to-volume ratio of the particle gets affected and consequently surface chemistry in terms of binding sites might be influenced. Altogether the excellent signal-to-noise ratio of UCNPs, due to the absence of background luminescence upon NIR excitation, can only beat the bright luminescence of the QDs and C-Dots in terms of lowest limit of detection for some analytes.

1.4.2 Imaging

Bioimaging has become a highly progressive field of research, regardless if one thinks on imaging within a cell line (*in vitro*) and within a living being (*in vivo*). Table 1.2 lists recent examples of cell and animal imaging based on the use of C-Dots, QDs, UCNPs, or FPs as luminescent probes to demonstrate the wide range of applications. Despite the many reports in literature, one has to be critical in terms of deep-tissue penetration. Even for UCNPs, when excited in the NIR at 980 nm, the emissions in the visual range of the spectrum hardly can be imaged due to scattering effects. It would be much better to address such a task by NIR emitting probes, which can also be from the NaLnF_4 type, but with doping of Yb, Er or Ce, which boosts the Stokes emission at wavelengths in the NIR-IIb window ranging from 1500 to 1700 nm [236]. Fluorescent proteins comprise by the direct introduction into cells (*in vitro* and *in vivo*) *via* transfection and by their simple modification using well established techniques, as it is demonstrated in an example where tissue-specific promoters with a high subcellular specificity have been attached [74].

Table 1.2| Overview of *in vivo* and *in vitro* imaging using UCNPs, C-Dots, QDs and FPs.

Composition of the probe (diameter)	Excitation [nm]	Emission [nm]	Applications	Comments	Ref
C-Dots(citric acid/ethylenediamine) (2.5 nm)	360	460	Labeling of cell membrane and cytoplasm of L929 cells	Quantum yield of 35%	[237]
C-Dots (polyethyleneimine)@folic acid (5.8 nm)	365	370 / 452	Distinguish between cancer cells and normal cells using the interaction between folic acid and folate receptor molecules	Specific and efficient cell labeling. High biocompatibility Wavelength independent emission	[238]
C-Dots(glucose/glutamic acid)@angiopep-2 (4 nm)	500	600	Glioma imaging in normal brain tissue	Higher glioma imaging sensitivity	[239]
NaYF ₄ (Yb,Er,Tm)@RGD ^a (14 nm)	980	490 / 522 / 543 / 654 / 695 / 800	Imaging of human glioblastoma U87MG tumor cells	Minimal autofluorescence and light scattering from tissue. Ultrahigh imaging contrast	[240]
NaYF ₄ (Yb,Er)@silica@RGDS ^b and NaYF ₄ (Yb,Er)@silica@TATb (both 32 nm)	975	476 / 650 / 700 / 800	Targeting and imaging of specific tumor phenotypes	Controlled extra - and intracellular nanoparticle uptake, deep tissue penetration	[140]
NaYbF ₄ (Nd)@NaGdF ₄ (Yb,Er)@NaGdF ₄ @chlorin e6 (nm) (~30 nm)	976 / 808	525 / 550 / 660	Simultaneously imaging and PDT of cancer cells	Change of excitation wavelength to 808 nm, reduction of overheating effect	[241]

UCNPs _s	NaYbF ₄ (Tm)CaF ₂ @hyaluronic acid (27 nm)	980	520 / 550	Whole body photoluminescent imaging of mice	Deep tissue penetration due to NIR excitation [242]
	NaYF ₄ (Yb,Er)@NaYF ₄ (Yb,Tm)@C ₆₀ MA ^{c)} (34 nm)	980 / 808	360 / 407 / 450 / 475 / 540 / 650 / 696 / 800	<i>In vivo</i> Hepa1-6 tumor targeting and PDT	Remarkable therapeutic efficacy, change of excitation wavelength [243]
QDs _s	CuInSe ₂ @InS@CGKPK ^{d)} (36 nm)	450	675	Optical imaging/targeting of glioblastoma tumor in mice	High cellular uptake, photostability and chemical inertness [244]
	[⁶⁴ Cu]CuInS@ZnS@glutathione (6.5 nm)	470	680	Active targeting to glioblastoma U87MG tumor in mice for PET imaging	Intrinsic radioactivity with excellent stability. [245]
FPs _s	CuInS@ZnS@DSPE-PEG2000 ^{e)} (5 nm)	660	730	Diagnosis and efficient destruction of tumors	PDT and multispectral optical tomography effects [246]
	mKeima (red FPs)	440 / 590	620	pH sensing in MIN6-beta cells	High resistance against degradation enzymes, dual excitation [247]
FPs _s	GEM-GECO1 (Ca ²⁺ -sensitive FP)	453	513	Ca ²⁺ sensing in MIN6 beta-cells	High resistance against pH [247]
	FP fusion SoNar (YFP ^{f)} derivative and NADH binding domain)	420 / 490	528	Detection of biological processes	Bright, pH-resistant and fast probe enabling high throughput screening [248]

a) RGD refers to an arginine-glycine-aspartic peptide; b) TAT and RGDS refer to cell penetratin and cell adhesive peptides; c) C60MA is a monomalonic fullerene; d) CGKPK refers to a tumor targeting peptide; e) DSPE-PEG2000 refers to 1,2-distearoyl-sn-glycero-3-phosphoethanolamine-N-[polyethylene glycol]-2000; f) YFP yellow fluorescent protein

Nowadays live-cell imaging using FPs has become almost a gold standard for biological imaging [249]. It is impressive to see all the possibilities which can be retrieved, *e.g.* to analyze organelle contact sites *in vivo* using split-GFP proteins [250]. Thereby the FP was split into two fragments and only fluorescence occurs in close distance of the two organelles as seen in Figure 1.19.

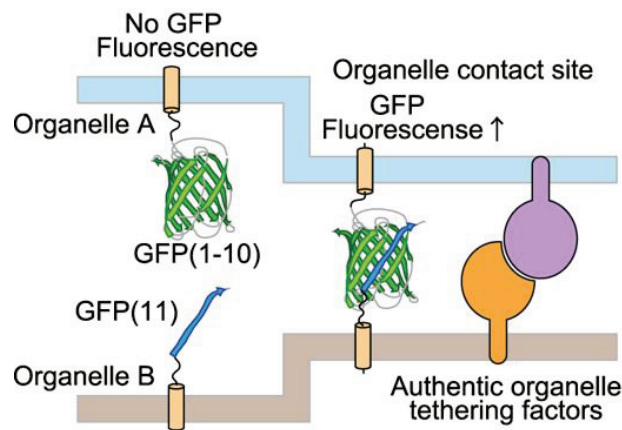


Figure 1.19| Scheme of the split-GFP system for detection of the interaction between organelles. Adapted from [250].

Deyev *et al.* have developed a FP (Dendra2) which is capable to visualize the mitochondrial and cytoplasmic pH in HEK293 cells [251]. Beside the intercellular pH value, the emission of different fluorescent proteins is also sensitive to the amount of chlorides, calcium and other compounds like cyclic adenosine monophosphate (cAMP), cyclic guanosine monophosphate (cGMP) or ATP as reported in a review by Germond *et al.* [252]. Compared to FPs, the cellular uptake is much more elaborate for fluorescent nanoparticles. On one side, the surface of the particles needs to have a functionality so that recognition of cell specific processes can occur. On the other side, the particles need to be able to enter a cell without being embedded in lysosomes, which is often the case when cellular uptake is induced by endocytosis. Beside this mechanism, the uptake can also occur *e.g. via* passive diffusion, hole formations, direct microinjection or electroporation. Nowadays alongside the classical staining of cell compartments also the tracking of the nucleus has gained more scientific interest, however, the narrow pore size is limiting for most luminescent nanomaterials. C-Dots, with the smallest average size, can be used to stain the nucleus of cells as shown by the group of Yin [253]. Thereby the size of the C-Dots (~2.3 nm) together with positive charged dopamine mimicking surface groups was essential for the crossing through the nucleus pores. By further tuning the surface of the nanoparticles, those probes can be used for the selective targeting and photostable staining of the nucleus [254]. On the other side, UCNPs are advantageous due to their NIR excitation either at 980 or 808 nm, enabling deep tissue penetration due to the higher optical transparency in the low energy range [255]. Beside low phototoxicity to tissues, animals or cells, also minimized light scattering gains ultrahigh imaging contrast. Methods like time-gated imaging can lead to further improvements in resolution as demonstrated by the group of Jaque [256]. The comparison of UCNPs and QDs, injected into mice, showed that the *in vivo* detection sensitivity of the UCNPs is one order of magnitude higher than that of the QDs [257]. Based on this, the usage of the multi-photon microscopy has become a valuable alternative for QDs [173, 258–260], C-Dots [261–264] and fluorescent proteins [265–268]. By using high-power pulsed laser, the absorption of two or more photons in the same timeframe occurs and lead to an anti-Stokes shift comparable to the upconversion nanoparticles.

1.5 Conclusion and perspective

In this review, we compared UCNPs with QDs, C-Dots and FPs regarding optical and physical properties (Figure 1.20) and their performance in biosensing and bioimaging applications. Due to the unique origin of photoluminescence, UCNPs can be excited in the NIR, which results in a low background signal from matrix compounds like proteins, or DNA. Also, their luminescence lifetimes are longer compared to the other probes and the particles show high photostability upon long-term excitation. Concerning physical properties, the particles with a uniform size distribution and clear crystal structure can be prepared by a huge variety of methods. Particles of large variations in sizes between 10 and 200 nm and with different shapes can be obtained in contrast to QDs and C-Dots. Additionally, C-Dots suffer so far from poor reproducibility and uniformity of the obtained particles.

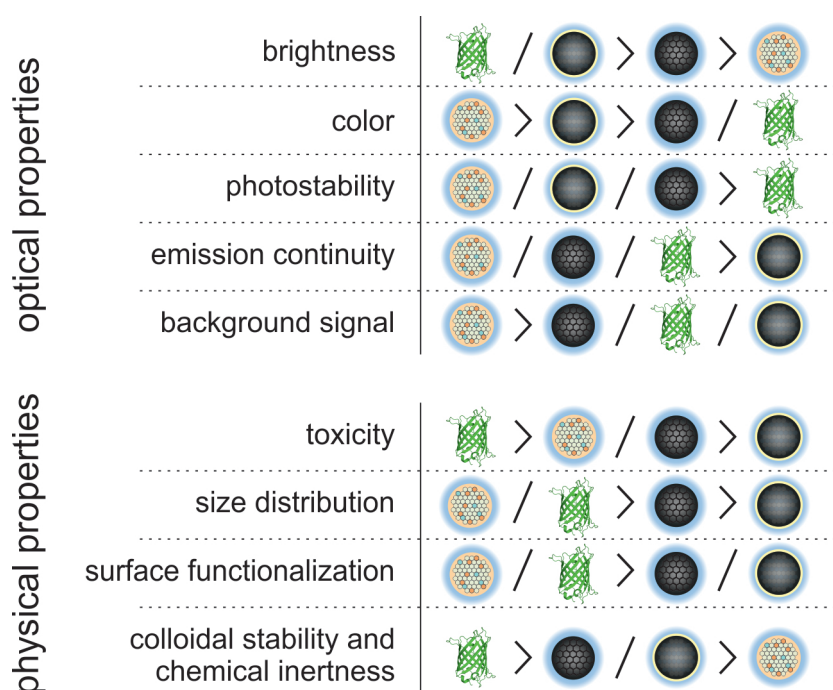


Figure 1.20| Comparison of UCNPs, QDs, C-Dots and FPs concerning their usability for biosensing and bioimaging.

The surface of all probes can be easily modified with a desired surface ligand by many (bio-) conjugation techniques. For stability issues, crosslinking of the surface ligand as well as covalent attachment of the biomolecule should be preferred. Fluorescent proteins offer naturally several functional groups. However, those are not distributed equally among the surface, which sometimes makes bioconjugation challenging and only poor efficiency can be achieved. For C-Dots there is also no defined surface chemistry, so that UCNPs and QDs are favourable in terms of the possibility of controlled surface engineering. Nevertheless, UCNPs suffer from low quantum yields and small absorption coefficients in comparison to the other fluorescent probes. This drawback affects the sensitivity of UCNPs achieved in sensors for common analytes when compared to the other probes. There is still room of improvement by finding strategies to boost the brightness which will enable smaller particles to be used as probes in sensors. In imaging applications UCNPs have an advantage due to their low excitation energy and the absence of background fluorescence. This can be also achieved for QDs, C-Dots and FPs by using two-photon spectroscopy. However, high-power laser

sources are required, which could be harmful in biological applications. Recent studies concerning the dissolution of highly diluted UCNPs have to be kept in mind and demand an improvement in stability by surface chemistry preventing the access of water to the NaYF₄ core. Alternatives would be to change the host material to the well-known oxides or other materials which are not prone for dissolution. Both suggestions are in contradiction to minimize the total particle size, which is important for *in vivo* applications. In general, it is difficult to judge the toxicity of all probes discussed here. More fundamental studies are needed to fully understand the impact on cells and even more so for animals. Compared to other fluorescent probes, UCNPs have already established as a powerful alternative but there are still plenty of hurdles which need to be overcome as summarized in Figure 1.21.

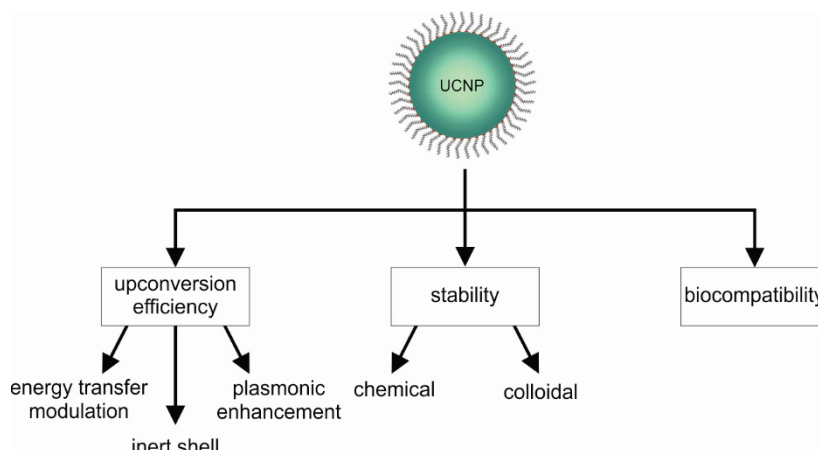


Figure 1.21| Challenges and issues, which need to be addressed to make upconversion nanoparticles more attractive for sensing or imaging applications.

1.6 References

- [1] Sun T, Ai F, Zhu G, Wang F (2018) Upconversion in Nanostructured Materials: From Optical Tuning to Biomedical Applications. *Chem. Asian J.* 13(4):373-85.
- [2] Sun L, Wei R, Feng J, Zhang H (2018) Tailored Lanthanide-Doped Upconversion Nanoparticles and their Promising Bioapplication Prospects. *Coord. Chem. Rev.* 364:10-32.
- [3] Buchner M, Muhr V, Himmelstoß SF, Hirsch T (2016) 4 Functionalization Aspects of Water Dispersible Upconversion Nanoparticles. In *Upconverting Nanomaterials* (pp 69-100). CRC Press, Boca Raton.
- [4] Liu H, Huang K, Valiev RR, Zhan Q, Zhang Y, Ågren H (2018) Photon Upconversion Kinetic Nanosystems and Their Optical Response. *Laser Photonics Rev.* 12(1):1700144.
- [5] Homann C, Krukewitt L, Frenzel F, Grauel B, Würth C, Resch-Genger U, Haase M (2018) NaYF₄:Yb,Er/NaYF₄ Core/Shell Nanocrystals with High Upconversion Luminescence Quantum Yield. *Angew. Chem. Int. Ed.* 57(28):8765-69.
- [6] Fernández-Luna V, Coto PB, Costa RD (2018) When Fluorescent Proteins Meet White Light-Emitting Diodes. *Angew. Chem. Int. Ed.* 57(29):8826-36.
- [7] Miyawaki A, Niino Y (2015) Molecular Spies for Bioimaging - Fluorescent Protein-based Probes. *Mol. Cell* 58(4):632-43.
- [8] Biju V, Itoh T, Ishikawa M (2010) Delivering Quantum Dots to Cells: Bioconjugated Quantum Dots for Targeted and Nonspecific Extracellular and Intracellular Imaging. *Chem. Soc. Rev.* 39(8):3031-56.
- [9] Rakovich A, Rakovich T (2018) Semiconductor versus Graphene Quantum Dots as Fluorescent Probes for Cancer Diagnosis and Therapy Applications. *J. Mater. Chem. B* 6(18):2690-712.
- [10] Sharma VK, McDonald TJ, Sohn M, Anquandah GAK, Pettine M, Zboril R (2017) Assessment of Toxicity of Selenium and Cadmium Selenium Quantum Dots: A Review. *Chemosphere* 188:403-13.
- [11] Zhang Z, Zhang J, Chen N, Qu L (2012) Graphene Quantum Dots: An Emerging Material for Energy-related Applications and Beyond. *Energy Environ. Sci.* 5(10):8869-90.
- [12] Lim S Y, Shen W, Gao Z (2015) Carbon Quantum Dots and their Applications. *Chem. Soc. Rev.* 44(1):362-81.
- [13] Zuo P, Lu X, Sun Z, Guo Y, He H (2016) A Review on Syntheses, Properties, Characterization and Bioanalytical Applications of Fluorescent Carbon Dots. *Microchim. Acta* 183(2):519-42.
- [14] Sydor AM, Czymmek KJ, Puchner EM, Mennella V (2015) Super-Resolution Microscopy: From Single Molecules to Supramolecular Assemblies. *Trends Cell Biol.* 25(12):730-48.
- [15] Huang B, Wang W, Bates M, Zhuang X (2008) Three-Dimensional Super-Resolution Imaging by Stochastic Optical Reconstruction Microscopy. *Science* 319(5864):810-13.
- [16] Leung BO, Chou KC (2011) Review of Super-resolution Fluorescence Microscopy for Biology. *Appl. Spectrosc.* 65(9):967-80.
- [17] Mayer M, Baeumner AJ (2018) ABC Spotlight on Analytics 4.0. *Anal. Bioanal. Chem.* 410(21):5095-97.
- [18] Kumar D, Verma K, Verma S, Chaudhary B, Som S, Sharma V, Kumar V, Swart H C (2018) Recent Advances in Enhanced Luminescence Upconversion of Lanthanide-doped NaYF₄ Phosphors. *Physica B* 535:278-86.
- [19] Gu B, Zhang Q (2018) Recent Advances on Functionalized Upconversion Nanoparticles for Detection of Small Molecules and Ions in Biosystems. *Adv. Sci.* 5(3):1700609.
- [20] Zhou B, Shi B, Jin D, Liu X (2015) Controlling Upconversion Nanocrystals for Emerging Applications. *Nat. Nanotechnol.* 10(11):924-36.
- [21] Zheng W, Huang P, Tu D, Ma E, Zhu H, Chen X (2015) Lanthanide-doped Upconversion Nano-Bioprobes: Electronic Structures, Optical Properties, and Biodetection. *Chem. Soc. Rev.* 44(6):1379-415.
- [22] Chen G, Qiu H, Prasad PN, Chen X (2014) Upconversion Nanoparticles: Design, Nanochemistry, and Applications in Theranostics. *Chem. Rev.* 114(19):5161-214.

- [23] Zu F, Yan F, Bai Z, Xu J, Wang Y, Huang Y, Zhou X (2017) The Quenching of the Fluorescence of Carbon Dots: A Review on Mechanisms and Applications. *Microchim. Acta* 184(7):1899-914.
- [24] Du Y, Guo S (2016) Chemically Doped Fluorescent Carbon and Graphene Quantum Dots for Bioimaging, Sensor, Catalytic and Photoelectronic Applications. *Nanoscale* 8(5):2532-43.
- [25] Sanford L, Palmer A (2017) Recent Advances in Development of Genetically Encoded Fluorescent Sensors. In *Enzymes as sensors* (pp 1-49). Academic Press, Cambridge.
- [26] Dedecker P, Schryver FC de, Hofkens J (2013) Fluorescent Proteins: Shine On, You Crazy Diamond. *J. Am. Chem. Soc.* 135(7):2387-402.
- [27] Chudakov DM, Matz MV, Lukyanov S, Lukyanov KA (2010) Fluorescent Proteins and their Applications in Imaging Living Cells and Tissues. *Physiol. Rev.* 90(3):1103-63.
- [28] Seward HE, Bagshaw CR (2009) The Photochemistry of Fluorescent Proteins: Implications for their Biological Applications. *Chem. Soc. Rev.* 38(10):2842-51.
- [29] Chandan HR, Schiffman JD, Balakrishna RG (2018) Quantum Dots as Fluorescent Probes: Synthesis, Surface Chemistry, Energy Transfer Mechanisms, and Applications. *Sens. Actuator B Chem.* 258:1191-214.
- [30] Medintz IL, Uyeda HT, Goldman ER, Mattoussi H (2005) Quantum Dot Bioconjugates for Imaging, Labeling and Sensing. *Nat. Mater.* 4(6):435-46.
- [31] Chan WCW, Maxwell DJ, Gao X, Bailey RE, Han M, Nie S (2002) Luminescent Quantum Dots for Multiplexed Biological Detection and Imaging. *Curr. Opin. Biotechnol.* 13(1):40-6.
- [32] Pu C, Qin H, Gao Y, Zhou J, Wang P, Peng X (2017) Synthetic Control of Exciton Behavior in Colloidal Quantum Dots. *J. Am. Chem. Soc.* 139(9):3302-11.
- [33] Hemmer E, Benayas A, Légaré F, Vetrone F (2016) Exploiting the Biological Windows: Current Perspectives on Fluorescent Bioprobes Emitting above 1000 nm. *Nanoscale Horiz.* 1(3):168-84.
- [34] He S, Song J, Qu J, Cheng Z (2018) Crucial Breakthrough of Second Near-Infrared Biological Window Fluorophores: Design and Synthesis Toward Multimodal Imaging and Theranostics. *Chem. Soc. Rev.* 47(12):4258-78.
- [35] Cai Y, Wei Z, Song C, Tang C, Han W, Dong X (2019) Optical Nano-Agents in the Second Near-Infrared Window for Biomedical Applications. *Chem. Soc. Rev.* 48(1):22-37.
- [36] Svendsen A, Kiefer HV, Pedersen HB, Bochenkova AV, Andersen LH (2017) Origin of the Intrinsic Fluorescence of the Green Fluorescent Protein. *J. Am. Chem. Soc.* 139(25):8766-71.
- [37] Masumoto Y, Takagahara T (2002) *Semiconductor Quantum Dots: Physics, Spectroscopy and Applications*. Springer, Berlin.
- [38] Quintanilla M, Liz-Marzán LM (2018) Guiding Rules for Selecting a Nanothermometer. *Nano Today* 19:126-45.
- [39] Sharma S, Umar A, Sood S, Mehta SK, Kansal S K (2018) Photoluminescent C-dots: An Overview on the Recent Development in the Synthesis, Physiochemical Properties and Potential Applications. *J. Alloys Compd.* 748:818-53.
- [40] Wang J, Qiu J (2016) A Review of Carbon Dots in Biological Applications. *J. Mater. Sci.* 51(10):4728-38.
- [41] DaCosta MV, Doughan S, Han Y, Krull UJ (2014) Lanthanide Upconversion Nanoparticles and Applications in Bioassays and Bioimaging: A Review. *Anal. Chim. Acta* 832:1-33.
- [42] Auzel F (2004) Upconversion and Anti-Stokes Processes with f and d Ions in Solids. *Chem. Rev.* 104(1):139-73.
- [43] Chien YH, Chan KK, Yap SHK, Yong KT (2018) NIR-Responsive Nanomaterials and their Applications; Upconversion Nanoparticles and Carbon Dots: A Perspective. *J. Chem. Technol. Biotechnol.* 93(6):1519-28.
- [44] Naccache R, Yu Q, Capobianco JA (2015) The Fluoride Host: Nucleation, Growth, and Upconversion of Lanthanide-Doped Nanoparticles. *Adv. Opt. Mater.* 3(4):482-509.

- [45] Bazylińska U, Wawrzyńczyk D (2017) Encapsulation of TOPO stabilized NaYF₄:Er³⁺,Yb³⁺ Nanoparticles in Biocompatible Nanocarriers: Synthesis, Optical Properties and Colloidal Stability. *Colloids Surf. A* 532:556–63.
- [46] Yan C, Zhao H, Peregichka DF, Rosei F (2016) Lanthanide Ion Doped Upconverting Nanoparticles: Synthesis, Structure and Properties. *Small* 12(29):3888–907.
- [47] Bialecka-Fornal M, Makushok T, Rafelski SM (2016) A Review of Fluorescent Proteins for Use in Yeast. In *Yeast Cytokinesis* (pp. 309–346). Springer, New York.
- [48] Pletnev S, Shcherbakova DM, Subach O M, Pletneva NV, Malashkevich VN, Almo SC, Dauter Z, Verkhusha VV (2014) Orange Fluorescent Proteins: Structural Studies of LSSmOrange, PSMOrange and PSMOrange2. *PLoS One* 9(6):e99136.
- [49] Acharya A, Bogdanov AM, Grigorenko BL, Bravaya KB, Nemukhin AV, Lukyanov KA, Krylov AI (2017) Photoinduced Chemistry in Fluorescent Proteins: Curse or Blessing? *Chem. Rev.* 117(2):758–95.
- [50] Bomati EK, Haley JE, Noel JP, Deheyn DD (2014) Spectral and Structural Comparison Between Bright and Dim Green Fluorescent Proteins in *Amphioxus*. *Sci. Rep.* 4:5469.
- [51] Mishin AS, Belousov VV, Solntsev KM, Lukyanov KA (2015) Novel Uses of Fluorescent Proteins. *Curr. Opin. Chem. Biol.* 27:1–9.
- [52] Teng L, Wang K, Xu J, Xu C (2015) Flavin mononucleotide (FMN)-based fluorescent protein (FbFP) as reporter for promoter screening in *Clostridium cellulolyticum*. *J. Microbiol. Methods* 119:37–43.
- [53] Ng SM, Koneswaran M, Narayanaswamy R (2016) A Review on Fluorescent Inorganic Nanoparticles for Optical Sensing Applications. *RSC Adv.* 6(26):21624–61.
- [54] Altintas Z, Davis F, Scheller FW (2018) Applications of Quantum Dots. In *Biosensors and Diagnostics. In Biosensors and nanotechnology: Applications in health care diagnostics* (pp 183–99). Wiley, New York.
- [55] Chen O, Zhao J, Chauhan VP, Cui J, Wong C, Harris DK, Wei H, Han HS, Fukumura D, Jain RK, Bawendi MG (2013) Compact High-Quality CdSe–CdS Core-Shell Nanocrystals With Narrow Emission Linewidths and Suppressed Blinking. *Nat. Mater.* 12(5):445–51.
- [56] Binetti E, Tricoli M, Sibillano T, Giannini C, Brescia R, Falqui A, Comparelli R, Corricelli M, Tommasi R, Agostiano A, Curri ML (2015) Tuning Light Emission of PbS Nanocrystals From Infrared to Visible Range By Cation Exchange. *Sci. Technol. Adv. Mater. Technology* 16(5):055007.
- [57] Zhou J, Zhou H, Tang J, Deng S, Yan F, Li W, Qu M (2017) Carbon Dots Doped With Heteroatoms For Fluorescent Bioimaging: A Review. *Microchim. Acta* 184(2):343–68.
- [58] Zhu X, Su Q, Feng W, Li F (2017) Anti-Stokes Shift Luminescent Materials for Bio-Applications. *Chem. Soc. Rev.* 46(4):1025–39.
- [59] Wolfbeis OS (2015) An Overview of Nanoparticles Commonly Used in Fluorescent Bioimaging. *Chem. Soc. Rev.* 44(14):4743–68.
- [60] Wilhelm S, Kaiser M, Würth C, Heiland J, Carrillo-Carrion C, Muhr V, Wolfbeis OS, Parak WJ, Resch-Genger U, Hirsch T (2015) Water Dispersible Upconverting Nanoparticles: Effects of Surface Modification on their Luminescence and Colloidal Stability. *Nanoscale* 7(4):1403–10.
- [61] Han S, Deng R, Xie X, Liu X (2014) Enhancing Luminescence in Lanthanide-Doped Upconversion Nanoparticles. *Angew. Chem. Int. Ed.* 53(44):11702–15.
- [62] Cranfill PJ, Sell BR, Baird MA, Allen JR, Lavagnino Z, Gruiter HM de, Kremers G-J, Davidson MW, Ustione A, Piston DW (2016) Quantitative Assessment of Fluorescent Proteins. *Nat. Methods* 13(7):557–62.
- [63] Kang B-H, Lee JS, Lee SW, Kim SW, Lee JW, Gopalan SA, Park JS, Kwon DH, Bae JH, Kim HR, Kang SW (2016) Efficient Exciton Generation in Atomic Passivated CdSe/ZnS Quantum Dots Light-Emitting Devices. *Sci. Rep.* 6:34659.
- [64] Long Q, Li H, Zhang Y, Yao S (2015) Upconversion nanoparticle-based fluorescence resonance energy transfer assay for organophosphorus pesticides. *Biosens. Bioelectron.* 68:168–74.

- [65] Yang L, Jiang W, Qiu L, Jiang X, Zuo D, Wang D and Yang L (2015) One Pot Synthesis of Highly Luminescent Polyethylene Glycol Anchored Carbon Dots Functionalized with a Nuclear Localization Signal Peptide for Cell Nucleus Imaging. *Nanoscale* 7(14):6104-13.
- [66] Xu Q, Pu P, Zhao J, Dong C, Gao C, Chen Y, Chen J, Liu Y, Zhou H (2015) Preparation of Highly Photoluminescent Sulfur-Doped Carbon Dots for Fe(III) Detection. *J. Mater. Chem. A* 3(2):542-6.
- [67] Maestro LM, Rodriguez EM, Vetrone F, Naccache R, Ramirez HL, Jaque D, Capobianco JA, Solé JG (2010) Nanoparticles for Highly Efficient Multiphoton Fluorescence Bioimaging. *Opt. Express* 18(23):23544-53.
- [68] Tikhonov GV, Babkin AS, Seregina EA and Seregin AA (2017) Yb³⁺-Activated Inorganic Aprotic Liquids for Diode-Pumped Lasers. *Inorg. Mater.* 53(10):1097-102.
- [69] Würth C, Fischer S, Grauel B, Alivisatos AP, Resch-Genger U (2018) Quantum Yields, Surface Quenching, and Passivation Efficiency for Ultrasmall Core/Shell Upconverting Nanoparticles *J. Am. Chem. Soc.* 140(14):4922-8.
- [70] Wiesholler LM, Hirsch T (2018) Strategies for the Design of Bright Upconversion Nanoparticles for Bioanalytical Applications. *Opt. Mater.* 80:253-64.
- [71] Li X, Zhang F, Zhao D (2015) Lab on Upconversion Nanoparticles: Optical Properties and Applications Engineering *via* Designed Nanostructure. *Chem. Soc. Rev.* 44(6): 346-78.
- [72] Resch-Genger U, Gorris HH (2017) Perspectives and Challenges of Photon-Upconversion Nanoparticles - Part I: Routes to Brighter Particles and Quantitative Spectroscopic Studies. *Anal. Bioanal. Chem.* 409(25):5855-74.
- [73] Lakowicz JR (2010) *Principles of Fluorescence Spectroscopy*. Springer, New York.
- [74] Bajar BT, Wang ES, Zhang S, Lin MZ, Chu J (2016) A Guide to Fluorescent Protein FRET Pairs. *Sensors* 16(9):1488-1512.
- [75] Bindels DS, Haarbosch L, Van Weeren L, Postma M, Wiese KE, Mastop M, Aumonier S (2017) mScarlet: A Bright Monomeric Red Fluorescent Protein for Cellular Imaging. *Nat. Methods* 14(1):53-6.
- [76] Hutton GAM, Martindale BCM, Reisner E (2017) Carbon dots as Photosensitisers for Solar-Driven Catalysis. *Chem. Soc. Rev.* 46(20):6111-23.
- [77] Schneider J, Reckmeier C J, Xiong Y, Seckendorff M von, Susa A S, Kasák P, Rogach AL (2017) Molecular Fluorescence in Citric Acid-Based Carbon Dots. *J. Phys. Chem. C* 121(3):2014-22.
- [78] Li H, Sun C, Vijayaraghavan R, Zhou F, Zhang X, MacFarlane DR (2016) Long lifetime Photoluminescence in N, S Co-Doped Carbon Quantum Dots From an Ionic Liquid and their Applications in Ultrasensitive Detection of Pesticides. *Carbon* 104:33-9.
- [79] Bhuckory S, Hemmer E, Wu Y-T, Yahia-Ammar A, Vetrone F, Hildebrandt N (2017) Core or Shell? Er³⁺ FRET Donors in Upconversion Nanoparticles. *Eur. J. Inorg. Chem.* 2017(44): 5186-95.
- [80] Chen X, Peng D, Ju Q, Wang F (2015) Photon Upconversion in Core-Shell Nanoparticles. *Chem. Soc. Rev.* 44(6):1318-30.
- [81] Wang Y, Deng R, Xie X, Huang L and Liu X (2016) Nonlinear Spectral and Lifetime Management in Upconversion Nanoparticles by Controlling Energy Distribution. *Nanoscale* 8(12):6666-73.
- [82] Efros AL, Nesbitt DJ (2016) Origin and Control of Blinking in Quantum Dots. *Nat. Nanotechnol.* 11(8):661-71.
- [83] Yang Z, Sharma A, Qi J, Peng X, Lee DY, Hu R, Lin D, Qu J, Kim JS (2016) Super-Resolution Fluorescent Materials: An Insight into Design and Bioimaging Applications. *Chem. Soc. Rev.* 45(17):4651-67.
- [84] Dertinger T, Heilemann M, Vogel R, Sauer M, Weiss S (2010) Superresolution Optical Fluctuation Imaging with Organic Dyes. *Angew. Chem. Int. Ed.* 49(49):9441-3.
- [85] Zeng Z, Chen X, Wang H, Huang N, Shan C, Zhang H, Teng J, Xi P (2015) Fast Super-Resolution Imaging with Ultra-High Labeling Density Achieved by Joint Tagging Super-Resolution Optical Fluctuation Imaging. *Sci. Rep.* 5:8359.

- [86] Zheng XT, Ananthanarayanan A, Luo KQ, Chen P (2015) Glowing Graphene Quantum Dots and Carbon Dots: Properties, Syntheses, and Biological Applications. *Small* 11(14):1620-36.
- [87] Mamontova AV, Grigoryev AP, Tsarkova AS, Lukyanov KA, Bogdanov AM (2017) Struggle for Photostability: Bleaching Mechanisms of Fluorescent Proteins. *Russ. J. Bioorg. Chem.* 43(6):625-33.
- [88] Muhr V, Würth C, Kraft M, Buchner M, Baeumner AJ, Resch-Genger U, Hirsch T (2017) Particle- Size- Dependent Förster Resonance Energy Transfer from Upconversion Nanoparticles to Organic Dyes. *Anal. Chem.* 89(9):4868-74.
- [89] Nyk M, Wawrzynczyk D, Parjaszewski K, Samoc M (2011) Spectrally Resolved Nonlinear Optical Response of Upconversion Lanthanide-Doped NaYF₄ Nanoparticles. *J. Phys. Chem. C* 115(34):16849-55.
- [90] Meiling TT, Cywiński PJ, Löhmansröben HG (2018) Two-Photon Excitation Fluorescence Spectroscopy of Quantum Dots: Photophysical Properties and Application in Bioassays. *J. Phys. Chem. C* 122(17):9641-47.
- [91] Drobizhev M, Makarov NS, Tillo SE, Hughes TE, Rebane A (2011) Two-Photon Absorption Properties of Fluorescent Proteins. *Nat. Methods* 8(5):393-9.
- [92] Liu Y, Tan J, Thomas A, Ou-Yang D, Muzykantov VR (2012) The Shape of Things to Come: Importance of Design in Nanotechnology for Drug Delivery. *Therapeutic Delivery* 3(2):181-94.
- [93] Wen HQ, Peng HY, Liu K, Bian MH, Xu YJ, Dong L, Yan X, Xu WP, Tao W, Shen JL, Lu Y (2017) Sequential Growth of NaYF₄:Yb/Er@NaGdF₄ Nanodumbbells for Dual-Modality Fluorescence and Magnetic Resonance Imaging. *ACS Appl. Mater. Interfaces* 9(11):9226-32.
- [94] Xu B, Zhang X, Huang W, Yang Y, Ma Y, Gu Z, Zhai T, Zhao Y (2016) Nd³⁺ Sensitized Dumbbell-Like Upconversion Nanoparticles for Photodynamic Therapy Application. *J. Mater. Chem. B* 4(16):2776-84.
- [95] Liu D, Xu X, Du Y, Qin X, Zhang Y, Ma C, Wen S, Ren W, Goldys EM, Piper JA, Dou S (2016) Three - Dimensional Controlled Growth of Monodisperse Sub-50 nm Heterogeneous Nanocrystals. *Nat. Commun.* 7:10254.
- [96] Makrides SC (1999) Components of Vectors for Gene Transfer and Expression in Mammalian Cells. *Protein Expr. Purif.* 17(2):183-202.
- [97] Grishammer RK (2006) *Structural Biology of Membrane Proteins*, RSC, Cambridge.
- [98] Craggs TD (2009) Green Fluorescent Protein: Structure, Folding and Chromophore Maturation. *Chem. Soc. Rev.* 38(10):2865-75.
- [99] Ma Y, Sun Q, Smith SC (2017) The Mechanism of Oxidation in Chromophore Maturation of Wild - Type Green Fluorescent Protein: A Theoretical study. *Phys. Chem. Chem. Phys.* 19(20):12942-52.
- [100] Balleza E, Kim JM, Cluzel P (2018) Systematic Characterization of Maturation Time of Fluorescent Proteins in Living Cells. *Nat. Methods* 15(1):47-51.
- [101] Murray CB, Norris DJ, Bawendi MG (1993) Synthesis and Characterization of Nearly Monodisperse CdE (E = sulfur, selenium, tellurium) Semiconductor Nanocrystallites. *J. Am. Chem. Soc.* 115(19):8706-15.
- [102] Wegner KD, Hildebrandt N (2015) Quantum Dots: Bright and Versatile *in vitro* and *in vivo* Fluorescence Imaging Biosensors. *Chem. Soc. Rev.* 44(14):4792-834.
- [103] Vasudevan D, Gaddam RR, Trinchì A, Cole I (2015) Core-shell Quantum Dots: Properties and Applications. *J. Alloys Compd.* 636:395-404.
- [104] Zhao H, Chaker M, Wu N, Ma D (2011) Towards Controlled Synthesis and Better Understanding of Highly Luminescent PbS/CdS Core/Shell Quantum Dots. *J. Mater. Chem.* 21(24):8898-8904.
- [105] Peng ZA, Peng X (2001) Formation of High-Quality CdTe, CdSe, and CdS Nanocrystals Using CdO as Precursor. *J. Am. Chem. Soc.* 123(1):183-4.
- [106] Jing L, Kershaw SV, Li Y, Huang X, Li Y, Rogach AL, Gao M (2016) Aqueous Based Semiconductor Nanocrystals. *Chem. Rev.* 116(18):10623-730.
- [107] Choi Y, Choi Y, Kwon O-H, Kim B-S (2018) Carbon Dots: Bottom-Up Syntheses, Properties, and Light-Harvesting Applications. *Chem. Asian J.* 13(6):586-98.

- [108] Papaioannou N, Marinovic A, Yoshizawa N, Goode AE, Fay M, Khlobystov A, Titirici MM, Sapelkin A (2018) Structure and Solvents Effects on the Optical Properties of Sugar-Derived Carbon Nanodots. *Sci. Rep.* 8:6559.
- [109] Liu H, Li Z, Sun Y, Geng X, Hu Y, Meng H, Ge J, Qu L (2018) Synthesis of Luminescent Carbon Dots with Ultrahigh Quantum Yield and Inherent Folate Receptor-Positive Cancer Cell Targetability. *Sci. Rep.* 8:1086.
- [110] Qian H-S, Zhang Y (2008) Synthesis of Hexagonal-Phase Core-Shell NaYF₄ Nanocrystals with Tunable Upconversion Fluorescence. *Langmuir* 24(21):12123-5.
- [111] Rojas-Gutierrez PA, DeWolf C, Capobianco JA (2016) Formation of a Supported Lipid Bilayer on Faceted LiYF₄:Tm³⁺/Yb³⁺ Upconversion Nanoparticles. *Part. Part. Syst. Charact.* 33(12):865-70.
- [112] Chen C, Li C, Shi Z (2016) Current Advances in Lanthanide-Doped Upconversion Nanostructures for Detection and Bioapplication. *Adv. Sci.* 3(10):1600029.
- [113] Wang X, Zhuang J, Peng Q, Li Y (2005) A General Strategy for Nanocrystal Synthesis. *Nature* 437(7055):121-4.
- [114] Du P, Zhang P, Kang S H, Yu JS (2017) Hydrothermal Synthesis and Application of Ho³⁺-Activated NaYbF₄ Bifunctional Upconverting Nanoparticles for *In Vitro* Cell Imaging and Latent Fingerprint Detection. *Sens. Actuator B Chem.* 252:584-91.
- [115] Reddy KL, Prabhakar N, Arppe R, Rosenholm JM, Krishnan V (2017) Microwave-Assisted One-Step Synthesis of Acetate-Capped NaYF₄:Yb/Er Upconversion Nanocrystals and their Application in Bioimaging. *J. Mater. Sci.* 52(10):5738-50.
- [116] Liu Q, Zhang Y, Peng CS, Yang T, Joubert L-M, Chu S (2018) Single Upconversion Nanoparticle Imaging at Sub-10 W cm⁻² Irradiance. *Nat. Photonics* 12(9):548-53.
- [117] Lin X, Chen X, Zhang W, Sun T, Fang P, Liao Q, Chen X, He J, Liu M, Wang F, Shi P (2018) Core - Shell-Shell Upconversion Nanoparticles with Enhanced Emission for Wireless Optogenetic Inhibition. *Nano Lett.* 18(2):948-56.
- [118] Voß B, Nordmann J, Uhl A, Kombar R, Haase M (2013) Effect of the Crystal Structure of Small Precursor Particles on the Growth of β-NaREF₄ (RE = Sm, Eu, Gd, Tb) Nanocrystals. *Nanoscale* 5(2):806-12.
- [119] Baziulyte-Paulaviciene D, Karabanovas V, Stasys M, Jarockyte G, Poderys V, Sakirzanovas S, Rotomskis R (2017) Synthesis and Functionalization of NaGdF₄:Yb,Er@NaGdF₄ Core - Shell Nanoparticles for Possible Application as Multimodal Contrast Agents. *Beilstein J. Nanotechnol.* 8(1):1815-24.
- [120] Ma D, Meng L, Chen Y, Hu M, Chen Y, Huang C, Shang J, Wang R, Guo Y, Yang J (2015) NaGdF₄:Yb³⁺/Er³⁺@NaGdF₄:Nd³⁺@Sodium-Gluconate: Multifunctional and Biocompatible Ultrasmall Core-Shell Nanohybrids for UCL/MR/CT Multimodal Imaging. *ACS Appl. Mater. Interfaces* 7(30):16257-65.
- [121] He S, Johnson NJ, Nguyen Huu VA, Cory E, Huang Y, Sah RL, Jokerst JV, Almutairi A (2017) Simultaneous Enhancement of Photoluminescence, MRI Relaxivity, and CT Contrast by Tuning the Interfacial Layer of Lanthanide Heteroepitaxial Nanoparticles. *Nano Lett.* 17:4873-80.
- [122] Dong H, Du SR, Zheng XY, Lyu GM, Sun LD, Li LD, Zhang PZ, Zhang C, Yan CH (2015) Lanthanide Nanoparticles: From Design toward Bioimaging and Therapy. *Chem. Rev.* 115(19):10725-815.
- [123] Liu C, Gao Z, Zeng J, Hou Y, Fang F, Li Y, Qiao R, Shen L, Lei H, Yang W, Gao M (2013) Magnetic/upconversion Fluorescent NaGdF₄:Yb,Er Nanoparticle-Based Dual-Modal Molecular Probes for Imaging Tiny Tumors *in vivo*. *ACS Nano* 7(8):7227-40.
- [124] Xu Y, Jia XH, Yin XB, He XW, Zhang YK (2014) Carbon Quantum Dot Stabilized Gadolinium Nanoprobe Prepared *via* a One-Pot Hydrothermal Approach for Magnetic Resonance and Fluorescence Dual-Modality Bioimaging. *Anal. Chem.* 86(24):12122-9.
- [125] Pan Y, Yang J, Fang Y, Zheng J, Song R, Yi C (2017) One-pot Synthesis of Gadolinium-Doped Carbon Quantum Dots for High-Performance Multimodal Bioimaging. *J. Mater. Chem. B* 5(1):92-101.
- [126] Bozrova SV, Baryshnikova MA, Sokolova ZA, Nabiev IR, Sukhanova AV (2018) *In Vitro* Cytotoxicity of CdSe/ZnS Quantum Dots and Their Interaction with Biological Systems. *KEn Energy* 3(2):58-63.
- [127] Snapp EL (2009) Fluorescent Proteins: A Cell Biologist's User Guide. *Trends Cell Biol.* 19(11):649-55.

- [128] Davis CM, Gruebele M (2018) Labeling for Quantitative Comparison of Imaging Measurements *in Vitro* and in Cells. *Biochemistry* 57(13):1929-38.
- [129] Dean KM, Palmer AE (2014) Advances In Fluorescence Labeling Strategies for Dynamic Cellular Imaging. *Nat. Chem. Biol.* 10(7):512-23.
- [130] Gao S, You C, Rennecker S, Bao J, Zhang YHP (2014) New Insights into Enzymatic Hydrolysis of Heterogeneous Cellulose by Using Carbohydrate-Binding Module 3 Containing GFP and Carbohydrate-Binding Module 17 Containing CFP. *Biotechnol. Biofuels* 7(1):24.
- [131] Naccache R, Chevallier P, Lagueux J, Gossuin Y, Laurent S, Vander Elst L, Chilian C, Capobianco JA, Fortin MA (2013) High Relaxivities and Strong Vascular Signal Enhancement for NaGdF₄ Nanoparticles designed for Dual MR/optical imaging. *Adv. Healthc. Mater.* 2(11):1478-88.
- [132] Nsubuga A, Sgarzi M, Zarschler K, Kubeil M, Hübner R, Steudtner R, Graham B, Joshi T, Stephan H (2018) Facile Preparation of Multifunctionalisable 'Stealth' Upconverting Nanoparticles for Biomedical Applications. *Dalton Trans.* 47(26):8595-8604.
- [133] Kong W, Sun T, Chen B, Chen X, Ai F, Zhu X, Li M, Zhang W, Zhu G, Wang F (2017) A General Strategy for Ligand Exchange on Upconversion Nanoparticles. *Inorg. Chem.* 56(2):872-7.
- [134] Wang X, Valiev RR, Ohulchanskyy TY, Ågren H, Yang C, Chen G (2017) Dye-sensitized lanthanide-doped upconversion nanoparticles. *Chem. Soc. Rev.* 46(14):4150-67.
- [135] Huang Y, Hemmer E, Rosei F, Vetrone F (2016) Multifunctional Liposome Nanocarriers Combining Upconverting Nanoparticles and Anticancer Drugs. *J. Phys. Chem. B.* 120(22):4992-5001.
- [136] Muhr V, Wilhelm S, Hirsch T, Wolfbeis OS (2014) Upconversion Nanoparticles: From Hydrophobic to Hydrophilic Surfaces. *Acc. Chem. Res.* 47(12):3481-93.
- [137] Zhou J, Yang Y, Zhang CY (2015) Toward Biocompatible Semiconductor Quantum Dots: From Biosynthesis and Bioconjugation to Biomedical Application. *Chem. Rev.* 115(21):11669-717.
- [138] Zhang Z, Pan Y, Fang Y, Zhang L, Chen J, Yi C (2016) Tuning Photoluminescence and Surface Properties of Carbon Nanodots for Chemical Sensing. *Nanoscale* 8(1):500-7.
- [139] Zhu J, Shao H, Bai X, Zhai Y, Zhu Y, Chen X, Pan G, Dong B, Xu L, Zhang H, Song H (2018) Modulation of the Photoluminescence in Carbon Dots through Surface Modification: from Mechanism to White Light-Emitting Diodes. *Nanotechnology* 29(24): 245702.
- [140] Kostiv U, Kotelnikov I, Proks V, Šlouf M, Kučka J, Engstová H, Ježek P, Horák D (2016) RGDS- and TAT-Conjugated Upconversion of NaYF₄:Yb³⁺/Er³⁺@SiO₂ Nanoparticles: *In Vitro* Human Epithelioid Cervix Carcinoma Cellular Uptake, Imaging, and Targeting. *ACS Appl. Mater. Interfaces* 8(31):20422-31.
- [141] Cui X, Zhu L, Wu J, Hou Y, Wang P, Wang Z, Yang M (2015) A Fluorescent Biosensor Based on Carbon Dots-Labeled Oligodeoxyribonucleotide and Graphene Oxide for Mercury (II) Detection. *Biosens. Bioelectron.* 63:506-12.
- [142] Bhuckory S, Mattera L, Wegner KD, Qiu X, Wu YT, Charbonnière LJ, Reiss P, Hildebrandt N (2016) Direct Conjugation of Antibodies to the ZnS Shell of Quantum Dots for FRET Immunoassays with Low Picomolar Detection Limits. *Chem. Commun.* 52(100):14423-5.
- [143] Costantini LM, Baloban M, Markwardt ML, Rizzo M, Guo F, Verkhusha VV, Snapp EL (2015) A Palette of Fluorescent Proteins Optimized for Diverse Cellular Environments. *Nat. Commun.* 6:229.
- [144] Feliu N, Sun X, Alvarez Puebla RA, Parak W J (2017) Quantitative Particle-Cell Interaction: Some Basic Physicochemical Pitfalls. *Langmuir* 33(27):6639-46.
- [145] Tadros T (2011) General Principles of Colloid Stability and the Role of Surface Forces. In *Colloid Stability: Vol. 1, Pt. 1: The Role of Surface Forces* (pp, 1-22). Wiley, New York.
- [146] Zhang H, Dasbiswas K, Ludwig NB, Han G, Lee B, Vaikuntanathan S, Talapin DV (2017) Stable Colloids in Molten Inorganic Salts. *Nature* 542(7641):328-31.
- [147] Falco G de, Commodo M, Minutolo P, D'Anna A (2015) Flame-Formed Carbon Nanoparticles: Morphology, Interaction Forces, and Hamaker Constant from AFM. *Aerosol Sci. Technol.* 49(5):281-9.
- [148] Sahaman MN (2017) *Ceramic Processing*. CRC Press, Boca Raton.

- [149] Bhattacharjee S (2016) DLS and Zeta potential - What they are and What they are not? *J. Control. Release* 235:337-51.
- [150] Qiao R, Liu C, Liu M, Hu H, Liu C, Hou Y, Wu K, Lin Y, Liang J, Gao M (2015) Ultrasensitive *In vivo* Detection of Primary Gastric Tumor and Lymphatic Metastasis Using Upconversion Nanoparticles. *ACS Nano* 9(2):2120-9.
- [151] Kamrani S, Rezaei M, Kord M, Baalousha M (2018) Transport and Retention of Carbon Dots (CDs) in Saturated and Unsaturated Porous Media: Role of Ionic Strength, pH, and Collector Grain Size. *Water Res.* 133:338-47.
- [152] Datta KKR, Qi G, Zboril R, Giannelis EP (2016) Yellow Emitting Carbon Dots with Superior Colloidal, Thermal, and Photochemical Stabilities. *J. Mater. Chem. C* 4(41):9798-803
- [153] Yang S, Liu J, Chen Y, Guo J, Zhao L, Wei X, Peng X, Pu Q (2015) A Facile One-Step Photochemical Strategy for Preparation of Polyacrylamide Functionalized CdTe(S) Quantum Dots and their Application in Sensitive Determination of 2,4,6-trinitrotoluene. *Sens. Actuator B Chem.* 212:1-9.
- [154] Stepanenko OV, Stepanenko OV, Kuznetsova IM, Verkhusha VV, Turoverov KK (2013) Beta - Barrel Scaffold of Fluorescent Proteins: Folding, Stability and Role in Chromophore Formation. *Int. Rev. Cell Mol. Biol.* 302:22178.
- [155] Ward WW (2005) Biochemical and Physical Properties of Green Fluorescent Protein. In *Green Fluorescent Protein (Methods of Biochemical Analysis)* (pp. 39-65). Wiley, New York.
- [156] Soenen SJ, Abe S, Manshian BB, Aubert T, Hens Z, Smedt SC de, Braeckmans K (2015) The Effect of Intracellular Degradation on Cytotoxicity and Cell Labeling Efficacy of Inorganic Ligand-Stabilized Colloidal CdSe/CdS Quantum Dots. *J Biomed Nanotechnol* 11(4):631-43.
- [157] Lahtinen S, Lyytikäinen A, Pääkkilä H, Hömppi E, Perälä N, Lastusaari M, Soukka T (2017) Disintegration of Hexagonal NaYF₄:Yb³⁺,Er³⁺ Upconverting Nanoparticles in Aqueous Media: The Role of Fluoride in Solubility Equilibrium. *J. Phys. Chem. C* 121(1):656-65.
- [158] Lisjak D, Plohl O, Ponikvar-Svet M, Majaron B (2015) Dissolution of Upconverting Fluoride Nanoparticles in Aqueous Suspensions. *RSC Adv.* 5(35):27393-7.
- [159] Plohl O, Kraft M, Kovač J, Belec B, Ponikvar-Svet M, Würth C, Lisjak D, Resch-Genger U (2017) Optically Detected Degradation of NaYF₄:Yb,Tm-Based Upconversion Nanoparticles in Phosphate Buffered Saline Solution. *Langmuir* 33(2):553-60.
- [160] Li R, Ji Z, Dong J, Chang CH, Wang X, Sun B, Wang M, Liao YP, Zink JI, Nel AE, Xia T (2015) Enhancing the Imaging and Biosafety of Upconversion Nanoparticles through Phosphonate Coating. *ACS Nano* 9(3):3293-306.
- [161] Dukhno O, Przybilla F, Muhr V, Buchner M, Hirsch T, Mély Y (2018) Time-Dependent Luminescence Loss for Individual Upconversion Nanoparticles upon Dilution in Aqueous Solution. *Nanoscale* 10(34):15904-10.
- [162] Shiri S, Pajouheshpoor N, Khoshshafar H, Amidi S, Bagheri H (2017) An Electrochemical Sensor for the Simultaneous Determination of Fampicin and Isoniazid Using a C-dots@CuFe₂O₄ Nanocomposite Modified Carbon Paste Electrode. *New J. Chem.* 41(24):15564-73.
- [163] Tian X, Peng H, Li Y, Yang C, Zhou Z, Wang Y (2017) Highly Sensitive and Selective Paper Sensor Based on Carbon Quantum Dots for Visual Detection of TNT Residues in Groundwater. *Sensors and Actuator. B: Chemical* 243:1002-9.
- [164] Behzadi S, Serpooshan V, Tao W, Hamaly MA, Alkawareek MY, Dreaden EC, Brown D, Alkilany AM, Farokhzad OC, Mahmoudi M (2017) Cellular Uptake of Nanoparticles: Journey Inside the Cell. *Chem. Soc. Rev.* 46(14):4218-44.
- [165] Betzer O, Shilo M, Oepochinsky R, Barnoy E, Motiei M, Okun E, Yadid G, Popovtzer R (2017) The Effect of Nanoparticle Size on the ability to Cross the Blood-Brain Barrier: An *In Vivo* Study. *Nanomedicine* 12(13):1533-46.
- [166] Hoshyar N, Gray S, Han H, Bao G (2016) The Effect of Nanoparticle Size on *In Vivo* Pharmacokinetics and Cellular Interaction. *Nanomedicine* 11(6):673-92.

- [167] Yu J, Yin W, Peng T, Chang YN, Zu Y, Li J, He X, Ma X, Gu Z, Zhao Y (2017) Biodistribution, Excretion, and Toxicity of Polyethyleneimine Modified NaYF₄:Yb,Er Upconversion Nanoparticles in Mice *via* Different Administration Routes. *Nanoscale* 9(13):4497-507.
- [168] Gao Y, Zhu X, Zhang Y, Chen X, Wang L, Feng W, Huang C, Li F (2017) *In Vivo* Biodistribution and Passive Accumulation of Upconversion Nanoparticles in Colorectal Cancer Models *via* Intraperitoneal Injection. *RSC Adv.* 7(50):31588-96.
- [169] Guller A E, Generalova AN, Petersen EV, Nechaev AV, Trusova IA, Landyshev NN, Nadort A, Grebenik EA, Deyev SM, Shekhter AB, Zvyagin AV (2015) Cytotoxicity and Non-Specific Cellular Uptake of Bare and Surface-Modified Upconversion Nanoparticles in Human Skin Cells. *Nano Res.* 8(5):1546-62.
- [170] Ganini D, Leinisch F, Kumar A, Jiang J, Tokar EJ, Malone CC, Petrovich RM, Mason RP (2017) Fluorescent Proteins such as eGFP Lead to Catalytic Oxidative Etreess in Cells. *Redox Biol.* 12:462-8.
- [171] Kalyanaraman B, Zielonka J (2017) Green Fluorescent Proteins Induce Oxidative Stress in Cells: A Worrisome New Wrinkle in the Application of the GFP Reporter System to Biological Systems? *Redox Biol.* 12:755-7.
- [172] Liu W, Li C, Ren Y, Sun X, Pan W, Li Y, Wang J, Wang W (2016) Carbon Dots: Surface Engineering and Applications. *J. Mater. Chem. B* 4(35):5772-88.
- [173] Bwatanglang IB, Mohammad F, Yusof NA, Abdullah J, Hussein MZ, Alitheen NB, Abu N (2016) Folic Acid Targeted Mn:ZnS Quantum Dots for Theranostic Applications of Cancer Cell Imaging and Therapy. *Int. J. Nanomedicine* 11:413-28.
- [174] Ximendes EC, Rocha U, del Rosal B, Vaquero A, Sanz-Rodríguez F, Monge L, Ren F, Vetrone F, Ma D, García-Solé J, Jacinto C (2017) *In Vivo* Ischemia Detection by Luminescent Nanothermometers. *Adv. Healthc. Mater.* 6(4):1601195.
- [175] Ximendes EC, Santos WQ, Rocha U, Kagola UK, Sanz-Rodríguez F, Fernández N, Gouveia-Neto AD, Bravo D, Domingo AM, del Rosal B, Brites CD (2016) Unveiling *in Vivo* Subcutaneous Thermal Dynamics by Infrared Luminescent Nanothermometers. *Nano Lett.* 16(3):1695-703.
- [176] Ximendes EC, Rocha U, Sales TO, Fernández N, Sanz-Rodríguez F, Martín IR, Jacinto C, Jaque D (2017) *In Vivo* Subcutaneous Thermal Video Recording by Supersensitive Infrared Nanothermometers. *Adv. Funct. Mater.* 27(38):1702249.
- [177] Zhu X, Feng W, Chang J, Tan YW, Li J, Chen M, Sun Y, Li F (2016) Temperature-Feedback Upconversion Nanocomposite for Accurate Photothermal Therapy at Facile Temperature. *Nat Commun.* 7:10437.
- [178] del Rosal B, Carrasco E, Ren F, Benayas A, Vetrone F, Sanz-Rodríguez F, Ma D, Juarranz Á, Jaque D (2016) Infrared-Emitting QDs for Thermal Therapy with Real-Time Subcutaneous Temperature Feedback. *Adv. Funct. Mater.* 26(33):6060-8.
- [179] Vetrone F, Naccache R, Zamarrón A, La Juarranz de Fuente A, Sanz-Rodríguez F, Martínez Maestro L, Martín Rodríguez E, Jaque D, García Solé J, Capobianco JA (2010) Temperature Sensing Using Fluorescent Nanothermometers. *ACS Nano* 4(6):3254-8.
- [180] Shi Z, Duan Y, Zhu X, Wang Q, Li D, Hu K, Feng W, Li F, Xu C (2018) Dual Functional NaYF₄:Yb³⁺, Er³⁺@NaYF₄:Yb³⁺, Nd³⁺ Core-Shell Nanoparticles for Cell Temperature Sensing and Imaging. *Nanotechnology* 29(9):94001.
- [181] Hemmer E, Quintanilla M, Légaré F, Vetrone F (2015) Temperature-Induced Energy Transfer in Dye-Conjugated Upconverting Nanoparticles: A New Candidate for Nanothermometry. *Chem. Mater.* 27(1):235-44.
- [182] Wortmann L, Suyari S, Ube T, Kamimura M, Soga K (2018) Tuning the Thermal Sensitivity of β-NaYF₄: Yb³⁺, Ho³⁺, Er³⁺ Nanothermometers for Optimal Temperature Sensing in OTN-NIR (NIR II/III) biological window. *J. Lumin.* 198:236-42.
- [183] Quintanilla M, Cantelar E, Cussó F, Villegas M, Caballero A C (2011) Temperature Sensing with Up-Converting Submicron-Sized LiNbO₃:Er³⁺/Yb³⁺ Particles. *Appl. Phys. Express* 4(2):22601.

- [184] Cerón EN, Ortgies DH, Del Rosal B, Ren F, Benayas A, Vetrone F, Ma D, Sanz-Rodríguez F, Solé JG, Jaque D, Rodríguez EM (2015) Hybrid Nanostructures for High-Sensitivity Luminescence Nanothermometry in the Second Biological Window. *Adv. Mater.* 27(32):4781-7.
- [185] Yang Y, Kong W, Li H, Liu J, Yang M, Huang H, Liu Y, Wang Z, Wang Z, Sham TK, Zhong J (2015) Fluorescent N-Doped Carbon Dots as *in Vitro* and *in Vivo* Nanothermometer. *ACS Appl. Mater. Interfaces* 7(49):27324-30.
- [186] Wu J, Liu W, Ge J, Zhang H, Wang P (2011) New Sensing Mechanisms for Design of Fluorescent Chemosensors Emerging in Recent Years. *Chem. Soc. Rev.* 40(7):3483-95.
- [187] Howes PD, Chandrawati R, Stevens MM (2014) Colloidal Nanoparticles as Advanced Biological Sensors. *Science* 346(6205):1247390.
- [188] Mattsson L, Wegner KD, Hildebrandt N, Soukka T (2015) Upconverting Nanoparticle to Quantum Dot FRET for Homogeneous Double-Nano Biosensors. *RSC Adv.* 5(18):13270-7.
- [189] Cheng X, Cen Y, Xu G, Wei F, Shi M, Xu X, Sohail M, Hu Q (2018) Aptamer Based Fluorometric Determination of ATP by Exploiting the FRET between Carbon Dots and Graphene Oxide. *Microchim. Acta* 185(2):144.
- [190] Long Q, Wen Y, Li H, Zhang Y, Yao S (2017) A Novel Fluorescent Biosensor for Detection of Silver Ions Based on Upconversion Nanoparticles. *J. Fluoresc.* 27(1):205-11.
- [191] Wei R, Wei Z, Sun L, Zhang J Z, Liu J, Ge X, Shi L (2016) Nile Red Derivative-Modified Nanostructure for Upconversion Luminescence Sensing and Intracellular Detection of Fe³⁺ and MR Imaging. *ACS Appl. Mater. Interfaces* 8(1):400-10.
- [192] Li Z, Yuan H, Yuan W, Su Q, Li F (2018) Upconversion Nanoprobes for Biodetections. *Coord. Chem. Rev.* 354:155-68.
- [193] Wang F, Zhang C, Xue Q, Li H, Xian Y (2017) Label-Free Upconversion Nanoparticles-Based Fluorescent Probes for Sequential Sensing of Cu²⁺, Pyrophosphate and Alkaline Phosphatase Activity. *Biosens. Bioelectron.* 95:21-6.
- [194] Cui S, Xu S, Song H, Xu W, Chen X, Zhou D, Yin Z, Han W (2015) Highly Sensitive and Selective Detection of Mercury Ions Based on Up-Conversion FRET from NaYF₄:Yb³⁺/Er³⁺ Nanophosphors to CdTe Quantum Dots. *RSC Adv.* 5(120):99099-106.
- [195] Fang A, Chen H, Li H, Liu M, Zhang Y, Yao S (2017) Glutathione Regulation-Based Dual-Functional Upconversion Sensing-Platform for Acetylcholinesterase Activity and Cadmium Ions. *Biosens. Bioelectron.* 87:545-51.
- [196] Li Z, Lv S, Wang Y, Chen S, Liu Z (2015) Construction of LRET-based Nanoprobe Using Upconversion Nanoparticles with Confined Emitters and Bared Surface as Luminophore. *J. Am. Chem. Soc.* 137(9):3421-7.
- [197] Chen H, Fang A, He L, Zhang Y, Yao S (2017) Sensitive Fluorescent Detection of H₂O₂ and Glucose in Human Serum Based on Inner Filter Effect of Squaric Acid-Iron(III) on the Fluorescence of Upconversion Nanoparticle. *Talanta* 164:580-7.
- [198] Zhao B, Li Y (2018) Facile Synthesis of Near-Infrared-Excited NaYF₄:Yb³⁺,Tm³⁺ Nanoparticles for Label-Free Detection of Dopamine in Biological Fluids. *Talanta* 179:478-84.
- [199] Cen Y, Tang J, Kong X-J, Wu S, Yuan J, Yu R-Q, Chu X (2015) A Cobalt Oxyhydroxide-Modified Upconversion Nanosystem for Sensitive Fluorescence Sensing of Ascorbic Acid in Human Plasma. *Nanoscale* 7(33):13951-7.
- [200] Guan Y, Qu S, Li B, Zhang L, Ma H, Zhang L (2016) Ratiometric Fluorescent Nanosensors for Selective Detecting Cysteine with Upconversion Luminescence. *Biosens. Bioelectron.* 77:124-30.
- [201] Long Q, Fang A, Wen Y, Li H, Zhang Y, Yao S (2016) Rapid and Highly-Sensitive Uric Acid Sensing Based on Enzymatic Catalysis-Induced Upconversion Inner Filter Effect. *Biosens. Bioelectron.* 86:109-14.
- [202] Alonso-Cristobal P, Vilela P, El-Sagheer A, Lopez-Cabarcos E, Brown T, Muskens OL, Rubio-Retama J, Kanaras AG (2015) Highly Sensitive DNA Sensor Based on Upconversion Nanoparticles and Graphene Oxide. *ACS Appl. Mater. Interfaces* 7(23):12422-9.

- [203] Yuan F, Chen H, Xu J, Zhang Y, Wu Y, Wang L (2014) Aptamer-Based Luminescence Energy Transfer from Near-Infrared-to-Near-Infrared Upconverting Nanoparticles to Gold Nanorods and its Application for the Detection of Thrombin. *Chem. Eur. J.* 20(10):2888-94.
- [204] Zhang L, Ling B, Wang L, Chen H (2017) A Near-Infrared Luminescent Mn²⁺-doped NaYF₄:Yb,Tm/Fe³⁺ Upconversion Nanoparticles Redox Reaction System for the Detection of GSH/Cys/AA. *Talanta* 172:95-101.
- [205] Li J, Zuo G, Pan X, Wei W, Qi X, Su T, Dong W (2018) Nitrogen-Doped Carbon Dots as a Fluorescent Probe for the Highly Sensitive Detection of Ag⁺ and Cell Imaging. *Luminescence* 33(1):243-8.
- [206] Yu J, Song N, Zhang YK, Zhong SX, Wang AJ, Chen J (2015) Green Preparation of Carbon Dots by *Jinhua Bergamot* for Sensitive and Selective Fluorescent Detection of Hg²⁺ and Fe³⁺. *Sens. Actuator. B. Chem.* 214:29-35.
- [207] Zhang Z, Shi Y, Pan Y, Cheng X, Zhang L, Chen J, Li MJ, Yi C (2014) Quinoline Derivative- Functionalized Carbon Dots as a Fluorescent Nanosensor for Sensing and Intracellular Imaging of Zn²⁺. *J. Mater. Chem. B* 2(31):5020-7.
- [208] Chen J, Li Y, Lv K, Zhong W, Wang H, Wu Z, Yi P, Jiang J (2016) Cyclam-Functionalized Carbon Dots sensor for Sensitive and Selective Detection of Copper(II) Ion and Sulfide Anion in Aqueous Media and its Imaging in Live Cells. *Sens. Actuator. B. Chem.* 224:298-306.
- [209] Hou Y, Lu Q, Deng J, Li H, Zhang Y (2015) One-Pot Electrochemical Synthesis of Functionalized Fluorescent Carbon Dots and their Selective Sensing for Mercury Ion. *Anal. Chim. Acta* 866:69-74.
- [210] Kumar A, Chowdhuri AR, Laha D, Mahto TK, Karmakar P, Sahu SK (2017) Green Synthesis of Carbon Dots from *Ocimum Sanctum* for Effective Fluorescent Sensing of Pb²⁺ Ions and Live Cell Imaging. *Sens. Actuators B Chem.* 242:679-86.
- [211] Karfa P, Roy E, Patra S, Kumar S, Tarafdar A, Madhuri R, Sharma PK (2015) Amino Acid Derived Highly Luminescent, Heteroatom-Doped Carbon Dots for Label-Free Detection of Cd²⁺/Fe³⁺, Cell Imaging and Enhanced Antibacterial Activity. *RSC Adv.* 5:58141-53.
- [212] Ankireddy SR, Kim J (2018) Highly Selective and Sensitive Detection of Calcium (II) Ions in Human Serum Using Novel Fluorescent Carbon Dots. *Sens. Actuator. B Chem.* 255:3425-33.
- [213] Zhang Y, Yang X, Gao Z (2015) *In Situ* Polymerization of Aniline on Carbon Quantum Dots: A New Platform for Ultrasensitive Detection of Glucose and Hydrogen Peroxide. *RSC Adv.* 5(28):21675-80.
- [214] Zhu L, Xu G, Song Q, Tang T, Wang X, Wei F, Hu Q (2016) Highly Sensitive Determination of Dopamine by a Turn-On Fluorescent Biosensor Based on Aptamer Labeled Carbon Dots and Nano-Graphite. *Sens. Actuator. B Chem.* 231:506-12.
- [215] Kong W, Di Wu, Li G, Chen X, Gong P, Sun Z, Chen G, Xia L, You J, Wu Y (2017) A Facile Carbon Dots Based Fluorescent Probe for Ultrasensitive Detection of Ascorbic Acid in Biological Fluids *via* Non-Oxidation Reduction Strategy. *Talanta* 165:677-84.
- [216] Zhang Y, Cui P, Zhang F, Feng X, Wang Y, Yang Y, Liu X (2016) Fluorescent Probes for "Off-On" Highly Sensitive Detection of Hg²⁺ and L-Cysteine Based on Nitrogen-Doped Carbon Dots. *Talanta* 152:288-300.
- [217] Wang H, Lu Q, Hou Y, Liu Y, Zhang Y (2016) High Fluorescence S, N Co-Doped Carbon Dots as an Ultra-Sensitive Fluorescent Probe for the Determination of Uric Acid. *Talanta* 155:62-9.
- [218] Qaddare SH, Salimi A (2017) Amplified Fluorescent Sensing of DNA Using Luminescent Carbon Dots and AuNPs/GO as a Sensing Platform: A Novel Coupling of FRET and DNA Hybridization for Homogeneous HIV-1 Gene Detection at Femtomolar Level. *Biosens. Bioelectron.* 89:773-80.
- [219] Zhang L, Cui P, Zhang B, Gao F (2013) Aptamer-Based Turn-on Detection of Thrombin in Biological Fluids Based on Efficient Phosphorescence Energy Transfer from Mn-doped ZnS Quantum Dots to Carbon Nanodots. *Chem.: Eur. J.* 19(28):9242-50.
- [220] Zhong Q, Chen Y, Su A, Wang Y (2018) Synthesis of Catalytically Active Carbon Quantum Dots and its Application for Colorimetric Detection of Glutathione. *Sensors and Actuators B: Chemical* 273:1098-102.

- [221] Jia K, He X, Zhou X, Zhang D, Wang P, Huang Y, Xiaobo L (2018) Solid State Effective Luminescent Probe Based on CdSe@CdS/Amphiphilic Co-Polyarylene Ether Nitrile Core-Shell Superparticles for Ag⁺ Detection and Optical Strain Sensing. *Sens. Acutator. B Chem.* 257:442-50.
- [222] Zhou M, Guo J, Yang C (2018) Ratiometric Fluorescence Sensor for Fe³⁺ Ions Detection Based on Quantum Dot-Doped Hydrogel Optical Fiber. *Sens. Acutator. B Chem.* 264:52-8.
- [223] Wu L, Guo QS, Liu YQ, Sun QJ (2015) Fluorescence Resonance Energy Transfer-Based Ratiometric Fluorescent Probe for Detection of Zn²⁺ Using a Dual-Emission Silica-Coated Quantum Dots Mixture. *Anal. Chem.* 87(10):5318-23.
- [224] Zhang K, Guo J, Nie J, Du B, Xu D (2014) Ultrasensitive and Selective Detection of Cu²⁺ in Aqueous Solution with Fluorescence Enhanced CdSe Quantum Dots. *Sens. Acutator. B Chem.* 190:279-87.
- [225] Wang S, Liu R, Li C (2018) Highly Selective and Sensitive Detection of Hg²⁺ Based on Förster Resonance Energy Transfer between CdSe Quantum Dots and gC₃N₄ Nanosheets. *Nanoscale Res. Lett.* 13(1):235.
- [226] Lou Y, Zhao Y, Chen J, Zhu JJ (2014) Metal Ions Optical Sensing by Semiconductor Quantum Dots. *J. Mater. Chem. C* 2:595-613.
- [227] Liu S, Wang H, Cheng Z, Liu H (2016) Hexametaphosphate-Capped Quantum Dots as Fluorescent Probes for Detection of Calcium Ion and Fluoride. *Sens. Actuator. B Chem.* 232:306-12.
- [228] Miao Y, Yang M, Yan G (2016) Self-Assembly of Phosphorescent Quantum Dots/Boronic-Acid - Substituted Viologen Nanohybrids Based on Photoinduced Electron Transfer for Glucose Eetection in Aqueous Solution. *RSC Adv.* 6:8588-93.
- [229] Ankireddy SR, Kim J (2015) Selective Detection of Dopamine in the Presence of Ascorbic Acid *via* Fluorescence Quenching of InP/ZnS Quantum Dots. *International Journal of Nanomedicine* 10:113-9.
- [230] Ganiga M, Cyriac J (2016) An Ascorbic Acid Sensor Based on Cadmium Sulphide Quantum Dots. *Anal. Bioanal. Chem.* 408:3699-706.
- [231] Chao MR, Hu CW, Chen JL (2014) Fluorescent Turn-On Detection of Cysteine using a Molecularly Imprinted Polyacrylate Linked to Allylthiol-Capped CdTe Quantum Dots. *Microchim Acta* 181:1085-91.
- [232] Azmi NE, Ramli NI, Abdullah J, Abdul Hamid MA, Sidek H, Abd Rahman S, Ariffin N, Yusof NA (2015) A Simple and Sensitive Fluorescence Based Biosensor for the Determination of Uric Acid Using H₂O₂-Sensitive Quantum Dots/Dual Enzymes. *Biosens. Bioelectron.* 67:129-33.
- [233] Jie G, Qin Y, Meng Q, Wang J (2015) Autocatalytic Amplified Detection of DNA Based on a CdSe Quantum Dot/Folic Acid Electrochemiluminescence Energy Transfer System. *Analyst* 140:79-82.
- [234] Wang GL, Hu XL, Wu XM, Dong YM, Li ZJ (2016) Fluorescent Aptamer-Based Assay for Thrombin with Large Signal Amplification Using Peroxidase Mimetics. *Microchim. Acta* 183:765-71.
- [235] Chen J, Huang Z, Meng H, Zhang L, Ji D, Liu J, Yu F, Qu L, Li Z (2018) A Facile Fluorescence Lateral Flow Biosensor for Glutathione Detection Based on Quantum Dots-MnO₂ Nanocomposites. *Sens. Actuator. B Chem.* 260:770-7.
- [236] Zhong Y, Ma Z, Zhu S, Yue J, Zhang M, Antaris AL, Yuan J, Cui R, Wan H, Zhou Y, Wang W (2017) Boosting the Down-Shifting Luminescence of Rare-Earth Nanocrystals for Biological Imaging beyond 1500 nm *Nat. Commun.* 8:737.
- [237] Zhai X, Zhang P, Liu C, Bai T, Li W, Dai L, Liu W (2012) Highly Luminescent Carbon Nanodots by Microwave-Assisted Pyrolysis. *Chem. Commun.* 48:7955-7.
- [238] Yang X, Wang Y, Shen X, Su C, Yang J, Piao M, Jia F, Gao G, Zhang L, Lin Q (2017) One-Step Synthesis of Photoluminescent Carbon Dots with Excitation-Independent Emission for Selective Bioimaging and Gene Delivery. *J. Colloid Interface Sci.* 492:1-7.
- [239] Ruan S, Qian J, Shen S, Chen J, Zhu J, Jiang X, He Q, Yang W, Gao H (2014) Fluorescent Carbonaceous Nanodots for Noninvasive Glioma Imaging After Angiopep-2 Decoration, *Bioconjugate Chem.* 25:2252-9.
- [240] Xiong L, Chen Z, Tian Q, Cao T, Xu C, Li F (2009) High Contrast Upconversion Luminescence Targeted Imaging *in Vivo* Using Peptide-Labeled Nanophosphors. *Anal. Chem.* 81:8687-94.

- [241] Ai F, Ju Q, Zhang X, Chen X, Wang F, Zhu G (2015) A Core-Shell-Shell Nanoplatform Upconverting Near-Infrared Light at 808 nm for Luminescence Imaging and Photodynamic Therapy of Cancer. *Sci. Rep.* 5:10785.
- [242] Chen G, Shen J, Ohulchanskyy TY, Patel NJ, Kutikov A, Li Z, Song J, Pandey RK, Ågren H, Prasad PN, Han G (2012) $(\alpha\text{-NaYbF}_4\text{:Tm}^{3+})/\text{CaF}_2$ core/shell Nanoparticles with Efficient Near-Infrared to Near-Infrared Upconversion for High-Contrast Deep Tissue Bioimaging. *ACS Nano* 6:8280-7.
- [243] Liu X, Que I, Kong X, Zhang Y, Tu L, Chang Y, Wang TT, Chan A, Löwik CW, Zhang H (2015) *In Vivo* 808 nm Image-Guided Photodynamic Therapy Based on an Upconversion Theranostic Nanoplatform. *Nanoscale* 7:14914-23.
- [244] Liu X, Braun GB, Zhong H, Hall DJ, Han W, Qin M, Zhao C, Wang M, She ZG, Cao C, Sailor MJ (2016) Tumor-Targeted Multimodal Optical Imaging with Versatile Cadmium-Free Quantum Dots. *Adv. Funct. Mater.* 26:267-76.
- [245] Guo W, Sun X, Jacobson O, Yan X, Min K, Srivatsan A, Niu G, Kiesewetter DO, Chang J, Chen X (2015) Intrinsically Radioactive $^{64}\text{CuCuInS/ZnS}$ Quantum Dots for PET and Optical Imaging: Improved Radiochemical Stability and Controllable Cerenkov Luminescence. *ACS Nano* 9:488-95.
- [246] Lv G, Guo W, Zhang W, Zhang T, Li S, Chen S, Eltahan AS, Wang D, Wang Y, Zhang J, Wang PC (2016) Near-Infrared Emission CuInS/ZnS Quantum Dots: All-in-One Theranostic Nanomedicines with Intrinsic Fluorescence/Photoacoustic Imaging for Tumor Phototherapy. *ACS Nano* 10:9637-45.
- [247] Albrecht T, Zhao Y, Nguyen TH, Campbell RE, Johnson JD (2015) Fluorescent Biosensors Illuminate Calcium Levels within Defined Beta-Cell Endosome Subpopulations. *Cell Calcium* 57:263-74.
- [248] Zhao Y, Hu Q, Cheng F, Su N, Wang A, Zou Y, Hu H, Chen X, Zhou HM, Huang X, Yang K (2015) SoNar, a Highly Responsive NAD^+/NADH Sensor, Allows High-Throughput Metabolic Screening of Anti-tumor Agents. *Cell Metab.* 21(5):777-89.
- [249] Suzuki K, Kimura T, Shinoda H, Bai G, Daniels MJ, Arai Y, Nakano M, Nagai T (2016) Five Color Variants of Bright Luminescent Protein for Real-Time Multicolor Bioimaging. *Nat. Commun.* 7:13718.
- [250] Kakimoto Y, Tashiro S, Kojima R, Morozumi Y, Endo T, Tamura Y (2018) Visualizing Multiple Interorganelle Contact Sites Using the Organelle-Targeted Split-GFP System. *Sci. Rep.* 8(1):6175.
- [251] Pakhomov AA, Martynov VI, Orsa AN, Bondarenko AA, Chertkova RV, Lukyanov KA, Petrenko AG, Deyev IE (2017) Fluorescent Protein Dendra2 as a Ratiometric Genetically Encoded pH-Sensor. *Biochem. Biophys. Res. Commun.* 493 (4):1518-21.
- [252] Germond A, Fujita H, Ichimura T, Watanabe TM (2016) Design and Development of Genetically Encoded Fluorescent Sensors to Monitor Intracellular Chemical and Physical Parameters. *Biophys. Rev.* 8(2):121-38.
- [253] Kang YF, Fang YW, Li YH, Li W, Yin XB (2015) Nucleus-Staining with Biomolecule-Mimicking Nitrogen-Doped Carbon Dots Prepared by a Fast Neutralization Heat Strategy. *Chem. Commun.* 51(95):16956-9.
- [254] Hua XW, Bao YW, Wu FG (2018) Fluorescent Carbon Quantum Dots with Intrinsic Nucleolus-Targeting Capability for Nucleolus Imaging and Enhanced Cytosolic and Nuclear Drug Delivery. *ACS Appl. Mater. Interfaces* 10(13):10664-77.
- [255] Duan C, Liang L, Li L, Zhang R, Xu ZP (2018) Recent Progress in Upconversion Luminescence Nanomaterials for Biomedical Applications. *J. Mater. Chem. B* 6(2):192-209.
- [256] Tan M, del Rosal B, Zhang Y, Rodríguez EM, Hu J, Zhou Z, Fan R, Ortgies DH, Fernández N, Chaves-Coira I, Núñez Á, Jaque D, Chen G (2018) Rare-Earth-Doped Fluoride Nanoparticles with Engineered Long Luminescence Lifetime for Time-Gated *in Vivo* Optical Imaging in the Second Biological Window. *Nanoscale* 10(37):17771-80.
- [257] Park YI, Lee KT, Suh YD, Hyeon T (2015) Upconverting Nanoparticles: A Versatile Platform for Wide-Field Two-Photon Microscopy and Multi-Modal *in Vivo* Imaging. *Chem. Soc. Rev.* 44(6):1302-17.

- [258] Liang X, Grice JE, Zhu Y, Liu D, Sanchez WY, Li Z, Crawford DH, Le Couteur DG, Cogger VC, Liu X, Xu ZP (2015) Intravital Multiphoton Imaging of the Selective Uptake of Water-Dispersible Quantum Dots into Sinusoidal Liver Cells. *Small* 11(14):1711-20.
- [259] Ramos-Gomes F, Bode J, Sukhanova A, Bozrova SV, Saccomano M, Mitkovski M, Krueger JE, Wege AK, Stuehmer W, Samokhvalov PS, Baty D (2018) Single- and Two-Photon Imaging of Human Micrometastases and Disseminated Tumour Cells with Conjugates of Nanobodies and Quantum Dots. *Sci. Rep.* 8(1):4595.
- [260] Sukhanova A, Hafian H, Turini M, Chames P, Baty D, Pluot M, Cohen JHM, Millot JM, Nabiev I (2016) Multiphoton Imaging of Tumor Biomarkers *in situ* Using Single-domain Antibodies Conjugated with Quantum Dots in a Set Orientation. *Mater. Today: Proceedings* 3(2):523-6.
- [261] Dehghani A, Ardekani SM, Hassan M, Gomes VG (2018) Collagen Derived Carbon Quantum Dots for Cell Imaging in 3D scaffolds *via* Two-Photon Spectroscopy. *Carbon* 131:238-45.
- [262] Lan M, Zhao S, Zhang Z, Yan L, Guo L, Niu G, Zhang J, Zhao J, Zhang H, Wang P, Zhu G (2017) Two-Photon-Excited Near-Infrared Emissive Carbon Dots as Multifunctional Agents for Fluorescence Imaging and Photothermal Therapy. *Nano Res.* 10(9):3113-23.
- [263] Di Yang, Guan S, Niu Y, Xie Z, Zhou S, Qu X (2018) Construction of a Hypoxia Responsive Upconversion Nanosensor for Tumor Imaging by Fluorescence Resonance Energy Transfer from Carbon Dots to Ruthenium Complex. *J. Mater. Chem. B* 6(15):2315-22.
- [264] Wong G, Wang J, Wang R, Guo X, He L, Qiu F, Wang G, Zhu B, Zhu X, Liu T (2015) Amorphous Carbon Dots with High Two-Photon Fluorescence for Cellular Imaging Passivated by Hyperbranched Poly(amino amine). *J. Mater. Chem. B* 3(34):700-6.
- [265] Sato M, Kawano M, Yanagawa Y, Hayashi Y (2016) *In Vivo* Two-Photon Imaging of Striatal Neuronal Circuits in Mice. *Neurobiol. Learn. Mem.* 135:146-51.
- [266] Guo D, Zou J, Rensing N, Wong M (2017) *In vivo* Two-Photon Imaging of Astrocytes in GFAP-GFP Transgenic Mice. *PLoS One* 12(1):e0170005.
- [267] Chu J, Oh Y, Sens A, Ataie N, Dana H, Macklin JJ, Laviv T, Welf ES, Dean KM, Zhang F, Kim BB (2016) A Bright Cyan-Excitable Orange Fluorescent Protein Facilitates Dual-Emission Microscopy and Enhances Bioluminescence Imaging *in Vivo*. *Nat. Biotechnol.* 34(7):760-7.
- [268] Wu J, Abdelfattah AS, Miraucourt LS, Kutsarova E, Ruangkittisakul A, Zhou H, Ballanyi K, Wicks G, Drobizhev M, Rebane A, Ruthazer ES (2014) A Long Stokes Shift Red Fluorescent Ca^{2+} Indicator Protein for Two-Photon and Ratiometric Imaging. *Nat. Commun.* 5:5262.

CHAPTER 2

Motivation and aim of the work

Upconversion nanoparticles (UCNPs) are a class of fascinating materials with many promising properties. Those make them useful probes in bioanalysis as shown in Chapter 1. However, the low upconversion efficiency as well as the challenging physical properties of UCNPs including colloidal and chemical stability are critical issues that need to be addressed to bring UCNPs into bioanalytical applications.

Motivated by this the aim of the work was

- a) to provide a detailed insight and understanding on the impact of the UCNPs' surface chemistry for chemical and colloidal stability in aqueous dispersions,
- b) to derive and realize a concept to apply UCNPs in a biosensing application enabling self-referenced continuous online monitoring in a complex matrix.

Upconversion nanoparticles can be excited in the NIR leading to a high signal-to-noise ratio due to limited autofluorescence. Additionally, due to the presence of several emission bands of lanthanide doped NaYF₄ those particles are very attractive for the development of an enzymatic sensor.

So far, a major drawback of UCNPs is their low quantum yield demanding high excitation laser power density or extremely sensitive detection systems to achieve high sensitivity in a sensing application. This limits the practical application. To make these particles accessible for bioanalytics sophisticated architectures are required, *e.g.* realized by surface engineering *via* the growth of an additional inert shell. Also, the ligands attached to the UCNPs are essential to obtain a colloidal stable system. Up to now, there is only limited information available and only recently it was reported that the chemical stability of particles based on a NaYF₄ host material is limited in water [1,2]. Therefore, a thorough study of different surface cappings should reveal valuable information for designing UCNPs for biosensor applications.

After the successful design of the nanoprobe itself, the requirements for its bioanalytical applications need to be considered. One task was to design a self-referenced continuous online monitoring setup. However, under the common excitation wavelength of 980 nm, water quenching and sample heating is a major problem that needs to be addressed during this sensor engineering. A possibility to overcome this problem is the change of the excitation wavelength to 808 nm using tandem sensitized UCNPs. Those particles have a special core/shell architecture with a NaYF₄(Yb,Tm) core and a NaYF₄(Yb,Nd) shell.

To gain selectivity for a sensor a functionalization by a receptor needs to be realized. For the online measurement of an analyte *via* an enzymatic linked reaction, the particles and the enzyme need to be linked together to warrant colloidal and chemical stability. A hydrogel was chosen as a matrix to host

both, the nanoprobe, as well as the bioreceptor. Based on this a sensor for the continuous monitoring of lactate in serum was realized.

References

- [1] Estebanez N, González-Béjar M, Pérez-Prieto J (2019) Polysulfonate Cappings on Upconversion Nanoparticles Prevent Their Disintegration in Water and Provide Superior Stability in a Highly Acidic Medium. *ACS Omega*. 4(2):3012-9.
- [2] Dukhno O, Przybilla F, Muhr V, Buchner M, Hirsch T, Mély Y (2018) Time-Dependent Luminescence Loss for Individual Upconversion Nanoparticles upon Dilution in Aqueous Solution. *Nanoscale*. 10(34):15904-10.

CHAPTER 3

Long-term colloidal and chemical stability in aqueous media of NaYF₄-type upconversion nanoparticles modified by ligand-exchange

The surface capping is the essential component of nanoparticles as it provides access to their outstanding properties to the real world. Upconversion nanoparticles are predominantly interesting to be used in a biological environment, due to their excellent optical properties such as the conversion of near-infrared excitation light into emissions in the visible or UV range of the spectrum, high photostability, or the absence of any intermittence. One of the most efficient upconversion nanoparticles, consisting of lanthanide doped NaYF₄, suffers from limited stability in aqueous media. This study investigates a set of five types of surface coatings ranging from small ligands to polymers of different charge and different coordinating groups on monodisperse 28 ± 0.9 nm sized NaYF₄(Yb,Er) nanoparticles modified by a two-step ligand exchange mediated by NOBF₄. Information on the long-term chemical and colloidal stability for highly diluted aqueous dispersions of these particles are acquired by transmission electron microscopy, dynamic light scattering and, the luminescence spectroscopy. The findings are of importance for the development of probes and labels based on upconversion nanoparticles for biological applications.

This chapter has been submitted for publication in “Particle and Particle Systems Characterization” (impact factor 4.4):

Himmelstoß SF, Hirsch T. Long-term Colloidal and Chemical Stability in Aqueous Media of NaYF₄-type Upconversion Nanoparticles Modified by Ligand-Exchange. *Particle and Particle Systems Characterization*, 2019 (accepted July 2019)

Author contributions:

All measurements and synthesis were carried out by SFH. The initial particles NaYF₄(Yb,Er)@OA were prepared during the master’s study of SFH. The manuscript was written by SFH. The article was revised by TH. TH is corresponding author.

3.1 Introduction

Upconversion nanoparticles (UCNPs) established in the last years as versatile luminescent probes due to intense progress in the synthesis enabling complex particle architectures of controlled dimensions [1–3]. As a consequence, also the photophysical principles of photon upconversion, including luminescence efficiency affected by surface quenching and passivation processes have been excessively studied [4–6]. The absence of any background fluorescence in biological media due to the unique optical properties of the upconversion of low energy photons in the near-infrared (NIR) region into high energy emissions in the visible or UV [7] makes this material promising for biological applications. But this comes with several challenges like chemical and colloidal stability in aqueous media or the controlled functionalization by a defined number of receptor molecules [8–10].

Most upconversion nanoparticles described in literature are consisting of a NaYF₄ host lattice as this materials has a preferable low phonon-energy [11] ($\sim 300\text{ cm}^{-1}$) compared to other host materials like fluorides (LiYbF₄, $\sim 460\text{ cm}^{-1}$ [12]), oxides (Y₂O₃, $\sim 591\text{ cm}^{-1}$ [13]) or vanadates (YVO₃, $\sim 890\text{ cm}^{-1}$ [14]). Therefore, it is not surprising that this host material together with Yb³⁺ and Er³⁺ has been used to design the most efficient upconversion nanoparticles [1,15]. However, the synthesis of those nanoparticles is often based on thermal decomposition of lanthanide oleates [16] or acetates [1] in high boiling organic solvents, ending up with a hydrophobic surface ligand (*e.g.* oleic acid) [17]. To make the particles accessible for biological applications, different surface engineering strategies have been developed to render the particles water dispersible [18,19]. Thereby, the simplest method is the removal of the surface ligands assisted by an acid [20]. Alternatively, the removal of the ligands is performed before the addition of a stabilizing agent like citrate. The oleic acid can be removed *via* the acidic form of the surface ligand (*e.g.* citric acid [21]) or by NOBF₄ [22].

Other techniques not requiring the removal of the oleic acid are based on the interaction of amphiphilic molecules and hydrophobic capping agents. As reported by the group of Wolfgang Parak [23] a comb-like polymer consisting of a poly(maleic anhydride) backbone with a modified hydrophobic chain can be used for the successful transfer of colloidal nanoparticles into a hydrophilic environment. During this process, also polymer micelles with no UCNPs inside are generated [24]. This is attributed by the intention to ensure a complete coating of the UCNPs by using an excess of the amphiphilic polymer. Such empty micelles cannot be separated easily from the modified particles and may affect certain applications. For instance, when the polymer is labeled with additional dyes, those empty structures may falsify the results. Another popular strategy is the coating of the particles with silica. Such silica shells can be prepared by the Stöber method, which involves the controlled hydrolysis and condensation of siloxane monomers [25]. However, particles with silica coating often show poor temporal stability under physiological conditions in aqueous dispersions of high salt concentration or in the presence of highly charged ions like phosphates [18].

In many studies, the impact of the surface chemistry is neglected or only tackled with a minor interest in terms of introducing functionalities such as receptors for targeting or labels for imaging. In this study, the colloidal and chemical stability of NaYF₄(Yb,Er) nanoparticles modified by five different surface coatings *via* a two-step ligand exchange assisted by NOBF₄ has been investigated in detail. As this method is not only one of the most versatile ones [26], but also fast and easy to handle, we have focused on this strategy. Regarding the colloidal stability, the relevant forces within a nanoscopic system must be taken into account. Particles without any surface capping tend to minimize their

surface energy by aggregation so that further efforts are inalienable to obtain stable nanoparticles [27].

The five different surface ligands attached to UCNPs of identical size consist of three polymers (poly(acrylic acid) (PAA), polyallylamine (PAH), and polyethylene glycol (PEG)) and two small ligands (citrate (CIT) and N,N-bis(phosphonomethyl)glycine (PG)). This set of particles was used to investigate the concentration dependent colloidal and chemical stability in water over time. Detailed information is presented on different coordination groups stabilizing a particle and how the disintegration of the particles is influenced by ions present in the solution.

3.2 Materials and methods

3.2.1 Chemicals

Oleic acid and 1-octadecene (both technical grade, 90%) were purchased from Alfa Aesar (www.alfa.com). Lanthanide chloride hexahydrates (YbCl₃ · 6 H₂O, YCl₃ · 6 H₂O and ErCl₃ · 6 H₂O each >99.99%) were obtained from Sigma Aldrich and Treibacher Industrie AG. Ammonium fluoride, sodium hydroxide (both analytical grade), nitrosyl tetrafluoroborate (95%), N,N bis(phosphonomethyl)glycine (PG, 98%), sodium fluoride (KF), ytterbium nitrate (Y(NO₃)₃), poly(acrylic acid) sodium salt (PAA, M_w ≈ 2,100), trisodium citrate (CIT), polyallylamine hydrochloride (PAH, M_w ≈ 15,000), polyethylene glycol (M_w ≈ 12,000) and ethylenediaminetetraacetic acid (EDTA) were obtained from Sigma Aldrich. The water standard (Aquastar, 5 mg·mL⁻¹) and the CombiCoulomat fritless Karl Fischer reagent were purchased from Merck. All other chemicals were of analytical grade. All chemicals were used as received without further purification. Double distilled (dd) water was used for the preparation of all aqueous solutions.

3.2.2 Characterization and measurement methods

Transmission electron microscopy (TEM) was carried out with a 120 kV Phillips CM12 microscope. For sample preparation, a particle dispersion (~1.5 mg·mL⁻¹ in cyclohexane or dd water) was dropped on a copper grid (coated with carbon, 400 mesh). The obtained micrographs were analyzed with the software ImageJ. Dynamic light scattering and ζ-potential measurements were carried out on a Malvern Zetasizer Nano ZS at 20 °C. For the determination of the particle concentration and the doping ratios of the rare-earth ions within the UCNPs, mass spectrometry combined with inductively coupled plasma (ICP-MS, ELAN 9000 from Perkin Elmer) was used. For calibration, a multielement standard solution from Perkin Elmer (10000 ppb with various dilutions ranging between 200 and 1 ppb in 5% HNO₃) was utilized. A rhodium standard solution (10000 ppb) in 5% HNO₃ dealt as internal standard. Upconversion samples were prepared by an acidic decomposition of the nanoparticles (~0.3 mg) in 417 μL H₂SO₄ (96% w/v) assisted by ultrasonication. Afterward, the solution was diluted by the addition of 7.083 mL water and 7.5 mL 1 M HNO₃. For the ICP-MS measurement, the particles (1 mL) were diluted additionally with 49 mL 5% HNO₃ and 10 μL of the rhodium standard was added.

For Raman measurements, a DXR Raman microscope from ThermoFischer equipped with a 100× magnification Mplan N objective, a 532 nm laser excitation (0.5 mW) and a 50 μm slit was used. X-ray diffraction patterns were obtained on a STOE STADI P diffractometer equipped with a Dectris Mythen 1K detector (K_{α1} Cu source, λ = 1.54060 Å). Luminescence spectra of UCNPs were recorded with an Aminco Bowman Series 2 luminescence spectrometer equipped with an external continuous wave (CW) 980 nm laser module (200 mW) from Picotronic. All luminescence spectra were recorded at room temperature. For lifetime-measurements, an in-house setup consisting of a 980 nm CW laser module (200 mW, ~15 W·cm⁻²) and an optical chopper was assembled. For the thermogravimetric analysis (TGA) a Perkin Elmer TGA 7 was used. Fourier-transform infrared spectroscopy measurements were performed by an Agilent Technologies Cary630 FTIR spectrometer.

3.2.3 Surface modification of upconversion nanoparticles *via* NOBF₄

For bioanalytical applications, the surface of oleate-capped UCNPs must be engineered *via* a two-step ligand exchange method with the assistance of nitrosyl tetrafluoroborate [28]. Oleate-capped UCNPs (1 mg) and an equal amount of NOBF₄ are added to a two-phase system consisting of equivalent volumes of cyclohexane and N,N-dimethylformamide (DMF). The mixture was stirred vigorously for 10 min at 30 °C. Thereby the oleic acid gets protonated and remains in the cyclohexane (upper) phase, whereas the ligand-free UCNPs get stabilized *via* BF₄⁻ in the DMF phase. The cyclohexane phase is discarded. The UCNPs were precipitated from the DMF phase by addition of an excess of chloroform and centrifuged (1000 g, 5 min). The obtained transparent pellet is washed with chloroform / DMF at least one more time, and then the finally obtained BF₄⁻ stabilized UCNPs were dispersed in DMF.

For the surface modification with CIT, PAA, PAH, PEG, or PG, the dispersion with the BF₄⁻ stabilized UCNPs (~30 mg, 2 mL) was slowly added to a solution of the respective ligand (~30 mg) in water (2 mL) and stirred for additional 20 min. The particles are collected from the solution by centrifugation (21000 g, 30 min) and washed three times to remove the excess of surface ligands. Aggregates are removed by centrifugation (1000 g, 3 min) and the supernatant is collected and stored in the refrigerator at 4 °C.

3.2.4 Surface modification of upconversion nanoparticles *via* HCl

Oleate capped particles are dried (50 mg) and then dissolved in 5 mL HCl (pH 3, 1 mM). The solution was stirred for at least 3 h at 30 °C. Afterwards, the remaining oleate was extracted with 5 mL diethyl ether (three times) to remove the free oleic acid molecules. The particles in water were then precipitated with an excess of acetone and centrifuged at 1000 g for 15 min. The supernatant is discarded. The pellet was redispersed in 5 mL water and stored in the refrigerator at 4 °C.

For the surface modification with PG, the dispersion with the bare UCNPs (~5 mg·mL⁻¹, 1 mL) was slowly added to a solution of the desired ligand (~5 mg) in water (1 mL) and stirred for additional 30 min. The particles are collected from the solution by centrifugation (21000 g, 30 min) and washed three times to remove the excess of the surface ligand. The final dispersion is stored in the refrigerator at 4 °C.

3.2.5 Time-dependent colloidal stability study and the influence of different solution systems

UCNPs with different surface coatings (CIT, PEG, PG, PAA, or PAH) were dispersed in dd water at pH 7. Thereby the mass concentration was varied between 5, 1, 0.5 and 0.1 mg·mL⁻¹. The particles (1 mL) were filled in a mini dialysis device (Slide-A-Lyzer, MWCO = 10 kDa, total volume of 2 mL) and dialysed at 37 °C for several hours. At distinct time steps (2.5, 5, 7.5, 10 and 24 h) the solution for dialysis (50 mL) was changed.

3.3 Results and discussion

3.3.1 Synthesis and design of hydrophilic upconversion nanoparticles

Predominately green emitting UCNPs based on the most common host material NaYF₄ with a doping ratio of 20% Yb³⁺ and 2% Er³⁺ have been synthesized on large-scale by a bottom-up approach [29]. The oleate coated particles of pure hexagonal crystal phase show a diameter of 28 ± 0.9 nm with a narrow size distribution (Figure 3.1 A, B and D) and a phonon energy of 300 cm⁻¹ determined *via* Raman spectroscopy (Figure S3.1). Dynamic light scattering (DLS) measurements of the UCNP dispersion (~5 mg·mL⁻¹) revealed the outstanding long-term colloidal stability of the nanoparticles for at least 4 years in organic solvents (Figure 3.1C).

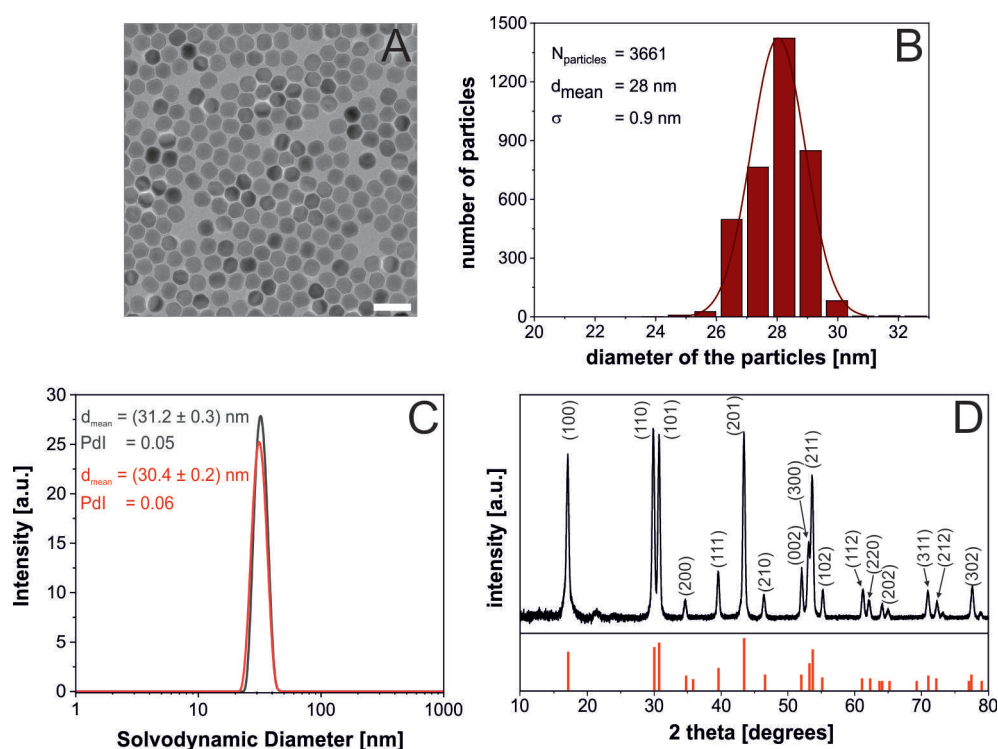


Figure 3.1 | (A) Transmission electron micrographs (scale bar: 60 nm) and (B) corresponding size distribution of oleate-capped NaYF₄(20%Yb,2%Er). (C) Intensity-weighted particle-size distribution obtained by dynamic light scattering of a particle dispersion in cyclohexane (~5 mg·mL⁻¹, n = 3) of UCNPs shortly after the synthesis (red) and after a storage of ~4 years (grey) (D) X-ray diffraction patterns of UCNPs. The pattern in red refers to the standard pattern (ICDD PDF #16-0334) of hexagonal phase NaYF₄.

The doping ratio of the lanthanide ions in the particles matches the ratio of the respective lanthanide chlorides used in the synthesis as confirmed *via* ICP-MS measurements (Table S3.1). These UCNPs co-doped with Yb³⁺ and Er³⁺ show emissions at 522 nm (²H_{11/2} → ⁴I_{15/2}, green) 540 nm (⁴S_{3/2} → ⁴I_{15/2}, green) and 650 nm (⁴F_{9/2} → ⁴I_{15/2}; red) (Figure 3.2) upon excitation with a low-power 980 nm laser module. The absorption cross-section of the Yb³⁺-ions within the nanocrystal was estimated to be $\sim(2.5 \pm 0.1) \cdot 10^{-20}$ cm² (Table S3.2), which corresponds to the value reported in the literature [30]. For the green emission, a decay time of (156 ± 1) μs and for the red emission, one of (226 ± 3) μs was measured with a home-built lifetime-setup (Figure S3.2).

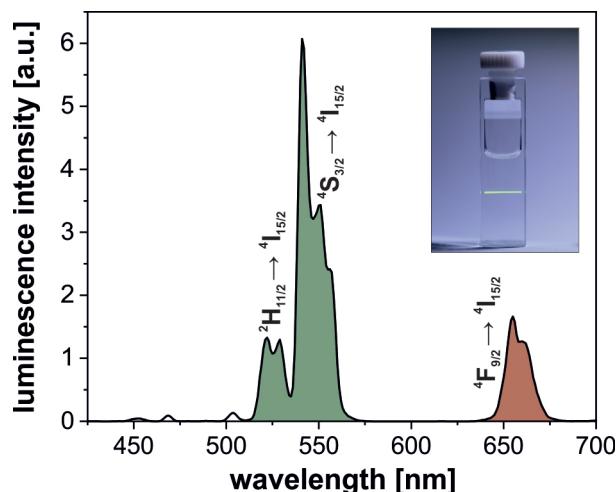


Figure 3.2| Luminescence spectra of NaYF₄(Yb,Er) dispersed in cyclohexane (13 mg·mL⁻¹). A 980 nm CW laser module (200 mW, 15 W·cm⁻²) was used as excitation source. In the insert one can see a digital photograph of UCNPs coated with oleic acid under NIR excitation.

Five different surface-modifications (UCNP@CIT, UCNP@PAA, UCNP@PEG, UCNP@PAH, and UCNP@PG) have been chosen to study the colloidal and luminescence properties of these particles in water. All surface modifications have been prepared from the same batch of oleate capped particles *via* a ligand exchange process assisted by NOBF₄ (Figure 3.3) [28,31].

In the first step, the hydrophobic oleate-capped UCNPs (UCNP@OA) in cyclohexane are mixed with an equivalent volume of DMF leading to a two-phase system. After the addition of NOBF₄ a slightly acidic environment is created, as the NO⁺-ions react with water residues in the DMF and form nitrous acid and H⁺ as reported in the literature (Equation 3.1) [28].



It is desired to strip off the oleate completely. Therefore, an excess of protons is needed. The coverage of oleate on the surface of UCNPs is 60% determined by thermal gravimetric analysis (TGA) (Figure S3.3 and Figure S3.4). Under the assumption that all H⁺, required for this process, come from the reaction of residual water in DMF (~0.2% determined *via* Karl Fischer titration, refer to Chapter 3.6.6 and Figure S3.5) with NO⁺, the minimal required amount of water is depending on the size of the nanoparticles. *E.g.*, for the 28 nm-sized UCNPs ~7300 water molecules per particle are needed (Figure S3.4 and Figure S3.6).

In the course of the reaction, the oleic acid gets removed from the surface of the nanoparticles remaining in the cyclohexane phase. The UCNPs are transferred to the DMF phase, where they are stabilized by BF₄⁻ (UCNP@BF₄). As shown by FTIR-spectroscopy, the typical vibrations of oleic acid can be found only in the cyclohexane phase (Figure S3.7). After ~15 min the phase transfer is complete and no upconversion luminescence can be excited any longer in the cyclohexane phase. The total yield and the composition of the BF₄⁻ stabilized nanoparticles has been determined *via* ICP-MS to be approx. 95% (according to TGA, ~8250 BF₄⁻ molecules coordinate to the surface of one nanoparticle). Figure S3.8 shows the particle-size distribution of BF₄⁻-stabilized UCNPs in DMF in comparison to UCNPs with oleate capping in cyclohexane, indicating colloidal stability of the particles in DMF after the ligand removal due to weakly coordinating BF₄⁻ ions [32].

To complete the phase transfer, BF₄⁻ stabilized UCNPs dispersed in DMF are mixed with an aqueous solution, containing the desired hydrophilic surface ligand. For this study small molecules (like PG and CIT) and polymers (PAH, PAA and PEG) have been investigated in detail. It has to be mentioned that also the composition of the UCNP has to be considered when thinking on the coordination of ligands to the particle surface, as different lanthanide ions prefer different coordination numbers.

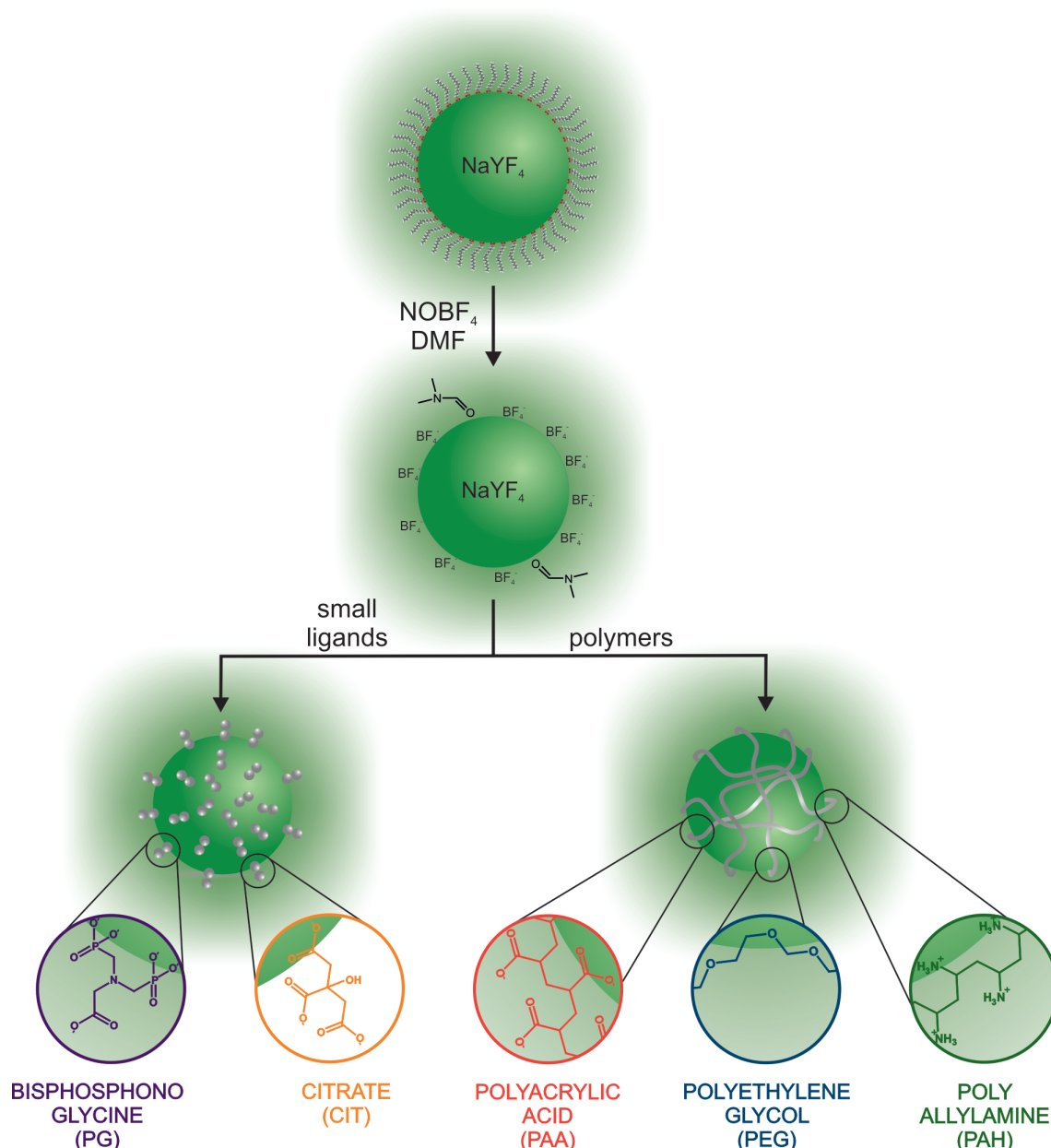


Figure 3.3| Scheme of the two-step ligand exchange for the surface modification of upconversion nanoparticles. In the first step the oleate is removed *via* the addition of NOBF₄. The bare UCNPs are stabilized *via* BF₄⁻ ions. In the next step the particles are modified with the desired ligand (here PG, CIT, PAA, PEG and PAH).

Within a nanocrystal, consisting of NaYF₄, the Y³⁺ ions are coordinated by nine neighboring ions as shown by molecular dynamics simulations [33]. At the surface of bare particles, this number is unsaturated due to the missing of coordination partners and it is possible for ligands to attach *via* coordination towards the Y³⁺ ions. In principle, a large number of free electron pairs provided by the surface ligand could lead to the maximum coordination number. In contrast to this, six-fold coordination is more likely for Yb³⁺ ions [34].

Thereby, changes in the surface coverage as well as in the binding stability for different host materials (e.g. NaYF₄ or NaYbF₄) are expected. Additionally, the shape of the nanoparticles is essential. As shown by the group of Jin [35] phosphate headgroups are capable to coordinate with up to three oxygen atoms towards the Y³⁺. However, the binding energies of the ligands at rod-like structures (hexagonal prism) are changing with the crystal plane, allowing anisotropic surface modifications.

The oleate can also be stripped off by an alternative method, where the particle dispersion is treated by an acid, most likely HCl [20,36–38]. Thereby, the hydrophobic oleate capped UCNPs need to be dispersed in an acidic aqueous system for 2 h (Figure S3.9). Regarding the pK_a of the ligand, which needs to be replaced from the particle surface, the reaction protocol has to be adjusted in terms of reaction time and pH. For the oleate capped particles used in this study, pH 3 and 2 h reaction time are sufficient. This method is somehow trickier than the ligand exchange *via* BF₄⁻, as the mixing of hydrophobic particles with the acidic aqueous phase can come with difficulties, and also due to the tendency of bare particles to minimize their surface energy by forming agglomerates (Figure S3.10 and Figure S3.11). Therefore, it is not surprising that the yield of this method is only in the range of 30 - 35%, according to the ICP-MS measurements. In contrast, the ligand exchange with the BF₄⁻ mediated method yields up to 95%. When comparing both methods for an identical particle system, it was found that the surface coverage achieved by the acid mediated ligand exchange is slightly higher compared to the BF₄⁻ mediated ligand exchange (Figure S3.3). In case of PG as new surface ligand, ~1600 molecules get attached to the surface of the nanoparticles. For the two-step ligand exchange, only ~1200 molecules have been bound. The reason might be, especially for this surface ligand that the pH was more acidic and therefore not all groups of this ligand have been deprotonated. By this, the electrostatic repulsion between two neighboring surface ligands might be lower, which minimizes the distance and therefore leads to a higher surface coverage. By directly comparing both methods, the ligand exchange with NOBF₄ shows several advantages: Besides the short reaction time and easy purification protocol, the particles are electrostatically stabilized throughout the whole process, which reduces the aggregation during the ligand exchange process and increases the yield of the modified UCNPs.

3.3.2 Surface coverage by using small ligands or polymers

Phosphate groups show a very high binding affinity followed by carboxylic groups, when looking at the binding ability of the functional group of the ligand towards the surface of the nanoparticles [17]. Nevertheless, also amine groups [30] and ether groups [39] are capable to coordinate to the lanthanide ions to obtain water dispersible nanoparticles. Consequently, all these kinds have been investigated regarding colloidal as well as chemical stability in aqueous solutions.

PG, with two phosphate groups, is expected to coordinate best to the UCNPs but a surface coverage of only ~20% (Figure S3.3) was found (~1200 PG ligands per UCNP (size 28 nm)). Such low coverage can be explained by electrostatic effects. At neutral pH, PG is four times negatively charged, which leads to a strong electrostatic repulsion at the surface of one nanoparticle (Figure S3.12). Therefore, it is quite obvious that those surfaces cannot be densely covered, a distance between two neighboring PGs can be calculated to be 1.6 nm. The situation is completely different, when a capping agent like poly(acrylic acid) is used. The polymer PAA (M_w ~2.1 kDa) used here consists in average of 30 monomers with each of them providing a carboxylic group which can bind to the surface of the nanoparticles. From TGA characteristics one can calculate from the loss of the total mass that ~520 polymers have been attached to the surface of one nanoparticle. The analysis of the particle size by DLS (as well as the particle distance on the TEM grid) indicates that the polymer forms only a thin layer. Similar findings have been reported for iron oxide

particles covered by PAA [40]. A very simplified assumption that all monomers can coordinate to the particle surface reveals a coverage of 120%. This demonstrates that a large fraction of the polymers does not bind with all carboxylates to the surface. The other extreme would be that the polymers are linked only by one single carboxylate to the surface (surface coverage of 4%) with a distance of 2.4 nm to the next neighbor. This is also quite unexpected and the reality should be somewhere in between.

Especially changes in pH might lead to more or fewer charges at the surface of the particles and prevent a dense surface coating due to electrostatic repulsion. In contrast to PG, PAA molecules are bearing more than one surface charge. In this case, an electrostatic repulsion of the charges is limited due to the polymeric nature of the capping agent. Complementary to the work of Tanmaya [41], the PAA molecules can be seen as crosslinked monomers bearing only one charge. A first glance at the Coulomb-potential shows that systems with a small charge show less repulsion leading to a lower distance between the surface ligands. For an even more detailed description of the electrostatic repulsion of the PAA polymers, it would be interesting to calculate the Coulomb-potential based on the charge density of the polymer (*e.g.* *via* molecular dynamics simulations).

3.3.3 Colloidal stability of hydrophilic upconversion nanoparticles

By comparison of the ligand exchange for small molecules and polymers, one can clearly see the advantage of the larger surface capping. Besides the higher surface coverage of the particles also a huge number of functional groups can contribute to the colloidal stability of these systems and create a dense surface coating. In the case of polymers with strongly coordinating groups like the carboxyl in PAA, the smaller hydrodynamic diameter indicates that the polymer gets tightly wrapped around the particle. For polymers with ether groups (like PEG) or with amine functionalization (PAH), the coordination to the Y³⁺ is slightly weaker. For instance, at pH 7 a large fraction of the amine groups is protonated so that only a few binding sites would be available, leading to a weaker attachment of the polymer chain towards the surface of the particles. An increased hydrodynamic diameter is the consequence. For small molecules like PG, steric reasons prevent the coordination *via* all possible groups and therefore a larger hydrodynamic diameter may be found. Despite the low surface loading of the PG molecules, the Pdl of those UCNPs is in the same range as for UCNPs with polymer coating or with a CIT capping. Also, from TEM studies, no agglomerates are found, and the clear dispersion of the UCNPs prove the colloidal stability of the nanoparticles (Figure 3.4, Figure S3.13 A).

As seen from Table S3.3, the surface ligands not only differ from their binding groups and size (small molecules vs. polymers) but also from their charge (Figure S3.13 B). At pH 7, PG bears four negative charges, whereas CIT is three times deprotonated. The difference of the charge of the surface ligands can also be seen in the ζ -potential. UCNP@PG have a slightly more negative ζ -potential than UCNP@CIT. In the case of polymers like PAA, which cannot distribute their charges by electrostatic repulsion, because of their linkage by chemical bonds, a higher surface coverage compared to the small capping molecules is expected. This is also indicated by a higher ζ -potential (Figure 3.4). In the case of the PAH – which has positively charged amine groups – a similar interaction of the polymer towards the nanoparticle as described for the PAA molecules is present. Consequently, the average surface charge is quite similar, as seen for the PAA.

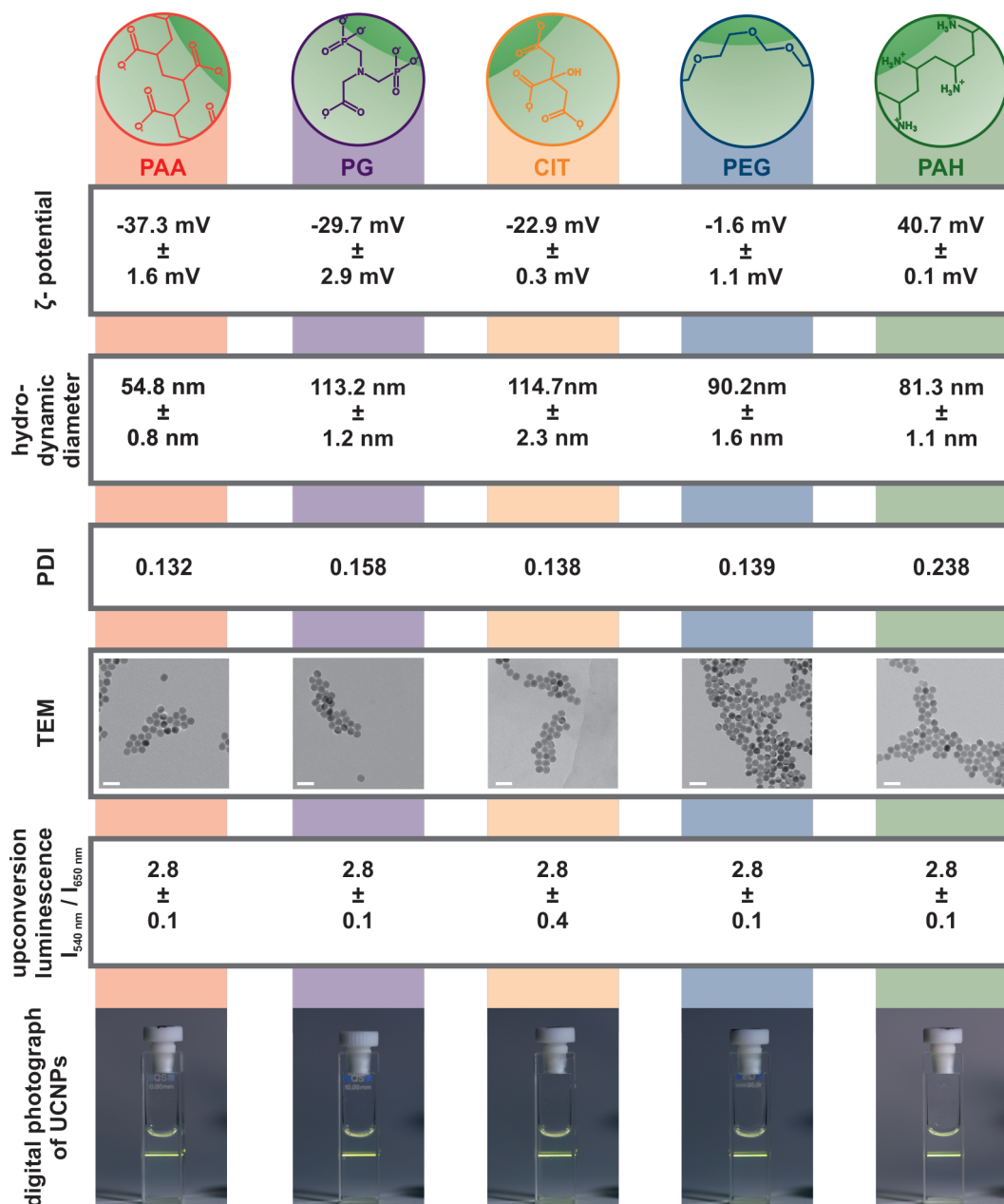


Figure 3.4| Overview of the ζ -potential measurements, intensity-weighted dynamic light scattering measurements and TEM measurements for all particle systems. At the bottom digital photographs of each particle system under 980 nm laser excitation (250 mW, CW, 1.6 mg·mL⁻¹), with corresponding ratio of the emission intensity at 540 nm and 650 nm, are shown. The clear dispersions are an indication for colloidal stability.

All hydrophilic UCNPs can be excited with a 980 nm CW laser module and the typical upconversion emission spectrum of Yb³⁺/Er³⁺ co-doped nanoparticles can be obtained (Figure S3.14). In contrast to the oleic acid capped UCNPs in cyclohexane, the ratio between the green and the red emission band is decreased due to the presence of water quenching. Whereas it is ~3.7:1 for UCNP@OA, $I_{\text{green}}/I_{\text{red}}$ is ~2.8:1 for all types of the here studied hydrophilic UCNPs. This indicates that the shielding against water access to the surface of the particles is very similar for all types of surface modification. Still many lanthanide ions seem not to be completely coordinated by a surface ligand. At those ions, water might act as ligand and consequently quench the upconversion luminescence.

3.3.4 Long-term stability of aqueous dispersion of upconversion nanoparticles

UCNPs with a NaYF₄ host lattice, which have been associated for a long time with excellent chemical stability [7, 42–44] show a very low solubility product of $1.6 \cdot 10^{-26} \text{ M}^6$ [45]. Nevertheless, a small amount of the particles gets dissolved [38,45–47] in water according to the equilibrium reported by the group of Mely [45] and displayed in Equation 3.2



In a saturated solution the concentration of the free ions ($[\text{Na}^+]$, $[\text{Y}^{3+}] = 20 \mu\text{M}$, $[\text{F}^-] = 80 \mu\text{M}$, refer to Chapter 3.6.14) is very low. For a typical stock solution consisting of NaYF₄(20%Yb,2%Er) nanoparticles (28 nm, $5 \text{ mg} \cdot \text{mL}^{-1}$), the amount of fluoride within the nanoparticle is around 900 times higher. Only a neglectable part of about 0.1% of the total F⁻ ions will get dissolved in steady state conditions. Highly diluted systems, with a mass concentrations of $100 \mu\text{g} \cdot \text{mL}^{-1}$, as often used in biological applications become critical. Here, ~5% of the ions get dissolved until the solution reaches its equilibrium.

As seen in the TEM images (Figure S3.15 and Figure S3.16) at $100 \mu\text{g} \cdot \text{mL}^{-1}$ dilution, the morphology of the UCNP@PAH is almost not affected compared to UCNP@OA or UCNP@BF₄⁻. This has also been confirmed by the luminescent signal at 540 nm as well as by the hydrodynamic diameter which both remain quite constant (Figure S3.17). Further reduction of the particle concentration leads to a higher dissolution rate (Figure S3.18). This has a tremendous influence on the storage and usage of highly diluted dispersion of upconversion nanoparticles. For instance, in UCNPs dispersions with $10 \mu\text{g} \cdot \text{mL}^{-1}$ ~50% of the particles will get dissolved in a short time period (Figure S3.19). Already 2.5 h after dilution the luminescence signal and size of the nanoparticles was strongly reduced. Mainly for *in vivo* / *in vitro* applications, the mass concentration is essential. As shown in Table S3.4, cytotoxicity studies are typically covering this range of concentrations. Due to the dissolution of the nanoparticles, one has to consider the potential toxic influence of the released F⁻ ions. In contrast, the amount of UCNPs for applications *in vivo* is often higher (the final concentration in e.g. a mouse (~25 – 35 mg, 1.5 mL blood volume) is ranging between 150 and $3000 \mu\text{g} \cdot \text{mL}^{-1}$) so that in steady state after dissolution of the particles the luminescent properties will only be minimally affected.

Analogous to the different surface coverage also the chemical stability and dissolution behavior of the UCNPs at high dilutions is affected by the presence of small molecules or polymers (Figure 3.5). At a closer look at the negatively charged nanoparticles including UCNPs with CIT, PAA, and PG, those modifications showed no good protection against dissolution. Particles with these surface ligands are characterized by a constant drop in the upconversion luminescence when dialyzed for 24 h. In each case, the luminescent intensity showed a drastic reduction of the luminescence at 650 nm (Figure S3.20) or at 540 nm (Figure S3.21) already at a high mass concentration of $5000 \mu\text{g} \cdot \text{mL}^{-1}$. Both UCNP@CIT and UCNP@PAA still retained ~30% of the initial luminescence intensity, whereas for UCNP@PG only ~15% of the original signal can be measured. An explanation can be found by analyzing the particles by DLS and TEM (Figure S3.21, Figure S3.22 – CIT, Figure S3.23 – PG, and Figure S3.24 – PAA), which indicates an ongoing aggregation of the particles especially for the PG modified UCNPs. Particles with PAA capping are much longer prone to those aggregation effects.

The increase of the Pdl with time is another hint for the instability of these systems (Figure S3.25). On the first glance, an inconsistency of the DLS data with those obtained from luminescence measurements and the electron microscopy might be suspected, but from the complete data set of complementary methods, one can suggest that the aggregation with following precipitation was the reason for the loss of

luminescence. Therefore, it is not easy to make an assumption from the data obtained only by one single technique.

For diluted dispersion of UCNPs (Figure S3.26 and Figure S3.27), the colloidal as well as the chemical stability is affected as expected. The low surface coverage of the small molecules does not sufficiently protect the particle surface against dissolution. Already after 450 min of dialysis for concentrations of 1000 $\mu\text{g}\cdot\text{mL}^{-1}$, a slight change of the morphology of the nanoparticles and a decrease in the upconversion luminescence intensity was observed (Figure S3.26). By using a dispersion with 500 $\mu\text{g}\cdot\text{mL}^{-1}$ the luminescent signal almost vanished for UCNP@CIT and UCNP@PG after 24 h of dialysis (Figure S3.27). For even lower particle concentrations (100 $\mu\text{g}\cdot\text{mL}^{-1}$), the disintegration (strongly) affects the morphology and size of all negatively charged nanoparticles as seen in the TEM images (Figure 3.5). Accompanied by this, a strong loss of the upconversion efficiency as well as an increase in the hydrodynamic diameter due to the agglomeration of the fragmented particles is found.

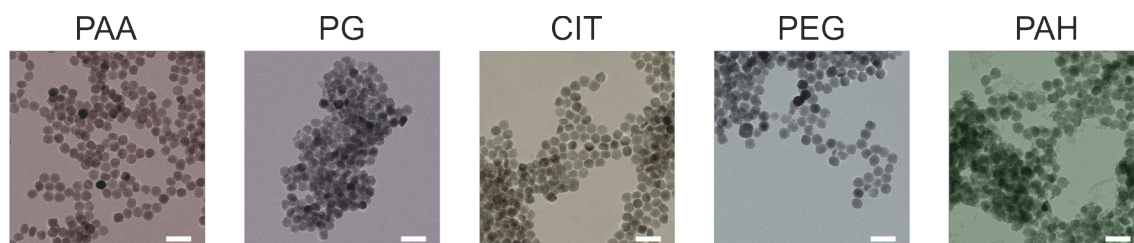


Figure 3.5| TEM images of UCNPs ($100 \mu\text{g}\cdot\text{mL}^{-1}$) with different surface capping (red = PAA, purple = PG, orange = CIT, blue = PEG and green = PAH) after dialysis for 300 min. In the case of a capping with small molecules, aggregation and strong dissolution can be observed. Dissolution effects can also be seen for UCNPs modified with PAH and PEG. UCNP@PAA are more prone to those negative effects.

The dissolution of particles at the smallest concentration reveals again a different trend between the three negative surfaces. For particles modified with small ligands like PG $\sim 70\%$ of the luminescence signal has vanished already after 150 min. For UCNPs with CIT capping a decrease of the luminescence to 30% has been observed after ~ 200 min. In contrast to this PAA modified particles were the most stable ones. After 300 min, the relative change of the luminescence signal has decreased to 30% (Figure 3.6).

For UCNPs with a PEG group at the first glance a much more stable system seems to be present. As seen in Figure S3.28 at the highest concentration, the particles are nearly unaffected in their stability. However due to the weaker binding of the ether groups towards the nanoparticles, at a mass concentration of 1000 $\mu\text{g}\cdot\text{mL}^{-1}$ (after 450 min) also a slight deformation of the nanoparticles can be observed and after 24 h the luminescent signal decreases to 70% (Figure S3.26). Further dilution to 100 $\mu\text{g}\cdot\text{mL}^{-1}$ leads to a similar course as for the other UCNPs (Figure 3.5 and Figure 3.6). After ~ 150 min, around 70% of the initial luminescence at 540 nm has vanished.

Remarkably colloidal and chemical stability was found for UCNPs functionalized by positively charged PAH (Figure S3.29). At a high mass concentration of 5000 $\mu\text{g}\cdot\text{mL}^{-1}$ the upconversion luminescence was almost not affected at all during a dialysis period of 24 h. However, also for the smaller amount (1000 $\mu\text{g}\cdot\text{mL}^{-1}$) a slight change of the morphology of the nanoparticles and an influence on the emission intensity has been observed. Further reduction of the mass concentration to 100 $\mu\text{g}\cdot\text{mL}^{-1}$ leads to a loss $\sim 70\%$ of the initial luminescence signal (Figure 3.6) after only 150 min of dialysis.

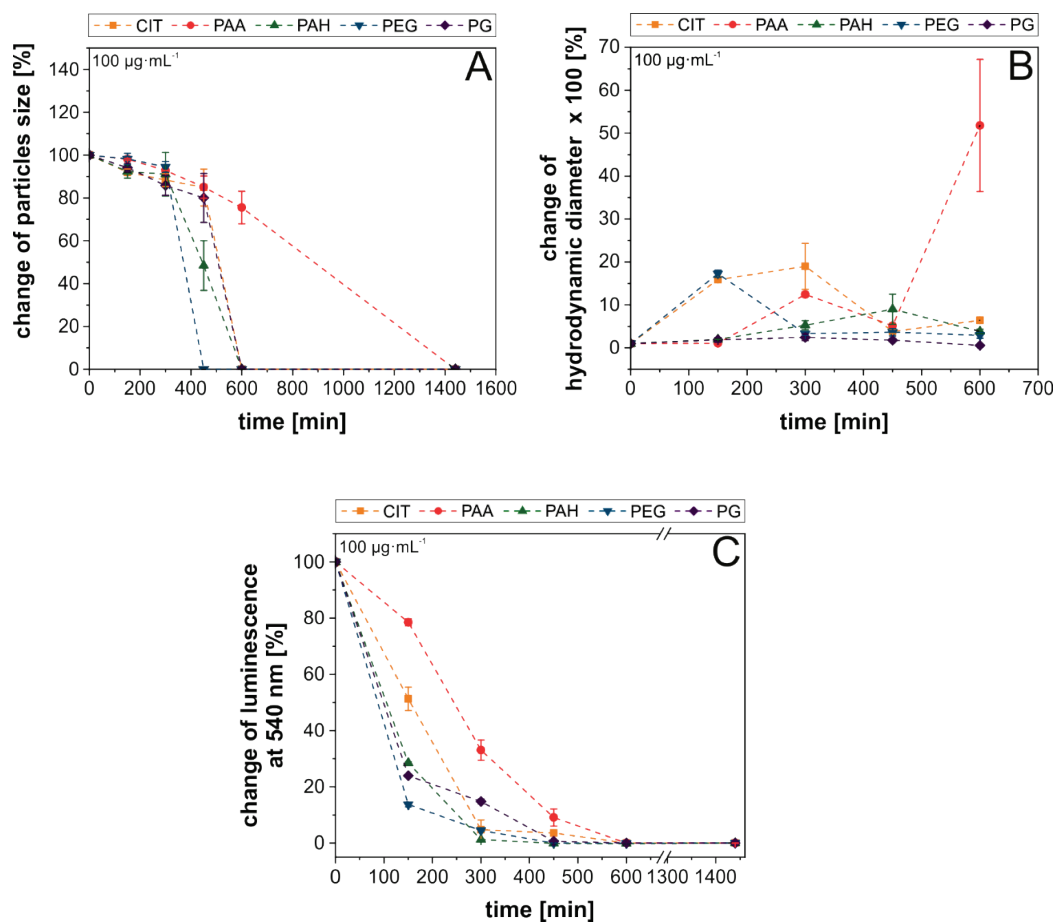


Figure 3.6] Analysis of the colloidal and chemical stability of UCNPs with different surface capping (PAA, PAH, PEG, PG, and CIT) and with a mass concentration of 100 µg·mL⁻¹. A: Change of particle size analyzed *via* TEM. B: Change of hydrodynamic diameter determined *via* intensity-weighted dynamic light scattering measurement. C: Change of luminescent signal at 540 nm for different times and surface capping. The particles were excited with a 980 nm laser module (250 mW, CW).

3.3.5 Stabilization of highly diluted aqueous upconversion nanoparticle dispersions

Due to the poor stabilization of the UCNPs *via* hydrophilic surface ligands directly attached to the particle surface one of the simplest possibilities to prevent the particle dissolution is given by the addition of respective ions to the dispersion media. For applications without toxicity issues, this might not be a problem at all. For single particle imaging as shown by the group of Yves Mely [45] UCNPs based on NaYF₄ host materials stay stable when 1 mmol·L⁻¹ fluoride was added to the solution. In order to study the presence of different ions for the stability of PAH and CIT, modified UCNPs dialysis not only against water but also against 1 mM KF solution, 1 mM NaNO₃, a solution with 100 µg·mL⁻¹ of the ligand (e.g. PAH or Na₃CIT), 1 mM Y(NO₃)₃, and 1 mM of KF and Y(NO₃)₃ has been performed. Additional F⁻ ions can entirely hinder the dissolution of highly diluted UCNPs due to the exceedance of the saturation concentration of the free F⁻. As seen in the TEM images of UCNP@PAH (Figure S3.30) and UCNP@CIT (Figure S3.31), the morphology of the particles at high dilution (100 µg·mL⁻¹) remains constant for 24 h.

In the case of Y³⁺ the equilibrium could be reached by a mechanism reported by the group of Liu [48]. They describe a change in the nanoparticle composition by cation exchange. Theoretically, surface-bound Yb³⁺ and Er³⁺ ions could be exchanged by Y³⁺, ideally leading to an “inert shell” preventing surface quenching of the upconversion luminescence. For the 28 nm-sized particles after dialysis against a pure Y(NO₃)₃ solution,

this could not be found. The different lanthanide ions have individual solubility constants, so that only the pathway with Y³⁺ disintegration is hindered, but the dissolution mechanism based on Yb³⁺ and Er³⁺ is still possible and leads to a drastic change of the morphology of the particles, as seen from the TEM images (Figure S3.30, Figure S3.31, and Figure S3.32).

By applying a mixture of KF and Y(NO₃)₃, the dissolution can be prevented. For a short dialysis time (~ up to 450 min) indeed an increase of the upconversion signal at 540 nm can be observed for UCNP@PAH (Figure S3.32). However, a closer look at the TEM showed no monodisperse UCNPs any longer as spark-like structures have grown around the particles. It is assumed that YF₃ is deposited on the UCNPs. In contrast to the UCNP@PAH, negatively charged UCNP@CIT suffer from fast crosslinking and aggregation. As shown by the group of Xu, the carboxylic groups of *e.g.* the poly(acrylic acid) are capable to complex lanthanide ions [49]. This effect has to be considered as the negatively charged UCNPs can interact with the Y³⁺ ions and lead to a crosslinking of the particles as schematically shown in Figure S3.33. Thereby especially in systems with a low number of surface ligands and a low number of functional groups – like it is the case for CIT and PG capped UCNPs – already minimal amounts of Y³⁺ would lead to strong crosslinking. For UCNP@PAA, where crosslinking is also a problem, the high number of functional groups prevents a complete aggregation of the colloidal system when only a small amount of the Y³⁺ is present. To study the phenomenon of Ln³⁺ induced crosslinking in a dispersion of UCNP@PAA (1000 µg·mL⁻¹) small amounts of Y³⁺ were added and their luminescence and colloidal properties were monitored over time. As seen in Figure S3.34 with the addition of more and more Y³⁺, an increase of the hydrodynamic diameter was measured. With increasing concentration of Y³⁺, the colloidal stability of the nanoparticles gets affected very strongly leading to large aggregates and a decrease of the luminescence at 540 nm. In the presence of 200 µM EDTA this effect can be shifted to higher concentrations of Y³⁺, as EDTA complexes the Y³⁺.

Due to the potential toxic effect of added fluoride ions and the limitation of this in the aspect of bioanalytical applications, it was also studied if the addition of the ligand itself or the addition of Na⁺ would have a positive effect. However, for the dissolution of the nanoparticles not only the pathway in Equation 3.2 but also a second one, described by the group of Yves Mely [45], would be possible:



Therefore, the addition of Na⁺ only hinders the pathway according to Equation 3.2, as it exceeds the saturation concentration of Na⁺ ions associated with the UCNPs. The one following Equation 3.3 is still possible. Due to the limitations to this route, the dissolution process is slowed down as seen from the TEM images (Figure S3.30, Figure S3.31, and Figure S3.32). The same phenomenon can be observed when using Na₃CIT as an additive for CIT capped UCNPs. The addition of a solution with only the ligand (PAH for PAH capped UCNPs) does not hinder the disintegration of the nanoparticles. Additionally, to the change of the morphology also the influence of the dissolution on the crystal structure of the nanoparticle was analyzed (Figure S3.35). In each case, whether the particles are stabilized *via* KF or get partly dissolved, no change of the lattice constant can be observed. This indicates that the KF prevents the leakage of the F⁻ ions. In the presence of both KF and Y(NO₃)₃ a “shell” is grown around the particles and for UCNP@PAH no crosslinking of the YF₃ shell occurs. It grows uniformly in one direction and also the lattice constant is still 0.5 nm.

3.4 Conclusion

In this study five different surface capping ligands – poly(acrylic acid) (PAA), polyallylamine (PAH), citrate (CIT), phosphonoglycine (PG), and polyethylene glycol (PEG) – were examined in terms of their shielding ability for long-term colloidal stability of NaYF₄(Yb,Er) upconversion nanoparticles in aqueous dispersions of low concentration.

The surface modification was performed by NOBF₄ assisted two-step ligand exchange, resulting in colloiddally stable aqueous dispersions when stored at high concentrations as demonstrated by a low polydispersity index. For colloidal stability, both the attractive van der Waals interaction of two particles ($E_{v.d.W.}$) and the repulsive forces due to the surface capping are essential. The luminescence data of UCNP@PAA, UCNP@PAH, and UCNP@PEG do not indicate better shielding and the hydrodynamic diameter of those modifications was in the same range as for surface coatings assembled by small molecules. It is assumed that the high colloidal stability at neutral pH is achieved by electrostatic repulsion of the nanoparticles due to charged molecules attached to the nanoparticle surface. Consequently, for the design of a hydrophilic surface, providing colloidal stability for the whole physiologically relevant pH range, the ligands should consist of molecules providing both, steric hindrance as well as electrostatic repulsion.

Under non-steady state conditions, like it is the case in flow systems for online monitoring or in high dilutions as for single particle imaging, the ligand-exchange method does not end up with a surface modification providing a tight coating to prevent particle disintegration with time. Due to the dominant electrostatic stabilization, almost identical low surface coverage rates have been found without any significant influence of the type of ligand. As a consequence, surfaces with a strong negative ζ -potential tend to aggregate in highly dilutions or in flow conditions already after a short period of time despite their theoretical high colloidal stability. A closer examination revealed that released Ln³⁺ might crosslink with the negative charged carboxylic groups and limit the colloidal stability of those systems. In contrast, UCNPs with PAH and PEG capping did not show this Ln³⁺ induced colloidal instability. However, by strong dilution of all examined particle systems, a strong loss of the luminescence due to the dissolution of the nanoparticles has been observed. The easiest way to prevent disintegration is given by the presence of fluoride ions in solution. Here one has to keep in mind that changes in the ionic strength of the dispersion media will also have an impact on the electrostatic stabilization. Therefore, this parameter will also be investigated, together with surface ligands, that have been reported for colloidal stability *via* steric repulsion [50,51], in the near future.

3.5 References

- [1] Homann C, Krukewitt L, Frenzel F, Grauel B, Würth C, Resch-Genger U, Haase M (2018) NaYF₄: Yb, Er/NaYF₄ Core/Shell Nanocrystals with High Upconversion Luminescence Quantum Yield. *Angew. Chem. Int. Ed.* 9;57(28):8765-9.
- [2] Cheng T, Marin R, Skripka A, Vetrone F (2018) Small and Bright Lithium-Based Upconverting Nanoparticles. *J. Am. Chem. Soc.* 140(40):12890-9.
- [3] Wen S, Zhou J, Zheng K, Bednarkiewicz A, Liu X, Jin D (2018) Advances in Highly Doped Upconversion Nanoparticles. *Nat. Commun.* 9(1):2415.
- [4] Würth C, Fischer S, Grauel B, Alivisatos AP, Resch-Genger U (2018) Quantum Yields, Surface Quenching, and Passivation Efficiency for Ultrasmall Core/Shell Upconverting Nanoparticles. *J. Am. Chem. Soc.* 140(14):4922-8.
- [5] Tian B, Fernandez-Bravo A, Najafiaghdam H, Torquato NA, Altoe MV, Teitelboim A, Tajon CA, Tian Y, Borys NJ, Barnard ES, Anwar M, Emory CM, James Schuk P, Cohen BE (2018) Low Irradiance Multiphoton Imaging with Alloyed Lanthanide Nanocrystals. *Nat. Commun.* ;9(1):3082.
- [6] Liang L, Qin X, Zheng K, Liu X (2018) Energy Flux Manipulation in Upconversion Nanosystems. *Acc. Chem. Res.* 52(1):228-36.
- [7] Haase M, Schäfer H (2011) Upconverting Nanoparticles. *Angew. Chem. Int. Ed.* 50(26):5808-29.
- [8] Himmelstoß SF, Hirsch T (2019) A Critical Comparison of Lanthanide Based Upconversion Nanoparticles to Fluorescent Proteins, Semiconductor Quantum Dots, and Carbon Dots for Use in Optical Sensing and Imaging Methods Appl. *Fluoresc* 7(2):022002.
- [9] Mandl G, Cooper D, Hirsch T, Seuntjens J, Capobianco JA (2019) Perspective: Lanthanide-Doped Upconverting Nanoparticles. *Methods Appl. Fluoresc* 7(1):012004.
- [10] Wilhelm S (2017) Perspectives for Upconverting Nanoparticles. *ACS Nano* 11(11):10644-53.
- [11] Mackenzie LE, Goode JA, Vakurov A, Nampi PP, Saha S, Jose G, Millner PA (2018) The Theoretical Molecular Weight of NaYF₄:RE Upconversion Nanoparticles. *Sci. Rep.* 8(1):1106.
- [12] Zou Q, Huang P, Zheng W, You W, Li R, Tu D, Xu J, Chen X (2017) Cooperative and Non-Cooperative Sensitization Upconversion in Lanthanide-Doped LiYbF₄ Nanoparticles. *Nanoscale* 9(19):6521-8.
- [13] Wang L, Huang H, Shen D, Zhang J, Chen H, Wang Y, Liu X, Tang D (2014) Room Temperature Continuous-Wave Laser Performance of LD Pumped Er:Lu₂O₃ and Er:Y₂O₃ Ceramic at 2.7 μm. *Opt. Express.* 22(16):19495-503.
- [14] Ryba-Romanowski W, Niedźwiedzki T, Komar J, Lisiecki R, Świrkowicz M (2015) Luminescence and Energy Transfer Phenomena in YVO₄ Single Crystal Co-Doped with Tm³⁺ and Eu³⁺. *J. Lumin.* 162:134-9.
- [15] Pin MW, Park EJ, Choi S, Kim YI, Jeon CH, Ha TH, Kim YH (2018) Atomistic Evolution During the Phase Transition on a Metastable Single NaYF₄: Yb, Er Upconversion Nanoparticle. *Sci. Rep.* 8(1):2199.
- [16] Rinkel T, Raj AN, Dühnen S, Haase M (2016) Synthesis of 10 nm β-NaYF₄: Yb, Er/NaYF₄ Core/Shell Upconversion Nanocrystals with 5 nm Particle Cores. *Angew. Chem. Int. Ed.* 55(3):1164-7.
- [17] Duong HT, Chen Y, Tawfik SA, Wen S, Parviz M, Shimoni O, Jin D (2014). Systematic Investigation of Functional Ligands for Colloidal Stable Upconversion Nanoparticles. *RSC Adv.* 8(9):4842-9.
- [18] Muhr V, Wilhelm S, Hirsch T, Wolfbeis OS (2014) Upconversion Nanoparticles: From Hydrophobic to Hydrophilic Surfaces. *Acc. Chem. Res.* 47(12):3481-93.
- [19] Buchner M, Muhr V, Himmelstoß SF and Hirsch T (2016) 4 Functionalization Aspects of Water Dispersible Upconversion Nanoparticles. In *Upconverting Nanomaterials* (pp. 69-100). CRC Press, Boca Raton.
- [20] Bogdan N, Vetrone F, Ozin GA, Capobianco JA (2011) Synthesis of Ligand-Free Colloidally Stable Water Dispersible Brightly Luminescent Lanthanide-Doped Upconverting Nanoparticles. *Nano Lett.* 11(2):835-40.
- [21] Naccache R, Chevallier P, Lagueur J, Gossuin Y, Laurent S, Vander Elst L, Chilian C, Capobianco JA, Fortin MA (2013) High Relaxivities and Strong Vascular Signal Enhancement for NaGdF₄ Nanoparticles Designed for Dual MR/Optical Imaging. *Adv. Healthc. Mater.* 2(11):1478-88.

- [22] Duan C, Liang L, Li L, Zhang R, Xu ZP (2018) Recent Progress in Upconversion Luminescence Nanomaterials for Niomedical Applications. *J. Mater. Chem. B*. 6(2):192-209.
- [23] Lin CA, Sperling RA, Li JK, Yang TY, Li PY, Zanella M, Chang WH, Parak WJ (2008) Design of an Amphiphilic Polymer for Nanoparticle Coating and Functionalization. *Small*. 4(3):334-41.
- [24] Dukhno O, Przybilla F, Collot M, Klymchenko A, Pivovarenko V, Buchner M, Muhr V, Hirsch T, Mély Y (2015) Quantitative Assessment of Energy Transfer in Upconverting Nanoparticles Grafted with Organic Dyes. *Nanoscale*. (33):11994-2004.
- [25] Chen X, Peng D, Ju Q, Wang F (2015) Photon Upconversion in Core-Shell Nanoparticles. *Chem. Soc. Rev.* 44(6):1318-30.
- [26] Rosen EL, Buonsanti R, Llordes A, Sawvel AM, Milliron DJ, Helms BA (2016) Exceptionally Mild Reactive Stripping of Native Ligands from Nanocrystal Surfaces by Using Meerwein's Salt. *Angew. Chem. Int. Ed.* 51(3):684-9.
- [27] Tsuda A, Konduru NV (2016) The Role of Natural Processes and Surface Energy of Inhaled Engineered Nanoparticles on Aggregation and Corona Formation. *NanoImpact* 2:38-44.
- [28] Dong A, Ye X, Chen J, Kang Y, Gordon T, Kikkawa JM, Murray CB (2010) A Generalized Ligand-Exchange Strategy Enabling Sequential Surface Functionalization of Colloidal Nanocrystals. *J. Am. Chem. Soc.* 133(4):998-1006.
- [29] Muhr V, Würth C, Kraft M, Buchner M, Baeumner AJ, Resch-Genger U, Hirsch T (2017) Particle-Size-Dependent Förster Resonance Energy Transfer from Upconversion Nanoparticles to Organic Dyes. *Anal. Chem.* 89(9):4868-74.
- [30] D Jaque D, Maestro LM, Del Rosal B, Haro-Gonzalez P, Benayas A, Plaza JL, Rodriguez EM, Sole JG (2014) Nanoparticles for Photothermal Therapies. *Nanoscale* 6(16):9494-530.
- [31] Wilhelm S, Kaiser M, Würth C, Heiland J, Carrillo-Carrion C, Muhr V, Wolfbeis OS, Parak WJ, Resch-Genger U, Hirsch T (2015) Water Dispersible Upconverting Nanoparticles: Effects of Surface Modification on their Luminescence and Colloidal Stability. *Nanoscale* 7(4):1403-10.
- [32] Ott LS, Finke RG (2006) Nanocluster Formation and Stabilization Fundamental Studies: Investigating "Solvent-Only" Stabilization En Route to Discovering Stabilization by the Traditionally Weakly Coordinating Anion BF₄⁻ Plus High Dielectric Constant Solvents. *Inorg. Chem.* 45(20):8382-93.
- [33] Szeftczyk B, Roszak R, Roszak S (2014). Structure of the Hexagonal NaYF₄ Phase from First-Principles Molecular Dynamics. *RSC Adv.* 4(43):22526-35.
- [34] Robinson CC, Fournier JT (1969) Coordination of Yb³⁺ in Some Inorganic Glasses from Optical Absorption and Emission Studies. *Chem. Phys. Lett.* 3(7):517-9.
- [35] Ren W, Wen S, Tawfik SA, Su QP, Lin G, Ju LA, Ford MJ, Ghodke H, van Oijen AM, Jin D (2018) Anisotropic Functionalization of Upconversion Nanoparticles. *Chem. Sci.* 9(18):4352-8.
- [36] Kong W, Sun T, Chen B, Chen X, Ai F, Zhu X, Li M, Zhang W, Zhu G, Wang F (2017) A General Strategy for Ligand Exchange on Upconversion Nanoparticles. *Inorg. Chem.* 56(2):872-7.
- [37] Estebanez N, Ferrera-González J, Francés-Soriano L, Arenal R, González-Béjar M, Pérez-Prieto J (2018) Breaking the Nd³⁺-Sensitized Upconversion Nanoparticles Myth about the Need of Onion-Layered Structures. *Nanoscale* 10(26):12297-301.
- [38] Estebanez N, González-Béjar M, Pérez-Prieto J (2019) Polysulfonate Cappings on Upconversion Nanoparticles Prevent Their Disintegration in Water and Provide Superior Stability in a Highly Acidic Medium. *ACS Omega* 4(2):3012-9.
- [39] León A, Reuquen P, Garín C, Segura R, Vargas P, Zapata P, Orihuela P (2017). FTIR and Raman Characterization of TiO₂ Nanoparticles Coated with Polyethylene Glycol as Carrier for 2-Methoxyestradiol. *Appl. Sci.* 7(1):49.
- [40] Li H, Wang K, Tuo X, Almásy L, Tian Q, Sun G, Henderson MJ, Li Q, Wacha A, Courtois J, Yan M (2018) Thickness Determination of Ultrathin Poly(acrylic acid) Shell on γ -Fe₂O₃ Nanocore *via* Small-Angle Scattering. *Mater. Chem. Phys.* 204:236-42.
- [41] Nsubuga A, Zarschler K, Sgarzi M, Graham B, Stephan H, Joshi T (2018) Towards Utilising Photocrosslinking of Polydiacetylenes for the Preparation of "Stealth" Upconverting Nanoparticles. *Angew. Chem. Int. Ed.* 130(49):16268-72.

- [42] DaCosta MV, Doughan S, Han Y, Krull UJ (2014). Lanthanide Upconversion Nanoparticles and Applications in Bioassays and Bioimaging: A Review. *Anal. Chim. Acta* 832:1-33.
- [43] Wang F, Liu X (2009) Recent Advances in the Chemistry of Lanthanide-Doped Upconversion Nanocrystals. *Chem. Soc. Rev.* 38(4):976-89.
- [44] Chen J, Zhao JX (2012) Upconversion Nanomaterials: Synthesis, Mechanism, and Applications in Sensing. *Sensors* 12(3):2414-35.
- [45] Dukhno O, Przybilla F, Muhr V, Buchner M, Hirsch T, Mély Y (2018) Time-Dependent Luminescence Loss for Individual Upconversion Nanoparticles upon Dilution in Aqueous Solution. *Nanoscale* 10(34):15904-10.
- [46] Lisjak D, Plohl O, Vidmar J, Majaron B, Ponikvar-Svet M (2016) Dissolution Mechanism of Upconverting AYF₄:Yb,Tm (A= Na or K) Nanoparticles in Aqueous Media. *Langmuir* 32(32):8222-9.
- [47] Lahtinen S, Lyytikäinen A, Pääkkilä H, Hömppi E, Perälä N, Lastusaari M, Soukka T (2016). Disintegration of Hexagonal NaYF₄:Yb³⁺, Er³⁺ Upconverting Nanoparticles in Aqueous Media: The Role of Fluoride in Solubility Equilibrium. *J. Phys. Chem. C* 121(1):656-65.
- [48] Han S, Qin X, An Z, Zhu Y, Liang L, Han Y, Huang W, Liu X (2016) Multicolour Synthesis in Lanthanide-Doped Nanocrystals through Cation Exchange in Water. *Nat. Commun.* 7:13059.
- [49] Qi X, Wang Z, Ma S, Wu L, Yang S, Xu J (2014) Complexation Behavior of Poly(acrylic acid) and Lanthanide Ions. *Polymer* 55(5):1183-9.
- [50] Heuer-Jungemann A, Feliu N, Bakaimi I, Hamaly M, Alkilany A, Chakraborty I, Masood A, Casula MF, Kostopoulou A, Oh E, Susumu K, Stewart MH, Igor L, Stratakis E, Parak WJ, Kanaras AG (2019) The Role of Ligands in the Chemical Synthesis and Applications of Inorganic Nanoparticles. *Chem. Rev.* 119:4819-80.
- [51] Pellegrino T, Kudera S, Liedl T, Muñoz Javier A, Manna L, Parak WJ (2005) On the Development of Colloidal Nanoparticles towards Multifunctional Structures and their Possible Use for Biological Applications. *Small* 1(1):48-63.

3.6 Supporting information

3.6.1 Synthesis and characterization of upconversion nanoparticles

Synthesis of upconversion nanoparticles

Oleate capped upconversion nanoparticles with a NaYF₄ host lattice co-doped with Yb³⁺ and Tm³⁺ were synthesized *via* a thermal decomposition method [1]. Therefore, the rare earth chlorides (here YCl₃ · 6 H₂O, YbCl₃ · 6 H₂O and ErCl₃ · 6 H₂O (with the corresponding molar doping ratio) were dissolved in methanol and transferred in a three-necked round bottom flask under nitrogen flow. Per 1 mmol total amount of the lanthanide ions, 8 mL oleic acid and 15 mL 1-octadecene were added to the solution. The resulting suspension was heated to 160 °C, and vacuum was applied 30 min to form a clear solution. The mixture was cooled to room temperature and per 1 mmol of the chlorides 2.5 mmol NaOH and 4.0 mmol NH₄F, dissolved in methanol, were added. The suspension was heated to 120 °C and kept there for additional 30 min. Then the mixture was heated to reflux (approx. 325 °C). The progress of the synthesis was controlled by illumination with a 980 nm CW laser module (250 mW). After upconversion luminescence can be observed for the first time, the solution was kept another 10 min above 300 °C and was then cooled to room temperature. For purification, the particles were precipitated with an excess of ethanol and centrifuged for 5 min at 1000 g. The resulting pellet was washed twice with chloroform / ethanol and three times with cyclohexane / ethanol. Finally, the precipitant was redispersed in cyclohexane and centrifuged (1000 g, 3 min) to remove aggregates. The supernatant was collected and stored at 4 °C.

Table S3.1| Overview of the elemental composition of upconversion nanoparticles with OA, stabilized with BF₄⁻ or with hydrophilic surface ligands (CIT, PAA, PAH, PEG, and PG) *via* mass spectrometry with inductively coupled plasma and the theoretical composition of NaYF₄ (Yb,Er).

element	theoretical [mol %]	real [mol %]						
		OA	BF ₄ ⁻	PAA	PAH	PEG	CIT	PG
yttrium (Y ³⁺)	78 %	77.57 ± 0.40	77.67 ± 1.40	78.01 ± 0.08	77.87 ± 0.45	77.84 ± 0.62	78.12 ± 0.56	77.9 ± 0.25
ytterbium (Yb ³⁺)	20 %	20.15 ± 0.08	20.10 ± 0.20	19.79 ± 0.09	19.91 ± 0.21	19.96 ± 0.29	19.70 ± 0.29	19.89 ± 0.27
erbium (Er ³⁺)	2 %	2.27 ± 0.01	2.26 ± 0.05	2.21 ± 0.01	2.22 ± 0.01	2.20 ± 0.04	2.19 ± 0.03	2.21 ± 0.03

3.6.2 Determination of the phonon energy

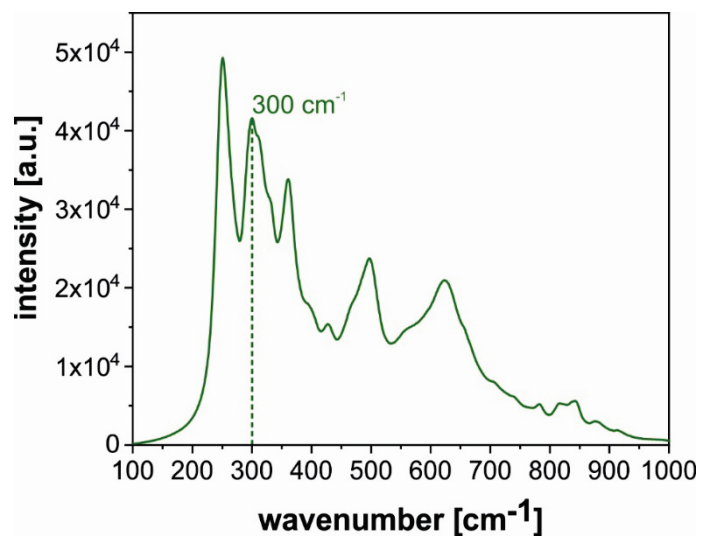


Figure S3.1| Raman spectrum of upconversion nanoparticles capped with oleic acid. The position of the phonon band at 300 cm⁻¹ is highlighted. The spectrum is an average over ten spectra with an acquisition time of 1 s.

3.6.3 Calculation of the absorption cross-section of Yb³⁺

For the determination of the absorption cross-section following equation [2] was used:

$$\sigma(\lambda) = \frac{1}{c \cdot l} \cdot \ln\left(\frac{P_0}{P_{\text{UCNPs}}}\right). \quad (\text{Equation S3.1})$$

Thereby the power density of both a quartz cuvette filled with the dispersion media (water or cyclohexane, P₀) is compared to the absorption of a quartz cuvette filled with a UCNP dispersion (UCNP@OA: 13 mg·mL⁻¹, water dispersible UCNPs: 1.6 mg·mL⁻¹, P_{UCNPs}). For the illumination of the particles, a 980 nm CW laser diode (200 mW) was used. For the measurement of both power densities, a 180 ° configuration with an optical power meter (PM400 equipped with a standard Si photodiode ranging from 400 to 1100 nm from Thorlabs) was used. As soon as the signal becomes constant, the power density of the individual particle's dispersion was measured for 60 s (600 data points). The mean value of the power density was used for the determination of the absorption cross-section. The concentration of the Yb³⁺ ions was determined *via* ICP-MS. *c* is the number concentration of molecular entities (number per volume) and *l* is the optical pathlength [2].

Table S3.2| Overview of the absorption cross-section upconversion nanoparticles with OA (13 mg·mL⁻¹) and with hydrophilic ligands (CIT, PAA, PAH, PEG, or PG, 1.6 mg·mL⁻¹).

upconversion nanoparticles	absorption cross-section [cm ²]
NaYF ₄ (Yb,Er)@OA	(2.54 ± 0.1) · 10 ⁻²⁰
NaYF ₄ (Yb,Er)@PAH	(3.40 ± 0.6) · 10 ⁻²⁰
NaYF ₄ (Yb,Er)@CIT	(3.13 ± 0.5) · 10 ⁻²⁰
NaYF ₄ (Yb,Er)@PAA	(2.67 ± 0.5) · 10 ⁻²⁰
NaYF ₄ (Yb,Er)@PG	(2.67 ± 0.7) · 10 ⁻²⁰
NaYF ₄ (Yb,Er)@PEG	(2.56 ± 0.7) · 10 ⁻²⁰

3.6.4 Lifetime

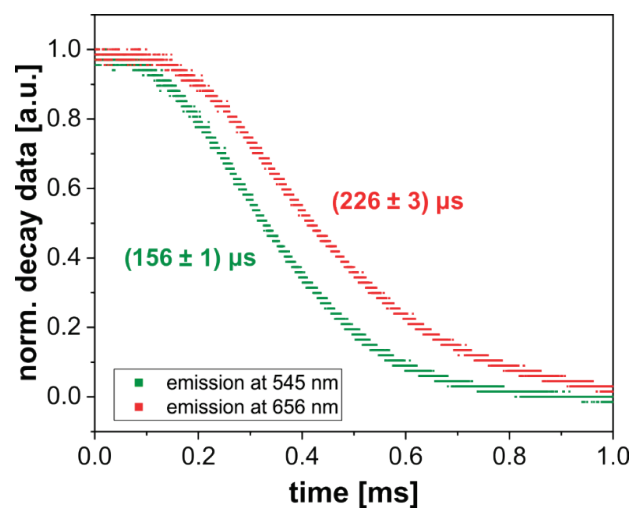


Figure S3.2| Normalized decay data of upconversion nanoparticles coated with oleic acid. The particles were dispersed in cyclohexane and excited with a 980 nm CW laser module (250 mW). The green and red emission around 545 nm (green) and 656 nm (red curve) was recorded.

3.6.5 Thermogravimetric analysis to determine the number of ligands attached to the surface of the nanoparticles

Thermogravimetric analysis (TGA) experiments were performed under air with a heating rate of 5 °C·min⁻¹ with the temperature ranging between 30 and 700 °C. The relative mass loss of the UCNP systems (capped with OA, stabilized with BF₄⁻ or modified with PAA or PG) can be extracted from Figure S3.3.

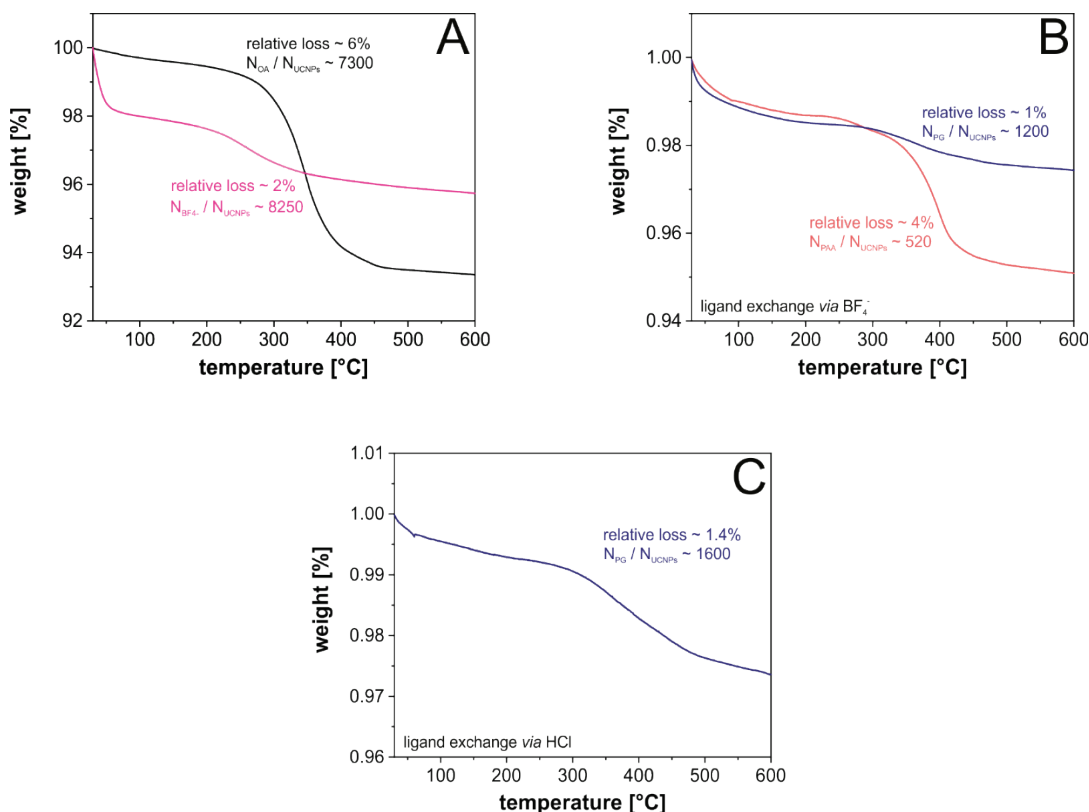


Figure S3.3| Thermogravimetric analysis of UCNP@OA and UCNP@BF₄(A), UCNP@PAA and UCNP@PG (B) and UCNP@PG obtained *via* the ligand removal by HCl (C). The relative mass loss and the calculated ratio of ligand molecules to the number of nanoparticles is inserted in the diagrams.

The number of the upconversion particles can be calculated from the absolute mass loss and the density of pure NaYF₄ (4.21 g·cm⁻³ [3]). The volume of the nanoparticles was calculated under the assumption of a spherical geometry of the particles. Together with the diameter determined *via* TEM (*d*) the surface (*A*_{UCNP}) and the volume (*V*_{UCNP}) of UCNPs can be determined using Equation S3.2 and Equation S3.3

$$A_{UCNP} = 4 \cdot \pi \cdot \left(\frac{d}{2}\right)^2 = \pi \cdot d^2 \quad (\text{Equation S3.2})$$

and

$$V_{UCNP} = \frac{4}{3} \cdot \pi \cdot \left(\frac{d}{2}\right)^3 \quad (\text{Equation S3.3})$$

Spherical upconversion nanoparticles with a size of 28 nm have a surface area of 2461 nm². At this area, oleic acid molecules can adsorb *via* their carboxylic head groups.

The mass of one single particle without any capping is obtained using Equation S3.4

$$m_{\text{UCNP}} = \frac{\rho_{\text{NaYF}_4}}{V_{\text{UCNP}}} \quad (\text{Equation S3.4})$$

For all examined systems, the mass of the nanoparticles did not change above ~600 °C, so that this absolute mass can be assumed to be the mass of plain UCNPs (UCNP^P). The number of particles can be calculated using Equation S3.5.

$$N_{\text{UCNP}^{\text{P}}} = \frac{m_{\text{UCNP}^{\text{P}}}}{m_{\text{UCNP}}} \quad (\text{Equation S3.5})$$

The total number of ligands per number of UCNPs ($N_{\text{Lig}/\text{UCNP}^{\text{P}}}$) can be determined from the mass loss of the TGA measurement using Equation S3.6 and Equation S3.7 together with the molar mass (M_{Ligand}) of the surface molecule. It is assumed that the mass loss is only due to the surface ligands

$$N_{\text{Ligand}} = \frac{m_{\text{loss}}}{M_{\text{Ligand}}} N_{\text{A}}, \quad (\text{Equation S3.6})$$

$$N_{\text{Lig}/\text{UCNP}^{\text{P}}} = \frac{N_{\text{Ligand}}}{N_{\text{UCNP}^{\text{P}}}} \quad (\text{Equation S3.7})$$

In the case, where the amount of binding sides is known – e.g. for oleate or PG the surface coverage of the nanoparticles can be calculated. For one phosphate group, a surface area of 0.23 nm² [4] and for the carboxylic group, a surface area of 0.2 nm² is taken [3]. Therefore ~60% of the UCNP surface is covered with OA whereas ~20% of the surface is modified with PG under the assumption that two phosphate groups are bound to the surface of the UCNPs.

For the UCNP@OA in total ~7300 OA molecules are attached to the surface of one UCNPs. For increasing the size of the nanoparticles, this value increases due to the bigger surface of the nanoparticles.

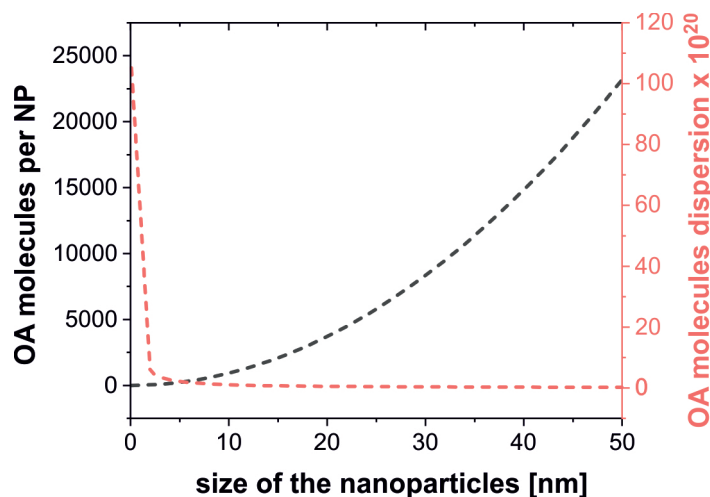


Figure S3.4| Size dependent calculation of the total amount of attached oleic acid (~60%) on the surface on one nanoparticle (black) and the total amount of OA in a UCNPs dispersion containing 25 mg UCNPs (red).

3.6.6 Determination of the required amount of water molecules for the ligand removal *via* NOBF₄

The ligand exchange mediated with the addition of NOBF₄ is induced by protons generated by the following reaction (Equation S3.8):



Thereby the NO⁺ reacts with traces of water in the DMF phase and forms nitrous acid and H⁺. This acidic environment allows the deprotonation of the oleate to form oleic acid, which gets detached from the surface of the nanoparticles.

Under the assumption that all H⁺ come from the water traces within the DMF and one UCNP would have ~7300 OA molecules, one would need an equivalent amount of water molecules for the complete deprotonation of the OA of one nanoparticle. As seen in Figure S3.4, the larger the particles become, the more OA molecules are attached to one NPs, leading to an increased amount of water molecules.

The amount of water in 1 mL of commercially available DMF ($\rho_{\text{DMF}} = 0.944 \text{ g}\cdot\text{cm}^{-3}$) was determined *via* Karl Fischer titration (Figure S3.5). Therefore 80 mL of a Karl-Fischer reagent were filled into the coulometric measurement chamber. Calibration of the device was done with different amounts of a water standard 5 mg·mL⁻¹ from Aquastar. The volume of the DMF phase was 0.5 mL. For the measurement of either the water standard or the DMF, the sample was injected, and the time was recorded until a decrease of the signal was observed, indicating that all water has been depleted. The time thereby is proportional to the mass of water present in the sample. For the DMF sample, the time for the complete consumption of the water was determined to be $10.1 \pm 0.2 \text{ min}$. This equals a water content of ~0.2%.

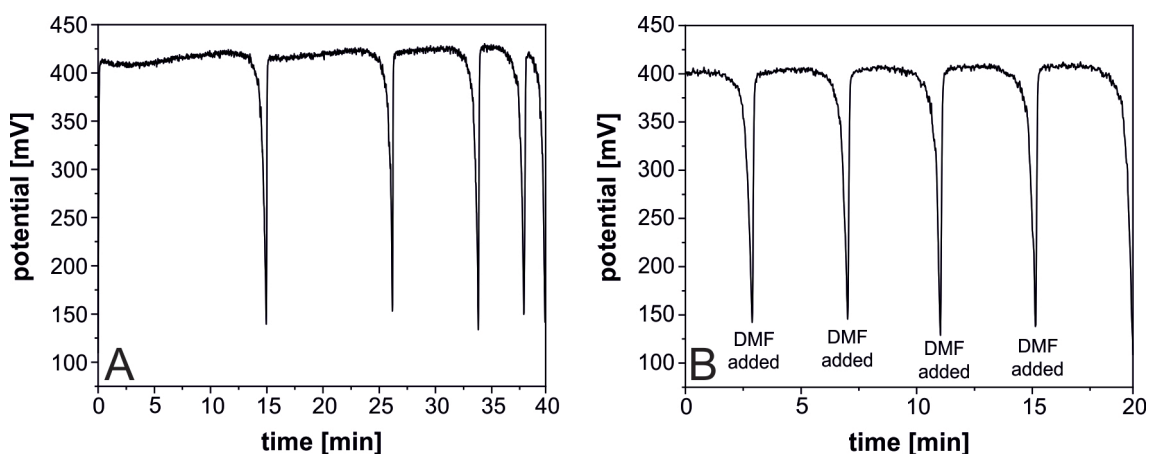


Figure S3.5] Dependency of the potential [mV] on the amount of water during the Karl Fischer Titration. (A) Different defined amounts of water (4 mg, 3 mg, 2 mg, 1 mg, and 0.5 mg) and the resulting variation of the titration time. (B) Volume of the DMF phase: 0.5 mL.

This equals a concentration of ~100 $\mu\text{mol}\cdot\text{mL}^{-1}$ of water. Under such a condition, the presence of water in the DMF phase is far enough for the protonation of the nanoparticle dispersion at any practically possible concentration. The theoretical amount of 28 nm-sized UCNPs, which can be modified *via* this method, is ~400 mg·mL⁻¹ ($8.7\cdot 10^{15}$ particles per mL) For smaller particles due to the increased surface-to-volume ratio, a higher amount can be modified as seen in Figure S3.6.

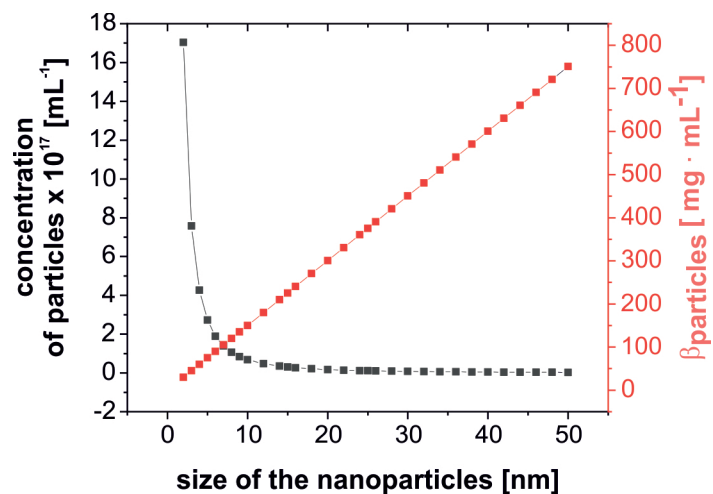


Figure S3.6] Amount of UCNPs per mL cyclohexane (grey) and mass concentration of the nanoparticles (red), which can be modified with the water residues present in an equivalent volume of DMF with a water content of 0.2%.

3.6.7 FT-IR measurements of the cyclohexane and DMF phase after ligand removal *via* NOBF₄

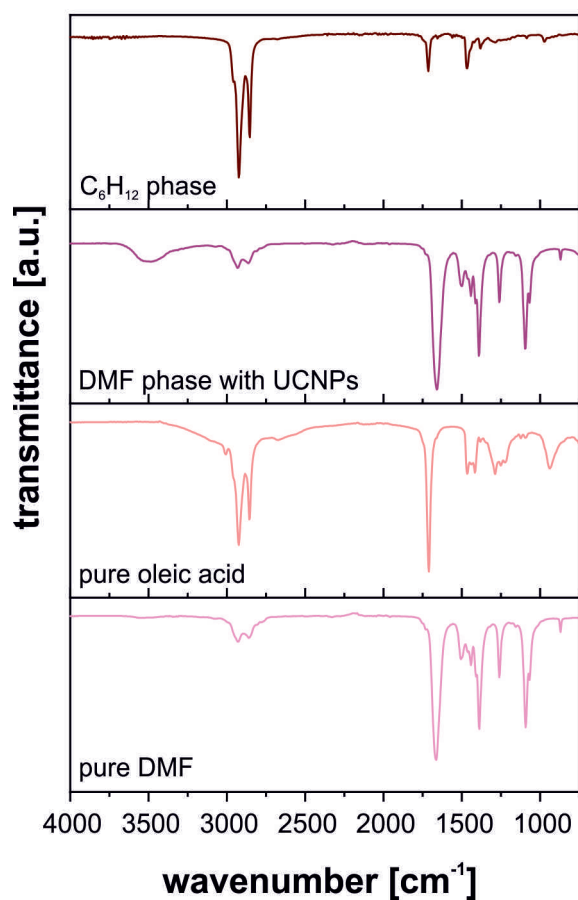


Figure S3.7| FT-IR measurement of the cyclohexane phase and the DMF phase after ligand removal *via* NOBF₄. The particles are now in the DMF phase. In the cyclohexane phase the signal (dark red curve) nicely overlaps with the signal of pure oleic acid (light red curve). In the DMF phase (purple curve) only the signal of pure DMF (light purple curves) can be found and no additional oleic acid peaks can be detected indicating that the ligand removal was successful, and the particles are stabilized *via* BF₄⁻ only.

3.6.8 Dynamic light scattering before and after ligand removal *via* NOBF₄

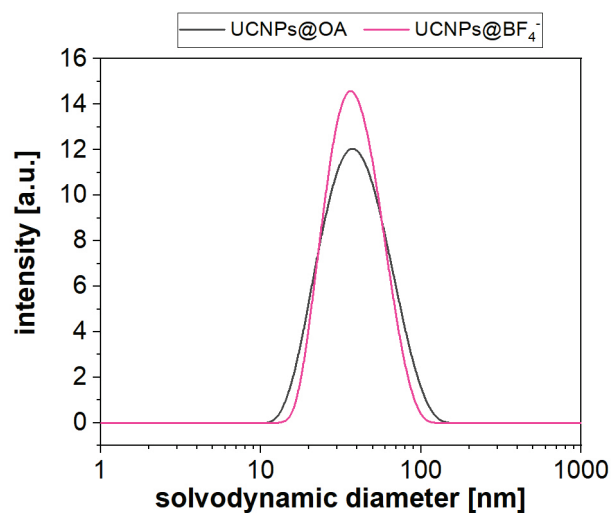


Figure S3.8| Intensity weighted dynamic light scattering measurement of oleate capped UCNPs (dark grey) in cyclohexane and BF₄⁻ stabilized UCNPs (pink) in DMF directly after their synthesis. The concentration of the nanoparticles was 1 mg·mL⁻¹.

3.6.9 Surface modification *via* HCl assisted ligand removal

The oleate can also be stripped off by an alternative method, where the particle dispersion is treated by an acid, most likely HCl. Thereby the hydrophobic oleate capped UCNPs need to be dispersed in an acidic aqueous system for 2 h. Regarding the pK_a of the ligand, which needs to be replaced from the particle surface, the reaction protocol has to be adjusted in terms of reaction time and pH. For the oleate capped particles used in this study, pH 3 and 2 h reaction time are enough.

For successful removal of the oleic acid, the “bare” UCNPs, dispersed in water, were washed with diethyl ether. An analysis of the water and ether phase *via* FT-IR showed that the oleic acid is found in the ether phase only (Figure S3.9). In the water phase, no typical vibrations of the oleic acid molecules could be found indicating that the organic surface ligand was successfully removed.

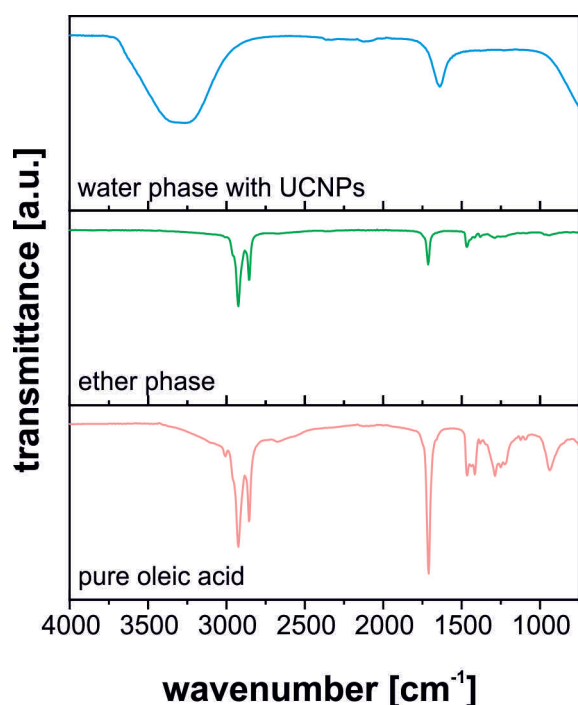


Figure S3.9| FT-IR measurement of the diethyl ether phase (green) and the water phase (blue) after ligand removal *via* NOBF₄. The particles are now in the water phase. In the diethyl ether phase the typical vibrations nicely overlap with the signal of pure oleic acid (light red curve). In the water phase (blue curve) those vibrations cannot be found indicating that the ligand removal was successful, and the particles are stabilized *via* BF₄⁻ only.

However, this method is somehow trickier than the ligand exchange *via* BF₄⁻, as the mixing of the organic phase containing the particles and the acidic aqueous phase can come with difficulties as well as the tendency of bare particles to minimize their surface energy by forming agglomerates (Figure S3.10). This could also be confirmed *via* TEM (Figure S3.11). To use lower particle concentrations does not help to get a lower fraction of agglomerates. With a reduced number of particles (~initial mass concentration was 1 mg·mL⁻¹) already a slight deformation of the shape of the UCNPs can be observed from the TEM images (Figure S3.11) which indicates the beginning of particle dissolution at this low concentration. When using a higher amount of UCNPs, this effect was not observed, so that for this technique, the concentration of UCNPs is recommended to be high.

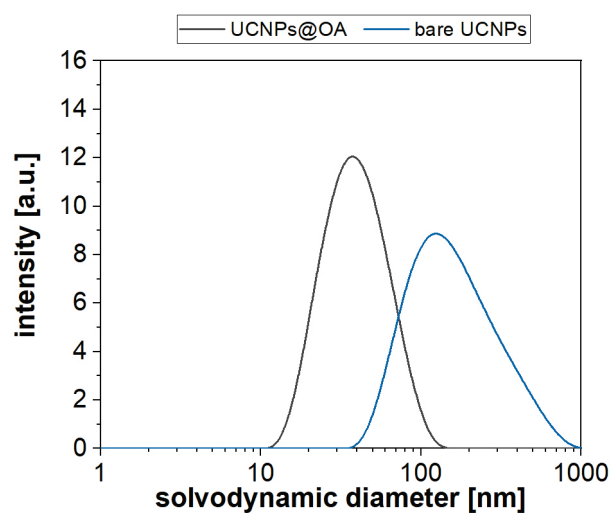


Figure S3.10| Intensity weighted dynamic light scattering measurement of oleate capped UCNPs (dark grey) in cyclohexane and bare UCNPs (blue) in water after their synthesis.

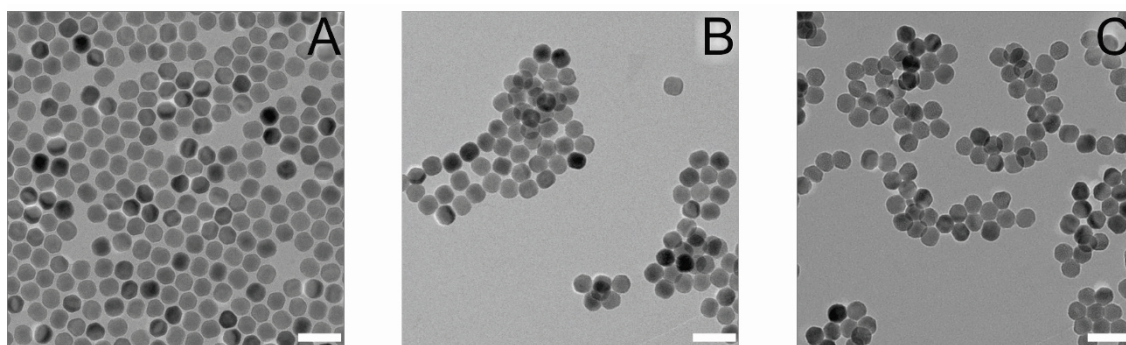


Figure S3.11| TEM images of UCNPs capped with oleic acid (A), (B) bare UCNPs obtained from the ligand removal of a high mass (10 mg·mL⁻¹) of UCNPs *via* HCl and (C) bare UCNPs obtained *via* a smaller batch size (1 mg·mL⁻¹).

3.6.10 Calculations of the distance between single ligands

The surface coverage of PG-capped UCNPs was determined to be 20%, whereas ~1200 PG molecules are attached to one nanoparticle with a size of 28 nm ($A_{UCNP} \sim 2400 \text{ nm}^2$). If one wants to have a complete surface loading (100%) with this number of molecules, the area occupied by one PG molecules can be calculated as follows:

$$100 \% = \frac{N_{PG} \cdot a_{ligand}}{A_{UCNPs}} = \frac{1200}{2463} \cdot a_{ligand} \quad (\text{Equation S3.9})$$

Under the assumption of a spherical surface area ($\pi \cdot r^2$) of the ligand, the diameter of this is 1.6 nm, which is also the distance between two PG molecules. Each of the PG molecules are bearing three functional groups, whereas it is assumed that the phosphate groups are attached to the UCNPs and the negative charged carboxylic group guarantees the colloidal stability. The total charge of the PG molecules (four negative charges) can be seen as point charge and following Coulomb's law the electrostatic repulsion potential, which decreases with r^{-1} , is given by

$$V(r) = \frac{1}{4\pi\epsilon_r\epsilon_0} \frac{q}{r} \quad (\text{Equation S3.10})$$

For the calculation of this potential, the relative permittivity ϵ_r of water at 20 °C ($\epsilon_r \sim 80$ [5]) was chosen. For one charge the elemental charge ($e = 1.6 \cdot 10^{-19} \text{ As}$) was used (Figure S3.12).

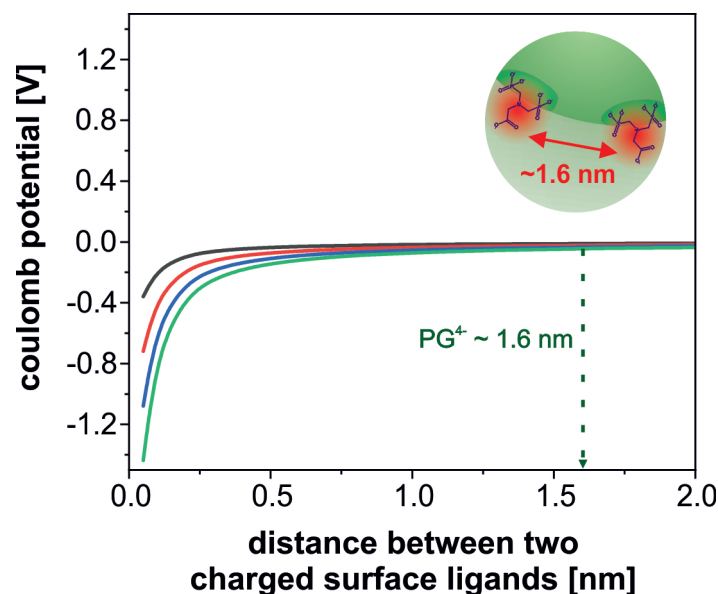


Figure S3.12] Calculation of the Coulomb-potential of charged surface ligands (black = $1 \cdot e^-$, red = $2 \cdot e^-$, blue = $3 \cdot e^-$ and green = $4 \cdot e^-$) and their repulsion distance. For the relative permittivity the influence of water was considered. PG-ligands are bearing 4 negative charges at pH 7 leading to a quite strong repulsion at small distances. Inserted is the average distance of two PG molecules attached to the surface of UCNPs.

3.6.11 Overview of the pK_a values of the surface ligands

Table S3.3| Overview of the pK_a value of citrate, (bis)phosphonoglycine, polyallylamine, poly(acrylic acid), and polyethylene glycol.

surface ligand	functional groups	pK _a	determined <i>via</i>	Ref
citrate	-COOH	3.13, 4.76, 6.4	potentiometric titration	[6,7]
			¹³ C-NMR	
(bis)phosphonoglycine	-COOH	pK _{a1} = 1.4	potentiometric titration	[8]
		pK _{a2} = 2.1		
		pK _{a3} = 5.0		
		pK _{a4} = 6.4		
		pK _{a5} = 11.2		
polyallylamine	-NH ₂	8.7	titration	[9]
poly(acrylic acid)	-COOH	4.52 – 4.55	potentiometric titration	[10]

3.6.12 Dynamic light scattering and surface charge of water dispersible UCNPs

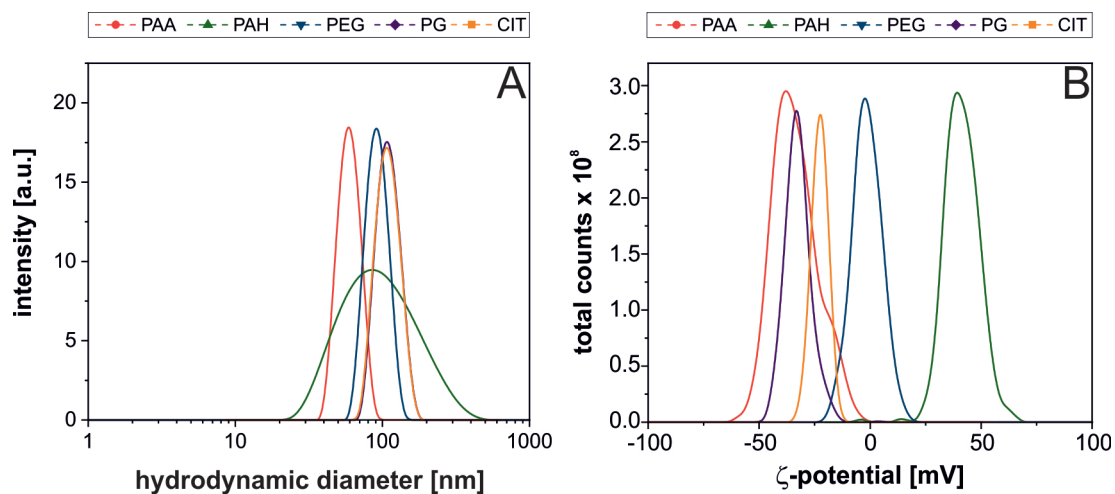


Figure S3.13| (A) Intensity-weighted dynamic light scattering measurements of hydrophilic NaYF₄(20%Yb,2%Er) with different surface cappings (PAA, PAH, PEG, PG, and CIT, each with a concentration of ~5 mg·mL⁻¹). (B) ζ-potential of these modified nanoparticles in water, pH 7.

3.6.13 Luminescence spectra of water dispersible UCNPs

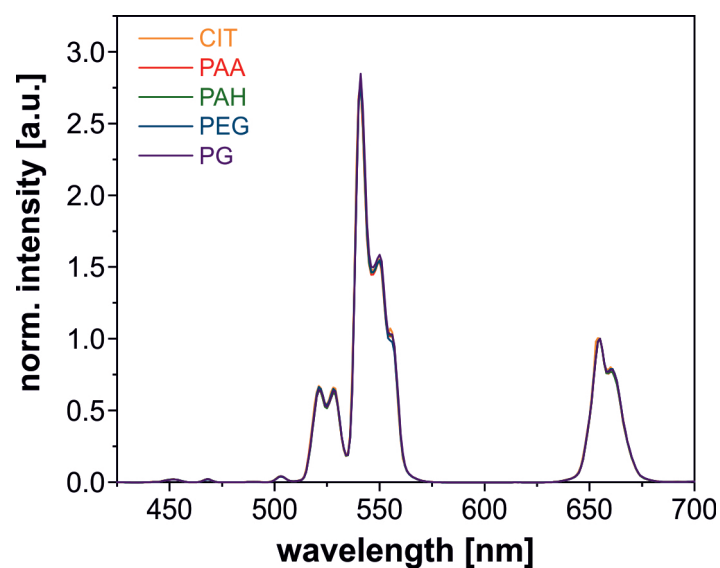


Figure S3.14| Normalized luminescence spectra of hydrophilic NaYF₄(20%Yb,2%Er) with different surface cappings (PAA, PAH, PEG, PG and CIT, each with a concentration of ~1 mg·mL⁻¹), upon 980 nm excitation (250 mW, CW). The spectra were normalized to the emission intensity at 650 nm.

3.6.14 Determination of number of unit cells and total amount of F⁻ ions within a 28 nm-sized upconversion nanoparticle

To calculate the number of unit cells both the surface (A_{UCNP}), the volume (V_{UCNP}) and the total amount of the upconversion nanoparticles (Equation S3.2 – S3.5) are required. UCNPs consisting of NaYF₄ can have either a cubic or hexagonal crystal structure affecting the unit cells and its parameters a_h or c_h . Typically those can be extracted from XRD measurements. For the here reported NaYF₄(20% Yb, 2% Er) a_h has the value 5.960 Å and $c_h = 3.510$ Å [11] Based on those parameters the number of unit cells within an upconversion nanoparticle can be estimated. Using hexagonal UCNPs the volume of the unit cell $V_{unit UCNP}$, given by Equation S3.11, can be used calculated. It has a value of 107.9 Å³.

$$V_{unit UCNP} = \frac{2}{4} \sqrt{3} a_h^2 c_h \quad (\text{Equation S3.11})$$

Dividing the total volume of the particle by the volume of the unit cell itself leads to the number of unit cells within one nanoparticle (Equation S3.12):

$$N_{Unit cells} = V_{UCNPs} / V_{unit cells} \quad (\text{Equation S3.12})$$

The concentration of unit cells can then be achieved with the number of particles determined before *via* Equation S3.2 – S3.5:

$$N_{unit total} = N_{UCNPs} \cdot N_{unit} \quad (\text{Equation S3.13})$$

Each of this unit cell has the formal composition of NaLnF₄, which gives the concentration of these ions within the nanocrystals (Equation S3.11, Equation S3.12 and Equation S3.13):

$$c_{Na^+} = c_{Unit} \quad (\text{Equation S3.14})$$

$$c_{Ln^{3+}} = c_{Unit} \quad (\text{Equation S3.15})$$

$$c_{F^-} = 4 \cdot c_{Unit} \quad (\text{Equation S3.16})$$

3.6.15 Disintegration of diluted upconversion nanoparticles

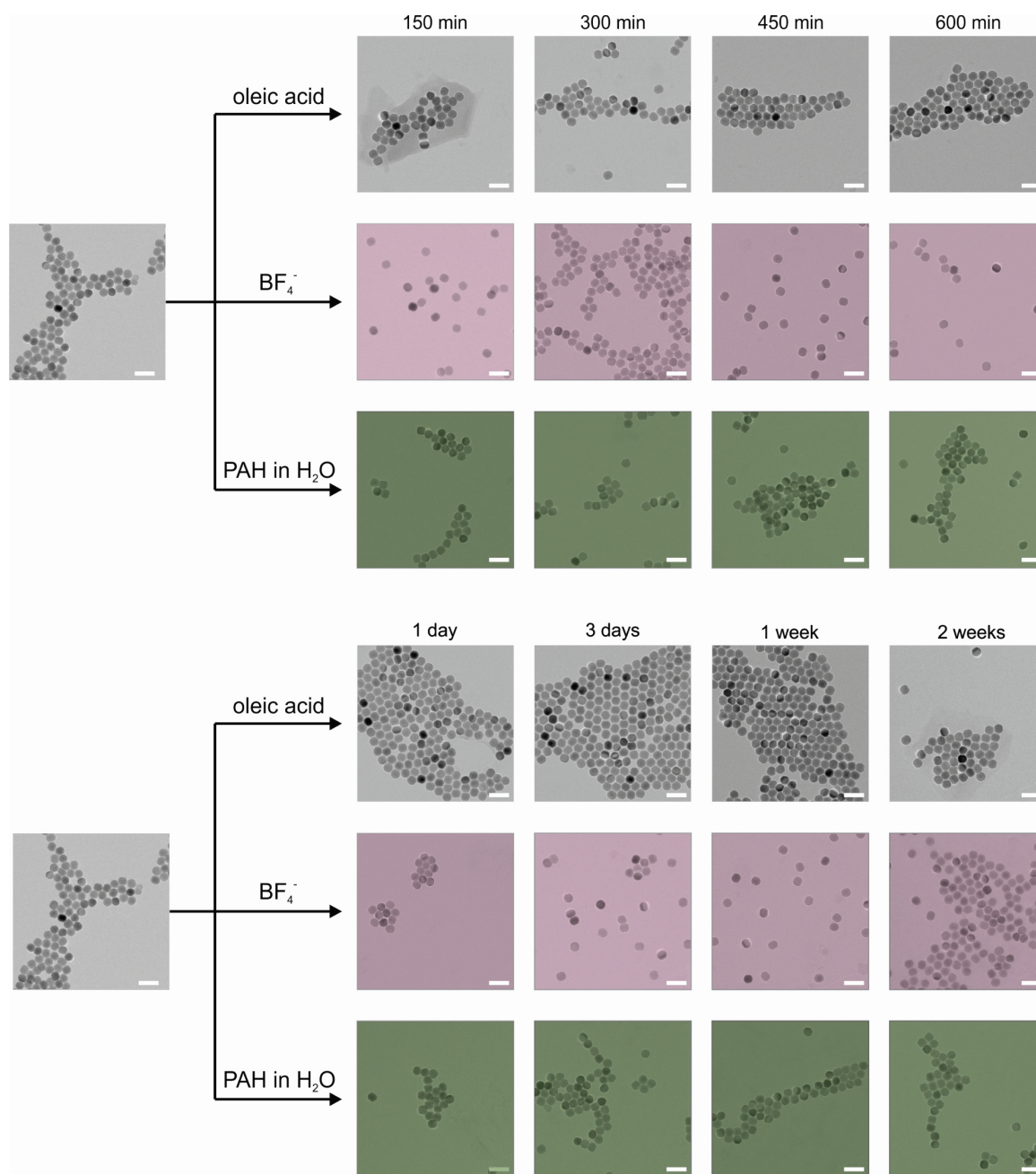


Figure S3.15| TEM image of the stability of NaYF₄(Yb,Er) with different surface capping (PAH, OA or stabilized by BF₄⁻ each with a concentration of 100 µg·mL⁻¹) for different time steps (0 min, 150 min, 300 min, and 600 min, 1 day, 2 days, 1 weeks, and 2 weeks). The scale bar is 60 nm.

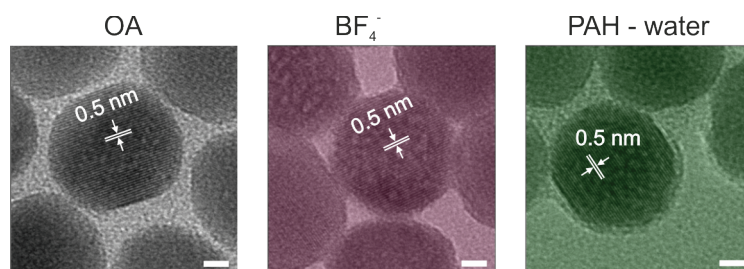


Figure S3.16| High resolution TEM image of NaYF₄(Yb,Er) with different surface capping (PAH, OA or stabilized by BF₄⁻ each with a concentration of 100 µg·mL⁻¹). The scale bar is 5 nm. Inserted is the value of lattice constant.

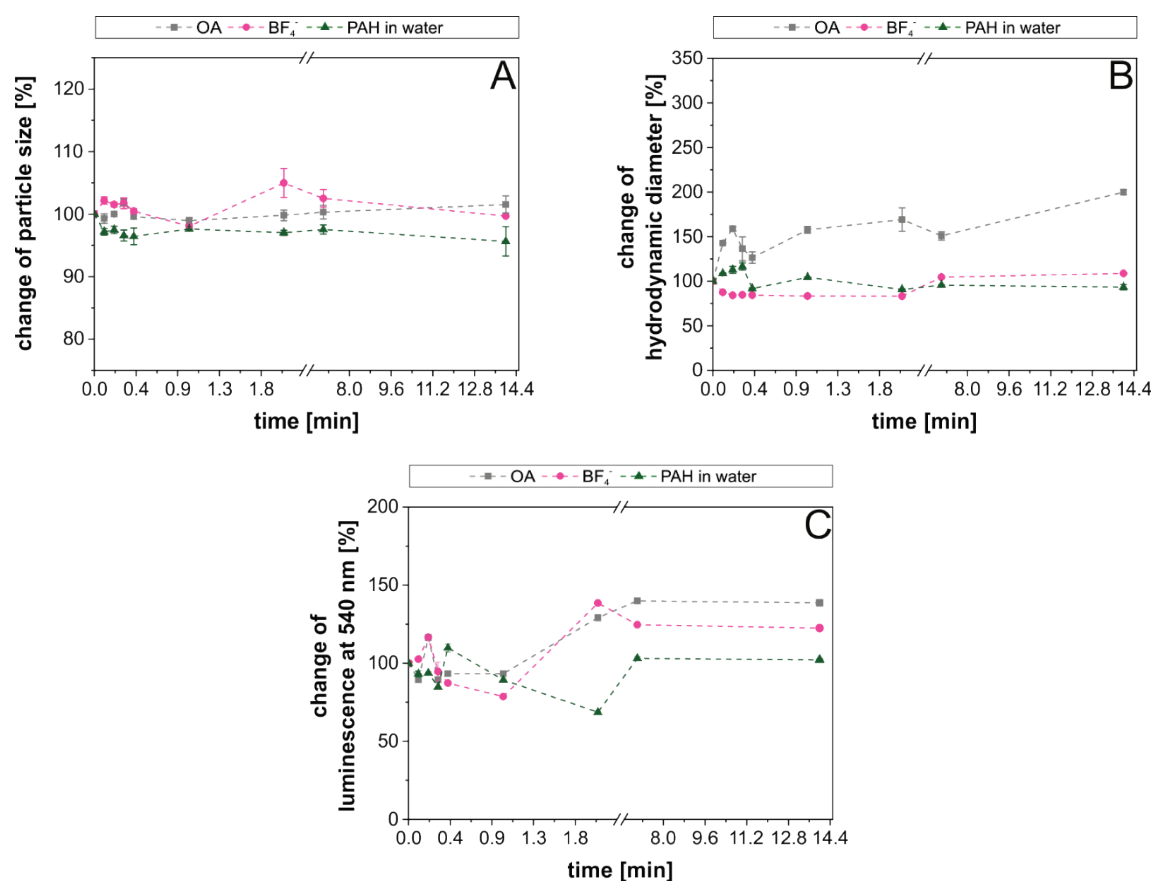


Figure 3.17| Long-term study of the colloidal and chemical stability of UCNPs with different surface cappings (OA, BF₄⁻ and PAH in water, each with a concentration of ~100 µg·mL⁻¹). (A): Change of particle size *via* TEM. The TEM images were analyzed using the software ImageJ. (B): Change of hydrodynamic diameter determined *via* intensity-weighted dynamic light scattering measurements. (C): Change of luminescent signal at 540 nm for different times and surface cappings. The particles were excited with a 980 nm laser module (250 mW, CW).

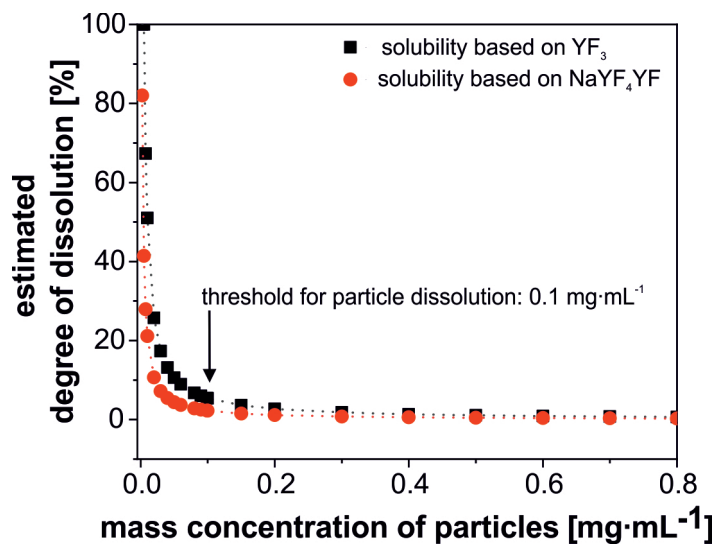


Figure S3.18| Calculation of particles dissolution based on the solubility constant of NaYF₄ (red) or YF₃ (black) and estimated threshold for particle dissolution. Below 100 $\mu\text{g}\cdot\text{mL}^{-1}$ a strong increase of the degree of dissolution can be observed.

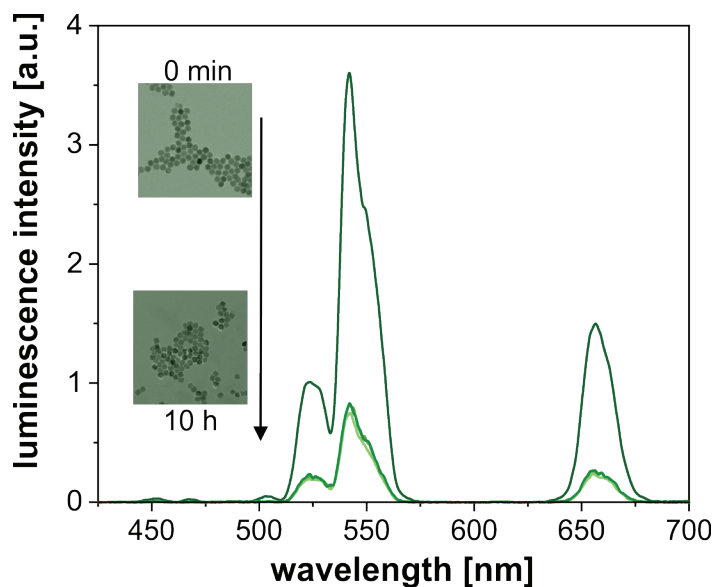


Figure 3.19| Luminescence spectra of PAH capped NaYF₄(Yb,Er) dispersed in dd water ($10 \mu\text{g}\cdot\text{mL}^{-1}$) at different time steps after dilution (0 min, 150 min, 300 min, 600 min). A 980 nm CW laser module (250 mW , $15 \text{ W}\cdot\text{cm}^{-2}$) was used as excitation source. Insert: TEM images of PAH capped NaYF₄(Yb,Er) 0 min and 10 h after dilution to $10 \mu\text{g}\cdot\text{mL}^{-1}$. The scale bar is 60 nm.

3.6.16 Overview of the mass concentration range of upconversion nanoparticles used for (bio)analytical application

Table S3.4 | Overview of the mass concentration range of UCNPs used for (bio)analytical application. For the calculation of the final concentration of nanoparticles in a mouse, a blood volume of 1.5 mL was assumed.

UCNPs	size [nm]	surface ligand	Mass concentration [$\mu\text{g}\cdot\text{mL}^{-1}$]		application	Ref
			Highest	Lowest		
NaYF ₄ :Yb,Er@NaYF ₄ :Yb, Nd	n.d.	DMSA ^{a)}	25	400	cytotoxicity of NIH-3T3 cells	[12]
NaYF ₄ :Yb,Er@NaYF ₄ @mSiO ₂ -Ru	75 - 80	mSiO ₂ -Ru	25	200	cytotoxicity of HepG2-cells	[13]
NaYF ₄ :Yb,Er	100	PLGA ^{b)}	10	50	cytotoxicity of HGC -cells	[14]
			10		imaging of HGC	
NaYF ₄ :Yb,Er	36	adipic acid	5	20	cell viability of SiHa cells	[15]
NaYF ₄ (20%Er)	17	ICG ^{c)} /DSPE-mPEG ^{d)}	2	60	cell viability in rat C6 cells	[16]
					cell viability in HeLa cells	
NaYF ₄ :Gd, Tb nanorod	~ 300	/ (ligand free)	50	1000	X-ray activated optical bioimaging in a mouse (20 g)	[17]
			200			
NaYF ₄ :Nd@NaLuF ₄ @SiO ₂	90	poly-styrene	50	800	cell viability in HeLa cells	[18]
			~ 150		bioimaging in a mouse	

^{a)}DMSA refers to dimercaptosuccinic acid; ^{b)}PLGA refers to poly(lactic-o-glycolic-acid) ^{c)}ICG refers to indocyanine green ^{d)}DSPE-mPEG refers to 1,2-distearoyl-sn-glycero-3-phosphoethanolamine-N-methoxy-(polyethylene glycol)-2000. N.d refers to not defined.

3.6.17 Analysis of the chemical and colloidal stability of hydrophilic UCNPs

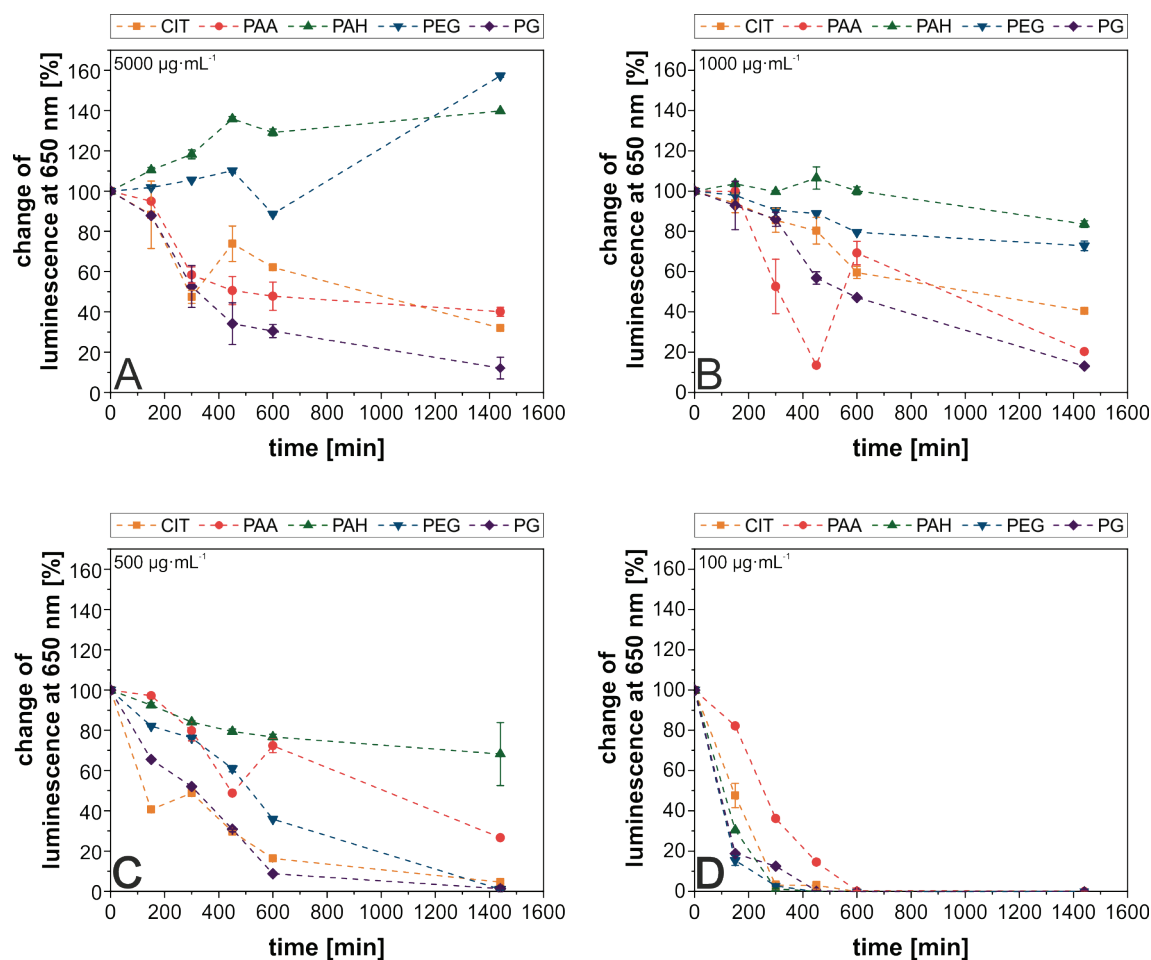


Figure S3.20] Monitoring of the change of luminescence at 650 nm of NaYF₄(Yb,Er) with different surface coatings (CIT, PAA, PAH, PEG, PG) and different particles concentrations (5000 µg·mL⁻¹ (A), 1000 µg·mL⁻¹ (B), 500 µg·mL⁻¹ (C), 100 µg·mL⁻¹ (D)) dialyzed against 50 mL dd H₂O. At each time step (2.5 h, 5 h, 7.5 h, 10 h, 24 h) the dialysis buffer was changed. The particles were excited with a 980 nm laser module (250 mW, CW).

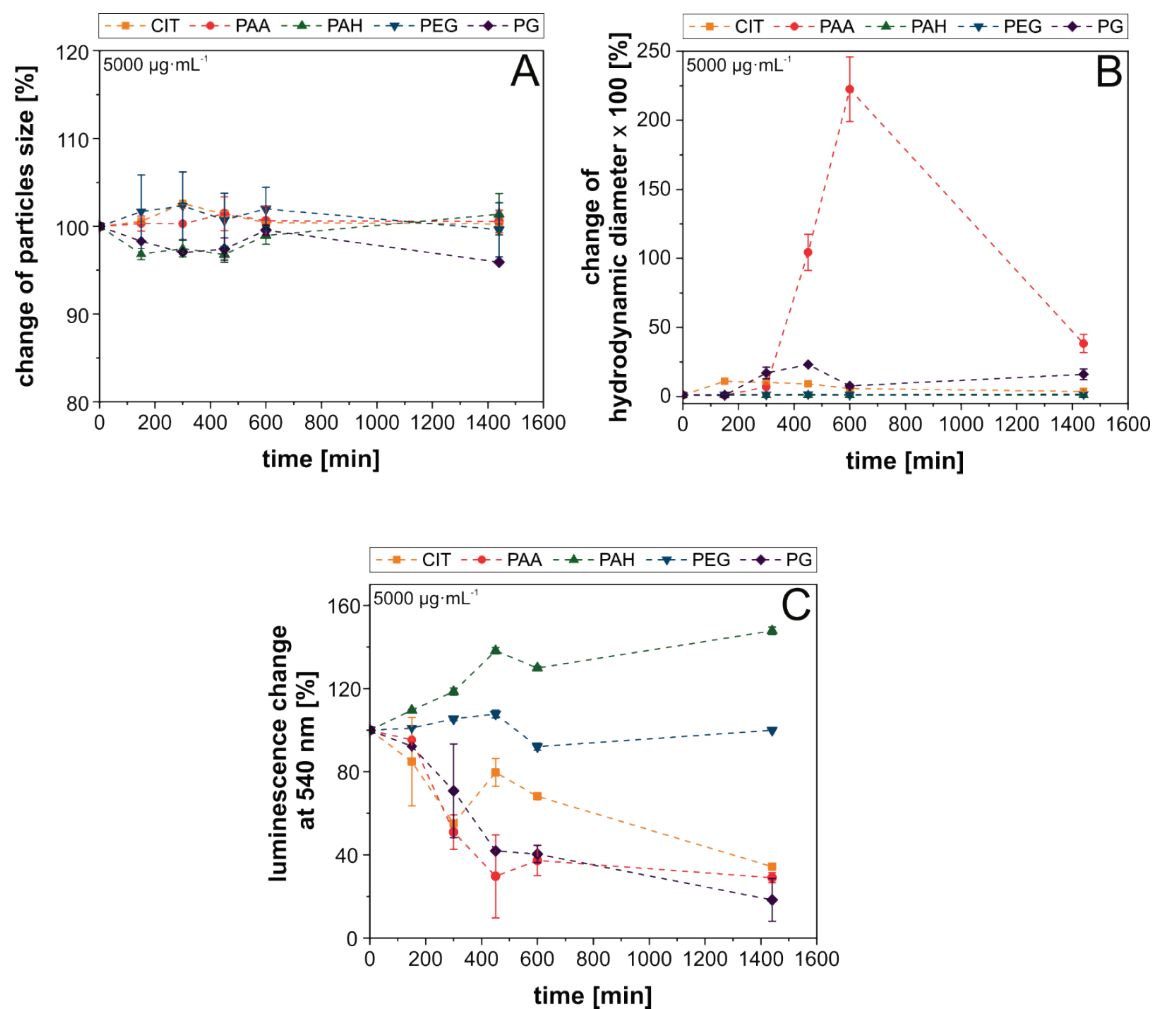


Figure S3.21| Analysis of the colloidal and chemical stability of UCNPs with different surface capping (PAA, PAH, PEG, PG, and CIT) and with a concentration of 5000 µg·mL⁻¹. (A): Change of particle size analyzed *via* TEM. (B): Change of hydrodynamic diameter determined *via* intensity-weighted dynamic light scattering measurement. (C): Change of luminescent signal at 540 nm for different times and surface cappings. The particles were excited with a 980 nm laser module (250 mW, CW).

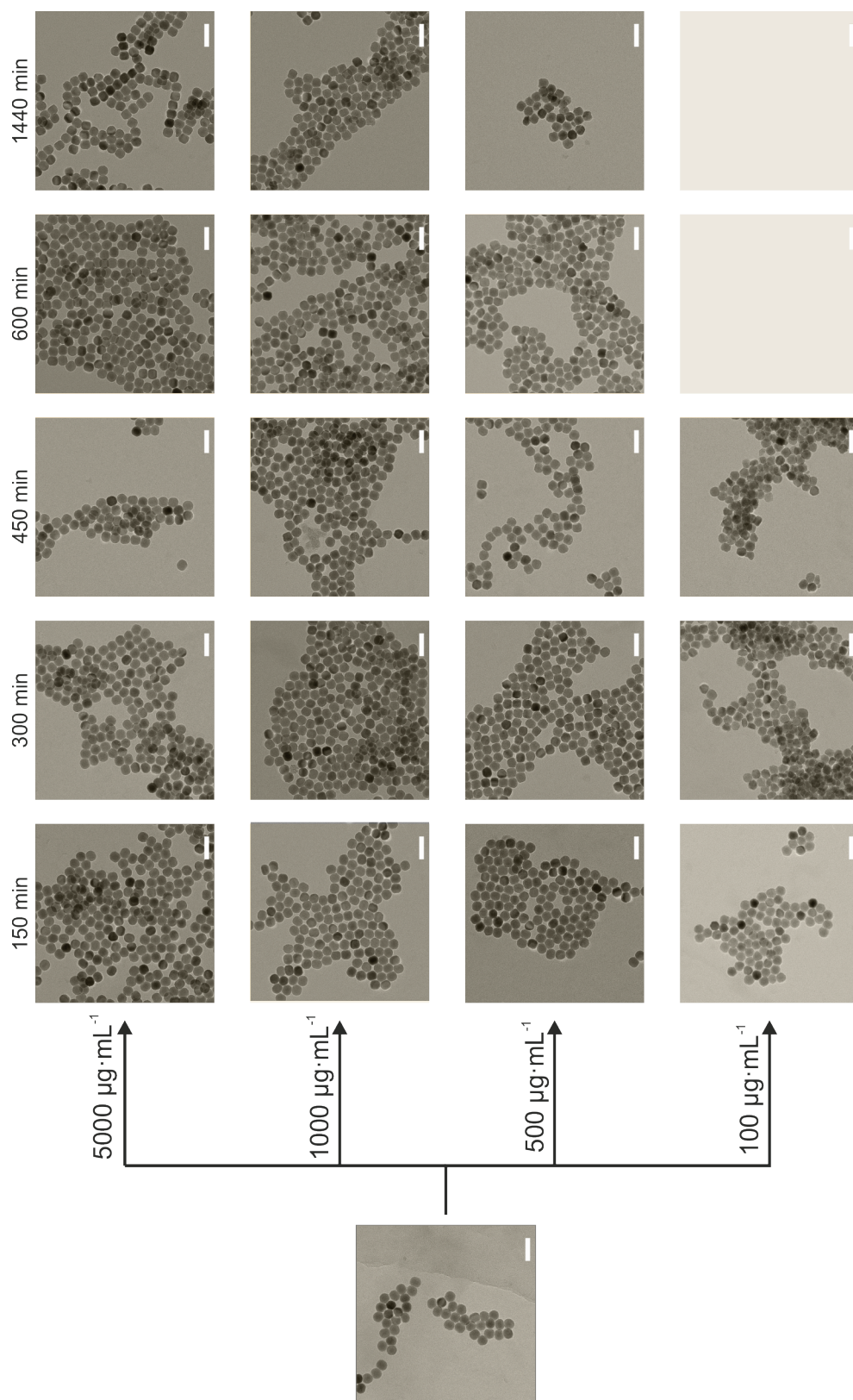


Figure S3.22| TEM image of NaYF₄(Yb,Er) with CIT capping and different concentrations (5000 μg·mL⁻¹, 1000 μg·mL⁻¹, 500 μg·mL⁻¹, 100 μg·mL⁻¹) dialyzed against 50 mL dd H₂O. The scale bar is 60 nm.

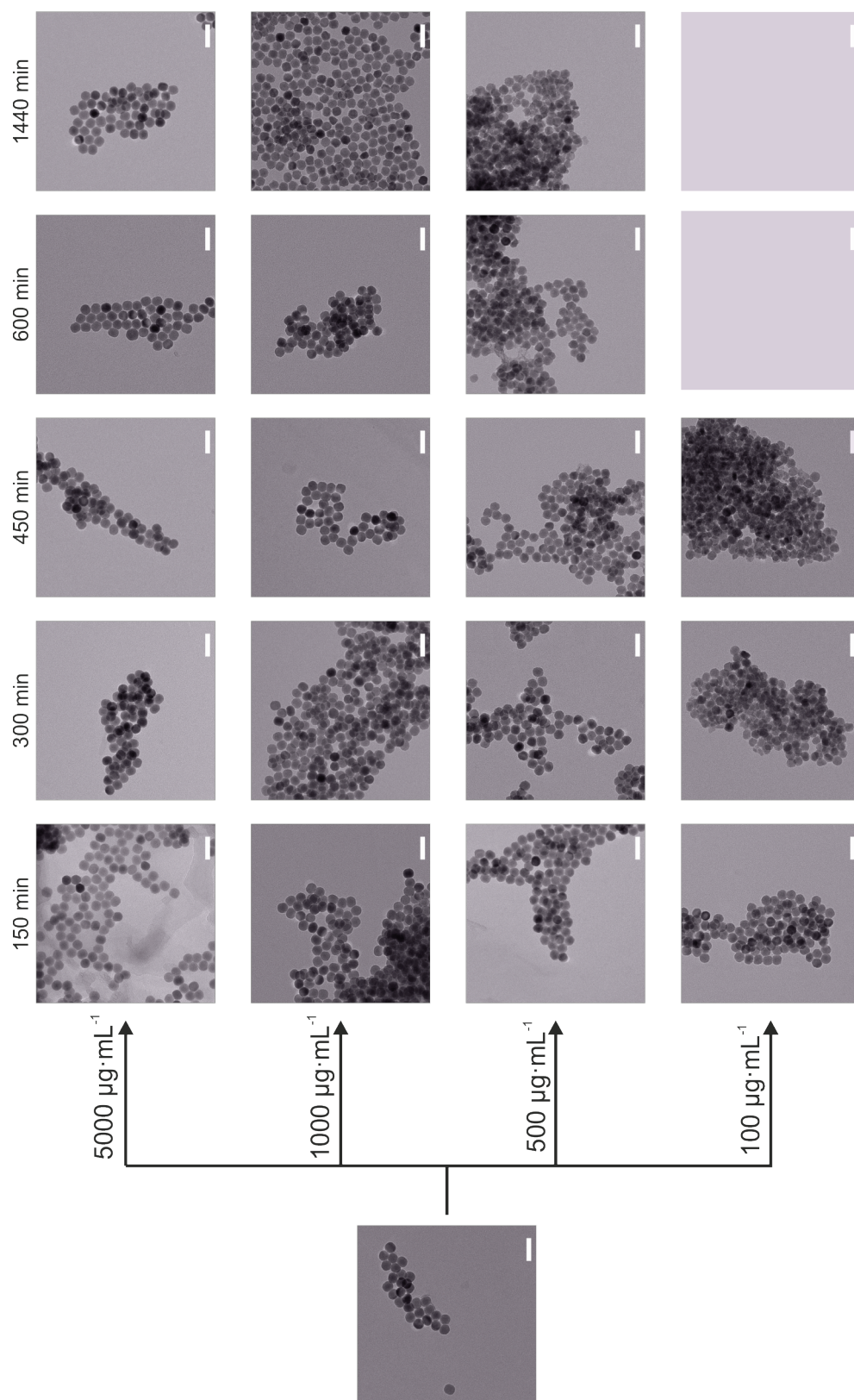


Figure S3.23 | TEM image of NaYF₄(Yb,Er) with PG capping and different concentrations (5000 µg·mL⁻¹, 1000 µg·mL⁻¹, 500 µg·mL⁻¹, 100 µg·mL⁻¹) dialyzed against 50 mL dd H₂O. The scale bar is 60 nm.

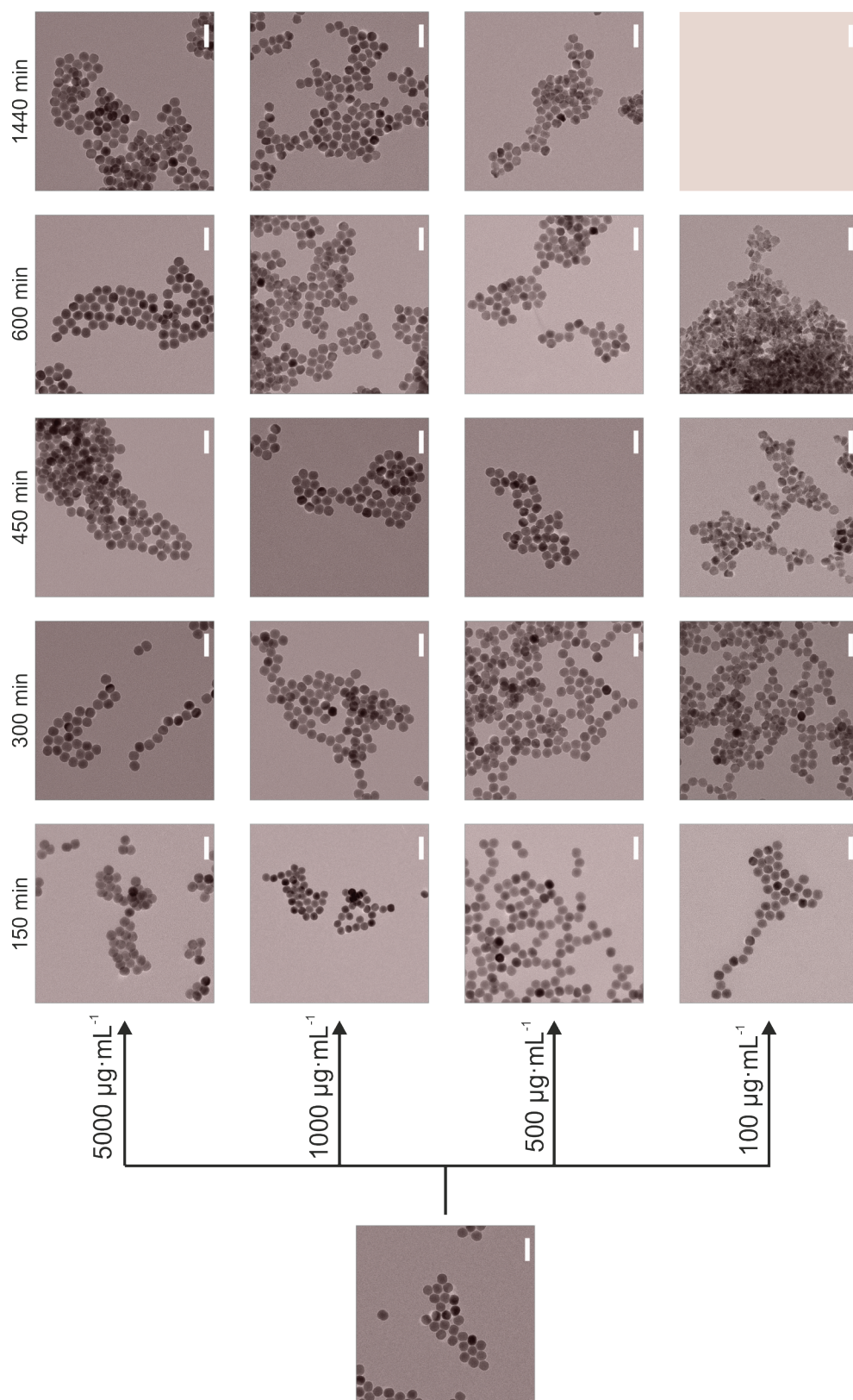


Figure S3.24| TEM image of NaYF₄(Yb,Er) with PAA capping and different concentrations (5000 μg·mL⁻¹, 1000 μg·mL⁻¹, 500 μg·mL⁻¹, 100 μg·mL⁻¹) dialyzed against 50 mL dd H₂O. The scale bar is 60 nm.

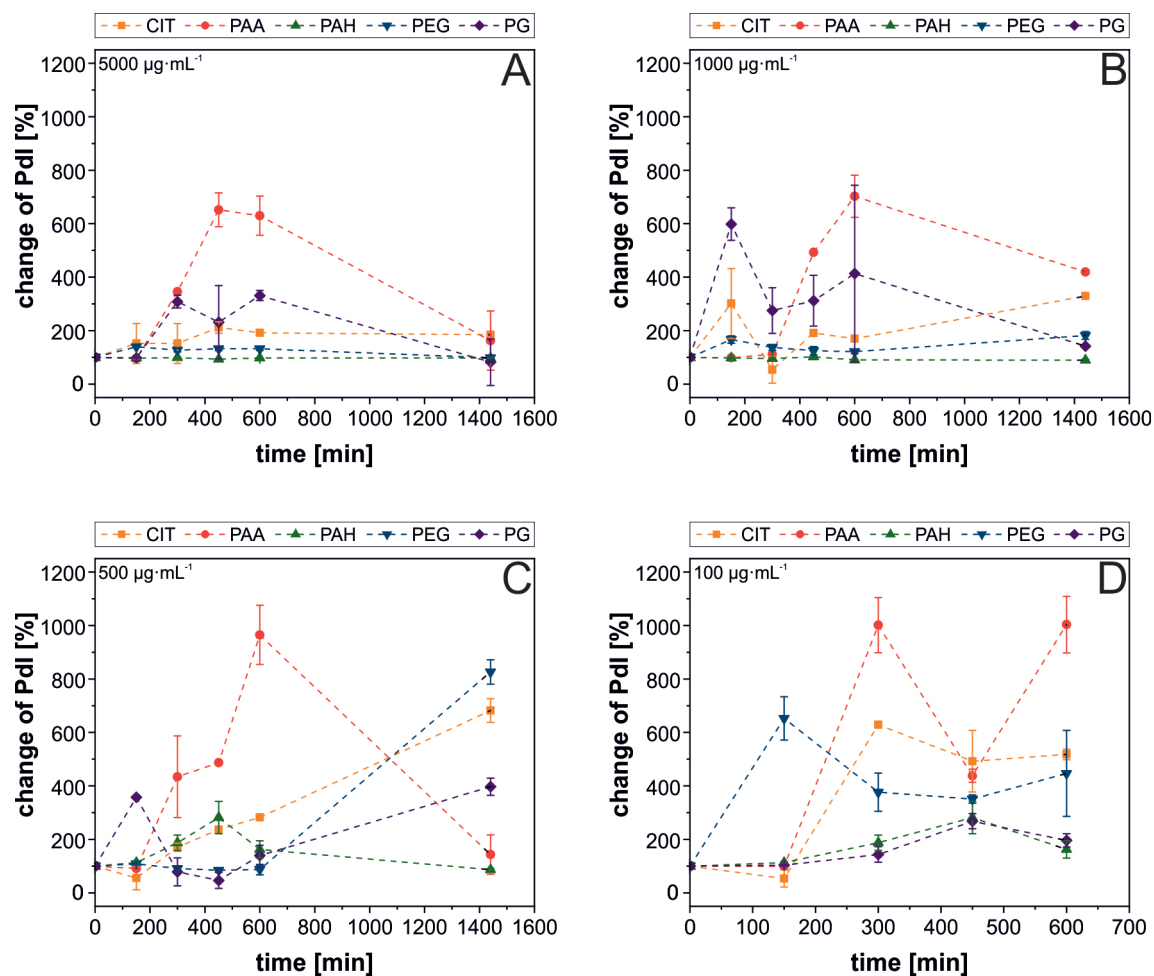


Figure S3.25| Monitoring of Pdl of NaYF₄(Yb,Er) with different surface coatings (CIT, PAA, PAH, PEG, PG) and different particles concentrations (5000 µg·mL⁻¹ (A), 1000 µg·mL⁻¹ (B), 500 µg·mL⁻¹ (C), 100 µg·mL⁻¹ (D)) dialyzed against 50 mL dd H₂O. At each time step (2.5 h, 5 h, 7.5 h, 10 h, 24 h) the dialysis buffer was changed.

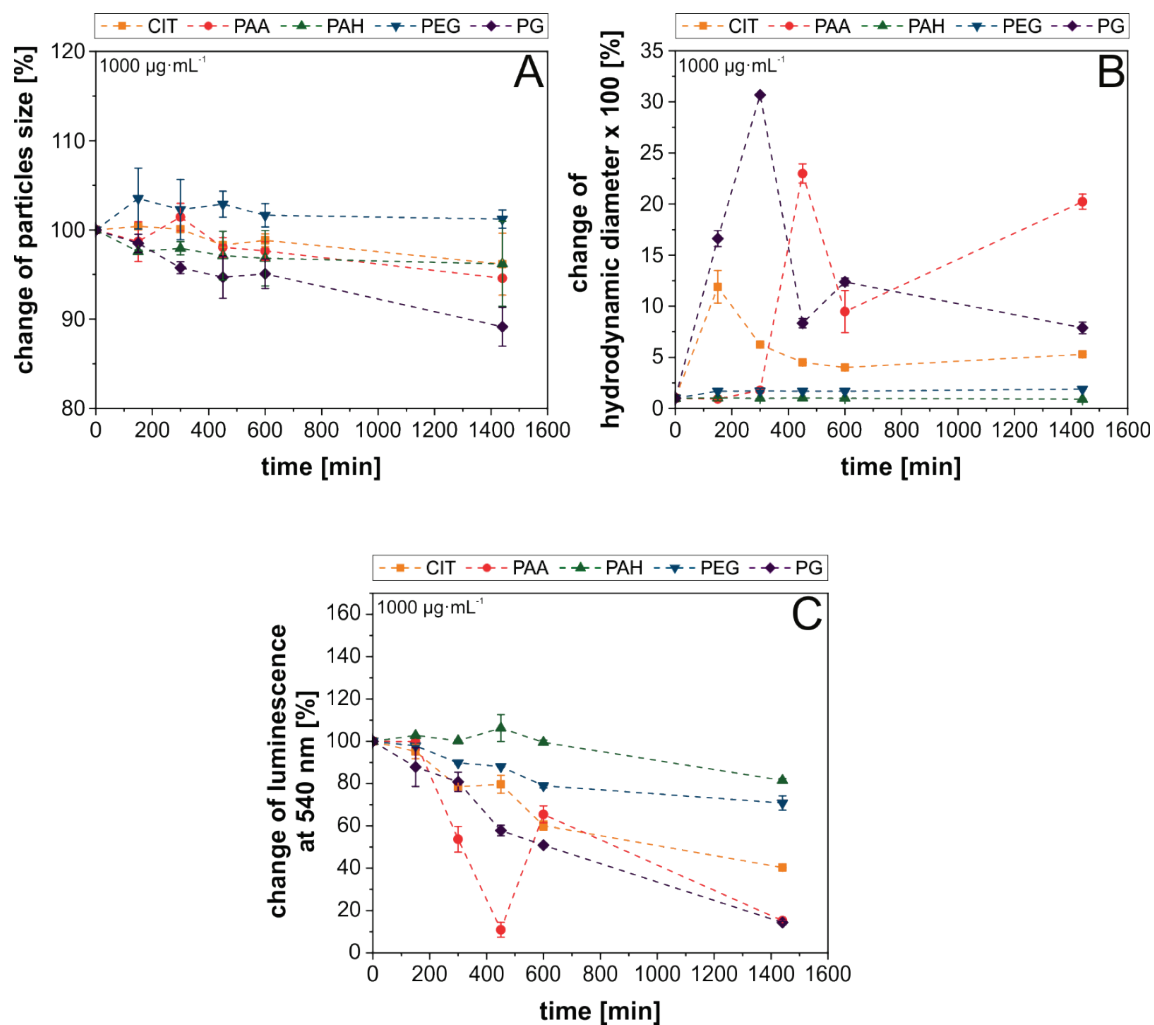


Figure S3.26 | Analysis of the colloidal and chemical stability of UCNPs with different surface cappings (PAA, PAH, PEG, PG, CIT) and with a concentration of 1000 µg·mL⁻¹. A: Change of particle size analyzed *via* TEM. B: Change of hydrodynamic diameter determined *via* intensity-weighted dynamic light scattering measurement. C: Change of luminescent signal at 540 nm for different times and surface capping. The particles were excited with a 980 nm laser module (250 mW, CW).

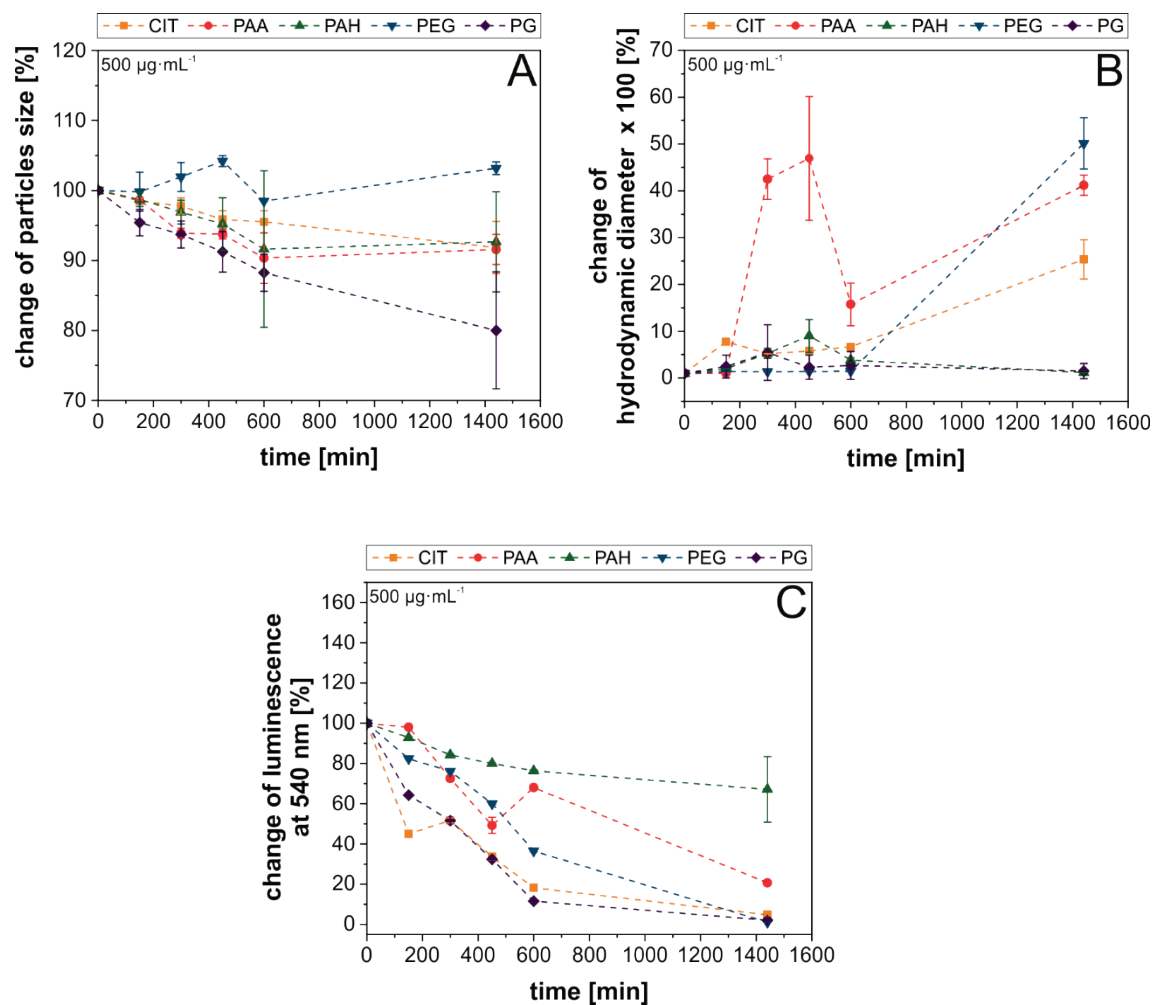


Figure S3.27| Analysis of the colloidal and chemical stability of UCNPs with different surface cappings (PAA, PAH, PEG, PG, CIT) and with a concentration of 500 µg·mL⁻¹. A: Change of particle size analyzed *via* TEM. B: Change of hydrodynamic diameter determined *via* intensity-weighted dynamic light scattering measurement. C: Change of luminescent signal at 540 nm for different times and surface capping. The particles were excited with a 980 nm laser module (250 mW, CW).

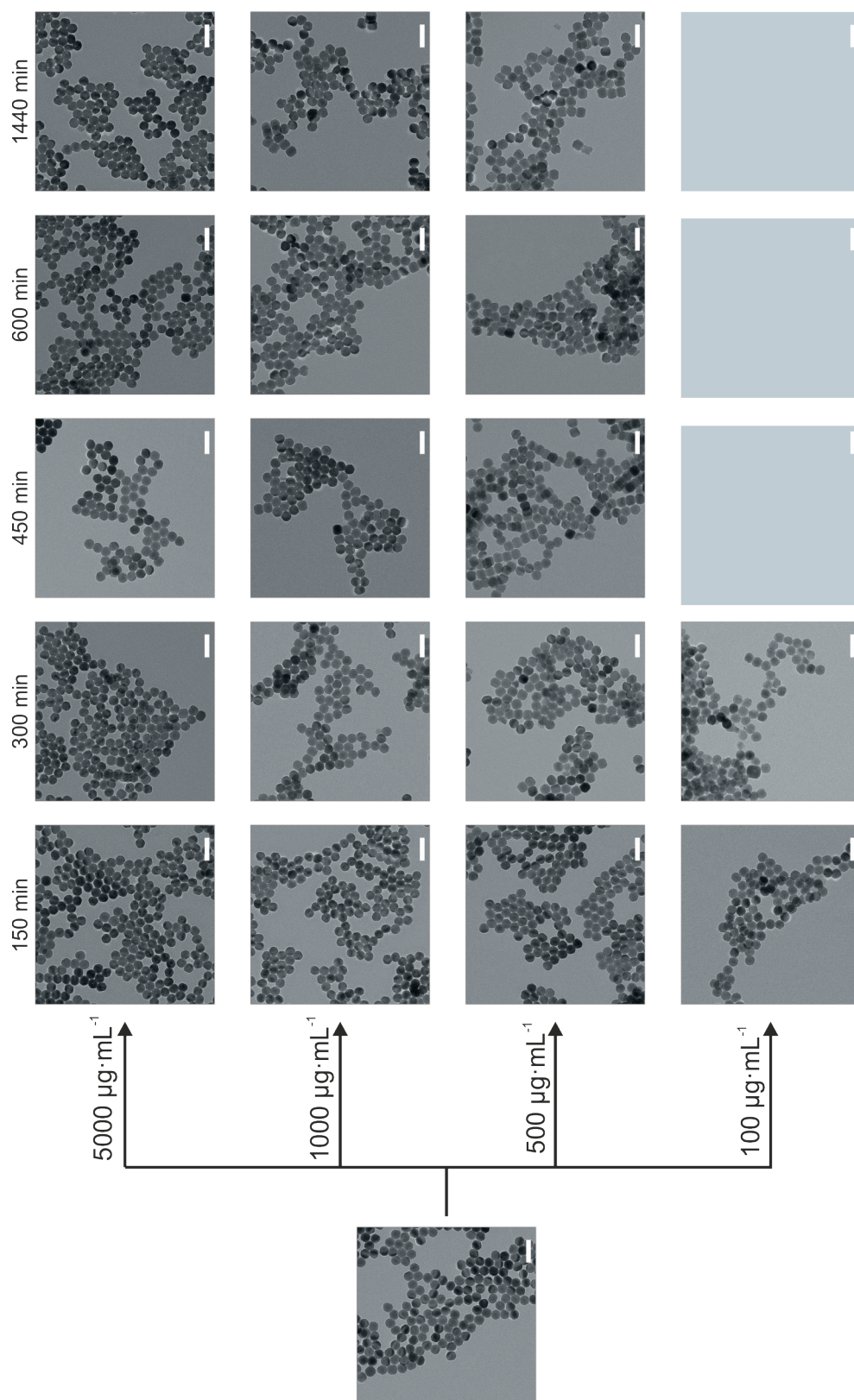


Figure S3.28| TEM image of NaYF₄(Yb,Er) with PEG capping and different concentrations (5000 μg·mL⁻¹, 1000 μg·mL⁻¹, 500 μg·mL⁻¹, 100 μg·mL⁻¹) dialyzed against 50 mL dd H₂O. The scale bar is 60 nm.

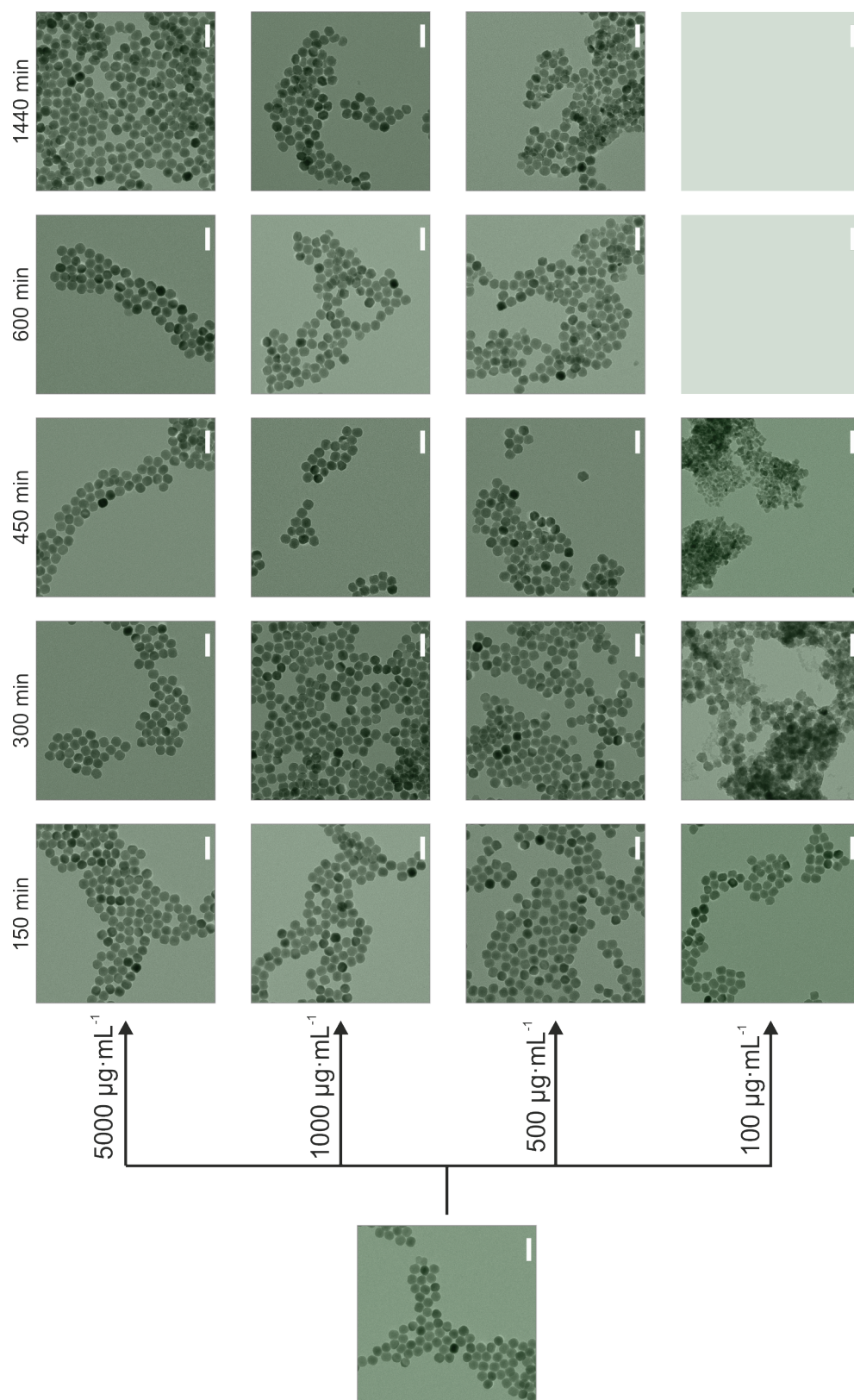


Figure S3.29| TEM image of NaYF₄(Yb,Er) with PAH capping and different concentrations (5000 μg·mL⁻¹, 1000 μg·mL⁻¹, 500 μg·mL⁻¹, 100 μg·mL⁻¹) dialyzed against 50 mL dd H₂O. The scale bar is 60 nm.

3.6.18 Influence of the dispersion media on the stability of UCNPs

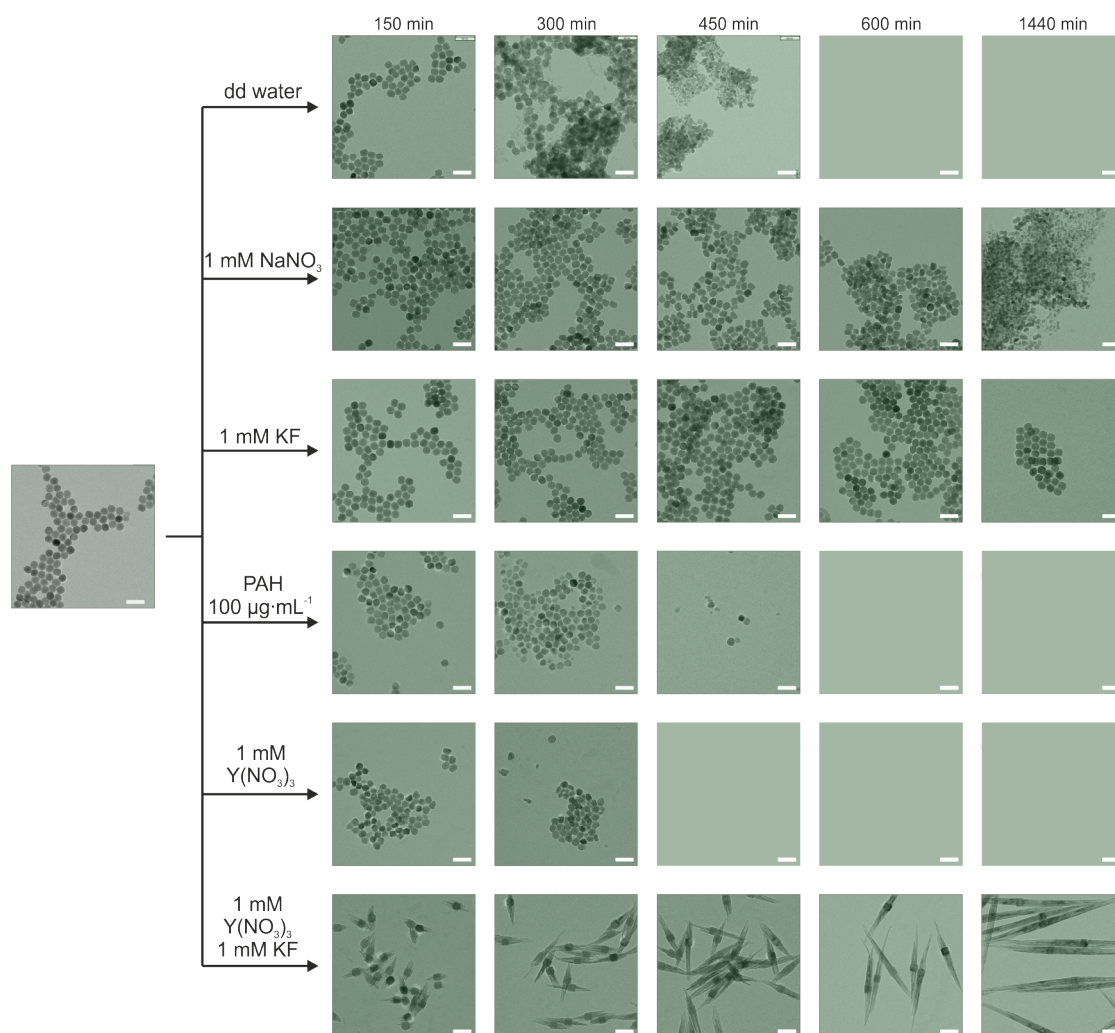


Figure S3.30| TEM images of NaYF₄(Yb,Er) with PAH capping (100 μg·mL⁻¹) dialyzed against 50 mL of following solutions: water, 1 mM NaNO₃, 1 mM KF, 100 μg·mL⁻¹ PAH, 1 mM Y(NO₃)₃, and (1 mM of KF, 1 mM of Y(NO₃)₃). The scale bar is 60 nm.

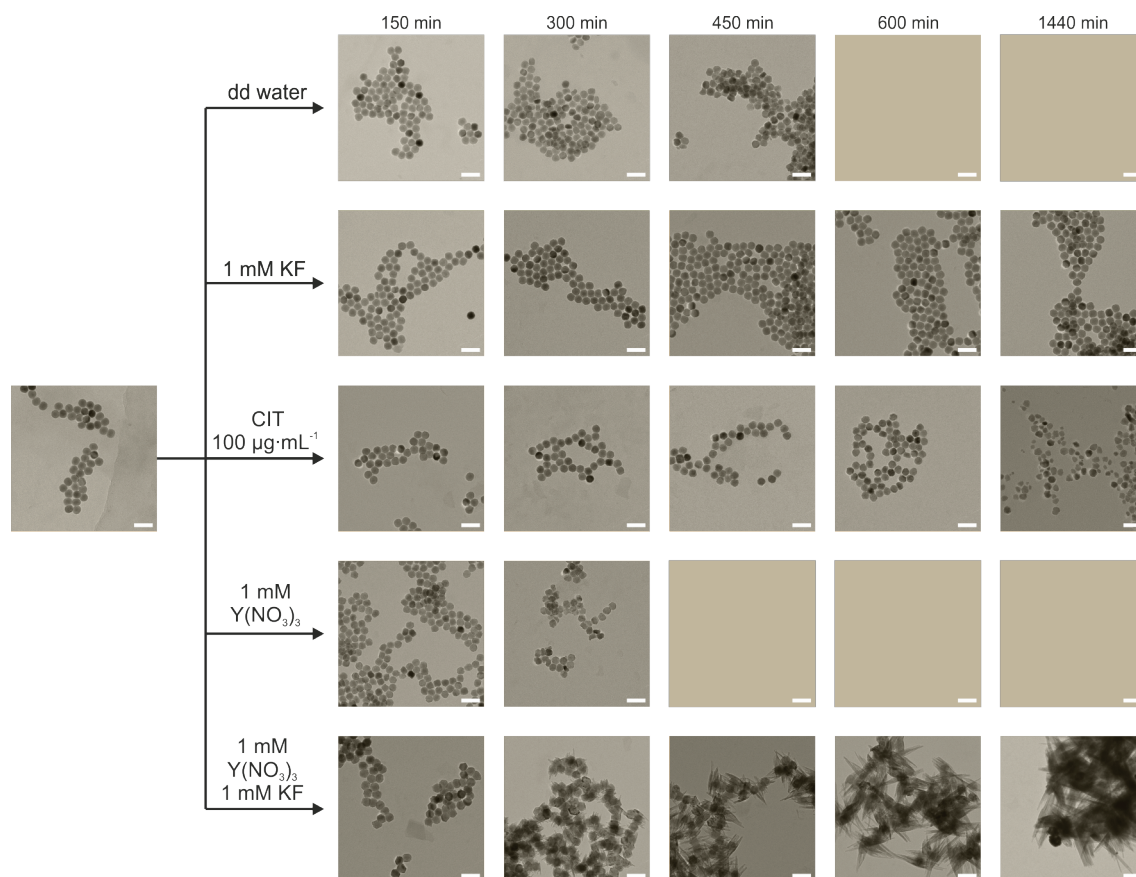


Figure S3.31| TEM image of NaYF₄(Yb,Er) with CIT capping (100 µg·mL⁻¹) dialyzed against 50 mL of following solutions: water, 1 mM KF, 100 µg·mL⁻¹ citrate, 1 mM Y(NO₃)₃, and (1 mM of KF, 1 mM of Y(NO₃)₃). The scale bar is 60 nm.

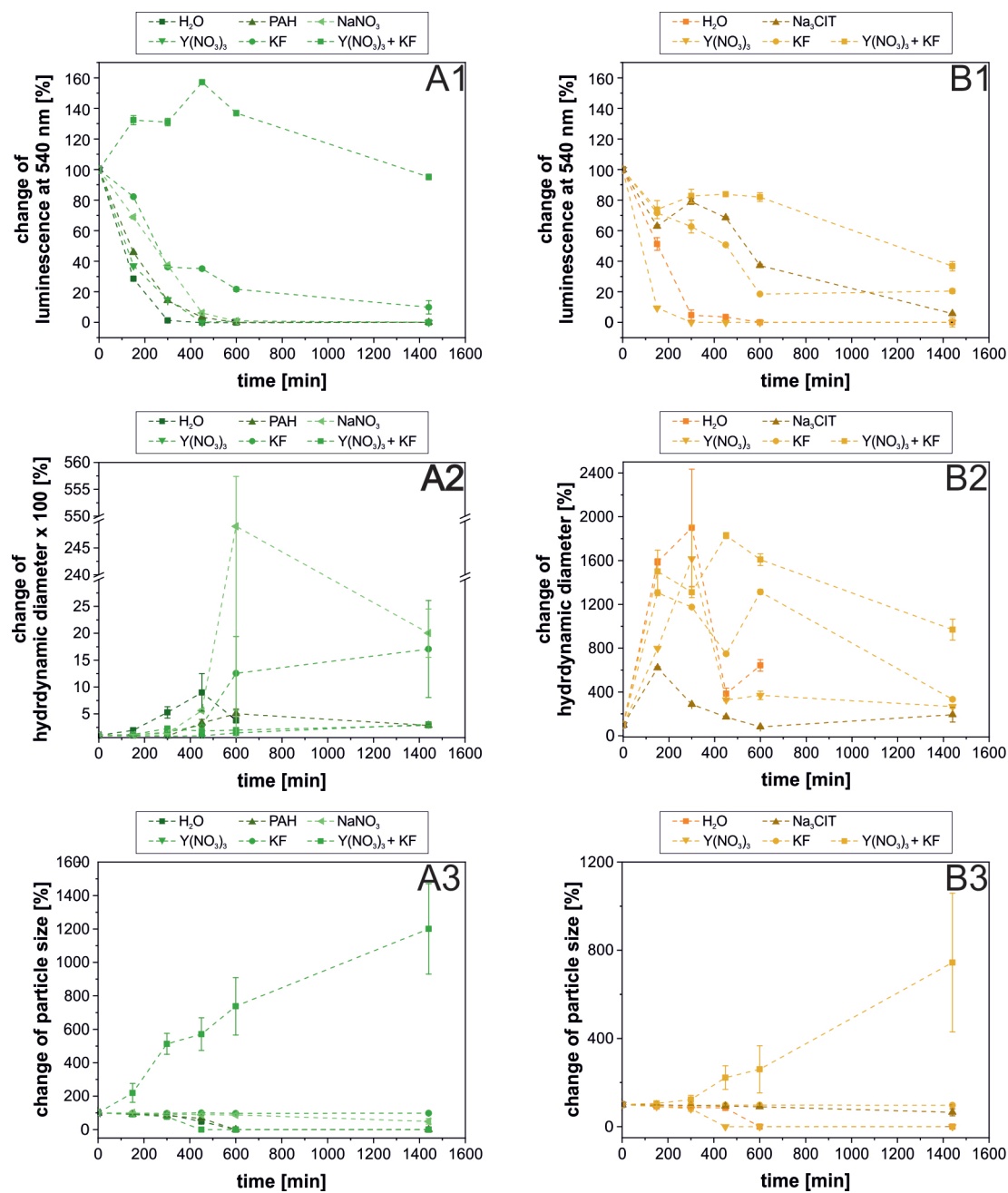


Figure S3.32| Analysis of the colloidal and chemical stability of UCNPs (with 100 µg·mL⁻¹ PAH (A) or CIT (B) *via* TEM (1), DLS (2) and their luminescent emission at 540 nm (980 nm, 250 mW, CW, C) under the influence of of following solutions: pure water, 1 mM KF, 100 µg·mL⁻¹ of additional surface ligand in the solution, 1 mM Y(NO₃)₃, and a mixture of 1 mM Y(NO₃)₃ and KF, 1 mM NaNO₃ (only for PAH).

3.6.19 Crosslinking of upconversion nanoparticles by dissolved Ln³⁺

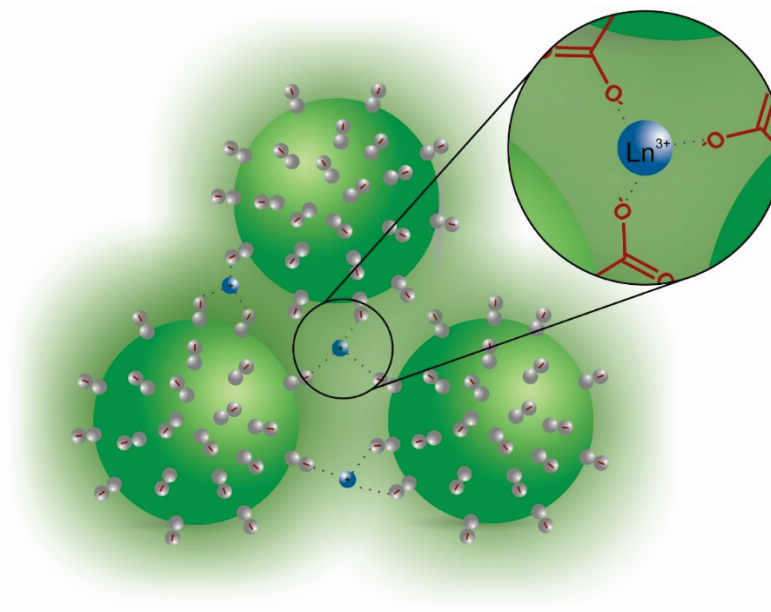


Figure S3.33| Schematic illustration of the crosslinking of UCNPs with negative surface charge (e.g. induced *via* carboxylic groups) and trivalent (positive) lanthanide ions.

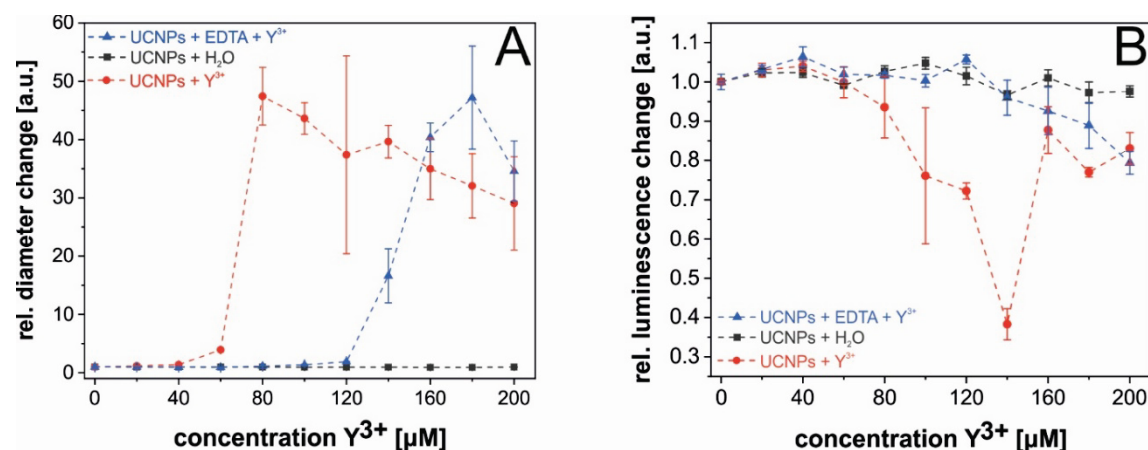


Figure S3.34| Analysis of the colloidal and chemical stability of PAA capped UCNPs by addition of an increasing amount of Y³⁺ (light red). As control experiment, equal amounts of water were added to the particles (grey red). To decrease the negative effect of the lanthanide ions 200 μM EDTA was added to complex the Y³⁺ (blue curve). For small concentrations, an increase of the stability could be obtained. With an increasing amount of Y³⁺, the free EDTA is not enough and crosslinking occurs again. The change of the hydrodynamic diameter was determined *via* intensity-weighted dynamic light scattering measurement (A). For the relative change of the luminescence at 540 nm, the particles were excited with a 980 nm laser module (250 mW, CW, (B).

3.6.20 Lattice constant of upconversion nanoparticles

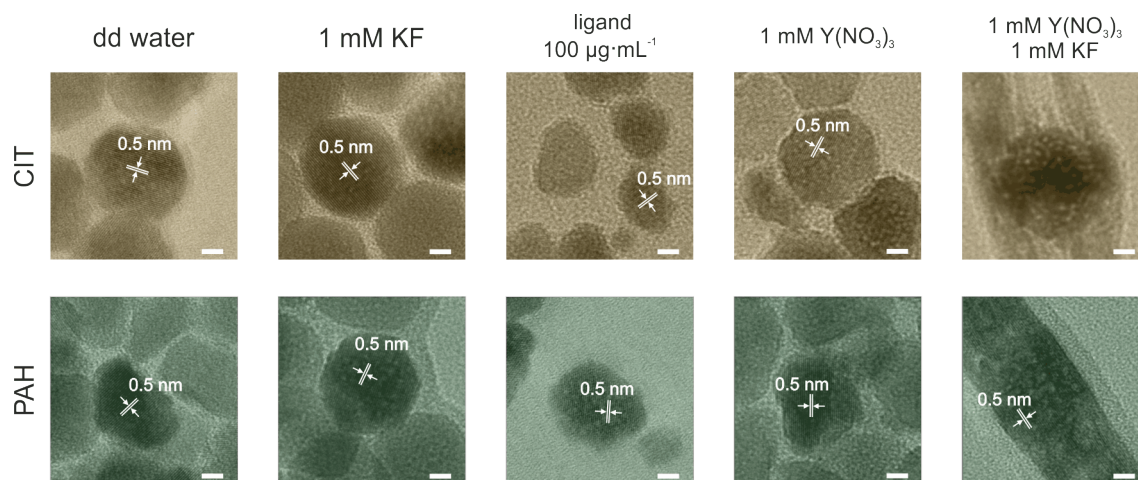


Figure S3.35| High resolution TEM image of $\text{NaYF}_4(\text{Yb},\text{Er})$ with CIT capping ($100 \mu\text{g}\cdot\text{mL}^{-1}$, upper row) upper row and with PAH capping ($100 \mu\text{g}\cdot\text{mL}^{-1}$, lower row) dialyzed against 50 mL of of following solutions: water, 1 mM KF, $100 \mu\text{g}\cdot\text{mL}^{-1}$ of trisodium citrate, 1 mM $\text{Y}(\text{NO}_3)_3$, and a mixture of 1 mM of KF and 1 mM of $\text{Y}(\text{NO}_3)_3$. The scale bar is 5 nm. Inserted is the value of lattice constant.

3.6.21 References

- [1] Muhr V, Würth C, Kraft M, Buchner M, Bäumner AJ, Resch-Genger U, Hirsch T (2017) Particle-Size-Dependent Förster Resonance Energy Transfer from Upconversion Nanoparticles to Organic Dyes. *Anal. Chem.* 89(9):4868-74.
- [2] Braslavsky SE (2007) Glossary of terms used in Photochemistry, IUPAC Recommendations 2006 79(3):293-465.
- [3] Wilhelm S, Kaiser M, Würth C, Heiland J, Carrillo-Carrion C, Muhr V, Wolfbeis OS, Parak WJ, Resch-Genger U, Hirsch T (2015) Water Dispersible Upconverting Nanoparticles: Effects of Surface Modification on their Luminescence and Colloidal Stability. *Nanoscale.* 7(4):1403-10.
- [4] Lushtinetz R, Oliveira AF, Duarte HA, Seifert G (2010) Self-Assembled Monolayers of Alkylphosphonic Acids on Aluminum Oxide Surfaces—A Theoretical Study. *Zeitschrift für anorganische und allgemeine Chemie* 636(8):1506-12.
- [5] Archer DG, Wang P (1990) The Dielectric Constant of Water and Debye-Hückel Limiting Law Slopes. *J. Phys. Chem. Ref. Data* 19(2):371-411.
- [6] Martell AE, Smith RM (1982) Inorganic Ligands. In *Critical Stability Constants* (pp. 393-424) Springer, Boston, MA.
- [7] Silva AM, Kong X, Hider RC (2009) Determination of the pKa Value of the Hydroxyl Group in the α -Hydroxycarboxylates Citrate, Malate and Lactate by ¹³C NMR: Implications for Metal Coordination in Biological Systems. *Biometals* 22(5):771-8.
- [8] Dhansay MA, Linder PW, Torrington RG, Modro TA (1990) Organophosphorus Herbicides and Plant Growth Regulators Part 1. Synthesis and Protonation Behaviour of Glyphosate and Related Compounds. *J. Phys. Org. Chem.* 3(4):248-54.
- [9] Sun L, Xiong X, Zou Q, Ouyang P, Burkhardt C, Krastev R. Design of Intelligent Chitosan/Heparin Hollow Microcapsules for Drug Delivery. *J. Appl. Polym. Sci.* 134(5).
- [10] Swift T, Swanson L, Geoghegan M, Rimmer S (2016) The pH-Responsive Behaviour of Poly(acrylic acid) in Aqueous Solution is Dependent on Molar Mass. *Soft Matter.* 12(9):2542-9.
- [11] Mackenzie LE, Goode JA, Vakurov A, Nampi PP, Saha S, Jose G, Millner PA (2018) The Theoretical Molecular Weight of NaYF₄:RE Upconversion Nanoparticles. *Sci. Rep.* 8(1):1106.
- [12] Shi Z, Duan Y, Zhu X, Wang Q, Li D, Hu K, Feng W, Li F, Xu C (2018). Dual Functional NaYF₄:Yb³⁺, Er³⁺@NaYF₄:Yb³⁺,Nd³⁺ Core-Shell Nanoparticles for Cell Temperature Sensing and Imaging. *Nachtechnol.* 29(9):094001.
- [13] Xu S, Yu Y, Gao Y, Zhang Y, Li X, Zhang J, Wang Y, Chen B (2018) Mesoporous Silica Coating NaYF₄:Yb,Er@NaYF₄ Upconversion Nanoparticles Loaded with Ruthenium (II) Complex Nanoparticles: Fluorometric Sensing and Cellular Imaging of Temperature by Upconversion and of Oxygen by Downconversion. *Microchim. Acta.* 185(10):454.
- [14] M Mancic, Djukic-Vukovic A, Dinic I, Nikolic MG, Rabasovic MD, Krmpot AJ, Costa AM, Trisic D, Lazarevic M, Mojovic L, Milosevic O (2018). NIR Photo-Driven Upconversion in NaYF₄:Yb,Er/PLGA Particles for *in Vitro* Bioimaging of Cancer Cells. *Mater. Sci. Eng. C* 91:597-605.
- [15] Wang M, Zhang T, Hu Y, Qin Y, Wei W (2019) *In Situ* Synthesis of Dicarboxylic Acid Functionalized Upconversion Nanoparticles for Bioimaging Applications. *ChemPhotoChem* 3(3):145-50.
- [16] Wang D, Wang D, Kuzmin A, Pliss A, Shao W, Xia J, Qu J, Prasad PN (2018) ICG-Sensitized NaYF₄:Er Nanostructure for Theranostics. *Adv. Opt. Mater.* 6(12):1701142.
- [17] Li X, Xue Z, Jiang M, Li Y, Zeng S, Liu H (2018) Soft X-ray Activated NaYF₄: Gd/Tb Scintillating Nanorods for *in Vivo* Dual-Modal X-Ray/X-Ray-Induced Optical Bioimaging. *Nanoscale* 10(1):342-50.
- [18] Yang D, Cao C, Feng W, Huang C, Li F (2018) Synthesis of NaYF₄: Nd@ NaLuF₄@ SiO₂@ PS Colloids for Fluorescence Imaging in the Second Biological Window. *J. of Rare Earths* 36(2):113-8.

CHAPTER 4

980 nm and 808 nm excitable upconversion nanoparticles for the detection of enzyme related reactions

Upconverting luminescent nanoparticles (UCNPs) represent an interesting class of nanomaterials for bioanalytical applications. Due to their excitation in the near infrared region of the spectra, no fluorescence of biological compounds is triggered. Compared to other nanomaterials like quantum dots, they exhibit low cytotoxicity, high photostability, no blinking and chemical inertness. Nevertheless, UCNPs suffer from low quantum efficiency. Here we report on two different core-shell particle systems which have a core consisting of NaYF₄ doped with Yb³⁺/Tm³⁺ and an additional inert shell (NaYF₄) or an active shell (NaYF₄ doped with Yb³⁺/Nd³⁺). Nanoparticles without Nd³⁺ as sensitizer can be excited at 980 nm. However, water has an absorption band in this region. This results in a reduction of the upconversion efficiency in aqueous systems and a heating of the solution. For bioanalytical application, more beneficial is the shifting of the wavelength to 808 nm by additional doping of the shell with Nd³⁺. Both core-shell systems were investigated with respect to monitor enzymatic reactions of dehydrogenases and oxidases involving the generation of either NADH or FADH₂.

This chapter has been published:

Himmelstoß SF, Wiesholler LM, Buchner M, Muhr V, Märkl S, Baeumner AJ, Hirsch T. 980 nm and 808 nm excitable upconversion nanoparticles for the detection of enzyme related reactions. SPIE BiOS 10077:100770L1-100770L6.

Author contributions:

Most of the experimental work was carried out by SFH. SFH and SM synthesized the UCNPs. Surface chemistry results were discussed with VM and MB. Shift of excitation wavelength was discussed with LMW. XRD measurements were performed by LMW. SFH wrote the manuscript. SFH, AJB and TH revised the article. TH is corresponding author.

4.1 Introduction

In the human body several enzymes, like oxidoreductases (*e.g.* lactate hydrogenase (LDH) or glucose oxidase (GOx)), are present to regulate the metabolism and guarantee the vital interplay of nerves, muscles or even whole organs. Some of the enzymes need a co-substrate like nicotinamide adenine dinucleotide (NADH) [1] or have a prosthetic group like flavin adenine dinucleotide (FAD) to enable their enzymatic function. These molecules can be found within biological electron transport chains [2], where they transfer electrons or hydrogen atoms from one metabolite to another. Besides this, they take part in the β -oxidation of fatty acids [3] and several other redox reactions [4] within the human body. This makes these molecules interesting candidates for monitoring enzymatic reactions and therefore to diagnose metabolic disorder or other diseases, especially when mutation occurred [5]. For example, patients suffering from amyotrophic lateral sclerosis (ALS), a degeneration of the nerve system, show an increased FAD level [6]. The easiest way to detect FAD or NAD⁺ is by their intrinsic fluorescence, but this is accompanied with low signals and therefore low sensitivity in complex matrices like body fluids or inside biological cells, due to high background fluorescence. Both molecules are excited in the UV at 450 nm (FAD) or 350 nm (NADH) [7,8], where also a lot of other biomolecules will get excited.

Upconversion nanoparticles (UCNPs) can overcome this drawback. Those inorganic nanocrystal (*e.g.* a NaYF₄ host crystal doped with Ytterbium and Thulium) are capable to convert low energy excitation into high energy radiation [9]. Thereby the Ytterbium ions work as sensitizer ions, which can absorb light in the near infrared region (NIR) of the spectra. The energy is then transferred to an activator ion like Thulium. During the relaxation from the excited state to the ground state, visible light is emitted [10]. As a consequence, autofluorescence of biological compounds can be prevented. This results in a low background signal and makes them ideal candidates for *in vitro* and *in vivo* imaging and labeling [11,12] or for the bioanalytical sensing application for NAD⁺ and FAD. The most studied UCNPs so far only consist of one sensitizer (*e.g.* Yb³⁺) and one activator ion (Tm³⁺) and their excitation is at around 980 nm. At this wavelength, also water exhibits a local absorption maximum which minimizes the efficiency of the upconversion process and can lead to sample heating. By increasing the diameter of the nanoparticles also the brightness of the particles gets enhanced [13]. This is in contradiction to the demand of small particles for bio-applications. The solution to get small but also bright particles is demonstrated by the design of core-shell particles. A thin shell of NaYF₄ around the UCNPs will lead to surface passivation [14]. Thereby the dopants of the UCNPs are kept at greater distance to the particle surface, whereas less interaction of water molecules and dopants occurs and a higher upconversion efficiency is achieved. Another attractive alternative to minimize the influence of water is the change of the excitation wavelength of the UCNPs towards the biological optical window. This can be achieved by doping the shell of the UCNPs with neodymium ions (Nd³⁺) to create a so-called activated shell. The Nd³⁺ ions can be excited at 808 nm and they can transfer the energy to the Yb³⁺ ions to excite the upconversion luminescence [15]. Here we report on the comparison of the optical properties of upconversion nanoparticles of the type NaYF₄(Yb,Tm) with two different shell types – an undoped shell and an activated shell with neodymium. Furthermore, the particles are examined concerning their ability to monitor enzymatic reactions *via* concentration changes of the co-factors.

4.2 Experimental Section

4.2.1 Materials

1-Octadecene and oleic acid (both technical 90%) were purchased from Alfa Aesar (www.alfa.com). Lanthanide chloride hexahydrate ($\text{YbCl}_3 \cdot 6 \text{H}_2\text{O}$, $\text{YCl}_3 \cdot 6 \text{H}_2\text{O}$, and $\text{TmCl}_3 \cdot 6 \text{H}_2\text{O}$, $\text{ErCl}_3 \cdot 6 \text{H}_2\text{O}$ each >99.99%) were obtained from Treibacher Industrie AG (www.treibacher.com) or Sigma Aldrich (www.sigmaaldrich.com). N,N-dimethylformamide (DMF) (99.5%) was from Acros Organics (www.acros.com). Chloroform (99.7%) and methanol (99.9%) were purchased from Fisher Chemicals (www.fisher.co.uk). Ammonium fluoride nitrosyl tetrafluoroborate (95%, NOBF_4), poly(acrylic acid) sodium salt ($M_w = 2100 \text{ Da}$, PAA), Sodium L-lactate and L-lactic dehydrogenase from rabbit muscle (lyophilized powder with activity of $816 \text{ U} \cdot \text{mg}^{-1}$ of the lyophilized solid), D-glucose, D-fructose, sucrose, L-ascorbic acid and hydrazine monohydrate were purchased from Sigma Aldrich (www.sigmaaldrich.com). Cyclohexane was obtained from VWR chemicals (www.vwr.com). Glycine was purchased from Merck (www.merckmillipore.com). Millipore water was used for the preparation of all buffers and aqueous solutions.

4.2.2 Characterization methods

Transmission electron microscopy (TEM) of UCNPs was carried out by wetting a carbon-copper grid (400 mesh, Plano GmbH, www.planoem.de) with 20 μL of a UCNP dispersion ($1.5 \text{ mg} \cdot \text{mL}^{-1}$) and measured with a 120 kV Phillips CM12 microscope (www.fei.com). The particle size distribution was analyzed by using the software ImageJ (<http://rsbweb.nih.gov/ij/>). For dynamic light scattering and ζ -potential measurements a Malvern Zetasizer Nano-ZS (www.malvern.com) at 20 °C was used. X-ray powder diffraction (XRD) analyses were obtained by using a STOE STADI P diffractometer with a Cu source (K_α radiation of 1.54060 Å). The measurements were performed at 40 kV and 30 mA with a resolution of 0.005° (2θ).

A Flame-EOP inductively coupled plasma optical emission spectrometer (ICP- OES) from Spectro (www.spectro.com) was used for the concentration determination of the lanthanide ions of the nanoparticles. Purification steps were done in a Hettich Universal 320 or a Hettich Mikro 200R centrifuge (www.hettichlab.com). Luminescence measurements were performed at room temperature with an Elmer-Perkin LS 50 (www.perkinelmer.com) luminescence spectrometer equipped with an external continuous wave (CW) 980 nm laser module (focusable, 200 mW and 120 mW) or an 808 nm laser module (500 mW) (www.picotronic.de). The spectra were recorded by using semi-microdisposable (1.5 mL) polymethylmethacrylate (PMMA) cuvettes with an optical pathway of 1 cm.

4.2.3 Synthesis of $\beta\text{-NaYF}_4$ nanoparticles doped with lanthanide ions

Hexagonal NaYF_4 nanoparticles doped with lanthanide ions (*e.g.* Yb^{3+} and Tm^{3+}) were obtained by solving in total 1 mmol of the desired rare earth trichlorides hexahydrates in methanol (5 mL). Under nitrogen flow this solution was mixed with oleic acid (6 mL) and 1-octadecene (15 mL) in a 50 mL three-necked round bottom flask. The solution was then heated to 160 °C and stirred for 30 min under vacuum until the solution gets clear. The mixture was cooled to room temperature und 2.5 mmol NaOH

and 4.0 mmol NH_4F in 10 mL methanol was added. The resulting suspension was heated to 120 °C for 30 min and then heated to reflux. The progress of the synthesis was controlled by illumination with a 980 nm CW laser module. After upconversion luminescence can be observed, the solution was kept another 5 - 10 min under reflux and then cooled to room temperature. The particles were precipitated with an excess of ethanol and separated from the solution by centrifugation (1000 g, 5 min). The resulting pellet was redispersed in chloroform, precipitated by ethanol and separated by centrifugation. This step was repeated twice for chloroform/ethanol and at least three times for cyclohexane/acetone. Finally, the pellet was dispersed in cyclohexane (5 mL) and centrifuged (1000 g, 3 min) to remove aggregates. The supernatant was collected.

4.2.4 Synthesis of α - NaYF_4 nanoparticles

Cubic phase NaYF_4 nanoparticles doped with lanthanide ions (e.g. Yb^{3+} , Nd^{3+}) were obtained by solving in total 1 mmol of rare earth trichlorides hexahydrates in methanol (5 mL). Under nitrogen flow this solution was mixed with oleic acid (6 mL) and 1-octadecene (15 mL) in a 50 mL three-necked round bottom flask. The solution was then heated to 160 °C and stirred for 30 min under vacuum. The mixture was cooled to room temperature and 2.5 mmol NaOH and 4.0 mmol NH_4F in 10 mL methanol was added. The resulting suspension was heated to 240 °C for 30 min and cooled to room temperature. The purification protocol was the same as described for the β -nanoparticles.

4.2.5 Synthesis of β -phase core/shell upconversion nanoparticles

Hexagonal phase core/shell nanostructures were prepared from the starting materials (lanthanide doped β - NaYF_4 particles (0.5 mmol) and lanthanide doped α - NaYF_4 -nanoparticles (1.5 mmol)). In a 50 mL three-necked round bottom flask per 1 mmol total content of the nanoparticles 5 mL oleic acid and 5 mL 1-octadecene were added. The β - NaYF_4 - particles and the shell precursor material were separately heated to 100 °C and vacuum was applied for 1 h unless a clear solution was obtained. Then the β - NaYF_4 nanoparticles were heated above 300 °C and the shell precursor was kept at 100 °C. Every 10 min a small volume of the shell precursor was added to the β - NaYF_4 -particles. When the precursor material was consumed, the solution was kept for another 10 min before it was cooled to room temperature. Purification was performed as described for the β -nanoparticles.

4.2.6 Surface modification of upconversion nanoparticles

Hydrophobic, oleate coated UCNPs were modified with PAA to render them water dispersible. In the first step, the oleic acid was removed *via* the addition of NOBF_4 . Therefore, particles in cyclohexane were mixed with an equivalent amount of DMF. NOBF_4 (around 1 mg per 1 mg nanoparticles) was added and the mixture was stirred for 20 min at 30 °C. The cyclohexane phase was rejected. The particles were precipitated with an excess of chloroform and separated by centrifugation (1000 g, 5 min). The resulting gel-like pellet was redispersed in DMF, precipitated by chloroform and separated by centrifugation. Finally, the pellet was dispersed in the desired amount of DMF (~5 mL) and centrifuged (1000 g, 3 min) in order to remove aggregates. The supernatant was collected. In the next step the UCNPs, stabilized by tetrafluoroborate, were mixed with a solution of PAA (around 1 mg polymer per 5 mg particles) and stirred for 15 min. The particles were purified either by dialysis against water or by centrifugation. Separation by centrifugation was performed at ~15.000 g for 60 min. The

pellet was then redispersed in dd water and centrifuged again. This step was repeated at least three times. Finally, the particles were dispersed in dd water (~5 mL) and centrifuged at 1000 g for 3 min to remove aggregates. The supernatant was collected.

4.3 Results and discussion

4.3.1 Characterization of upconversion nanoparticles

In this study, UCNPs of core-shell architecture have been used. Core particles with a diameter of 29.1 ± 1.1 nm have been prepared *via* a modified method reported by Zhang *et al.* [16]. For the growth of a shell precursor materials (cubic phase) α -NaYF₄ and α -NaYF₄(Yb,Nd) have been synthesized. By a frequent injection of the cubic nanoparticles into a boiling dispersion of the hexagonal nanoparticles a uniform shell can be formed. In order to control the quality of the nanoparticles and to determine the size TEM images were taken. Both the core and the core/shell system are monodisperse and have a narrow size distribution (Figure 4.1 A - C).

Closer looks at the size distribution show a homogenous increase of the diameter of 9.3 ± 2.5 nm. X-ray diffraction measurements confirmed that core-only as well as core-shell nanoparticles consist of pure hexagonal (β -phase) crystals only (Figure 4.1 D - F). The patterns are in good accordance with a reference pattern of NaYF₄ (ICDD PDF #16-0334) and show no reflexes of the cubic crystal lattice. The nanoparticles obtained by the bottom-up approach exhibit a hydrophobic character due to their oleate coating.

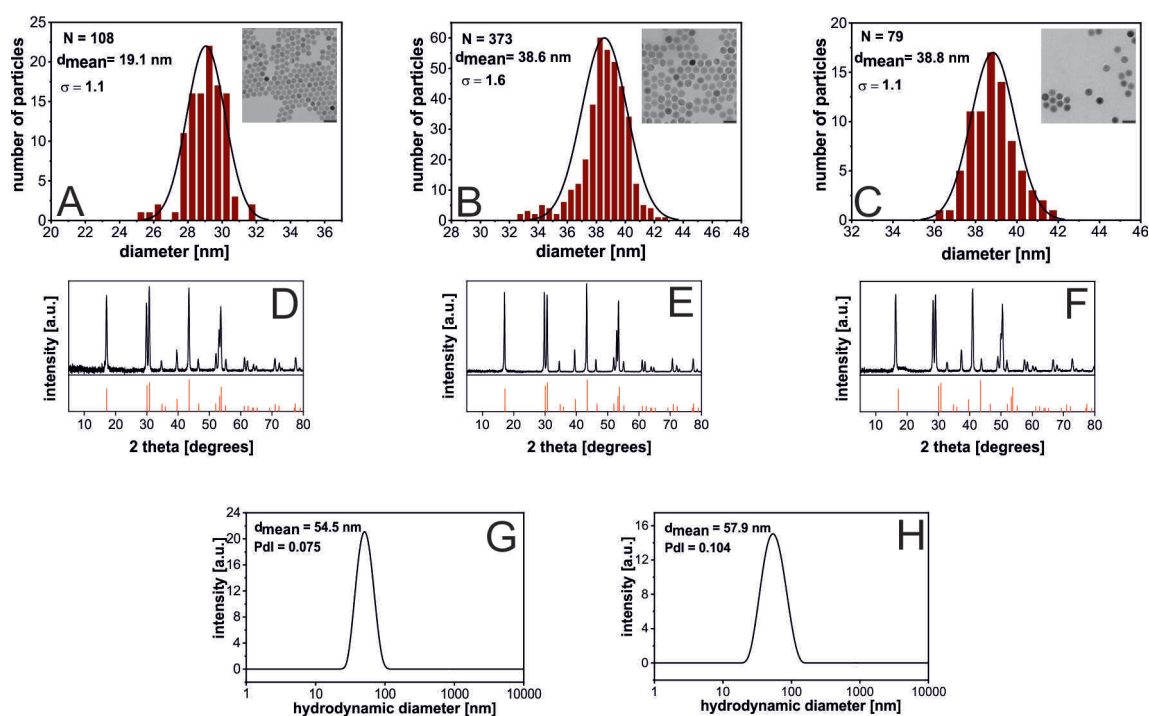


Figure 4.1| Top row: TEM image of β -NaYF₄(25% Yb, 0.3% Tm) (A), β -NaYF₄(25% Yb, 0.3% Tm)@NaYF₄(10% Yb, 10% Nd) (B), and β -NaYF₄(25% Yb, 0.3% Tm)@NaYF₄ (C). Scale bar is 60 nm. Middle row: X-Ray diffraction-pattern of NaYF₄(25% Yb, 0.3% Tm) (D), NaYF₄(25% Yb, 0.3% Tm)@NaYF₄ (E) and NaYF₄(25% Yb, 0.3% Tm)@NaYF₄(10% Yb, 10% Nd) (F) compared to a standard pattern of hexagonal NaYF₄ (red reflexes, ICDD PDF #16-0334) Bottom row: Particle size distribution of NaYF₄(25%Yb, 0.3% Tm)@NaYF₄(10% Yb, 10% Nd)@ PAA (G) and of NaYF₄ (25% Yb, 0.3% Tm)@ NaYF₄@PAA (H) is obtained from dynamic light scattering in double distilled water.

The surface of the UCNPs can be modified with different ligands, *e.g.* small organic molecules, dyes and polymers [17]. High colloidal stability can be achieved by polymer coatings providing a high binding affinity of the polymer and a large number of polar groups. Especially poly(acrylic acid) leads to water dispersible particles with remarkable colloid stability. A uniform particle size distribution with low polydispersity index (Pdl) has been obtained from dynamic light scattering (Figure 4.1 G - H).

The colloidal stability of the two core-shell particle systems is revealed by ζ -potential measurements. For UCNPs with an inert shell, it was determined to be -36.7 ± 1.4 mV and -35.6 ± 2.4 mV for those with an active shell. The particles are colloidal stable for at least six months, which is in good agreement with earlier reports [18].

4.3.2 Optical properties of 980 nm and 808 nm excitable upconversion nanoparticles

Both core-shell systems (inert shell and doped shell) can be excited at 980 nm. The shell decreases the probability of non-radiating relaxations by increasing the distance between the dopants and the surface ligands as well as the solvent. Thus, higher upconversion efficiency is achieved. By comparing the brightness, defined as peak intensity multiplied by the full width at half maximum, the emission at 340 nm of the core-shell particles is 21-times brighter than the ones of the core-only particles. Figure 4.2 displays the luminescence spectra of water dispersible core-shell particles with inert and active shell for excitation at 980 nm (A) as well as for 808 nm (B). The luminescence intensity is normalized to the concentration of Yb^{3+} in the solution, determined by ICP-OES.

Both spectra were recorded at the same power density of the 980 nm excitation source. Figure 4.2 A shows a slight decrease in the intensity and therefore the brightness when the shell contains Nd^{3+} . This can be attributed to some energy transfer from Yb^{3+} to Nd^{3+} at the interface between core and shell. For 808 nm irradiation, only particles with an activated shell can be excited. The content of Nd^{3+} of 10% in the shell was optimized to result in maximum energy transfer from Nd^{3+} to Yb^{3+} . The power density was about 2.5 times higher compared to the 980 nm excitation. Considering that the UV emission in the upconversion process is described by a two-photon process the brightness of the particles is enhanced by the 808 nm excitation as the intensity of the emission at 340 nm is about 2.8 times higher compared to the 980 nm excitation. This might also be attributed to the fact that at 808 nm excitation the aqueous solution will not absorb any excitation light.

980 nm and 808 nm excitable upconversion nanoparticles for the detection of enzyme related reactions

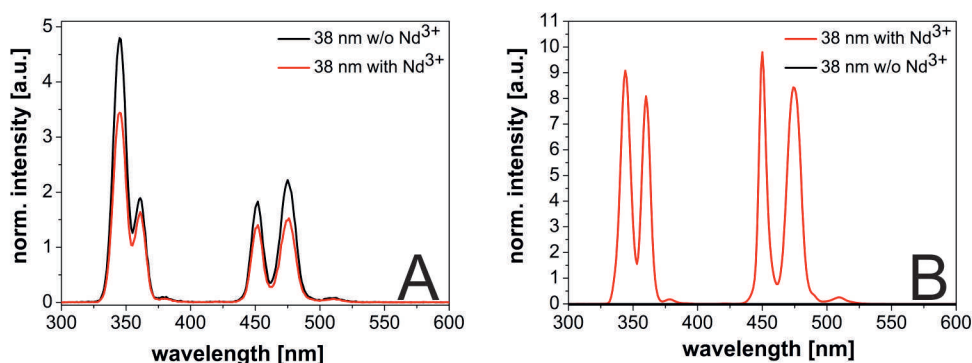


Figure 4.2| Emission spectra of UCNP normalized to the Yb³⁺ concentration. In (A): β -NaYF₄(25% Yb, 0.3% Tm)@NaYF₄@PAA (diameter 38.8 ± 1.1 nm) (black) and β -NaYF₄(25% Yb, 0.3% Tm)@NaYF₄(10% Yb, 10% Nd)@PAA core-shell UCNP (diameter 38.6 ± 1.6 nm) (red) dispersed in water under 980 nm CW laser excitation (200 mW) In (B): β -NaYF₄(25% Yb, 0.3% Tm)@NaYF₄@PAA (diameter 38.8 ± 1.1 nm) (red) and β -NaYF₄(25% Yb, 0.3% Tm)@NaYF₄(10% Yb, 10% Nd)@PAA core-shell UCNP (diameter 38.6 ± 1.6 nm) (black) dispersed in water under 808 nm CW laser excitation (500 mW). Particle concentration was in all cases set to 1.6 mg·mL⁻¹.

4.3.3 Inner filter effect of 980 nm and 808 nm excitable upconversion nanoparticles

The UCNP used in this study have several narrow emission bands between 300 and 500 nm when excited with a low power 980 nm or an 808 nm continuous wave laser source. These bands perfectly match the absorption spectra of essential co-factors (either FAD (450 nm) or NADH). This feature can be used to quantify the amount of FAD/NADH. By increasing the concentration of either NADH or FAD in the solution the emission intensity at 345 nm or 470 nm decreases (Figure 4.3). This can be attributed to an inner filter [19]. Both systems, UCNP with an active and an inert shell, are capable to detect very low concentration of the co-factors. NADH can be detected in the range between 30 to 150 μM and FAD between 30 and 100 μM by both systems. In case of 808 nm excitation, the sensitivity is slightly enhanced at lower concentrations.

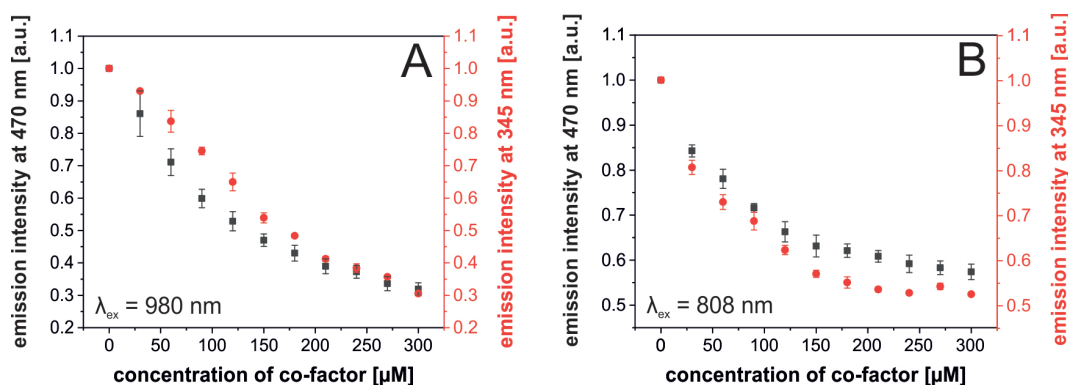


Figure 4.3| Decrease of emission intensity at 345 nm with increasing concentration of NADH and at 470 nm with increasing concentration of FAD due to the spectral overlap of the co-factors at 980 nm (200 mW, A) and 808 nm (500 mW, B) CW laser excitation. The concentration of the particles was 0.1 mg·mL⁻¹ (β -NaYF₄(25% Yb, 0.3% Tm)@NaYF₄@PAA) and 0.2 mg·mL⁻¹ (β -NaYF₄(25% Yb, 0.3% Tm)@NaYF₄(10% Yb, 10% Nd)@PAA).

4.4 Conclusion

Core-shell particles consisting of NaYF₄ doped with Yb³⁺ and Tm³⁺ with either an inert (NaYF₄) or an active shell (NaYF₄(10% Yb, 10% Nd) were prepared. A thin shell of about 5 nm enhances the brightness of upconversion luminescence. The additional doping of the shell by Nd³⁺ allows a shift in the excitation wavelength of the nanoparticles from 980 nm to 808 nm. This has several advantages for bioanalytical sensing applications. On one side, sample heating can be prevented. On the other side, a lower deactivation of the upconversion luminescence by non-radiative decay at the particle solvent interface is found. Therefore, an active shell is attractive for the monitoring of enzymatic reactions relying on co-factors like NADH or FAD which spectrally overlap with the emission of the UCNPs. Both systems, UCNPs with an inert and an active shell, can detect the amount of co-factors quantitatively including advantages like the reduction of background signal and high photo-stability of the particles.

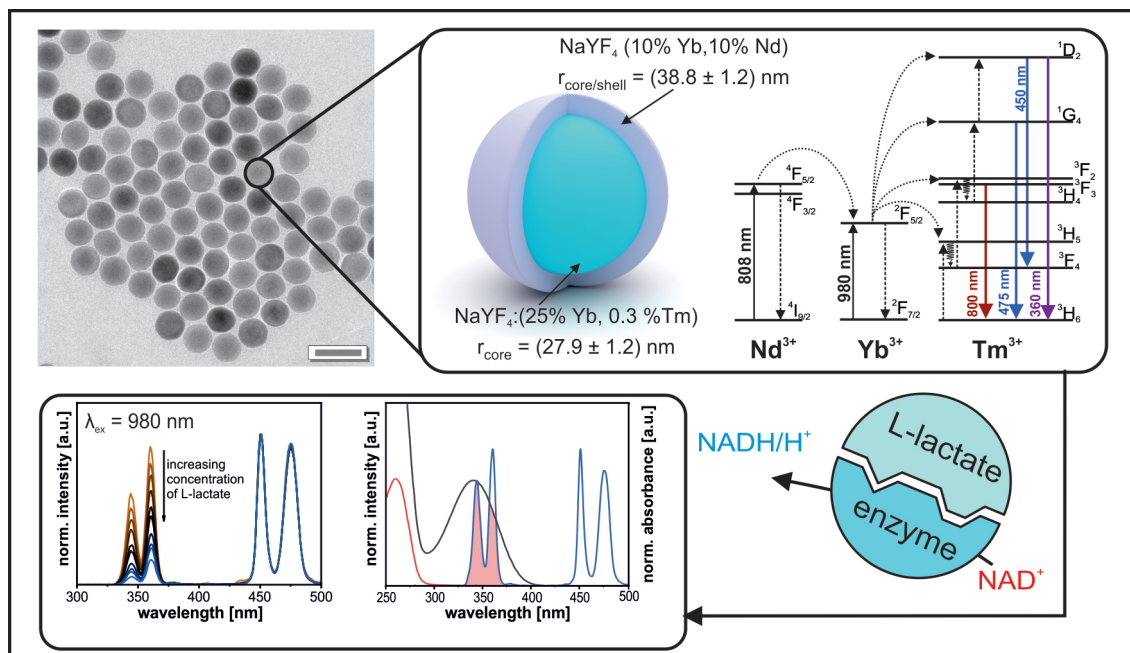
4.5 References

- [1] Pollak N, Dölle C, Ziegler M (2007) The Power to Reduce: Pyridine Nucleotides–Small Molecules with a Multitude of Functions. *Biochem. J.* 402(2):205-18.
- [2] Berg JM, Tymoczko JL, Stryer L (2002) *Biochemistry*. Freeman, New York.
- [3] Houten SM, Violante S, Ventura FV, Wanders RJ (2016) The Biochemistry and Physiology of Mitochondrial Fatty Acid β -oxidation and its Genetic Disorders. *Annu. Rev. Physiol.* 78, 23-44.
- [4] Nakamura M, Bhatnagar A, Sadoshima J. (2012) Overview of Pyridine Nucleotides Review Series. *Circ. Res.* 111 (5):604-10.
- [5] Lienhart WD, Gudipati V, Macheroux P (2013) The Human Flavoproteome. *Arch. Biochem. Biophys.* 535 (2):150-62.
- [6] Barile M, Anna Giancaspero T, Brizio C, Panebianco C, Indiveri C, Galluccio M, Vergani L, Eberini I, Gianazza E (2013) Biosynthesis of Flavin Cofactors in Man: Implications in Health and Disease. *Curr. Pharm. Des.* 19 (14):2649–75.
- [7] Mayevsky A, Barbiro-Michaely E (2009) Use of NADH Fluorescence to Determine Mitochondrial Function *in Vivo*. *Int. J. Biochem. Cell Biol.* 41 (10):1977-88.
- [8] Rhee HW, Choi HY, Han K, Hong JI (2007) Selective Fluorescent Detection of Flavin Adenine Dinucleotide in Human Eosinophils by Using bis(Zn²⁺-dipicolylamine) Complex. *J. Am. Chem. Soc.* 129 (15):4524-25.
- [9] Achatz DE, Ali R, Wolfbeis OS (2011) Luminescent Chemical Sensing, Biosensing, and Screening Using Upconverting Nanoparticles. *Top. Curr. Chem.* 300:29-50.
- [10] Auzel F (2004) Upconversion and Anti-Stokes Processes with f and d ions in Solids. *Chem. Rev.* 104 (1):139-173.
- [11] del Barrio M, de Marcos S, Cebolla V, Heiland J, Wilhelm S, Hirsch T, Galbán J (2014) Enzyme-Induced Modulation of the Emission of Upconverting Nanoparticles: Towards a New Sensing Scheme for Glucose. *Biosens. Bioelectron.* 59:14-20.
- [12] Wang F, Banerjee D, Liu Y, Chen X, Liu X (2010) Upconversion Nanoparticles in Biological Labeling, Imaging, and Therapy. *Analyst* 135 (8):1839-1854.
- [13] Dyck NC, Van Veggel FC, Demopoulos GP (2013) Size-Dependent Maximization of Upconversion Efficiency of Citrate-Stabilized Beta-Phase NaYF₄:Yb³⁺,Er³⁺ Crystals *via* Annealing. *ACS Appl. Mater. Interfaces* 5 (22):11661-11667.
- [14] Qiu H, Yang C, Shao W, Damasco J, Wang X, Ågren H, Prasad P, Chen G (2014) Enhanced Upconversion Luminescence in Yb³⁺/Tm³⁺-Codoped Fluoride Active Core/Active Shell/Inert Shell Nanoparticles through Directed Energy Migration. *Nanomaterials* 4 (1):55-68.
- [15] Wang YF, Liu GY, Sun LD, Xiao JW, Zhou JC, Yan CH (2013) Nd³⁺-Sensitized Upconversion Nanophosphors: Efficient *in Vivo* Bioimaging Probes with Minimized Heating Effect. *ACS Nano* 7(8): 7200.
- [16] Zhang F (2015) *Photon Upconversion Nanomaterials*. Springer, New York.
- [17] Muhr V, Wilhelm S, Hirsch T, Wolfbeis OS (2014) Upconversion Nanoparticles: From Hydrophobic to Hydrophilic Surfaces. *Acc. Chem. Res.* 47(12):3481-93.
- [18] Wilhelm S, Kaiser M, Würth C, Heiland J, Carrillo-Carrion C, Muhr V, Wolfbeis OS, Parak WJ, Resch-Genger U, Hirsch T (2015) Water Dispersible Upconverting Nanoparticles: Effects of Surface Modification on their Luminescence and Colloidal Stability. *Nanoscale* 7 (4):1403-10.
- [19] Wilhelm S, del Barrio M, Heiland J, Himmelstoß SF, Galbán J, Wolfbeis OS, Hirsch T (2014) Spectrally Matched Upconverting Luminescent Nanoparticles for Monitoring Enzymatic Reactions. *ACS Appl. Mater. Interfaces* 6(17):15427-33.

CHAPTER 5

Luminescence-based self-referenced enzymatic L-lactate sensing by tandem-sensitized NIR to UV NaYF₄(Yb,Tm) upconversion nanoparticles

Upconversion nanoparticles (UCNPs) are well-suited for sensing applications in complex biological samples because their excitation in the near-infrared reduces the auto-fluorescence of biomolecules and in contrast to other fluorescent nanoparticles photostability is no issue. Exploiting this property, a platform for long-term monitoring of L-lactate was developed. For this purpose, Yb³⁺/Tm³⁺ co-doped monodisperse core/shell NaYF₄ UCNPs of two types were synthesized. One system has an inert shell of NaYF₄, the second one a tandem-sensitized Nd³⁺/Yb³⁺ co-doped active shell. These particle architectures provide bright upconversion emissions upon excitation at 980 and 808 nm, respectively. The shift from Yb³⁺-sensitized 980 nm excitation to Nd³⁺/Yb³⁺ tandem sensitization at 808 nm was advantageous in online sensing due to less sample heating and better long-term stability. For short-term applications, both particle systems proved to be similar. Furthermore, upon low-power laser excitation they exhibit two emission bands peaking at 340 and 450 nm. Here, we demonstrate that highly reliable sensing is achieved by using the 340 nm emission for detection and the 450 nm emission for self-referencing. Specifically, as a good spectral overlap with the absorption of NADH is observed at 340 nm, all NAD⁺/NADH-dependent enzymatic reactions can be monitored. As a proof of principle, a flow-cell with UCNP-doped polyacrylamide hydrogel was developed for the reliable determination of L-lactate in serum down to 80 μM (808 nm excitable UCNPs) with continuous measurements of at least 120 minutes. Compared to UCNPs excited at 980 nm no significant advantage was found in terms of sensitivity. However, in terms of signal drift and long-term stability, it was possible to measure for over two hours using particles with tandem sensitization. This concept can easily be adapted for the determination of various analytes by simply employing other enzymes.



Scheme 5 | NaYF₄(Yb,Tm)@NaYF₄(Yb,Nd) nanoparticles with tandem sensitization absorb light at 808 nm. An energy transfer *via* Yb³⁺ to Tm³⁺ leads to emissions in the UV and blue region of the spectrum. Those emission bands overlap with the absorption characteristics of the enzymatic co-factor pair NAD⁺/NADH and can be used for the quantification of L-lactate.

This chapter is planned to be published in ACS Sensors:

Himmelstoß SF, Wiesholler LM, Märkl S, Baeumner AJ, Hirsch T. Luminescence-based self-referenced enzymatic L-lactate sensing by tandem-sensitized NIR to UV NaYF₄(Yb,Tm) upconversion nanoparticles.

Author contributions:

Most of the experimental work was carried out by SFH. SFH and MS synthesized the UCNPs. LMW performed XRD measurements and the absorption of the Nd³⁺. The shift of excitation wavelength was discussed with LMW. XRD measurements were performed by LMW. SFH, TH, AD, and AJB discussed the results. SFH will write the manuscript. TH and AJB will revise the article. TH will be corresponding author.

5.1 Introduction

Biosensors are powerful tools to improve the quality of life, which is demonstrated by covering a wide range of areas including biomedical diagnostics [1-3], food control [4], environmental monitoring [5], and forensic research [6]. One relevant analyte for monitoring health is lactate. For many years, L-lactate was not so much in the focus of diagnostics as it was considered only as a byproduct of the anaerobic metabolism within the human being. However, under oxygen deficit situations, as it is often the case for critically ill patients, more lactate is produced [7]. Here, lactate levels are above 4 mM, while the concentration of unstressed patients is reported to be between 0.5 and 1 mM. Whereas normal levels of lactate are removed very quickly in healthy humans, it is much more critical for higher levels and this can lead to several medical incidents including shock, seizures, anemia, and sepsis [8]. Recent studies showed that even tumor cells express an increased level of lactate, which further emphasizes its importance as a relevant biomarker [9].

So far, both optical and electrochemical techniques promise high sensitivity and selectivity for the determination of L-lactate. However, a glance at the literature shows that most biosensors are based on an electrochemical detection scheme (Table 5.1). Thereby, the lactate is determined specifically with the help of an enzyme, which translates the analytical signal directly and rapidly into an electrical answer [8]. As seen in Table 5.1, those biosensors are capable of reaching low limits of detection (LOD). Amperometric sensors for L-lactate are often based on oxidases. The flavin adenine dinucleotide (FAD) group within the enzyme produces H₂O₂, which can be transformed into an electrical signal *via* the transducer unit [10].

However, the main disadvantage of those sensors is the necessity of permanent background correction as a result of electroactive interfering substances like ascorbic acid [11]. As an alternative to the electrochemical methods, luminescence read-out can be utilized. Here, the signal is proportional to the amount of the analyte or the byproduct of an analyte specific enzymatic reaction. For this purpose, a suitable luminescent probe has to be designed, whereby several drawbacks need to be overcome. Most of the luminescence probes suffer from poor photostability and cannot be used for continuous monitoring [12]. In biological liquids scattering effects and autofluorescence demand complex sample pretreatment, calibration steps, and data evaluation. As a consequence, there are only a few systems reported so far that enable reliable sensing of L-lactate *via* luminescence read-out.

Another possibility for luminescent sensing of L-lactate is to monitor the intrinsic fluorescence of the enzymatic co-factor NAD⁺. The biomolecule has an absorption maximum at 360 nm leading to weak fluorescence at 450 nm. However, especially in biological fluids (*e.g.* serum) the direct excitation of the co-factor is challenging as also many other biological compounds like DNA or proteins are excited in the UV leading to a high background signal.

Table 5.1| Overview of sensors for L-lactate classified by the detection method and ordered by the limit of detection.

method	system	enzyme	LOD	Ref
amperometric	LDH immobilized onto graphene oxide nanoparticles modified pencil graphite electrodes	LDH	0.1 μM	[13]
amperometric	enzyme immobilized on carboxylated multiwalled carbon nanotubes/copper nanoparticles/polyaniline modified pencil graphite electrode	LOx ^a	0.3 μM	[14]
amperometric	polysulfone/carbon nanotubes membranes	LOx	0.4 μM	[15]
amperometric	enzyme immobilized in dimethylferrocene-modified LPEI ^b	LOx	3 μM	[16]
amperometric	Au nanoparticle enhanced amperometry	LOx	6 μM	[17]
amperometric	enzymatic sensing based on engineered <i>Aerococcus viridans</i> LOx	LOx	30 μM	[18]
amperometric	bienzymatic membrane produced by enzyme drop coating and crosslinking <i>via</i> glutaraldehyde	LDH / PyrOx ^c	17 μM	[19]
amperometric	chitosan/carbon nanotubes modified screen-printed graphite electrodes	LOx	23 μM	[20]
luminescence	upconversion nanoparticles – 808 nm excitation (in cuvette)	LDH	25 μM	This work
amperometric	printed graphite with the addition of Prussian Blue and Ag/AgCl	LOx	50 μM	[21]
luminescence	upconversion nanoparticles – 808 nm excitation (flow system)	LDH	81 μM	This work
surface plasmon resonance	fiber optic surface plasmon resonance	LDH	240 μM	[3]
amperometric	NiO electrode	/	530 μM	[22]
amperometric	bendable electro-chemical sensor with Ag nanoparticles	LOx	1 mM	[23]
amperometric	electrochemical tattoo with a three-electrode configuration consisting of Ag/AgCl ink and carbon ink). The working electrode is additionally modified with a CNT ^d and LOX immobilized <i>via</i> a chitosan polymer layer.	LOx	1 mM	[24]
transistor based conductometry	wearable sweat sensor consisting of an enzymatic ionogel as solid state electrolyte	LOx	10 mM	[25]

^a refers to L-lactate oxidase, ^b refers to linear polyethyleneimine, ^c refers to pyruvate oxidase, ^d refers to carboxy-functionalized multiwalled carbon nanotubes.

Here, UCNPs can provide an attractive solution to this challenge, as they can generate emissions in the UV/vis upon NIR excitation [26–29]. The excitation as well as the emission wavelength depend on the lanthanide composition within a crystal lattice [12]. For instance, UCNPs consisting of NaYF₄ co-

doped with Yb³⁺ and Tm³⁺ are capable of converting 980 nm light to high energy radiation in the visible (~450 nm) and ultraviolet region (~340 / ~360 nm) of the spectrum. This is advantageous for L-lactate sensing, as the emission of such nanoparticles overlaps with the absorption characteristics of the enzymatic co-factor, allowing the quantification of NAD⁺ within a sample of interest.

The upconversion effect by generating large anti-Stokes shifted emissions is particularly useful in biological systems where scattering effects are dominant and autofluorescence minimizes the signal-to-noise ratio. With this in mind, it is not surprising that UCNPs have been used in a wide range of bioanalytical sensors [30]. Beside the detection of ions like Zn²⁺ [31], Hg²⁺ [32] and Ca²⁺ [33], the sensing of pH [34], oxygen [35] or biomolecules like glucose [36,37] have been demonstrated. Additionally, UCNPs are used for drug delivery [38,39], photodynamic [40,41] and photothermal therapy [42] and imaging [43,44].

A significant obstacle in their use as a bioanalytical probe is the low upconversion efficiency when dispersed in an aqueous medium, due to the optical characteristics of water, also absorbing light at 980 nm [45] and quenching effects of surface-bound ligands. As reported in the literature, the upconversion efficiency of the nanoparticles can be improved by a core-shell approach, where the core of the particles is protected from non-radiative relaxations due to interactions of the dispersion media. Furthermore, a shell helps to prevent the leaking of sensitizer or activator ions, which will drastically alter the luminescence properties [46–48].

To efficiently decrease quenching effects due to the absorption of the excitation wavelength from the water molecules, the excitation wavelength of the nanoparticles can be shifted to 808 nm. This can be realized by the inclusion of Nd³⁺ into the host lattice of the shell material. Based on this, particles show an increased upconversion signal in aqueous systems compared to common nanoparticles excitable at 980 nm.

In our previous study [49], two different co-substrates have been used to study the proof of concept for monitoring enzymatic reactions *via* upconversion luminescence: NAD⁺/NADH and FAD/FADH₂. It was found that the FAD/FADH₂ system is affected by the presence of oxygen, which obviously limits its practicality strongly [36]. Thus, NAD⁺/NADH, together with the enzyme lactate dehydrogenase (LDH), is used here to develop a general platform technology for such co-factor dependent enzyme reactions. In the presence of L-lactate the enzyme co-factor NAD⁺ is reduced stoichiometrically leading to the formation of NADH and pyruvate. NADH absorbs the upconversion emission at 340 nm and therefore the particles can be used for the quantification of L-lactate. Figure 5.1 depicts the simplified design of an L-lactate biosensor based on UCNPs as developed in this study.

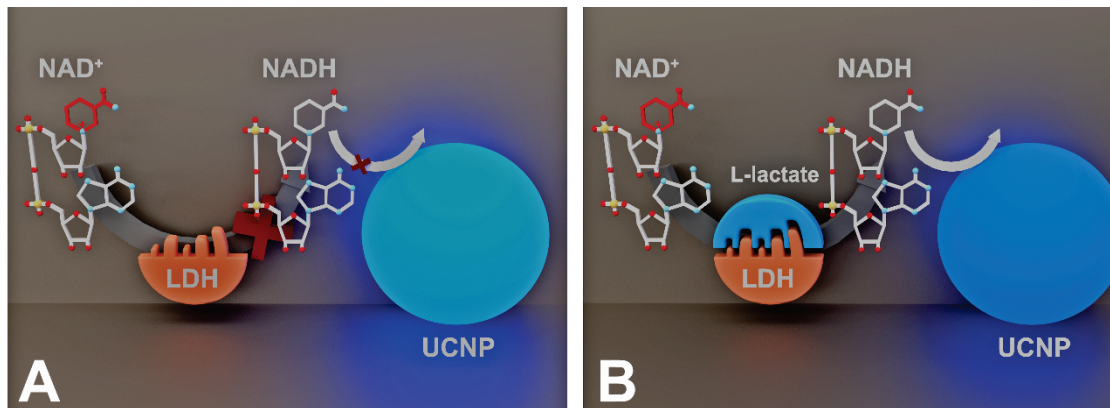


Figure 5.1 | Principle of L-lactate sensing based on the enzymatic conversion of the substrate by lactate dehydrogenase. A: In the absence of L-lactate, the reduction of NAD⁺ to NADH will not occur, so that the emission of the nanoparticles in the UV is not affected. B: In the presence of L-lactate, a substrate-enzyme-complex is generated, whereas NAD⁺ is reduced to NADH. The enzyme co-factor absorbs the UV emission of the nanoparticles and the overall upconversion emission gets weakened.

5.2 Methods and materials

5.2.1 Materials

Oleic acid and 1-octadecene (both technical 90%) were purchased from Alfa Aesar (www.alfa.com). Lanthanide chloride hexahydrate (YbCl₃ · 6 H₂O, YCl₃ · 6 H₂O and ErCl₃ · 6 H₂O, each >99.99%) were obtained from Treibacher Industrie AG (www.treibacher.com) or Sigma Aldrich (www.sigmaaldrich.com). N,N-dimethylformamide (DMF) (99.5%) was from Acros Organics (www.acros.com). Chloroform (99.7%) and methanol (99.9%) were purchased from Fisher Chemicals (www.fisher.co.uk). Ammonium fluoride (ACS reagent ≥ 98.0%), nitrosyl tetrafluoroborate (95%, NOBF₄), poly(acrylic acid) sodium salt (PAA, M_w = 2100 Da), sodium L-lactate and L-lactate dehydrogenase from rabbit muscle (lyophilized powder with activity of 816 U·mg⁻¹), 4-morpholineethanesulfonic acid (MES), N-(2-hydroxyethyl)piperazine-N'-(2-ethanesulfonic acid) (HEPES), N-hydroxysuccinimide (NHS), tris(hydroxymethyl)amino-methane (TRIS), N,N,N',N'-tetramethylethylenediamine (TEMED), ammonium persulfate (APTS) N-(3-dimethylaminopropyl)-N'-ethylcarbodiimide hydrochloride (EDC), D-glucose, D-fructose, sucrose, L-ascorbic acid, and hydrazine monohydrate were purchased from Sigma Aldrich (www.sigmaaldrich.com). Cyclohexane was from VWR chemicals (www.vwr.com). Glycine was purchased from Merck (www.merckmillipore.com). Millipore water was used for the preparation of all buffers and aqueous solutions.

5.2.2 Characterization methods

Transmission electron microscopy (TEM) of UCNPs was carried out with a 120 kV Phillips CM12 transmission electron microscope (www.fei.com). The obtained images of the UCNPs were analyzed by using the software ImageJ (<http://rsbweb.nih.gov/ij/>). Dynamic light scattering and ζ-potential measurements were performed by a Malvern Zetasizer Nano-ZS (www.malvern.com) at a constant temperature of 20 °C. An inductively coupled plasma optical emission spectrometer (ICP-OES) from Spectro (www.spectro.de) was used for the analysis of the concentration and the chemical composition of the nanoparticles. For the calibration, a series of solutions of different concentrations of the respective lanthanide ions were prepared from the lanthanide chloride hexahydrate salts dissolved in 0.5 M H₂SO₄ and 0.5 M HNO₃. The calibration of the Ln³⁺ was done in accordance with the emission lines of yttrium (363.312 nm), gadolinium (342.247 nm), erbium (349.910 nm), thulium (384.802 nm), ytterbium (328.937), neodymium (401.225 nm), and europium (381.970 nm). Argon (430.010 nm) was used as carrier gas. For the quantification of the nanoparticles, they were dissolved entirely by dispersing 0.3 mg UCNPs in sulfuric acid (96% w/v, 417 μL) and sonication for 10 min. The solution was diluted with water (7.083 mL) and 1 M HNO₃ (7.5 mL) before applying the solution to the ICP-OES.

For the measurement of X-ray diffraction (XRD) patterns, a STOE STADI P diffractometer (www.stoe.com) equipped with a Dectris Mythen 1 K detector (www.dectris.com), with a resolution of 0.005° (2θ) and a monochromatized Cu K_{α1} radiation (λ = 1.54056 Å) was used. Spectrophotometry was performed at room temperature with a Varian (former Varian now www.agilent.com) Cary® 50 UV/VIS spectrometer. Luminescence spectra were collected with an AMINCO-Bowman Series 2 luminescence spectrometer (formerly from Thermo Fisher) equipped with an external continuous wave

(CW) 980 nm (focusable, 250 mW, www.picotronic.de) or 808 nm (focusable, 200 mW or 500 mW, www.picotronic.de) laser module. All spectra were recorded at room temperature.

5.2.3 Synthesis of hexagonal β -NaYF₄(Yb,Tm) nanoparticles

For the synthesis of hexagonal phase, oleate capped NaYF₄(25% Yb, 0.3% Tm), the rare earth chlorides YCl₃ · 6 H₂O, YbCl₃ · 6 H₂O and TmCl₃ · 6 H₂O (with the corresponding molar doping ratio) were dissolved in methanol and transferred in a three-necked round bottom flask under nitrogen flow. Per 1 mmol total amount of the lanthanide ions, 8 mL oleic acid and 15 mL 1-octadecene was added to the solution. The resulting suspension was heated to 160 °C and vacuum was applied for 30 min to form a clear solution. The mixture was cooled to room temperature and per 1 mmol of the chlorides 2.5 mmol NaOH and 4.0 mmol NH₄F, dissolved in methanol, were added. The suspension was heated to 120 °C and kept there for additional 30 min. Then the mixture was heated to reflux (approx. 325 °C). Here, the progress of the synthesis was controlled by illumination with a 980 nm CW laser module (250 mW). When upconversion luminescence was observable for the first time, the solution was kept another 10 min at 325 °C before fast cooling to room temperature.

For purification, the particles were precipitated with an excess of ethanol and centrifuged at 1000 g for 5 min. The resulting pellet was washed twice with chloroform / ethanol and three times with cyclohexane / ethanol. Finally, the precipitant was dispersed in cyclohexane and centrifuged (1000 g, 3 min) to remove aggregates. The supernatant was collected and stored at 4 °C

5.2.4 Synthesis of α -NaYF₄ and α -NaYF₄(Yb, Nd)

The synthesis of cubic phase, oleate capped UCNPs is similar to the synthesis of hexagonal UCNPs until the suspension is heated to reflux. Instead of heating above 300 °C, the suspension was kept at 240 °C for 30 min before cooling to room temperature. The purification protocol was the same as described for the hexagonal phase nanoparticles.

5.2.5 Core-shell synthesis of β -NaYF₄(Yb, Tm)@NaYF₄ and β NaYF₄(Yb, Tm)@NaYF₄(Yb, Nd)

For the synthesis of hexagonal core-shell UCNPs, α -NaYF₄ or α -NaYF₄(10% Yb, 10% Nd) nanoparticles (shell material) and hexagonal phase NaYF₄(25% Yb, 0.3% Tm) (core material) dispersed in cyclohexane were used separately. Per 1 mmol of the particles 5 mL oleic acid and 5 mL 1-octadecene was added to the UCNP dispersion. To remove the cyclohexane, the dispersions were heated to 120 °C and vacuum was applied for 30 min. Afterwards, the core particles were heated to reflux (approx. 325 °C), whereas the shell precursor particles were kept at 120 °C. Every 10 min small volumes (less than 4 mL) of the cubic particle dispersion were injected into the boiling reaction mixture. After the last injection, the dispersion was kept at 325 °C for additional 10 min before it was cooled to room temperature. The purification protocol for the core-shell particles was the same as described in Chapter 5.2.3.

5.2.6 Surface modification with poly(acrylic acid)

Hydrophobic, oleate coated UCNPs were rendered water dispersible by a two-step ligand exchange. In the first step, the oleic acid was removed *via* NOBF₄. Therefore, the nanoparticles were dispersed in a two-phase system (equivalent volumes of cyclohexane and DMF), NOBF₄ (1 mg per 1 mg UCNPs) was added and the mixture was stirred vigorously at 30 °C for 20 min. Due to the protonation of the oleic acid, the nanoparticles were transferred from the cyclohexane phase to the DMF phase, whereas the free oleic acid stayed in the cyclohexane phase. The cyclohexane phase was rejected and the BF₄⁻ stabilized particles were precipitated with an excess of chloroform and separated by centrifugation (1000 g, 5 min). The resulting gel-like pellet was dispersed in DMF and washed two times with chloroform / DMF. Finally, the pellet was dispersed in DMF (~5 mL) and centrifuged (1000 g, 3 min) to remove aggregates. The supernatant was collected and stored in the dark at 4 °C.

In the second step, the BF₄⁻ stabilized nanoparticles were modified with poly(acrylic acid). Therefore, the particles in DMF (20 mg, 1 mL) were added to an aqueous solution of poly(acrylic acid) (2 mg, 4 mL). The mixture was stirred vigorously at 30 °C for 1 h. Afterwards, the particles were purified *via* centrifugation (~21000 g, 60 min). The pellet was dispersed in water and centrifuged again. This step was repeated at least three times. Finally, the particles were dispersed in water and centrifuged at 1000 g for 3 min to remove aggregates. The supernatant was collected and stored in the dark at 4 °C.

5.2.7 L-lactate assay

For the quantification of L-lactate in a cuvette, 100 µL of a nanoparticle dispersion in water (~2.0 mg·mL⁻¹), 50 µL of a NAD⁺ solution (40 mM), 50 µL of a L-lactate solution (different concentrations) and 10 µL of a lactate dehydrogenase (LDH) solution (3420 U·mL⁻¹) were mixed with 1.5 mL of a glycine / hydrazine buffer (pH 9, 500 mM glycine, 400 mM hydrazine) in a polymethyl methacrylate (PMMA) cuvette and incubated at 37 °C for 30 min. Afterwards, emission spectra were recorded for each examined L-lactate concentration. Therefore, the sample was excited with a 980 nm or an 808 nm CW laser module (200 mW each).

5.2.8 Preparation of a sensor film

The nanoparticles were encapsulated in a polyacrylamide hydrogel. Therefore 208 µL UCNPs dispersed in water (~4 mg·mL⁻¹), 99 mg acrylamide and 6.3 mg bisacrylamide were mixed with 288 µL water. Oxygen was removed by bubbling nitrogen through the vial, before the addition of 2 µL (10%) ammonium persulfate and 0.5 µL TEMED. The polymer cocktail was casted between two microscope slides separated by a layer of paraffin (thickness: 125 µm) and left for polymerization for 1 h (Figure 5.2). Afterward, the film was washed at least two times with an excess of water.

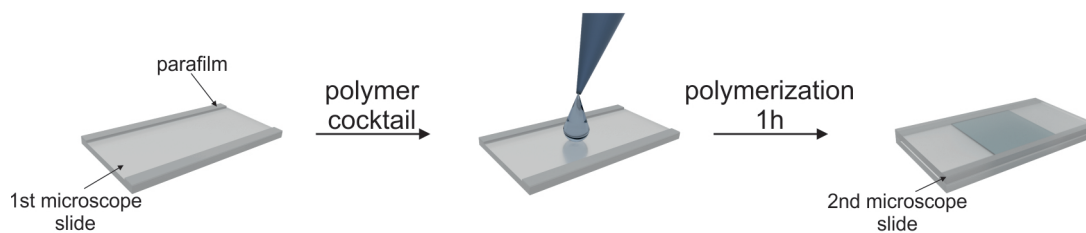


Figure 5.2] Schematic illustration of the production of a thin sensor film. Firstly one layer of paraffin (thickness = 125 μm) is attached to two sides of a microscope slide. Secondly a polymerization cocktail of the desired composition is drop casted on the microscope slide. In the next step a 2nd microscope slide is put on the paraffin layer in order to ensure the thickness of the hydrofilm layer. After 1 hour the polymerization is finished and the film can be washed with water.

5.2.9 Immobilization of L-lactate dehydrogenase on a polyacrylamide sensor film

The preparation of an enzyme modified gel is quite similar, as described above. Instead of an UCNPs dispersion, only pure water (498 μL) was mixed with 99 mg acrylamide and 6.3 mg bis-acrylamide. Oxygen was removed by bubbling nitrogen through the vial, before the addition of 2 μL (10%) ammonium persulfate and 0.5 μL TEMED. The polymer cocktail was casted between two microscope slides separated by a layer of paraffin (thickness: 125 μm) and left for polymerization for 1 h. Afterward, the film was washed two times with water and incubated in a mixture of 4.5 mL NaOH (1 M) and 0.5 mL TEMED for 10 min to hydrolyze the amid to carboxyl groups. The film was washed at least three times with water and then allowed to swell for 24 h in water. For the bioconjugation of the lactate dehydrogenase, the carboxyl groups of the sensor film were activated by incubating the gel in an EDC / NHS solution (100 mM / 200 mM in MES buffer, pH 6, 50 mM) for 1.5 h. The gel was washed at least two times with a HEPES buffer (pH 7, 50 mM) and then incubated in an enzyme solution (1200 $\text{U}\cdot\text{mL}^{-1}$ in HEPES buffer pH 7, 50 mM) for 1.5 h. In order to inactivate unbound carboxyl groups, the gel was then dipped in a TRIS buffer (pH 7, 10 mM) for additional 30 minutes. Afterwards, the film was washed a least two times with HEPES buffer (pH 7, 50 mM) and stored at 4 $^{\circ}\text{C}$.

5.2.10 Activity of L-lactate dehydrogenase on the enzyme film

For the determination of the enzyme activity of LDH after the immobilization on a polyacrylamide film, the intrinsic absorption behavior of NADH at 340 nm was used. Briefly, different concentrations of L-lactate, covering a concentration range from 1 to 6 mM, were added to a solution consisting of 20 mM NAD⁺ in a glycine/hydrazine buffer (500 mM / 400 mM, pH 9). The enzyme film was placed into the solution and the absorbance was measured at 340 nm against an L-lactate free solution. The increased absorption was recorded for 15 min with 1 min time steps. The change of the absorbance between each time step was converted into the product concentration by applying Lambert-Beer's-Law (with a molar absorption coefficient of 6600 $\text{L}\cdot\text{mol}^{-1}\cdot\text{cm}^{-1}$ for the NADH absorption at 340 nm [50]).

5.2.11 Online measurement of L-lactate

For the online quantification of L-lactate in a flow cell, both films (UCNPs film and enzyme film) were put in a home-made flow cell. During the measurement, the flow rate within the cell was set to

0.5 mL·min⁻¹ and L-lactate or possible interfering substances were injected for 2 min. After 10 min incubation, the system was washed with a glycine / hydrazine buffer (pH 9, 500 mM glycine, 400 mM hydrazine) for 5 minutes with a pump rate of 0.5 mL·min⁻¹

5.3 Results and discussion

5.3.1 Synthesis and surface modification of hydrophobic upconversion nanoparticles with tandem sensitization

Upconversion nanoparticles consisting of NaYF₄ co-doped with Yb³⁺ and Tm³⁺, prepared by a hydrothermal decomposition method [51], showed a diameter of 27.9 ± 1.1 nm (UCNP). For the core material, the molar doping ratio of 25% Yb³⁺ / 0.3% Tm³⁺ was chosen. Higher concentrations of both compounds have been reported to lead to self-quenching and thus to a decrease of the upconversion emission [52]. Two different core-shell particle systems were prepared with this core particles, one with a shell consisting of pure NaYF₄ (UCNPs-inert shell, UCNP^{IS}) and a second one with a shell of NaYF₄ co-doped with 10% Yb³⁺ and 10% Nd³⁺ (UCNPs-active shell, UCNP^{AS}). Both shells had a thickness of ~5.5 nm, as confirmed by TEM (Figure 5.3).

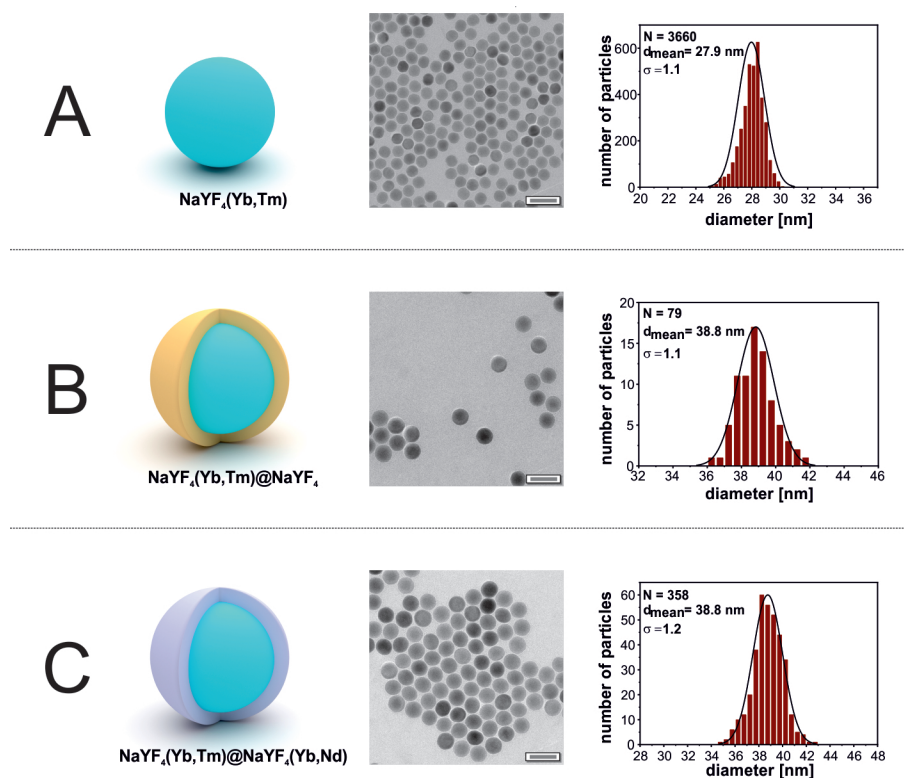


Figure 5.3| Transmission electron microscopy images (scale bar is 60 nm) and corresponding size distribution of hexagonal UCNP (A), UCNP^{IS} (B) and UCNP^{AS}(C).

As seen from the TEM images, the particles have a uniform size with a narrow size distribution. The difference between the core and the shell material cannot be visualized using TEM, due to the high similarity of the materials resulting in the same contrast. We were able to verify the elemental composition in the core and the core-shell particles with ICP-OES measurements, (Table 5.2). The compositions match those of the core and shell precursor material closely. We conclude that core-shell particles with the desired doping ratio were obtained. As it is known from the literature [53,54], the elements within the core and the shell are distributed homogeneously and no intermixing from shell to core can be observed. Additionally, the stability of the core-shell architecture was proven by

the optical properties of the nanoparticles. The luminescence spectra of oleate capped particles dispersed in cyclohexane do not change for at least two years (data not shown), so that any disintegration of the particles over time can be excluded. According to XRD studies (Figure 5.4) both, the core and the two core-shell systems, exhibit a pure hexagonal crystal structure when compared to the reference pattern of NaYF₄ (ICED PDF #16-334).

Table 5.2 Elemental composition of cubic α -NaYF₄, α -NaYF₄(10% Yb, 10% Nd), hexagonal NaYF₄(25% Yb, 0.3% Tm) (β -UCNPs), NaYF₄(25% Yb, 0.3% Tm)@NaYF₄(10% Yb, 10% Nd) (β -UCNP^{AS}), and NaYF₄(25% Yb, 0.3% Tm)@NaYF₄ (β -UCNP^{IS}) determined by ICP-OES measurements. For the UCNP^{AS} the Tm³⁺ was below 0.1% and was no longer reliably detectable (n.d.) with the given protocol.

particles			Y ³⁺	Yb ³⁺	Tm ³⁺	Nd ³⁺
hexagonal phase	β -UCNP	ideal	75%	25%	0.3%	/
		real	(77.1 ± 0.8)%	(22.6 ± 0.1)%	0.3%	/
	β -UCNP ^{IS}	ideal	93.1%	6.8%	0.1%	/
		real	(90.9 ± 0.4)%	(8.9 ± 0.1)%	0.1%	/
	β -UCNP ^{AS}	ideal	79.1%	13.5%	0.1%	7.3%
		real	(81.6 ± 0.6)%	(13.2 ± 0.1)%	n.d.	(5.1 ± 0.1)%
cubic phase	α -NaYF ₄	ideal	100 %	/	/	/
		real	(100 ± 0.4)%	/	/	/
	α - NaYF ₄ (10% Yb, 10% Nd)	ideal	80%	10%	/	10%
		real	(80.1 ± 0.7)%	(9.6 ± 0.2)%	/	(10.3 ± 0.1)%

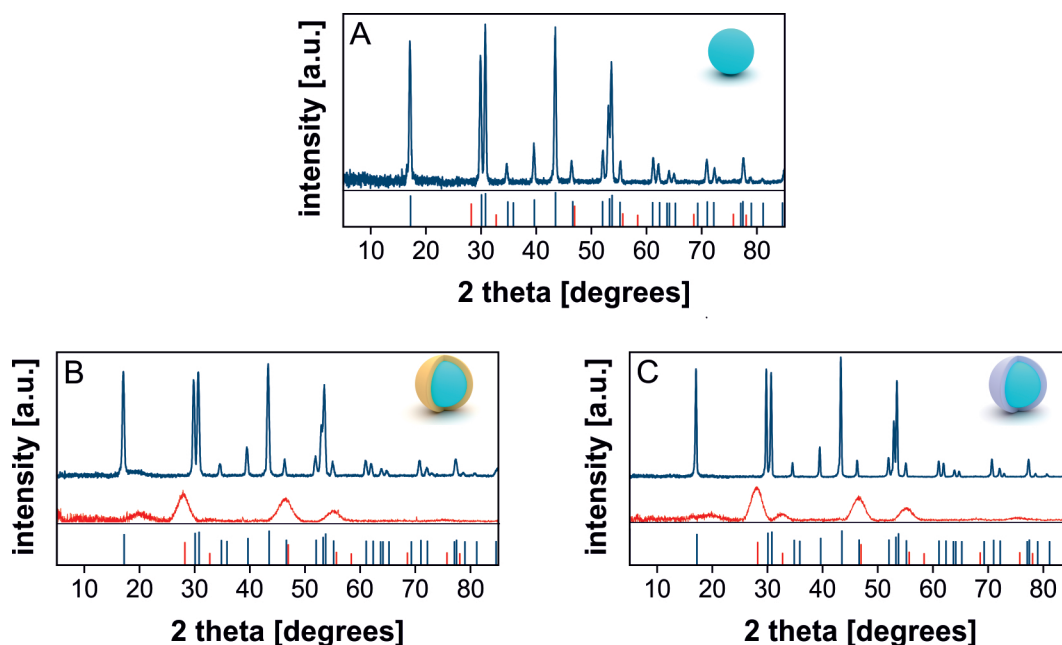


Figure 5.4| X-ray diffraction patterns of core and core-shell nanoparticles of the following types: UCNP (A) hexagonal UCNP^{IS} (blue) and cubic NaYF₄ (red) (B) and hexagonal UCNP^{AS} (blue) and cubic NaYF₄(10% Yb, 10% Nd) (red) (C) compared to a NaYF₄ standard pattern with hexagonal (blue, ICDD PDF# 16-334) and cubic (red, ICDD PDF# 16-2042) crystal phase.

The colloidal stability of the UCNPs was analyzed by dynamic light scattering in cyclohexane. In all cases, the particles did not aggregate (Figure 5.5), verified by homogeneous size distributions with

low polydispersity indices. UCNPs obtained by the thermal decomposition method are capped with oleate acid and are only dispersible in organic solvents. For the sensor application, the nanoparticles were modified *via* a two-step ligand exchange mediated by NOBF₄ [55,56].

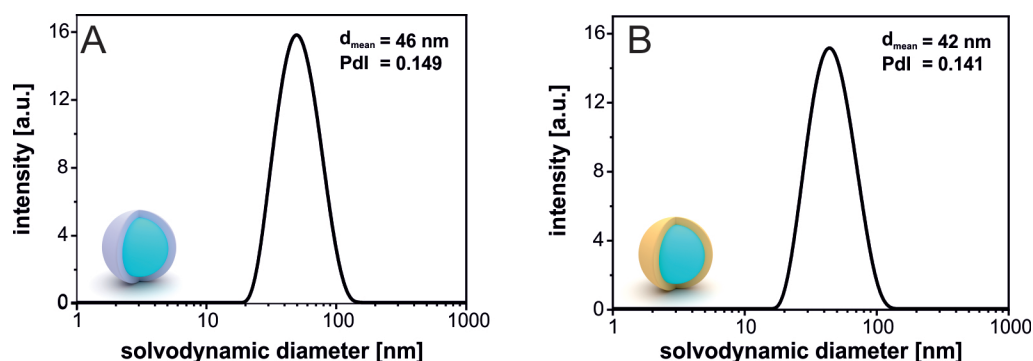


Figure 5.5| Dynamic light scattering measurements of hexagonal UCNP^{AS} (A) and UCNP^{IS} (B) in cyclohexane (each with a mass concentration of $\sim 10 \text{ mg}\cdot\text{mL}^{-1}$).

As stabilizing capping the ligand PAA was chosen since it provides a high density of carboxyl groups for coordination as well as for stabilization *via* electrostatic repulsion of the negatively charged surface of UCNP^{IS} (ζ -potential = $-36.7 \pm 1.4 \text{ mV}$) and UCNP^{AS} (ζ -potential = $-35.6 \pm 2.4 \text{ mV}$). The almost identical ζ -potential of both particle systems demonstrates the good reproducibility of this surface modification protocol. The functionalized particles have been characterized by DLS measurements (Figure 5.6) and both UCNP systems with inert as well as with active shell show low PDIs – again, an indicator for colloidal stability.

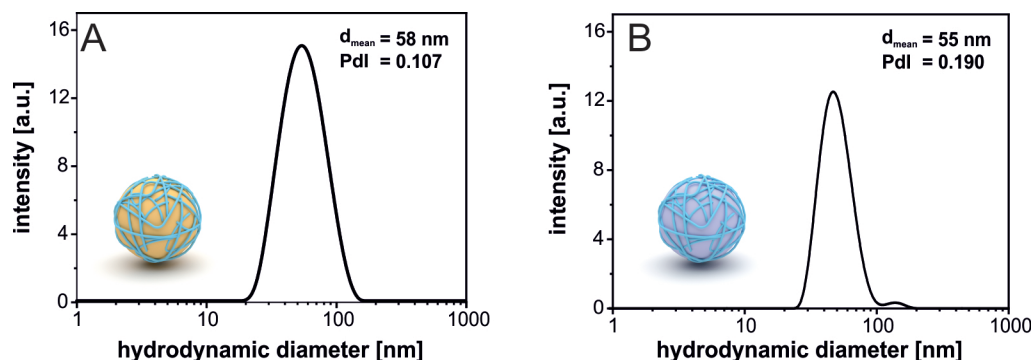


Figure 5.6| Dynamic light scattering measurements of hexagonal poly(acrylic acid) functionalized UCNP^{IS} and UCNP^{AS} in water (each with a mass concentration of $\sim 5 \text{ mg}\cdot\text{mL}^{-1}$).

5.3.2 Optical properties of upconversion nanoparticles with and without tandem sensitization

The UCNPs architecture and doping ratios selected for this work allow efficient conversion of low energy excitation in the NIR to high energy emissions in the spectral range of UV/VIS, as seen in Figure 5.7. Thereby, the energy is transferred from the Yb³⁺-ions, with an absorption maximum at 975 nm, towards the Tm³⁺ ions. Due to the stable electronic states of the lanthanide ions these phenomena happen several times so that high excited states can be reached. The transition back to the ground state of the Tm³⁺ leads to narrow emission bands in the UV (340 nm: $^1I_6 \rightarrow ^3F_4$; 360 nm: $^1D_2 \rightarrow ^3H_6$),

and blue (450 nm: $^1D_2 \rightarrow ^3F_4$, 475 nm: $^1G_4 \rightarrow ^3H_6$). Yet, in general, the outstanding properties of UCNPs compared to other fluorescent probes [12] are impaired by low quantum yields [57].

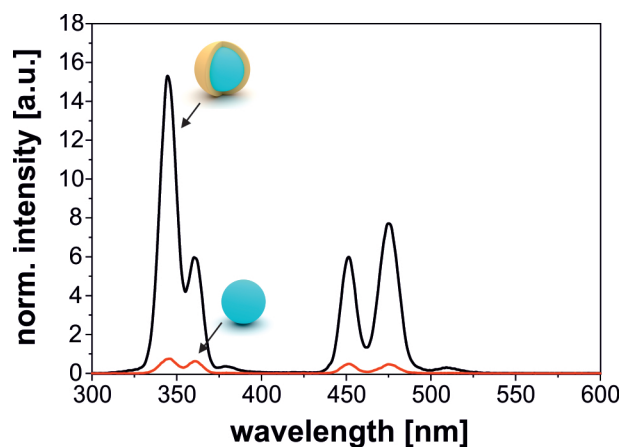


Figure 5.7 | Luminescence spectra of oleate capped UCNP and UCNP^{IS} dispersed in cyclohexane under 980 nm CW laser excitation (250 mW). The particle concentration was 1 mg·mL⁻¹, and the spectra were normalized to the Yb³⁺ concentration. Due to the presence of an inert shell, non-radiative deactivation processes were minimized.

This is mainly caused by non-radiative decay due to surface defects and interaction of the nanocrystal with the dispersion media and surface ligands (Figure 5.8). Several methods are reported in the literature to increase the efficiency of the upconversion, including the growth of an inert shell or the modulation of the energy transfer [58].

An inert NaYF₄ shell shields the surface defects of the particles. Compared to UCNPs without an inert shell, the intensity at 360 nm is already in cyclohexane about ~40 times higher (Figure 5.7). The enhancement in water is even higher but difficult to quantitate as an accurate comparison based on the evaluation of the peak intensity cannot be presented. The weak emission of the core particles makes a recording of the spectra under identical excitation power densities or photomultiplier voltages impossible. Nevertheless, due to the weak luminescence of core-only UCNPs, those particles were not further considered for the usage in a bioanalytical application. With increasing diameter, the potential force on the particles increases so that large particles tend to settle down over time [59]. The smaller the particles are, the more stable is the dispersion. A shell thickness of ~5 nm was chosen as a compromise between both, colloidal stability and effective shielding of the elements within the core.

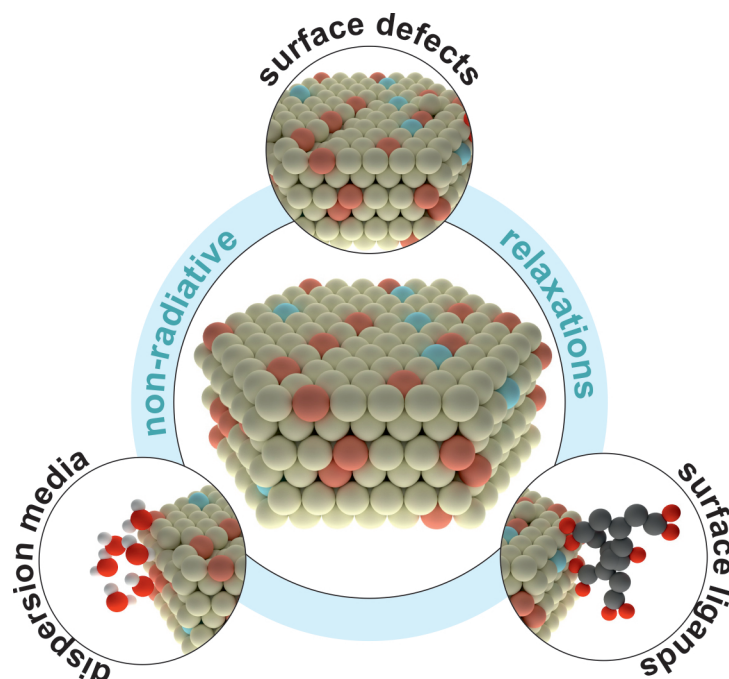


Figure 5.8| Schematic illustration of the contributions for non-radiative relaxations (dispersion media, surface ligands and surface defects) present at the surface of an NaYF₄(Yb,Tm) upconversion nanoparticle (beige sphere: Y³⁺, red sphere: Yb³⁺, blue sphere: Tm³⁺): The red sphere symbolizes oxygen atoms either present in water or in a surface ligands. Carbon atoms are illustrated in dark grey hydrogen atoms in white.

Instead of using an inert shell consisting only of NaYF₄, the shell can be doped with Yb³⁺. Additionally, to the shielding of the core, this structure would increase the absorbance at 980 nm and the efficiency of the upconversion nanoparticles as shown by Pilch *et al.* [60]. By further doping, the shell with Nd³⁺ the excitation wavelength of the particles can be shifted towards 808 nm as these ions absorb light at this region of the spectrum and tandem-sensitization occurs. Neodymium transfers the energy from its excited state to Yb³⁺, from where it migrates into the core to excite Tm³⁺, which consequently emits light in the blue and the UV. It should be noted that a core-only architecture with all lanthanide ions in one compartment is not favorable as an energy back transfer from Tm³⁺ towards Nd³⁺ was reported [61], which decreases the upconversion efficiency.

The core/shell architecture with active shell and tandem sensitization has several advantages as the excitation of the particles is shifted from 980 nm to 808 nm where water does not absorb light [62]. For example, this prevents any heating of the dispersion within a short time period, as seen in Figure 5.9. By illuminating a solution containing UCNP^{IS} with a 980 nm laser module, fast heating (15 °C within 15 min, 250 mW, CW) of the solution is observed. In contrast, the change of the particles' composition to UCNP^{AS} revealed a minimization of sample heating at 808 nm excitation. By using an even higher laser power (500 mW, CW) the temperature has only risen by ~5 °C within the same time, which is three times lower compared to a sample illuminated at 980 nm.

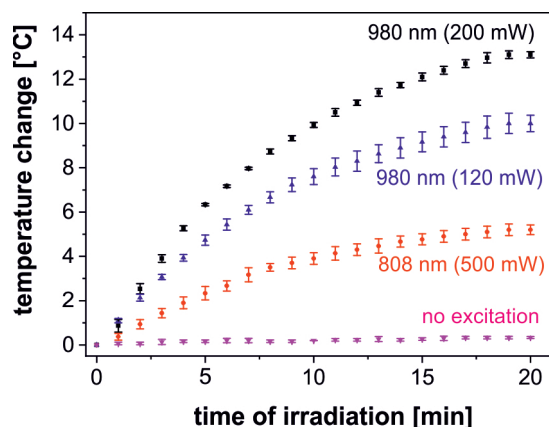


Figure 5.9| Temperature effect of 980 and 808 nm CW laser modules with different power (200 mW, 120 mW and 500 mW). The concentration of UCNP^{IS} was 1 mg·mL⁻¹.

For many applications, the heating problem of 980 nm excitation can also be overcome by pulsed excitation, but for continuous long-time online monitoring this is not desirable as a more complex experimental set-up would be required. Another advantage of the tandem sensitization becomes apparent when comparing UCNP^{IS} dispersed in cyclohexane or water. About 70% of the luminescence intensity at 345 nm is quenched due to the water molecules (Figure 5.10).

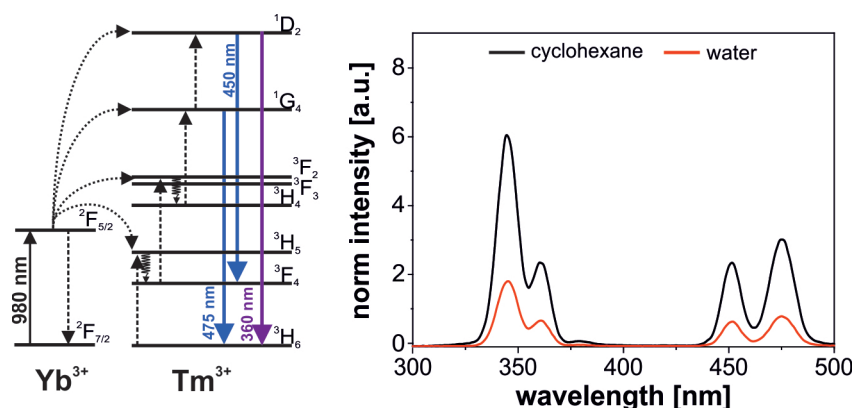


Figure 5.10| Left: Energy term scheme of UCNP^{IS}. Right: Influence of the dispersion media (cyclohexane or water) on the luminescence spectra of UCNP^{IS} normalized to the sensitizer concentration (Yb³⁺) under CW laser excitation (200 mW) at 980 nm.

By the introduction of Nd³⁺ this effect can be minimized, as seen in Figure 5.11. Upon 808 nm excitation only ~30% of the luminescence signal at 345 nm of the particles dispersed in water is quenched. In the end, as both systems demonstrated efficient upconversion in water (Figure 5.10, Figure 5.11) due to their core-shell structure, their usability for the enzymatic sensing of L-lactate was investigated. A comparison to the core-only particles at same excitation power density was not possible, as those particles show only a weak upconversion already in a cyclohexane phase.

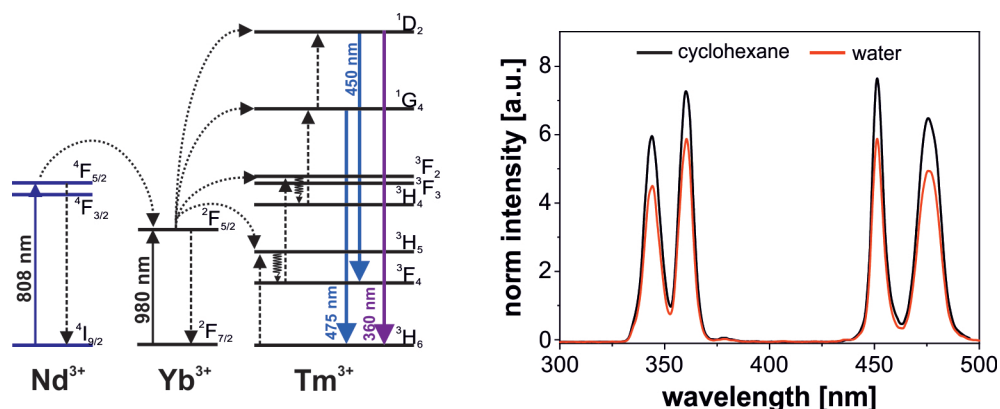


Figure 5.11| Left: Energy term schema of lanthanide ions in UCNP^{AS} with tandem sensitization. Right: Influence of the dispersion media (cyclohexane or water) on the luminescence spectra of UCNP^{AS} normalized to the sensitizer concentration (Nd³⁺) under CW laser excitation (200 mW) at 808 nm.

5.3.3 Determination of L-lactate

The principle of the L-lactate determination is based on an enzymatic reaction with L-lactate dehydrogenase (LDH). As seen in Figure 5.12, L-lactate reacts with the cofactor NAD⁺. Thereby L-lactate is oxidized to pyruvate whereas NAD⁺ gets reduced to NADH.

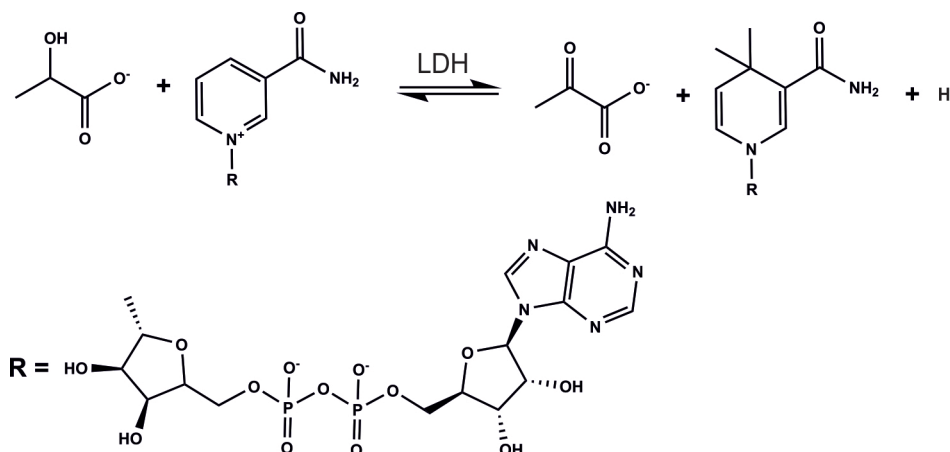


Figure 5.12| Enzymatic reversible reaction of LDH. Thereby, L-lactate is oxidized to pyruvate whereas NAD⁺ is reduced to NADH/H⁺.

However, under physiological conditions, the equilibrium of this reaction lies on the NADH side so that both H⁺ and the pyruvate need to be removed from the equilibrium to force a complete consumption of the substrate [63]. The usage of a glycine / hydrazine buffer turned out to be best for this task. The basic pH of 9 leads to the capture of the H⁺ ions, whereas the hydrazine reacts with pyruvate to hydrazone as depicted in Figure 5.13.

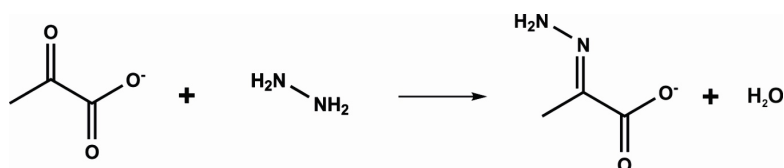


Figure 5.13| Reaction of pyruvate with hydrazine to hydrazone.

Upconversion nanoparticles from the type NaYF₄(Yb, Tm) exhibit several emission bands between 300 and 500 nm. As seen in Figure 5.14, those at higher energy nicely overlap with the absorption band of the enzymatic co-factor NADH. In contrast, the absorption spectrum of the oxidized form (NAD⁺) shows a hypsochromic shift so that there is no absorption of the light emitted by the UCNPs.

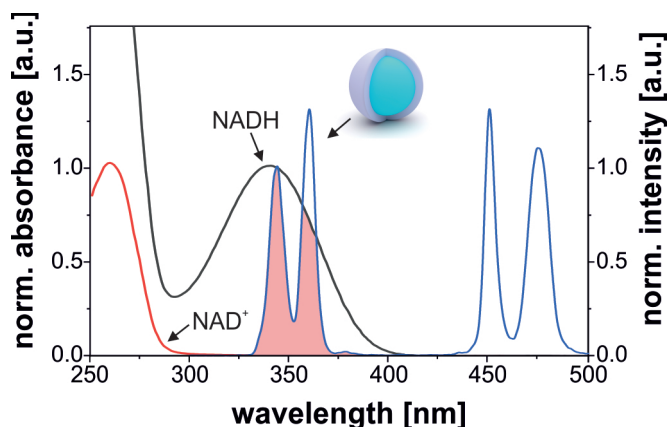


Figure 5.14| Normalized luminescence spectra of UCNP^{AS} nanoparticles in water (1.0 mg·mL⁻¹, blue line) under 808 nm CW laser excitation (200 mW) and normalized absorbance of enzymatic co-factors NADH (black line) and NAD⁺ (red line) in water. The light red area represents the spectral overlaps between NADH and the upconversion nanoparticles.

This effect can be used for the quantification of the enzymatic co-factor. The concentration of this biomolecule is also linked to the L-lactate concentration. Thus it is possible to quantify the amount of L-lactate, *via* the decrease of the upconversion emission in the UV at 345 nm by absorption due to an inner filter effect caused by NADH. Interestingly, the upconversion emission peaking at 450 nm is not affected at all by the enzymatic conversion of L-lactate and serves as an internal reference, useful for calibration and excluding influences like small fluctuations in temperature or excitation power density.

In Figure 5.15, the upconversion luminescence of UCNP^{IS} and UCNP^{AS} in the presence of LDH, NAD⁺ and various concentrations of L-lactate is shown. A limit of detection of (25 ± 9) μM (3 S/N) for UCNP^{AS} and of (30 ± 9) μM (3 S/N) for UCNP^{IS} was found. The physiological relevant L-lactate levels of a healthy human are around ~1 mM to 2.0 mM [64] and therefore both sensing systems can be used for the quantification of L-lactate up to 1 mM in such a media. In the case of higher concentrations higher than 1 mM the sensing is possible when the sample is diluted. As seen from the similar LOD in a simple cuvette assay, the difference between UCNP^{IS} and UCNP^{AS} seems to be quite small. However, for the UCNP^{AS} the absorption maximum of Nd³⁺ and the emission spectra of the laser diode does not show a perfect match (Figure 5.21) so that the full potential of those nanoparticles cannot be used. By using a laser diode with an emission peaking at 794 nm it is expected to further decrease the limit of detection further. However such diodes, especially cheap ones as required for sensing applications, are not commercially available so far.

Luminescence-based self-referenced enzymatic L-lactate sensing by tandem-sensitized NIR to UV NaYF₄(Yb,Tm) upconversion nanoparticles

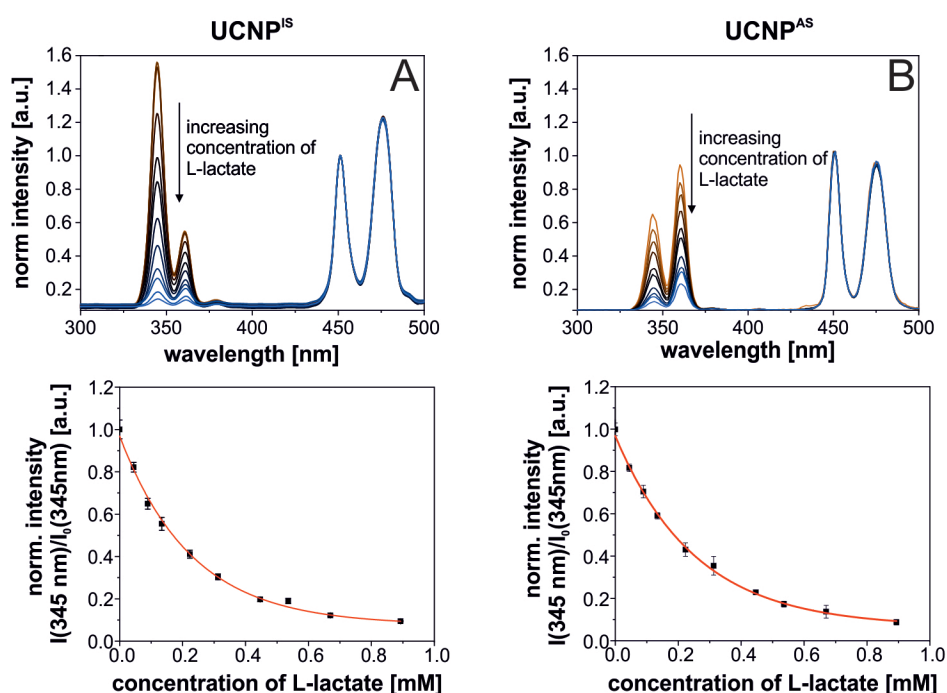


Figure 5.15| Luminescence spectra of UCNPIs(A) and UCNPAS(B) in a glycine / hydrazine buffer (pH 9) containing LDH (20 U·mL⁻¹) and NAD⁺(1.2 mM). The particle concentration was 0.1 mg·mL⁻¹ in both systems and excitation was performed with a 980 or 808 nm CW laser module (each 200 mW). Spectra are normalized to the emission at 450 nm.

5.3.4 Online monitoring of L-lactate

For the design of the online monitoring setup for L-lactate, two different strategies were investigated. One was the direct embedding of UCNP and the enzyme LDH within a polyacrylamide hydrogel (Figure 5.16).

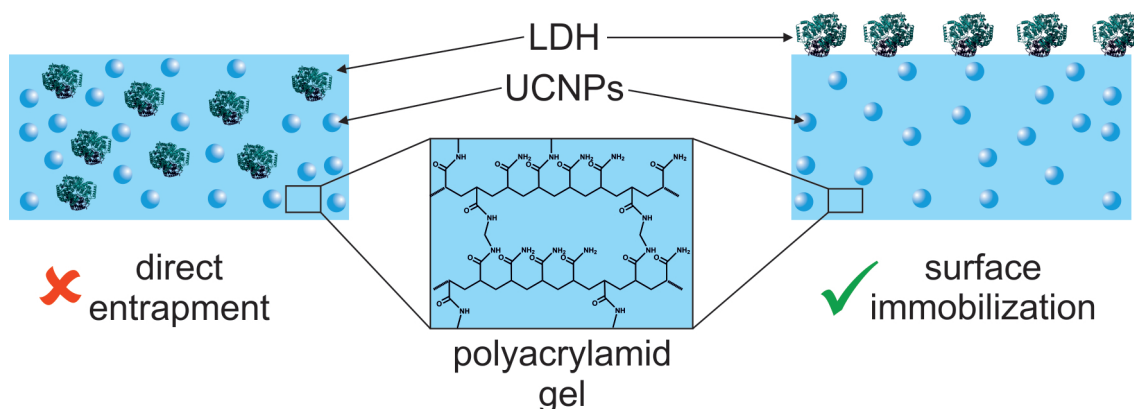


Figure 5.16| Strategies for the development of an online L-lactate sensor using upconversion nanoparticles.

The other one was to entrap only the UCNPs within the hydrogel, whereas the surface of the gel was covalently functionalized with the enzyme.

For the dual entrapment strategy, the enzyme and the particles were mixed with a solution containing the acrylamide monomers and initiator reagents (Figure 5.17).

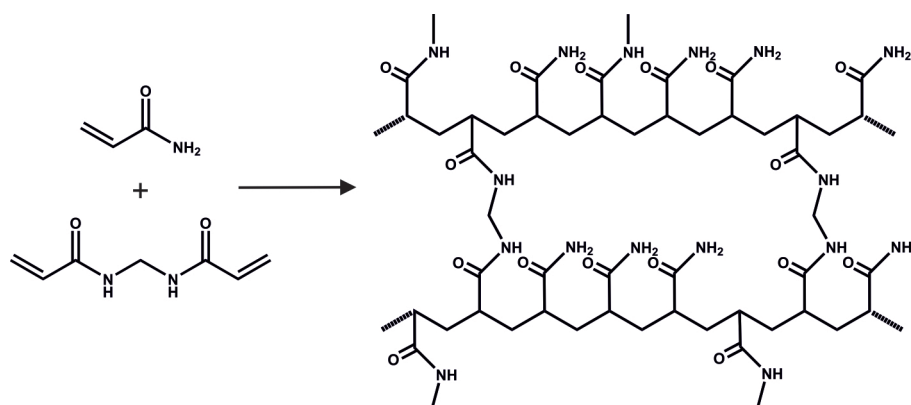


Figure 5.17| Polymerization reactions for the development of an online L-lactate sensor using upconversion nanoparticles. Reaction initiated by a radical starting agent, in this case APTS.

When tested in the flow-cell, no significant signal changes were observed within a reasonable time-frame (10 min). We assumed, this was due to a hampered diffusion of NAD⁺ and lactate into the hydrogel and the respective products again out of the hydrogel. Thus, LDH was directly immobilized on the surface of the hydrogel *via* a standard carbodiimide coupling reaction (Figure 5.18). The direct modification of the hydrogel containing the UCNPs lead to another difficulty.

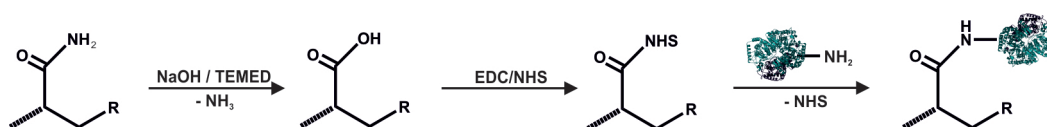


Figure 5.18| Reaction for the immobilization of LDH on the surface of the hydrogel. Amide groups at the surface are hydrolyzed by the addition of NaOH. The obtained carboxyl-groups are linked to the amine groups of the enzyme *via* EDC/NHS chemistry.

As the hydrolysis of the hydrogel's amide bonds leads to its swelling, the resulting nanoparticle leakage had to be overcome. A simple two-gel system within the home-made flow cell (Figure 5.19) solved the problem. The cell was made with a polyetheretherketone (PEEK) plastic. The chamber inside the cell had a length of 1.5 cm, a width of 0.4 cm and a height of 0.3 cm. This leads to a total volume of ~200 μ L.



Figure 5.19| Photograph of the home-made flow cell.

The activity of the enzyme film was determined from Michaelis Menten kinetics as $(1.45 \pm 0.1) \text{ mU} \cdot \text{cm}^{-2}$ (normalized to the surface of the enzyme film). A K_m value of $(2.99 \pm 0.3) \text{ mM}$ with a maximum reaction rate of $(3.7 \pm 0.2) \mu\text{M} \cdot \text{min}^{-1}$ was found (Figure 5.20).

For the design of the L-lactate online sensor, a small and affordable laser diode was used. However, those systems often show an increase in their temperature over a more extended measuring period

and a change of the emitted wavelength. Consequently, a precise temperature control system for the laser modules is inalienable. It is much simpler to use the upconversion emission intensity at 450 nm as an internal reference.

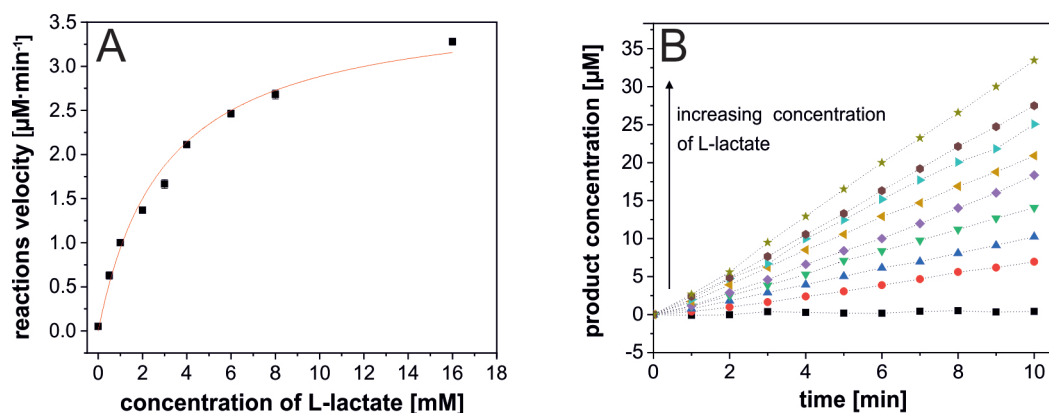


Figure 5.20| Absorbance of NADH at 340 nm as a function of the L-lactate concentration described in a Michaelis-Menten plot (A) with corresponding concentration-time dependency (B) for evaluation of the K_m -Value and maximum reaction rate with increasing L-lactate concentration from 0 mM up to 18 mM.

However, the cheap 808 nm low power laser modules show an emission profile that does not perfectly match the Nd³⁺ absorption, therefore already small fluctuations in the laser module temperature can shift the lasing wavelength outside the absorption region of the sensitizer (Figure 5.21).

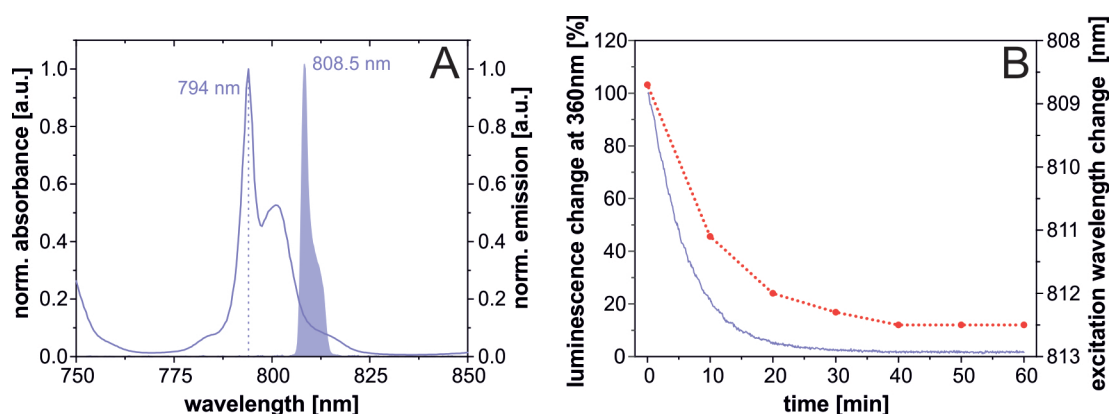


Figure 5.21| A: Normalized absorption spectrum of a NdCl₃ · 6H₂O (0.1 mol·L⁻¹, purple line) and the spectral overlap with the emission of the 808 nm (500 mW, light purple area) laser diode for online monitoring of L-lactate. The dotted line in purple indicates the ideal excitation wavelength (794 nm). The real excitation wavelength (808.5 nm) is shown in the figure. B: Stability of the emission wavelength of the excitation source (red dotted lines) and the resulting decrease of the upconversion emission at 360 nm (purple line).

The commercially available 980 nm low power laser modules are more robust to this effect (Figure 5.22). Therefore, an external cooling system was needed for the excitation at 808 nm to be able to perform long-term online monitoring (Figure 5.23).

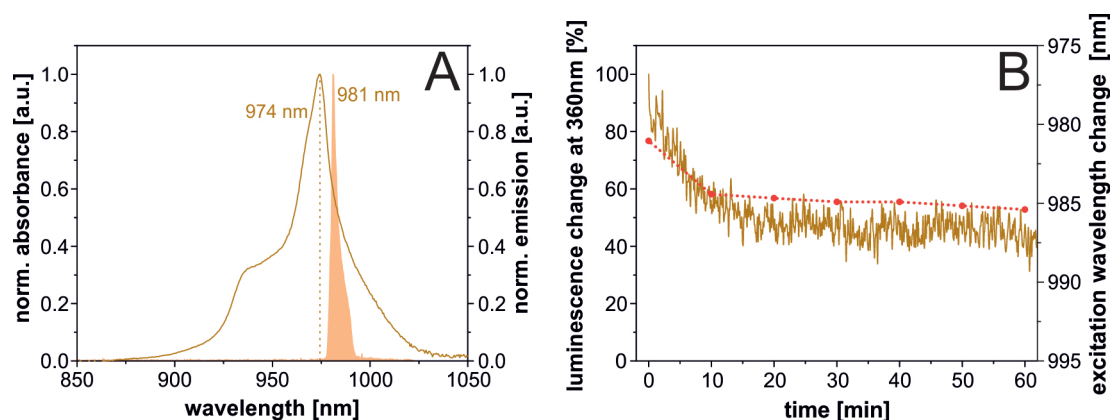


Figure 5.22| A: Normalized absorption spectrum of YbCl₃ · 6H₂O (0.1 mol·L⁻¹, orange line) and the spectral overlap with the emission of the 980 nm (200 mW, CW, light orange area) laser diode for online monitoring of L-lactate. The dotted line in purple indicates the ideal excitation wavelength (974 nm). The real excitation wavelength (981 nm) is shown in the figure. B: Stability of the emission wavelength of the excitation source (red dotted lines) and the resulting decrease of the upconversion emission at 360 nm (orange line).

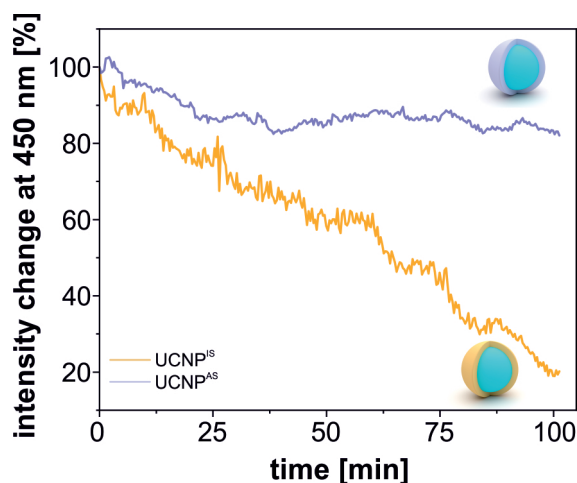


Figure 5.23| Stability of the emission signal at 450 nm of a hydrogel with either UCNP^{AS} (purple) and UCNP^{IS} (orange) in a glycine / hydrazine buffer (pH 9). The particle concentration was ~2 mg·mL⁻¹ in both systems and excitation was done with a 980 (200 mW) or 808 nm (500 mW) CW laser module.

Online measurements of L-lactate were performed in a flow cell at different concentrations of L-lactate for a period of around 2 h. When changing the solution to an L-lactate free solution, the initial signal was restored (Figure 5.24). Therefore, reversibility of the system for such a time scale can be claimed. In each case, the signal shows good stability. The larger error-bars for the 980 nm excitation in contrast to the 808 nm excitation can be assigned to the absence of a temperature control for the laser module whereas the 808 nm excitation source was cooled.

Comparing the two UCNP systems, surprisingly, a very similar behavior can be observed. The limit of detection was calculated to (130 ± 50) μM (3 S/N) for UCNP^{IS} and (81 ± 32) μM for UCNP^{AS}. However, for hydrogels illuminated at 980 nm the error bars are much higher due to the higher signal drift, which might be a consequence of gel swelling due to heating effects generated by the 980 nm excitation. In this study, due to environmental limitations, measurements were performed at room temperature only. However, as reported in the literature, the activity of L-lactate dehydrogenase increases nearly with a factor of 1.7 - 2.8 (depending on the type of the enzyme) with increasing temperature from 25

to 37 °C [65]. With the possibility to keep the temperature constant at 37 °C over a long time, it is expected to further increase the performance of this online detection system by lowering the limit of detection.

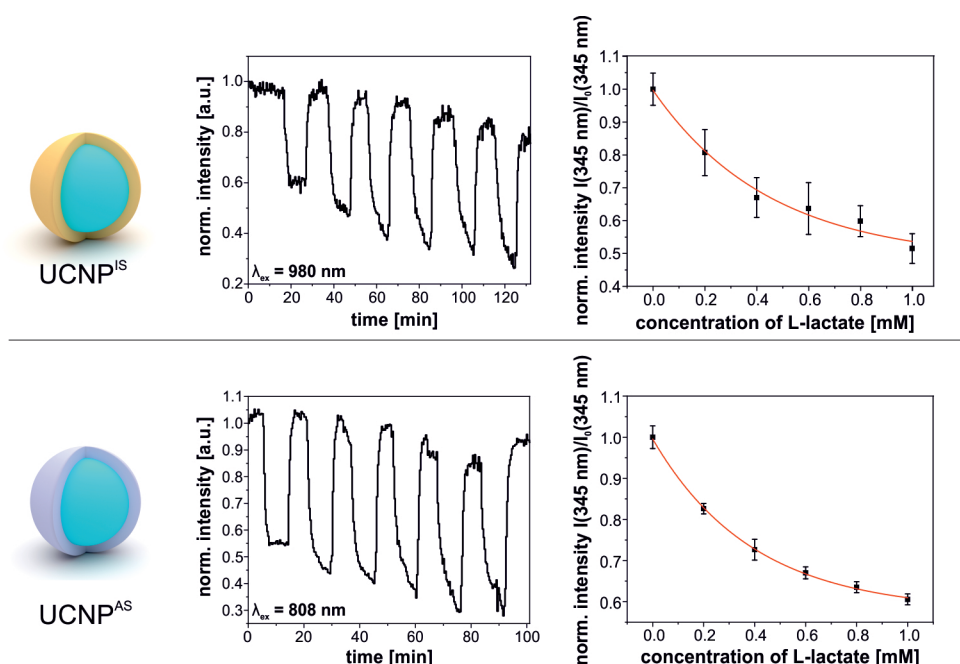


Figure 5.24| Luminescence spectra of UCNP^{IS} and UCNP^{AS} entrapped in a polyacrylamide hydrogel. The particle concentration was $\sim 2 \text{ mg}\cdot\text{mL}^{-1}$ in both systems and excitation was performed by a 980 nm (200 mW) or 808 nm (500 mW) CW laser module. On top of the particle hydrogel, an enzyme film $((1.45 \pm 0.1) \text{ mU}\cdot\text{cm}^{-2})$ was placed. After the injection of L-lactate, the signal 345 nm decreases due to the formation of NADH *via* LDH. After washing with a substrate-free solution the signal can be restored. The signal was normalized to the emission at 450 nm and $I_0(345 \text{ nm})$ refers to an L-lactate-free solution containing only NAD⁺ and the buffer.

For an application of this online monitoring system in more complex media like human serum, several interferences need to be studied. It was found that D-glucose, D-fructose, ascorbic acid, or sucrose had, no significant effect when applied in their physiologically occurring concentrations (Figure 5.25).

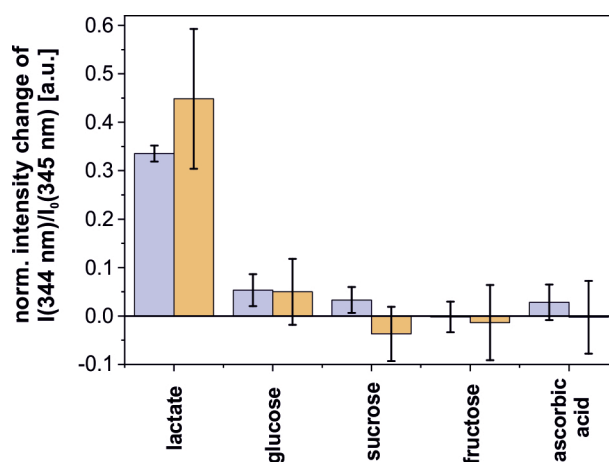


Figure 4.25| Selectivity investigation of the L-lactate online sensor using either UCNP^{IS} (beige) or UCNP^{AS} (purple). The concentration of each compound is equal to the physiological concentration of the compounds. The signal was normalized to the emission at 450 nm and $I_0(345 \text{ nm})$ refers to an L-lactate-free solution only containing NAD⁺ and the buffer.

Also, hemoglobin may influence the luminescence readout due to its absorption between 320 and 450 nm (with a maximum at 406 nm), which overlaps with the upconversion emission as seen in Figure 5.26.

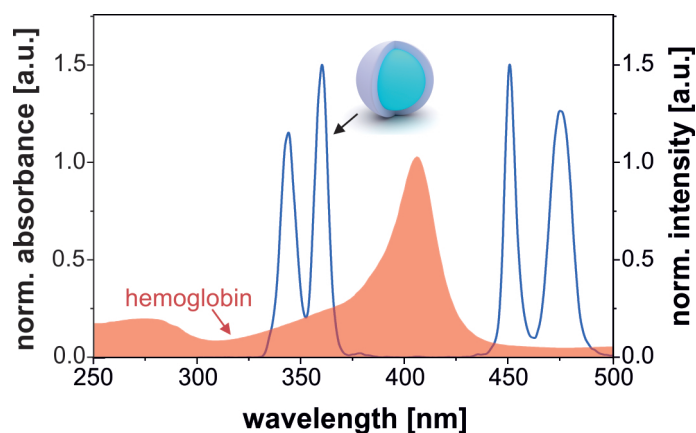


Figure 5.26| Normalized luminescence spectra of UCNPA^S nanoparticles in water (1.0 mg·mL⁻¹, blue line) under 808 nm CW laser excitation (200 mW) and normalized absorbance of hemoglobin (red area) in water. The spectra were normalized to the emission at 345 nm and to the absorbance maximum at 406 nm.

However, the absorption peak of hemoglobin covers both upconversion emission bands (UV and blue) and therefore its influence can be minimized by self-referencing of the intensity changes recorded at 360 nm to the emission at 450 nm. This may also be the main reason for the small signal decrease serum is injected (in addition to scattering effects). Finally, the addition of NAD⁺ to the serum didn't lead to signal increases hence ruling out nonspecific reactions with serum proteins. In a final experiment, the recovery rate of the system was determined (Figure 5.27), which leads to a highly satisfactory result yielding to a recovery of ~100 % (Table 5.3).

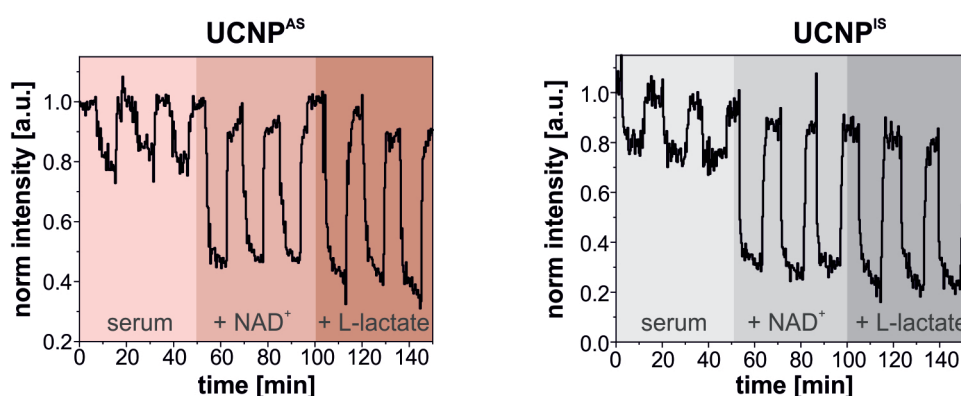


Figure 5.27| Investigation of sensor performance in a human serum sample using either UCNPs with an inert or with an active shell. The usability of the online setup for the detection of L-lactate in a complex media (like human serum) was analyzed with three different states: i) the influence of the serum itself, ii) the influence of interactions of the NAD⁺ with serum proteins, and iii) the recovery rate for the determination of L-lactate.

Table 5.3| Recovery rate of online measured L-lactate.

particle-system	added concentration [μM]	found concentration [μM]	recovery rate
UCNP ^{IS}	300	309 ± 12	103%
UCNP ^{AS}	300	314 ± 8	105%

5.4 Conclusion

In conclusion, we developed tandem-sensitized upconversion nanoparticles for efficient background-free sensing of L-lactate based on an inner filter effect. For high sensitivity, bright particles are required. NaYF₄(Yb,Tm) particles are prone to non-radiative relaxations due to surface defects and interactions of the particles with the dispersion media and the surface ligands. *Via* the growth of a thin inert shell (NaYF₄, UCNP^{IS}) the upconversion intensity at 340 nm can be increased with a factor of 40. It was also studied if an active shell consisting of NaYF₄(Nd,Yb) (UCNP^{AS}) can further enhance the sensitivity by shifting the excitation wavelength from 980 to 808 nm where the absorbance of water is much lower and therefore sample heating upon illumination can be prevented. In terms of sensitivity, no significant advantage was found. But in terms of signal drift and long-term stability, we were able to perform continuous measurements for over two hours using particles with tandem sensitization. Both particle systems show bright upconversion luminescence in aqueous media and can be used for an enzymatic sensor for L-lactate leading to a similar LOD (UCNP^{IS} = 30 μM and UCNP^{AS} = 25 μM). For the UCNP^{AS} the absorption maximum of Nd³⁺ and the emission spectra of the laser diode does not show a perfect match. Thus it is expected to further decrease the limit of detection by using a laser diode with an emission at 794 nm, but such diodes, especially cheap ones as required for sensing applications, are not commercially available so far.

The application of the particles in a long-term monitoring set-up demonstrated that the internal referencing by the 450 nm emission, their high photostability and excellent colloidal stability in an aqueous environment lead to a highly reliable online sensing platform. No interferences from the serum and additionally spiked molecules (such as glucose, ascorbic acid, *etc.*) affected the detection. We conclude that this online monitoring system can easily be adapted to other enzymatic linked reactions requiring NAD⁺/NADH as enzymatic co-factor to monitor analytes such as glucose or ethanol.

5.5 References

- [1] Jolly P, Formisano N, Estrela P (2015) DNA Aptamer-Based Detection of Prostate Cancer. *Chem. Pap.* 69(1):79-89.
- [2] Jolly P, Formisano N, Tkáč J, Kasák P, Frost CG, Estrela P (2015) Label-Free Impedimetric Aptasensor with Antifouling Surface Chemistry: A Prostate Specific Antigen Case Study. *Sens. Actuators B Chem.* 209:306-12.
- [3] Sharma P, Semwal V, Gupta B d (2019) Fiber Optic Surface Plasmon Resonance Based Lactate Sensor Using Co-Immobilization of Lactate Dehydrogenase and NAD⁺. *Opt. Fiber Technol.* 49:22-27.
- [4] Sharma TK, Ramanathan R, Rakwal R, Agrawal GK, Bansal V (2015) Moving Forward in Plant Food Safety and Security through NanoBioSensors: Adopt or Adapt Biomedical Technologies? *Proteomics* 15(10):1680-92.
- [5] Gavrilescu M, Demnerová K, Aamand J, Agathos S, Fava F (2015) Emerging Pollutants in the Environment: Present and Future Challenges in Biomonitoring, Ecological Risks and Bioremediation. *New Biotechnol.* 32(1):147-56.
- [6] Bhalla N, Jolly P, Formisano N, Estrela P (2016) Introduction to Biosensors. *Essays Biochem.* 60(1):1-8.
- [7] Bakker J, Nijsten MW, Jansen TC (2013) Clinical Use of Lactate Monitoring in Critically Ill Patients. *Ann. Intensive Care.* 3(1):12.
- [8] Alam F, RoyChoudhury S, Jalal AH, Umasankar Y, Forouzanfar S, Akter N, Bhansali S, Pala N (2018) Lactate Biosensing: The Emerging Point-of-Care and Personal Health Monitoring. *Biosens. and Bioelectron.* 117:818-29.
- [9] Faubert B, Li KY, Cai L, Hensley CT, Kim J, Zacharias LG, Yang C, Do QN, Doucette S, Burguete D, Li H (2017) Lactate Metabolism in Human Lung Tumors. *Cell* 171(2):358-71.
- [10] Rocchitta G, Spanu A, Babudieri S, Latte G, Madeddu G, Galleri G, Nuvoli S, Bagella P, Demartis M, Fiore V, Manetti R (2016) Enzyme Biosensors for Biomedical Applications: Strategies for Safeguarding Analytical Performances in Biological Fluids. *Sensors* 16(6):780.
- [11] Dzyadevych SV, Arkhypova VN, Soldatkin AP, El'skaya AV, Martelet C, Jaffrezic-Renault N (2008) Amperometric Enzyme Biosensors: Past, Present and Future. *Irbm* 29(2-3):171-80.
- [12] Himmelstoß SF, Hirsch T (2019) A Critical Comparison of Lanthanide Based Upconversion Nanoparticles to Fluorescent Proteins, Semiconductor Quantum Dots, and Carbon Dots for Use in Optical Sensing and Imaging. *Methods Appl. Fluoresc.* 7(2):22002.
- [13] Batra B, Narwal V, Pundir CS (2016) An Amperometric Lactate Biosensor Based on Lactate Dehydrogenase Immobilized onto Graphene Oxide Nanoparticles-Modified Pencil Graphite Electrode. *Eng. Life Sci.* 16(8):786-94.
- [14] Dagar K, Pundir CS (2017) An Improved Amperometric L-Lactate Biosensor Based on Covalent Immobilization of Microbial Lactate Oxidase onto Carboxylated Multiwalled Carbon Nanotubes/Copper Nanoparticles/Polyaniline Modified Pencil Graphite Electrode. *Enzyme Microb. Technol.* 96:177-86.
- [15] Pérez S, Sánchez S, Fàbregas E (2012) Enzymatic Strategies to Construct L-Lactate Biosensors Based on Polysulfone/Carbon Nanotubes Membranes. *Electroanalysis.* 24(4):967-74.
- [16] Hickey DP, Reid RC, Milton RD, Minteer SD (2016) A Self-Powered Amperometric Lactate Biosensor Based on Lactate Oxidase Immobilized in Simethylferrocene-Modified LPEI. *Biosens. Bioelectron.* 77:26-31.
- [17] Zhao Y, Fang X, Gu Y, Yan X, Kang Z, Zheng X, Lin P, Zhao L, Zhang Y (2015) Gold Nanoparticles Coated Zinc Oxide Nanorods as the Matrix for Enhanced L-Lactate Aensing. *Colloids Surf. B Biointerfaces* 126:476-80.
- [18] Hiraka K, Kojima K., Lin CE, Tsugawa W, Asano R, La Belle JT, Sode K (2018) Minimizing the Effects of Oxygen Interference on L-Lactate Sensors by a Single Amino Acid Mutation in *Aerococcus Viridans* L-Lactate Oxidase. *Biosens. Bioelectron.* 103:163-70.

- [19] Chan D, Barsan MM, Korpan Y, Brett CMA (2017) L-lactate Selective Impedimetric Biezymatic Biosensor Based on Lactate Dehydrogenase and Pyruvate Oxidase. *Electrochim. Acta* 231:209-15.
- [20] Hernández-Ibáñez N, García-Cruz L, Montiel V, Foster CW, Banks CE, Iniesta J (2016) Electrochemical Lactate Biosensor Based upon Chitosan/Carbon Nanotubes Modified Screen-Printed Graphite Electrodes for the Determination of Lactate in Embryonic Cell Cultures. *Biosens. Bioelectron.* 77:1168-74.
- [21] Kim J, Valdés-Ramírez G, Bandodkar AJ, Jia W, Martinez AG, Ramírez J, Mercier P, Wang J (2014) Non-Invasive Mouthguard Biosensor for Continuous Salivary Monitoring of Metabolites. *Analyst* 139(7):1632-36.
- [22] Kim S, Kim K, Kim HJ, Lee HN, Park TJ, Park YM (2018) Non-Enzymatic Electrochemical Lactate Sensing by NiO and Ni(OH)₂ Electrodes: A Mechanistic Investigation. *Electrochim. Acta* 276:240-46.
- [23] Abrar MA, Dong Y, Lee PK, Kim WS (2016). Bendable Electro-Chemical Lactate Sensor Printed with Silver Nanoparticles. *Sci. Rep.* 6:30565.
- [24] Jia W, Bandodkar AJ, Valdés-Ramírez G, Windmiller JR, Yang Z, Ramírez J, Chan G, Wang J (2013) Electrochemical Tattoo Biosensors for Real-Time Noninvasive Lactate Monitoring in Human Perspiration. *Anal. Chem.* 85(14):6553-60.
- [25] Khodagholy D, Curto VF, Fraser KJ, Gurfinkel M, Byrne R, Diamond D, Malliaras GG, Benito-Lopez F, Owens RM (2012) Organic Electrochemical Transistor Incorporating an Ionogel as a Solid State Electrolyte for Lactate Sensing. *J. Mater. Chem.* 22(10):4440.
- [26] Gu B, Zhang Q. (2018) Recent Advances on Functionalized Upconversion Nanoparticles for Detection of Small Molecules and Ions in Biosystems. *Adv. Sci.* 5(3):1700609.
- [27] Liu Y, Meng X, Bu W (2019) Upconversion-Based Photodynamic Cancer Therapy. *Coord. Chem. Rev.* 379:82-98.
- [28] Wen S, Zhou J, Zheng K, Bednarkiewicz A, Liu X, Jin D (2018) Advances in Highly Doped Upconversion Nanoparticles. *Nat. Commun.* 9(1):2415.
- [29] Sun L, Wei R, Feng J, Zhang H (2018) Tailored Lanthanide-Doped Upconversion Nanoparticles and their Promising Bioapplication Prospects. *Coord. Chem. Rev.* 364:10-32.
- [30] Zhou Y, Ling B, Chen H, Wang L (2017) Mn²⁺-doped NaYF₄: Yb,Er Upconversion Nanoparticles for Detection of Uric Acid Based on the Fenton Reaction. *Talanta.* 180:120-26.
- [31] Giust D, Lucío MI, El-Sagheer AH, Brown T, Williams LE, Muskens OL, Kanaras AG (2018) Graphene Oxide-Upconversion Nanoparticle Based Portable Sensors for Assessing Nutritional Deficiencies in Crops. *ACS Nano* 12(6):6273-79.
- [32] Gu B, Zhou Y, Zhang X, Liu X, Zhang Y, Marks R, Zhang H, Liu X, Zhang Q (2016) Thiazole Derivative-Modified Upconversion Nanoparticles for Hg²⁺ Detection in Living Cells. *Nanoscale.* 8(1):276-82.
- [33] Song X, Yue Z, Zhang J, Jiang Y, Wang Z, Zhang S (2018) Multicolor Upconversion Nanoprobes Based on a Dual Luminescence Resonance Energy Transfer Assay for Simultaneous Detection and Bioimaging of [Ca²⁺]_i and pH_i in Living Cells. *Chem. Eur. J.* 24(24):6458-63.
- [34] Mader HS, Wolfbeis OS (2010) Optical Ammonia Sensor Based on Upconverting Luminescent Nanoparticles. *Anal. Chem.* 82(12):5002-4.
- [35] Achatz DE, Meier RJ, Fischer LH, Wolfbeis OS (2011) Luminescent Sensing of Oxygen Using a Quenchable Probe and Upconverting Nanoparticles. *Angew. Chem. Int. Ed.* 50(1):260-3.
- [36] Wilhelm S, del Barrio M, Heiland J, Himmelstoß SF, Galbán J, Wolfbeis OS, Hirsch T (2014) Spectrally Matched Upconverting Luminescent Nanoparticles for Monitoring Enzymatic Reactions. *ACS Appl. Mater. Interfaces.* 6(17):15427-33.
- [37] Liu Y, Tu D, Zheng W, Lu L, You W, Zhou S, Huang P, Li R, Chen X (2018) A Strategy for Accurate Detection of Glucose in Human Serum and Whole Blood Based on an Upconversion Nanoparticles-Polydopamine Nanosystem. *Nano Res.* 11(6):3164-74.
- [38] Li X, Liu D, Wang Y, Xu S, Liu H (2018) Water Dispersive Upconversion Nanoparticles for Intelligent Drug Delivery System. *Colloids Surf. A* 555:55-62.

- [39] Li H, Wei R, Yan GH, Sun J, Li C, Wang H, Shi L, Capobianco JA, Sun L (2018) Smart Self-Assembled Nanosystem Based on Water-Soluble Pillararene and Rare-Earth-Doped Upconversion Nanoparticles for pH-Responsive Drug Delivery. *ACS Appl. Mater. Interfaces*. 10(5):4910-20.
- [40] Sabri T, Pawelek PD, Capobianco JA. (2018) Dual Activity of Rose Bengal Functionalized to Albumin-Coated Lanthanide-Doped Upconverting Nanoparticles: Targeting and Photodynamic Therapy. *ACS Appl. Mater. Interfaces*. 10(32):26947-53.
- [41] Li F, Du Y, Liu J, Sun H, Wang J, Li R, Kim D, Hyeon T, Ling D (2018) Responsive Assembly of Upconversion Nanoparticles for pH-Activated and Near-Infrared-Triggered Photodynamic Therapy of Deep Tumors. *Adv. Mater.* 30(35):e1802808.
- [42] Zhao H, Zhao L, Wang Z, Xi W, Dibaba ST, Wang S, Shi L, Sun L (2019) Heterogeneous Growth of Palladium Nanocrystals on Upconversion Nanoparticles for Multimodal Imaging and Photothermal Therapy. *J. Mater. Chem. B* 50:5808.
- [43] Tawfik SM, Sharipov M, Huy BT, Gerelkhuu Z, Biechele-Speziale D, Lee YI (2018) Naturally Modified Nonionic Alginate Functionalized Upconversion Nanoparticles for the Highly Efficient Targeted pH-Responsive Drug Delivery and Enhancement of NIR-Imaging. *J. Ind. Eng. Chem.* 57:424-435.
- [44] Zhang K, Zhao Q, Qin S, Fu Y, Liu R, Zhi J, Shan C (2019) Nanodiamonds Conjugated Upconversion Nanoparticles for Bio-imaging and Drug Delivery. *J. Colloid. Interface Sci.* 537:316-324.
- [45] Kraft M, Würth C, Muhr V, Hirsch T, Resch-Genger U. (2018) Particle-size-dependent upconversion luminescence of NaYF₄: Yb, Er nanoparticles in organic solvents and water at different excitation power densities. *Nano Res.* 11(12):6360-6374.
- [46] Dukhno O, Przybilla F, Muhr V, Buchner M, Hirsch T, Mély Y (2018) Time-dependent luminescence loss for individual upconversion nanoparticles upon dilution in aqueous solution. *Nanoscale* 10(34):15904-10.
- [47] Himmelstoß SF, Hirsch T. (2019) Long-Term Colloidal and Chemical Stability in Aqueous Media of NaYF₄-type Upconversion Nanoparticles Modified by Ligand-Exchange. *Part. Part. Syst. Char.* submitted
- [48] Lahtinen S, Lyytikäinen A, Pääkilä H, Hömppi E, Perälä N, Lastusaari M, Soukka T (2017) Disintegration of Hexagonal NaYF₄: Yb³⁺, Er³⁺ Upconverting Nanoparticles in Aqueous Media: The Role of Fluoride in Solubility Equilibrium. *J. Phys. Chem. C.* 121(1):656-65.
- [49] Himmelstoß SF, Wiesholler LM, Buchner M, Muhr V, Märkl S, Bäumner AJ, Hirsch T (2017) 980 nm and 808 nm Excitable Upconversion Nanoparticles for the Detection of Enzyme Related Reactions. *SPIE BiOS* 10077:100770L1-100770L6.
- [50] Ertek B, Akgül C, Dilgin Y (2016) Photoelectrochemical Glucose Biosensor Based on a Dehydrogenase Enzyme and NAD⁺/NADH Redox Couple using a Quantum Dot Modified Pencil Graphite Electrode. *RSC Adv.* 6(24):20058-66.
- [51] Wilhelm S, Kaiser M, Würth C, Heiland J, Carrillo-Carrion C, Muhr V, Wolfbeis OS, Parak WJ, Resch-Genger U, Hirsch T (2015) Water Dispersible Upconverting Nanoparticles: Effects of Surface Modification on their Luminescence and Colloidal Stability. *Nanoscale* 7(4):1403-10.
- [52] Haase M, Schäfer H (2011) Upconverting Nanoparticles. *Angew. Chem. Int. Ed.* 50(26):5808-29.
- [53] Hu J, Zhan S, Wu X, Hu S, Wu S, Liu Y (2018) Core/shell Upconversion Nanoparticles with Intense Fluorescence for Detecting Doxorubicin *in Vivo*. *RSC Adv.* 8(38):21505-12.
- [54] Abel KA, Boyer J-C, Andrei CM, van Veggel FCJM (2011) Analysis of the Shell Thickness Distribution on NaYF₄/ NaGdF₄ Core / Shell Nanocrystals by EELS and EDS. *J. Phys. Chem. Lett.* 2(3):185-89.
- [55] Dong A, Ye X, Chen J, Kang Y, Gordon T, Kikkawa JM, Murray CB (2011) A Generalized Ligand-Exchange Strategy Enabling Sequential Surface Functionalization of Colloidal Nanocrystals. *J. Am. Chem. Soc.* 133(4):998-1006.
- [56] Buchner M, Muhr V, Himmelstoß SF and Hirsch T (2016) 4 Functionalization Aspects of Water Dispersible Upconversion Nanoparticles. In *Upconverting Nanomaterials* (pp 69-100). CRC Press, Boca Raton.

- [57] Würth C, Kaiser M, Wilhelm S, Grauel B, Hirsch T, Resch-Genger U (2017) Excitation power dependent population pathways and absolute quantum yields of upconversion nanoparticles in different solvents. *Nanoscale* 9(12):4283-94.
- [58] Wiesholler LM, Hirsch T (2018) Strategies for the Design of Bright Upconversion Nanoparticles for Bioanalytical Applications. *Opt. Mater.* 80:253-64.
- [59] Feliu N, Sun X, Alvarez Puebla RA, Parak WJ (2017) Quantitative Particle-Cell Interaction: Some Basic Physicochemical Pitfalls. *Langmuir.* 33(27):6639-46.
- [60] Pilch A, Würth C, Kaiser M, Wawrzyńczyk D, Kurnatowska M, Arabasz S, Prorok K, Samoć M, Strek W, Resch-Genger U, Bednarkiewicz A (2017) Shaping Luminescent Properties of Yb³⁺ and Ho³⁺ Co-Doped Upconverting Core-Shell β-NaYF₄ Nanoparticles by Dopant Distribution and Spacing. *Small* 13(47):1701635.
- [61] Li Z, Zhang Y, La H, Zhu R, El-Banna G, Wei Y, Han G (2015) Upconverting NIR Photons for Bioimaging. *Nanomaterials* 5(4):2148-68.
- [62] Skripka A, Marin R, Benayas A, Canton P, Hemmer E, Vetrone F (2017) Covering the Optical Spectrum through Collective Rare-Earth Doping of NaGdF₄ Nanoparticles: 806 and 980 nm Excitation Routes. *Phys. Chem. Chem. Phys.* 19(19):11825-34.
- [63] Powers JL, Kiesman NE, Tran CM, Brown JH, Bevilacqua VL (2007) Lactate Dehydrogenase Kinetics and Inhibition Using a Microplate Reader. *Biochem. Educ.* 35(4):287-92.
- [64] Ewaschuk JB, Naylor JM, Zello GA (2005) D-lactate in Human and Ruminant Metabolism. *J. Nutr.* 135(7):1619-25.
- [65] Krieg AF, Gorton S, Henry JB (1967) Effect of Temperature on Activity and Lactate Optima of Ldh Isoenzymes. *Clin. Chim. Acta* 17(3):363-66.

CHAPTER 6

Conclusion and future perspectives

6.1 Nanomaterials in bioassays

According to a general definition, nanotechnology can be attributed to systems with a size smaller than 100 nm (at least in one dimension). In the last years, this field of research has become the driving motor for the development of new materials in nearly all aspects of daily life [1]. The reason therefore, is quite obvious after studying the properties of those systems. Each material, which is shrunk to the nanoscopic level, owns unique properties. For instance, the electron cloud of gold nanoparticles in contrast to the one of a bulky gold bar is capable of resonating with the irradiated light [2]. Depending on the size of the particles, different wavelengths can be absorbed, leading to a colored material as seen in the famous Lycurgus cup from the 4th century [3]. In other materials like semiconductor quantum dots, the luminescence is a consequence of the so-called quantum confinement. The dimensions of the materials are smaller than the Bohr-radius leading to discrete energy levels [4]. Those properties, together with the high surface-to-volume ratio of the nanoparticles, make them ideal candidates for the development of biosensors as a high amount of biorecognition elements can be attached to their surface [5].

In an extremely simplified picture, luminescent nanoparticles, such as presented in detail in Chapter 1, can be compared to modern Marvel® superheroes. Each of them has at least one superpower, which makes them unique in their field. However, a special weakness is always combined with this power, which seems to be very similar to the luminescent probes. For instance, the properties of the green fluorescent protein remind one somehow to the abilities of “HULK™”. Not only in size but also due to their special code in their (genomic) sequence, both are strong (and green) [6]. However, after a while, both systems are exhausted and are not active any longer (photobleaching). Quantum dots are more stable. Their luminescence properties change with their size, like the abilities of “ANT-MAN™” do. Additionally, this hero needs a special armor when he is shrinking in order to enable breathing any longer. Regarding the health effect, also quantum dots need a special shell to prevent damage due to leakage of toxic metals like cadmium [7]. Analogs to “ANT-MAN™”, also “IRON-MAN™” is dependent on his armor. Without this and his high energy reactor, this superhero is weak. Like him, UCNPs need a clever “armor” design as their unmodified form shows a very low quantum yield which increases with higher power density of the excitation source [8]. *Via* growing a shell around the nanoparticles or by clever surface engineering the brightness as well as the stability of the system rises strongly. Among the fluorescent probes, C-Dots are the youngest ones and might be compared to “SPIDER-MAN™”. At the current stage, the nanoparticles are strongly underestimated due to some lack in synthesis, in functionalization and also because of not fully understanding of all the exciting properties yet. Despite their fascinating properties like the ones of superheroes, the research is still missing some experience concerning their applications. In my opinion, UCNPs have the greatest potential of all luminescent nanoparticle heroes as they can be excited in the NIR region of the spectrum. Thus in

contrast to the other ones, the background signal due to autofluorescence of biological compounds is reduced [9]. Like “IRON-MAN™” they are not perfect by nature and there are still several challenges that need to be considered including the stability of the probes, the number and functionality of receptors and the design of surfaces. All these arguments directly describe the surface of the nanoparticles, which can be seen as interface between the bioassay world and the nature of the nanoparticles. In order to tune the nanoparticles for bioanalytical applications, it is mandatory to study the design of this interface in more detail. Therefore, it is not surprising that the number of publications for UCNPs, dealing with their surface chemistry has increased impressively in the last years (Figure 6.1).

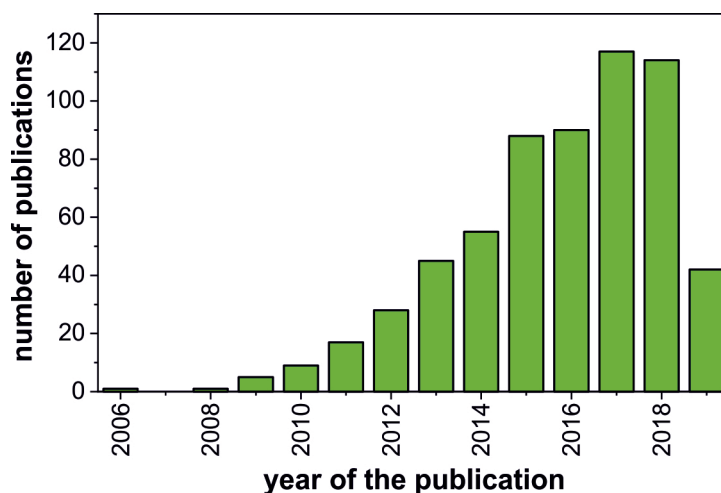


Figure 6.1| Web-of-Science survey about the publications dealing with the surface chemistry of upconversion nanoparticles.

In several systems, UCNPs have already been successfully modified and integrated [10]. For instance, as reported by He *et al.* [11], highly Er^{3+} and Tm^{3+} -doped 50 nm-sized UCNPs can be used for the detection of prostate specific antigen (PSA) based on a paper-based lateral flow assay ($\text{LOD} = 89 \text{ pg}\cdot\text{mL}^{-1}$). An even lower LOD for PSA was reported by the group of Gorris [12] by an upconversion immunosorbent assay on a single particle level. Here, the LOD was $1.2 \text{ pg}\cdot\text{mL}^{-1}$. However, in both systems, the assay is performed in a microtiter plate or on paper, with included washing steps. Especially for bioanalytical applications, online measurements with self-referencing are more interesting. This can be realized with UCNPs from the type $\text{NaYF}_4:\text{Yb},\text{Tm}$, which show several well separated emission bands ranging from the UV to the end of the visible spectrum at 800 nm. As seen in Chapter 4 the emission of those nanoparticles matches with the absorbance spectra of common enzymatic co-factors NAD^+/NADH and FAD/FADH_2 , so that it is possible to design a biosensor based on the reabsorption (inner filter effect) of those biomolecules. Consequently, the nanoparticles can be used to quantify the amount of co-factor after an enzymatic reaction. However, several challenges including leakage, colloidal and chemical stability need to be overcome. Most of them are directly related to the surface properties of the UCNPs.

6.2 Surface-engineering of upconversion nanoparticles

For the design of the surface of nanoparticles, several aspects need to be considered as suggested by the group of Wolfgang Parak [13, 14]. The choice of the ligand is a critical step to guarantee colloidal

stability and functionality of the nanoparticles. Furthermore, many parameters are involved in order to warrant a stable nanosystem: a) the UCNPs must have the right size and morphology for the desired applications, which determines the kind of surface modification, b) the chemical nature of the surface of the nanoparticles and their stability must be considered, and c) the environment of the nanoparticles must be known or even – when possible – controlled. Influences like pH, type and composition of the media, and competition with other possible ligands with higher binding strength towards the surface of the UCNPs need to be considered. Additionally, in order to apply the nanoparticles for *e.g.* *in vivo* application a bioconjugation of the nanoparticles with biomolecules is inalienable as this functionalization leads to a specific interaction of a nanoparticle with the (biological) system.

6.2.1 Particle size and the choice of the surface modification strategy

Upconversion nanoparticles can be found in different fields of application. Especially for bioanalytical applications *in vivo*, the size restricts the potential of the nanoparticles as it is often a stringent requirement for the uptake of the particles by the cells [15]. Moreover, the cellular uptake is strongly depending on different factors like the type of the cells. Generally, the interactions of the nanoparticles with the cells need to be investigated in detail for each cellular line. For instance, human melanoma cells (A375) are capable to uptake silica nanoparticles/nanorods with a length up to 450 nm [16]. By changing the cell line also the uptake behavior can be changed. As reported by Hsiao *et al.*, normal rat kidney cells (NRK-52E) rapidly incorporate 15 nm-sized SiO₂ nanoparticles but not particles with a size of 60 nm. In keratinocyte cells (HaCaT) both sizes (15 nm and 60 nm) are uptaken [17].

For the use of nanoparticles *in vivo*, the size of the particles is even more important. Beside the uptake also the clearance of the nanoparticles is essential [18]. The most effective and fast pathway is the renal one. However here the particles must have a size below the renal clearance barrier (6 - 8 nm) [19]. In the case of particles, which are bigger due to their original size or due to aggregation, the filtration by the kidney is not possible and therefore the preferred route of excretion is through the liver. However, during this route, the particles stay a long time in the reticuloendothelial system of the organism [19]. To get an FDA approval for the applications of nanomaterials the particles must leave the organism in a reasonable time period [19]. In the last years, the synthesis of bright UCNPs with sizes matching the renal clearance barrier has been realized [20], so that the choice of the post synthetic surface modifications has become more important, as the size of the nanoparticles should not increase dramatically.

In other applications, where the size is less relevant and only the brightness of the system counts, often bigger particles are chosen. Depending on the desired size, different surface strategies are more beneficial compared to others. In the literature as well as in Chapter 1 several methods are described to render upconversion nanoparticles water dispersible. Each of the methods (ligand removal, ligand exchange, ligand oxidation, inorganic shells, and polymer coating) has several benefits and drawbacks. In order to get a better understanding of the surface modification techniques, one can classify each system within a diagram where the complexity of the systems is plotted against the dimensions of the nanoparticles (0.1 nm to 80 nm, in a similar way as it was presented by Jeong *et al.* for the description of gold nanoparticles [21]). The complexity of the system is the sum of all elements present in the nanocrystal (Ln³⁺, Na⁺, F⁻) as well as the number of all surface ligands / elements attached to their surface. In the case of UCNPs after ligand removal, only the bare UCNPs are present with no

additional contributions of the surface ligands. After ligand exchange, up to 60% of the surface can be occupied with the new capping agent (a lower surface coverage is symbolized by the light blue area). In the case of an additional ligand (e.g. *via* an amphiphilic surface ligand) the amount of ligand compared to UCNPs with an oleate capping is nearly doubled. For the attachment of an inorganic shell (here SiO₂) the amount of the SiO₂ units in a 1 nm thick shell is added to the number of ligands.

As one can see from Figure 6.2, especially for small nanoparticles a very complex system is generated for all modification techniques. The ligand removal and the ligand exchange are counting to the simplest ones as here the number of additional surface molecules is smaller. In the case of the ligand removal, the particles need to be treated with acid in order to protonate the oleic acid leading to bare UCNPs. However, due to the missing stabilization, those particles are often colloidal unstable and less beneficial for bioanalytical applications. In the ligand exchange strategy, the nanoparticles are still covered with a surface ligand, which guarantees high colloidal stability, as shown in Chapter 3.

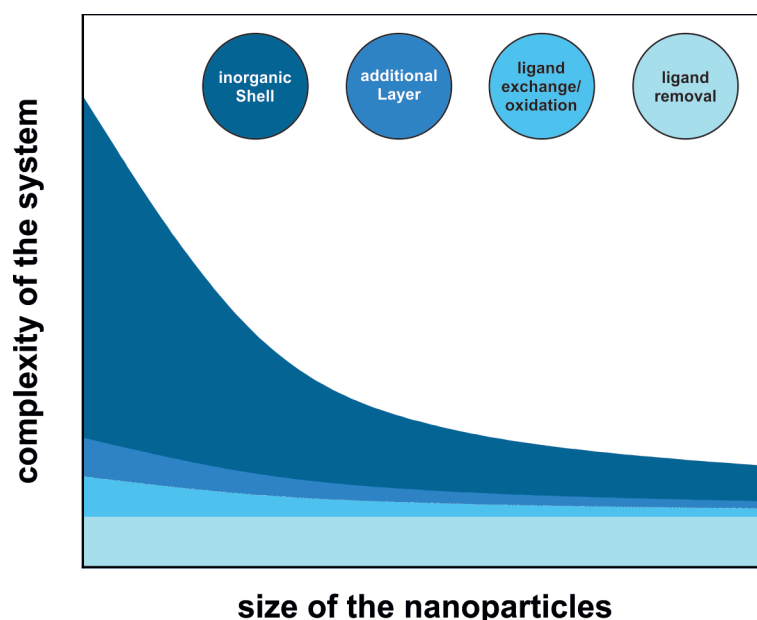


Figure 6.2| Schematic overview of the complexity of surface modified UCNPs with a 1 nm thick silica shell, with an additional polymer layer, with an exchanged ligand, after oxidation of the oleic acid or bare UCNPs after ligand removal. The x-axis is ranging from 0.1 to 80 nm.

Despite the potential of this method, it often suffers from poor surface coverage. Due to the smaller density of the surface layer, the shielding against water quenching is less effective as seen in Figure 6.3 and in Chapter 3. By the addition of a polymer or a silica layer, the system gets more complex, which needs more elaborate production methods. In both cases, the modification with a layer on top of the oleate capping (Type_Add) leads to a better shielding against water quenching as seen in Figure 6.3. For UCNPs with an additional polymer layer the size of the nanoparticles is increased, which makes them less beneficial for applications, where small structures (e.g. *in vivo* applications, FRET sensing) are required. In the case of a silica coating, it would be possible to generate a thin (and stable) shell around the particles which could have an additional positive effect on their chemical stability.

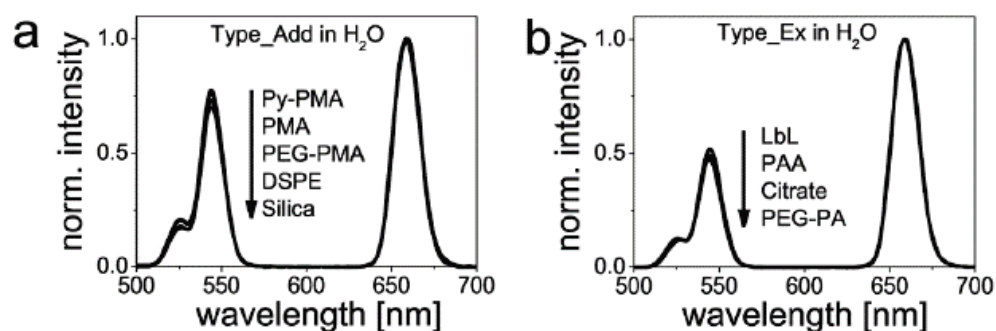


Figure 6.3| Normalized upconversion luminescence spectra of particles with coatings on top of the oleate (Type_Add) (A) and of particles modified by ligand exchange (Type_Ex) (B). Spectra were acquired at 980 nm laser excitation ($15 \text{ W}\cdot\text{cm}^{-2}$) and normalized to 658 nm [22] - Published by The Royal Society of Chemistry.

6.2.2 Chemical stability of upconversion nanoparticles

As seen in Chapter 3 and reported by the group of Mely [23], UCNPs modified *via* ligand exchange or with an additional polymer coating are not prone to particle dissolution. Especially for *in vivo* applications and continuous online measurements, this is a major drawback. Besides the loss of luminescence, also the released fluoride and lanthanide ions to the organism must be considered.

Many cellular studies use low concentrations of UCNPs. As shown in Chapter 3, the UCNPs start to dissolve when concentrations become lower than $100 \mu\text{g}\cdot\text{mL}^{-1}$. Consequently, cellular studies with dispersions of $25 \mu\text{g}\cdot\text{mL}^{-1}$ or less often do not cover the influence of the nanoparticles but of the free ions. Therefore, it is not surprising that for those particle concentrations often a high cell viability is observed as reported in an overview by Capobianco [24]. However, here also the effect of the released Ln^{3+} and the F^- on the health of the cells must be considered. For instance, fluoride at elevated concentrations has a toxic effect on the health of a human being and cells. In the case of UCNPs, the amount of free fluoride is $\sim 33 - 80 \mu\text{M}$ (depending on the assumed dissolution mechanism) and a detailed analysis of the influence of this concentration value on a cellular level should be mandatory for future cellular experiments. Additionally, also the morphology of those particles should not only be investigated prior to the applications but also after the dilution or the applications (e.g. *via* TEM).

Besides the more detailed study about the toxicity of UCNPs also alternative systems providing higher chemical stability are desirable. For upconversion nanoparticles consisting of NaYF_4 two possible dissolution mechanisms based on NaYF_4 ($K_s = 1.6 \cdot 10^{-26} \text{ mol}^6\cdot\text{L}^{-6}$) and YF_3 ($K_s = 3.98 \cdot 10^{-19} \text{ mol}^4\cdot\text{L}^{-4}$) have been reported [23]. By using highly concentrated dispersions of those nanoparticles or entrapping them within a polyacrylamide gel the dissolution can be reduced in the way that they can be used for a long online measurement. This observation matches with recently published studies to increase the chemical stability of UCNPs. The group of Lastusaari [25,26] has used a cross-linked surface coating consisting of poly(acrylic acid) and polyallylamine. The denser layer around the nanoparticle leads to a lower release rate of the fluoride ions. However, for *in vivo* applications, such systems are not useful as still a small amount of fluoride can get released, which does not fulfill the standards of the FDA. A glance at UCNPs completely based on a Y_2O_3 ($K_s = 1.6 \cdot 10^{-23} \text{ mol}^5\cdot\text{L}^{-5}$ [27]) host lattice shows that the change to this system is not recommendable as the higher phonon energy

($\sim 600 \text{ cm}^{-2}$ [28]) leads to a weaker upconversion luminescence. Additionally, the synthesis of those nanoparticles is performed in the autoclave so far, leading to lower size control.

However, as the solubility product of Y_2O_3 is between the solubility constants described for NaYF_4 the influence of a thin shielding shell of Y_2O_3 at NaYF_4 core particles would be worth to be studied in the future.

6.2.3 Influence of the dispersion media on the stability of upconversion nanoparticles

Not only the choice of the type of surface modification but also the influence of the dispersion media or the buffer must be considered, as not all surface ligands can be dispersed in the same buffer. To provide high colloidal stability, the surface of the nanoparticles should be electrically charged in order to ensure a strong electrostatic repulsion. Therefore, the pH value of the buffer should match the pK_a of the capping ligands. For instance, particles modified with polyallylamine with a pK_a of 8.7, as reported in Chapter 3, may lead to colloidal instability due to deprotonation of the amine groups when dispersed in slightly basic buffers. Additionally, to the influence of the pH of the buffer, also the composition of the buffer must be considered. For instance, buffers containing phosphate or their derivatives (like the phosphate buffered saline (PBS) or the Britton–Robinson buffer) should be used with UCNPs cautiously as those compounds show strong interaction with the surface of the nanoparticles. A possibility to overcome this issue is to use particles with a phosphate functionalization. In this case, the surface of the nanoparticles is saturated with phosphate and so the destabilizing influence of the buffer itself can be overcome as shown by Duong *et al.* [29]. Here the three different functional groups (phosphate, sulphonic acid and carboxyl) have been investigated regarding the stability of the nanoparticles in two buffer systems (2-(N-morpholino)ethanesulfonic acid (MES), pH 4.5 and PBS, pH 7.4). For the study, the particles were modified with poly oligo(ethylene glycol) methyl ether acrylate (POEGA), which was further functionalized with poly(acrylic acid) (PAA), poly monoacryloxyethyl phosphate (PMAEP) and poly 1-acrylamido-2-methylpropane sulphonic acid (PAMPS). An analysis of the adsorption energy showed that phosphate groups have the strongest affinity to bind to the surface of the UCNPs ($-90 \text{ kcal}\cdot\text{mol}^{-1}$). Carboxylic acid and sulphonic acid show similar values ($\sim -80 \text{ kcal}\cdot\text{mol}^{-1}$). Consequently, the nanoparticles with a phosphate capping (Figure 6.4 – first row) show remarkable colloidal stability in all buffer systems whereas the other coatings form aggregates (Figure 6.4 – second and third row), when dispersed in PBS.

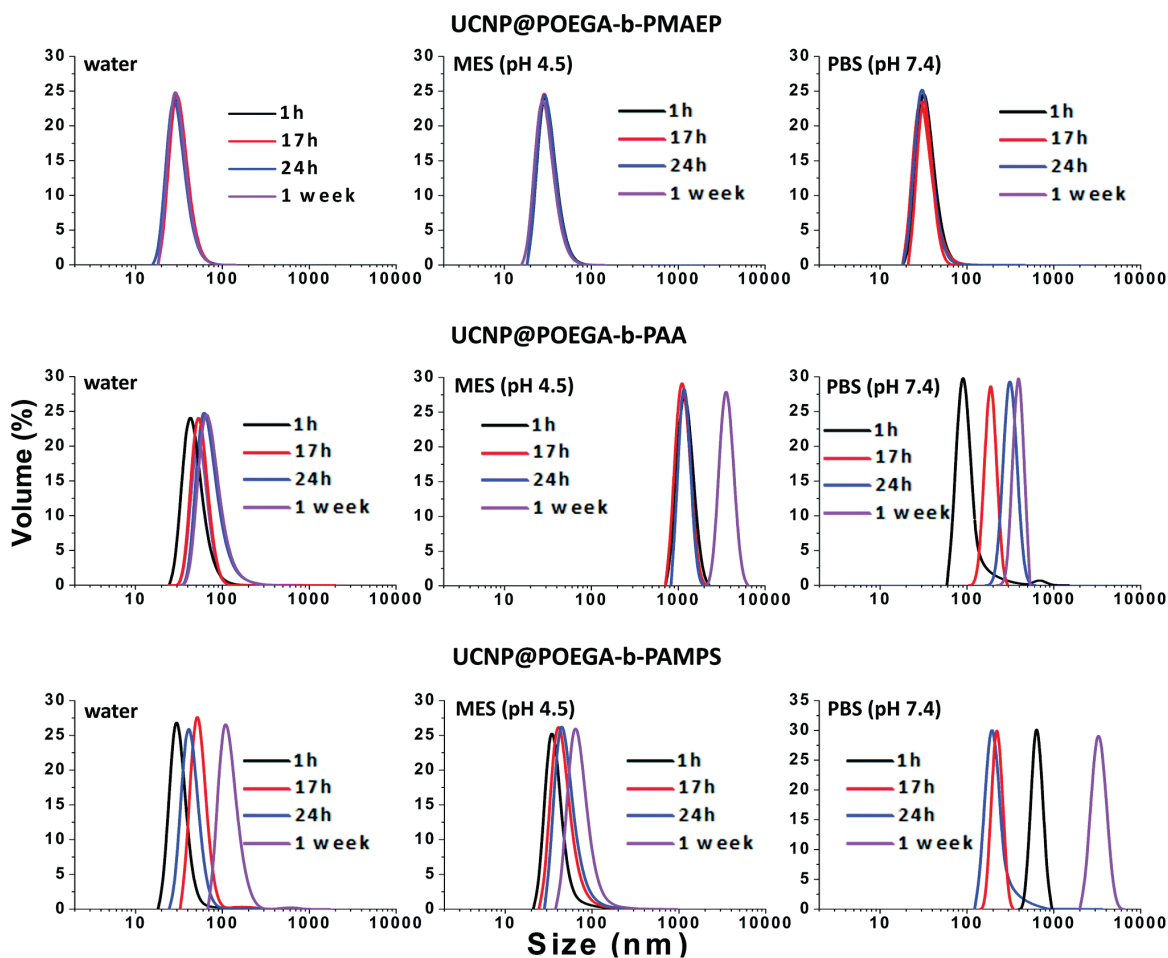


Figure 6.4| Colloidal stability of UCNP@POEGA-b-PMAEP, UCNP@POEGA-b-PAA and UCNP@POEGA-b-PAMPS over one week storage in water, MES (pH 4.5) and PBS (pH 7.4) [29] - Published by The Royal Society of Chemistry.

Another possibility to shield the UCNPs is their entrapment. For instance, the nanoparticles can be entrapped in polyvinyl pyrrolidone nanofibers, as shown by Buchner *et al.* [30] or within a hydrogel, as shown in Chapter 5. With this, it was possible to design an online sensor based on the enzymatic turnover of L-lactate *via* L-lactate dehydrogenase and NAD^+ . The byproduct of the reaction NADH was used for quantification and it was possible to detect L-lactate levels down to $82 \mu\text{mol}\cdot\text{L}^{-1}$ using $\text{NaYF}_4:\text{Yb}:\text{Tm}@\text{NaYF}_4:\text{Yb}:\text{Nd}$. The usability of the system was also investigated in human serum with a recovery rate of nearly 100%.

6.2.4 Surface functionalization for analytical applications

Nowadays, a smart design of the surface of UCNPs enables the usage of those nanoparticles for drug and gene delivery [31,32]. However, in order to make UCNPs attractive for those bioanalytical applications, the surface of the nanoparticle must be modified with receptor molecules like proteins, DNA or aptamers. Also simpler systems like the labeling of the UCNPs with a pH-sensitive dye would be possible. As shown in Chapter 1, the attachment of a functionality can happen *via* different routes. For instance, it is possible to design a pH-sensitive probe based on the electrostatic interaction between positively charged UCNPs and a negatively charged pH sensitive dye. In cooperation with the working group of Prof. Elizabeth Hall from Cambridge University, such a sensor was designed. Thereby,

Alizarin Red S – an anthraquinone derivate – was bound electrostatically to the surface of polyethyleneimine functionalized UCNPs (Figure 6.5). Thereby the pH sensitive absorption spectrum overlaps with the emission of NaYF₄:Yb,Er nanoparticles (540 nm). Based on this inner filter effect, the pH could be determined between pH 4 and 7, which makes this probe attractive for the detection of the pH changes within a cellular system.

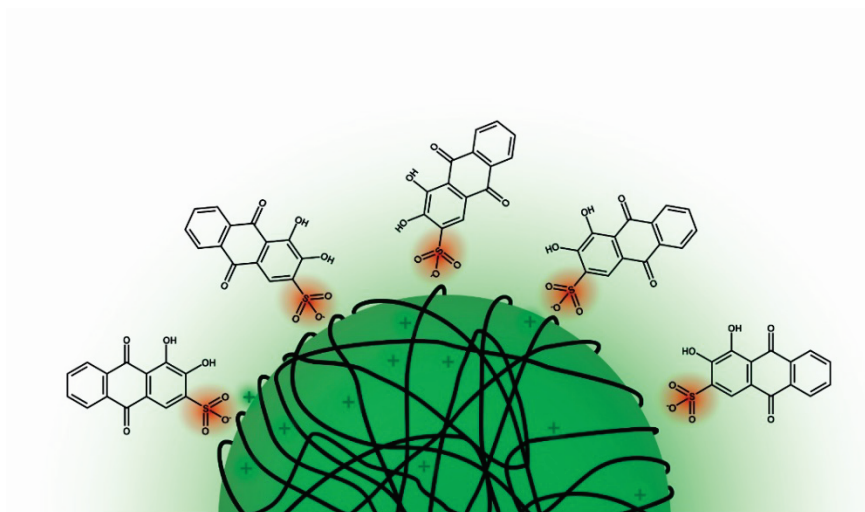


Figure 6.5| Schematic illustration of a pH sensitive UCNP probe. The Alizarin Red S molecules are bound electrostatically to the PEI modified UCNPs via negatively charged sulfonate groups.

However, especially for analytical applications in biological cells, such a coupling strategy is difficult as the possible leakage of the dye from the surface of the UCNPs must be considered. More promising is the covalent binding of the recognition element to the surface of the nanoparticles. An attractive alternative route for bioconjugation was presented by the group of Jin [33]. Thereby the UCNPs are modified with a cucurbit[7]uril macrocycle, which provides a binding cavity for most biomolecules. Based on a supramolecular host-guest self-assembly the biomolecules are then attached to the surface of the nanoparticles. For the conjugation with immunoglobulin G, this method allows a ten times higher concentration of the biomolecule on the surface of the particles than commonly known EDC/NHS chemistry. Another smart, fast, efficient and controllable surface modification can be based on photoinduced click chemistry as shown by Lederhose *et al.* [34]. Here, UCNPs consisting of NaY₄:Yb,Tm are used for the conversion of tetrazole into a reactive nitrile imine. This molecule can then react with an electron deficient double bond and build a pyrazoline cycloadduct.

6.3 Future perspectives of upconversion nanoparticles

The group of Alam [35] has shown that the performance limits of an electric nanobiosensor are based on the reaction diffusion theory as well as the time any analyte needs to be captured via the biorecognition element (settling time). With decreasing concentration, this gets more elaborate and the geometry of the biosensor plays (Figure 6.6) an important role to detect an analyte in a reasonable time (e.g. 100 s).

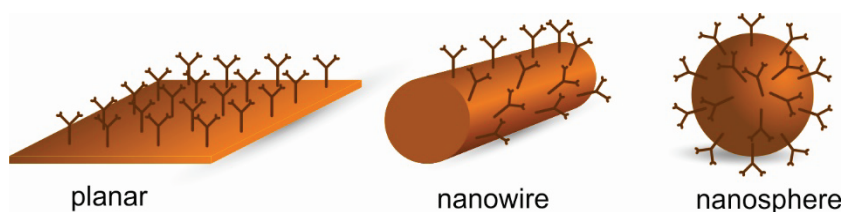


Figure 6.6] Schematic illustration of a sensor immersed in an analyte solution. The diffusion of the analyte towards a planar surface is done in one dimension. Towards a cylindrical nanostructure in two dimension and that to a spherical surface (nanosphere) is done in three dimensions.

The lower the concentration, the fewer molecules are swimming around the sensor element, and it will take longer to create a response signal. As shown in Figure 6.7, a cylindrical sensor setup is more sensitive than a planar sensor setup. However, there is little difference compared to a sensor using nanospheres.

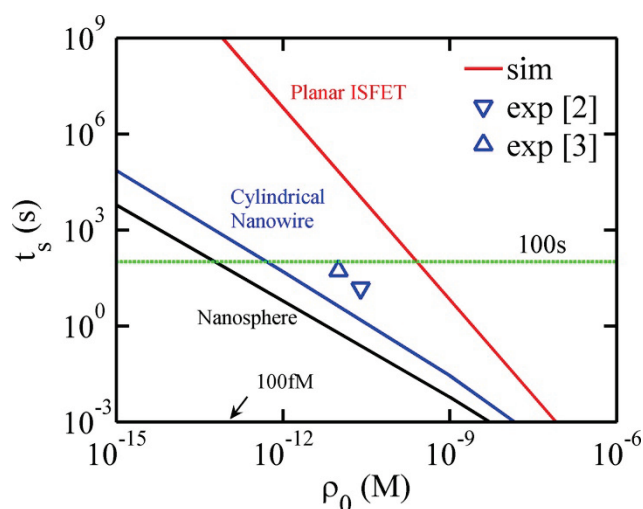


Figure 6.7] Relationship between settling time and detectable concentration of an analyte. For a detection time of 100 s (green line), the 2D cylindrical system can detect picomolar concentrations while the planar system cannot reach this level. Reprinted from [35], with the permission of AIP Publishing.

This study reveals a new insight into the design of biosensors and can be easily transferred to systems based on fluorescent probes. As shown in Chapter 1 the limit of detection of quantum dots and carbon dots with low settling times are ranging in the nM range, which is quite similar to Figure 6.7. For upconversion nanoparticles, this LOD is slightly elevated (1-10 μM) due to the larger size of the nanoparticles and weaker luminescence efficiency compared to other fluorescent probes. In Chapter 5 the development of a L-lactate sensor based on upconversion nanoparticles was discussed with a LOD ranging between $\sim 20 \mu\text{M}$ (cuvette) and $\sim 80 \mu\text{M}$ (hydrogel). Compared to the common reported LODs by using UCNPs, one can see that a further reduction of the limit of detection is only possible in exceptional circumstances.

Besides the application of UCNPs for bioanalytical sensing, the unique properties of the systems allow their usage in theranostics applications *in vivo*. UCNPs can be excited in the near-infrared region of the spectra. This provides not only a low background signal, but also allows a deep tissue penetration of the excitation source and enables to create a combined system for both, diagnosis and therapy.

In contrast to “IRON-MAN™”, who only exists in graphic novels and in the cinema auditorium, my superhero under the luminescent probes – the UCNP – can have a bright future and become a real superhero in our world if the challenges addressed in this work are a major part of research in the upcoming years. The first step in this direction has already been realized by the group of Xue [36] with their work about ocular injectable photoreceptor-binding UCNPs. Those nanoparticles can be seen as miniaturized NIR light transducers which create a NIR image vision in mice leading to an increased spectral range above 700 nm. This work has triggered a major public interest and was also discussed in a German newspaper [37] as those nanomaterials are capable to give mice their own real superpower, the sight in the NIR.

6.4 References

- [1] Rubahn HG (2008) Mesoscopic and Microscopic Physics In Basics of nanotechnology (pp.1-7) Wiley, New York.
- [2] Yeh YC, Creran B, Rotello VM (2012) Gold Nanoparticles: Preparation, Properties, and Applications in Bionanotechnology. *Nanoscale* 4(6):1871-80.
- [3] Freestone I, Meeks N, Sax M, Higgitt C (2007) The Lycurgus Cup — A Roman Nanotechnology. *Gold Bull.* 40(4):270-7.
- [4] Rakovich A, Rakovich T (2018) Semiconductor Versus Graphene Quantum Dots as Fluorescent Probes for Cancer Diagnosis and Therapy Applications. *J. Mater. Chem. B.* 6(18):2690-712.
- [5] Lan L, Yao Y, Ping J, Ying Y (2017) Recent Advances in Nanomaterial-Based Biosensors for Antibiotics Detection. *Biosens. Bioelectron.* 91:504-14.
- [6] Yang F, Moss LG, Phillips GN (1996) The Molecular Structure of Green Fluorescent Protein. *Nat. Biotechnol.* 14(10):1246-51.
- [7] Owen J, Brus L (2017) Chemical Synthesis and Luminescence Applications of Colloidal Semiconductor Quantum Dots. *J. Am. Chem. Soc.* 139(32):10939-43.
- [8] Kaiser M, Würth C, Kraft M, Hyppänen I, Soukka T, Resch-Genger U (2017) Power-Dependent Upconversion Quantum Yield of NaYF₄:Yb³⁺,Er³⁺ Nano- and Micrometer-Sized Particles - Measurements and Simulations. *Nanoscale* 9(28):10051-8.
- [9] Chen C, Wang F, Wen S, Su QP, Wu MC, Liu Y, Wang B, Li D, Shan X, Kianinia M, Aharonovich I (2018) Multi-Photon Near-Infrared Emission Saturation Nanoscopy Using Upconversion Nanoparticles. *Nat. Commun.* 9(1):3290.
- [10] Zhang Z, Shikha S, Liu J, Zhang J, Mei Q, Zhang Y (2019) Upconversion Nanoprobes: Recent Advances in Sensing Applications. *Anal. Chem.* 91(1):548-68.
- [11] He H, Liu B, Wen S, Liao J, Lin G, Zhou J, Jin D (2018) Quantitative Lateral Flow Strip Sensor Using Highly Doped Upconversion Nanoparticles. *Anal. Chem.* 90(21):12356-60.
- [12] Farka Z, Mickert MJ, Hlaváček A, Skládal P, Gorris HH (2017) Single Molecule Upconversion-Linked Immunosorbent Assay with Extended Dynamic Range for the Sensitive Detection of Diagnostic Biomarkers. *Anal. Chem.* 89(21):11825-30.
- [13] Heuer-Jungemann A, Feliu N, Bakaimi I, Hamaly M, Alkilany A, Chakraborty I, Masood A, Casula MF, Kostopoulou A, Oh E, Susumu K (2019) The Role of Ligands in the Chemical Synthesis and Applications of Inorganic Nanoparticles. *Chem. Rev.* 119(8):4819-80.
- [14] Sperling RA, Parak WJ (2010) Surface Modification, Functionalization and Bioconjugation of Colloidal Inorganic Nanoparticles. *Philos. Trans. Royal Soc. A.* 368(1915):1333-83.
- [15] Cheng T, Marin R, Skripka A, Vetrone F (2018) Small and Bright Lithium-Based Upconverting Nanoparticles. *J. Am. Chem. Soc.* 140(40):12890-9.
- [16] Huang X, Teng X, Chen D, Tang F, He J (2010) The Effect of the Shape of Mesoporous Silica Nanoparticles on Cellular Uptake and Cell Function. *Biomaterials* 31(3):438-448.
- [17] Hsiao IL, Gramatke AM, Joksimovic R, Sokolowski M, Gradzielski M, Haase A (2014) Size and Cell Type Dependent Uptake of Silica Nanoparticles. *J. Nanomed. Nanotechnol.* 5(6):248.
- [18] Zhang XD, Luo Z, Chen J, Song S, Yuan X, Shen X, Wang H, Sun Y, Gao K, Zhang L, Fan S (2015) Ultrasmall Glutathione-Protected Gold Nanoclusters as Next Generation Radiotherapy Sensitizers with High Tumor Uptake and High Renal Clearance. *Sci. Rep.* 5:8669.
- [19] Yu M, Zheng J (2015) Clearance Pathways and Tumor Targeting of Imaging Nanoparticles. *ACS Nano* 9(7):6655-6674.

- [20] Zhang Y, Yu Z, Li J, Ao Y, Xue J, Zeng Z, Yang X, Tan TT (2017) Ultrasmall-Superbright Neodymium-Upconversion Nanoparticles *via* Energy Migration Manipulation and Lattice Modification: 808 nm-Activated Drug Release. *ACS Nano* 11(3):2846-2857.
- [21] Jeong HH, Choi E, Ellis E, Lee TC (2019) Recent Advances in Gold Nanoparticles for Biomedical Applications: from Hybrid Structures to Multi-Functionality. *J. Mater. Chem. B.* doi:10.1039/C9TB00557A; *advance article*.
- [22] Wilhelm S, Kaiser M, Würth C, Heiland J, Carrillo-Carrion C, Muhr V, Wolfbeis OS, Parak WJ, Resch-Genger U, Hirsch T (2015) Water Dispersible Upconverting Nanoparticles: Effects of Surface Modification on their Luminescence and Colloidal Stability. *Nanoscale* 7(4):1403-1410.
- [23] Dukhno O, Przybilla F, Muhr V, Buchner M, Hirsch T, Mély Y (2018) Time-Dependent Luminescence Loss for Individual Upconversion Nanoparticles upon Dilution in Aqueous Solution. *Nanoscale* 10(34):15904-15910.
- [24] Gnach A, Lipinski T, Bednarkiewicz A, Rybka J, Capobianco JA (2015) Upconverting Nanoparticles: Assessing the Toxicity. *Chem. Soc. Rev.* 44(6):1561-1584.
- [25] Palo E, Lahtinen S, Pääkilä H, Salomäki M, Soukka T, Lastusaari M (2018) Effective Shielding of NaYF₄:Yb³⁺,Er³⁺ Upconverting Nanoparticles in Aqueous Environments Using Layer-by-Layer Assembly. *Langmuir* 34(26):7759-7766.
- [26] Palo E, Salomäki M, Lastusaari M. (2019) Restraining Fluoride Loss from NaYF₄:Yb³⁺,Er³⁺ Upconverting Nanoparticles in Aqueous Environments using Crosslinked Poly(Acrylic Acid)/Poly(Allylamine Hydrochloride) Multilayers. *J. Colloid Interface Sci.* 538:320-326.
- [27] Moeller T, Fogel N (1951) Observations on the Rare Earths. LXI. Precipitation of Hydrous Oxides or Hydroxides from Perchlorate Solutions 1. *J. Am. Chem. Soc.* 73(9):4481.
- [28] Wang L, Huang H, Shen D, Zhang J, Chen H, Wang Y, Liu X, Tang D (2014) Room Temperature Continuous-Wave Laser Performance of LD Pumped Er:Lu₂O₃ and Er:Y₂O₃ ceramic at 2.7 μm. *Opt. Express.* 22(16):19495-19503.
- [29] Duong HT, Chen Y, Tawfik SA, Wen S, Parviz M, Shimoni O, Jin D (2018) Systematic Investigation of Functional Ligands for Colloidal Stable Upconversion Nanoparticles. *RSC Adv.* 8(9):4842-4849.
- [30] Buchner M, Ngoensawat U, Schenck M, Fenzl C, Wongkaew N, Matlock-Colangelo L, Hirsch T, Duerkop A, Baeumner AJ (2017) Embedded Nanolamps in Electrospun Nanofibers Enabling Online Monitoring and Ratiometric Measurements. *J. Mater. Chem. C.* 5(37):9712-20.
- [31] Yao C, Wang P, Li X, Hu X, Hou J, Wang L, Zhang F (2016) Near-Infrared-Triggered Azobenzene-Liposome/Upconversion Nanoparticle Hybrid Vesicles for Remotely Controlled Drug Delivery to Overcome Cancer Multidrug Resistance. *Adv. Mater.* 28(42):9341-8.
- [32] Zhao H, Hu W, Ma H, Jiang R, Tang Y, Ji Y, Lu X, Hou B, Deng W, Huang W, Fan Q (2017) Photo-Induced Charge-Variable Conjugated Polyelectrolyte Brushes Encapsulating Upconversion Nanoparticles for Promoted siRNA Release and Collaborative Photodynamic Therapy under NIR Light Irradiation. *Adv. Funct. Mater.* 27(44):1702592.
- [33] Sun Y, Zhang W, Wang B, Xu X, Chou J, Shimoni O, Ung AT, Jin D (2018) A Supramolecular Self-Assembly Strategy for Upconversion Nanoparticle Bioconjugation. *Chem. Commun.* 54(31):3851-4.
- [34] Lederhose P, Chen Z, Müller R, Blinco JP, Wu S, Barner-Kowollik C (2016) Near-Infrared Photoinduced Coupling Reactions Assisted by Upconversion Nanoparticles. *Angew. Chem. Int. Ed.* 55(40):12195-9.
- [35] Nair PR, Alam MA. (2006) Performance Limits of Nanobiosensors. *Appl. Phys. Lett.* 88(23):233120.
- [36] Ma Y, Bao J, Zhang Y, Li Z, Zhou X, Wan C, Huang L, Zhao Y, Han G, Xue T (2019) Mammalian Near-Infrared Image Vision through Injectable and Self-Powered Retinal Nanoantennae. *Cell.* 177(2):243-55.
- [37] Retrieved April 26, 2019 from <https://www.sueddeutsche.de/wissen/infrarotsicht-nanopartikel-verleihen-maesenssuperblick-1.4350363>.

CURRICULUM VITAE

Persönliche Daten

Name	Sandy Franziska Himmelstoß
Adresse	Mauttafelstraße 1, 93053 Regensburg
Geburtsdatum	30. Juni 1991
Geburtsort	Straubing
Staatsangehörigkeit	Deutsch

Hochschulausbildung

11/2015 – 06/2019	Promotionsstudium Chemie , Universität Regensburg <i>“Surface Engineering of Upconversion Nanoparticles for Bioassays”</i> Institut für Analytische Chemie, Chemo- und Biosensorik (Dr. Thomas Hirsch, Prof. Antje J. Bäumner)
10/2013 - 09/2015	Masterstudium Chemie , Universität Regensburg <i>“Liposomes Encapsulating Upconverting Nanoparticles”</i> Institut für Analytische Chemie, Chemo- und Biosensorik (Dr. Thomas Hirsch, Prof. Antje J. Bäumner)
10/2010 - 09/2013	Bachelorstudium Chemie , Universität Regensburg <i>“Upconverting nanoparticles for cellular imaging: Synthesis, characterization and cytotoxicity”</i> Institut für Analytische Chemie, Chemo- und Biosensorik (Dr. Thomas Hirsch, Prof. Otto S. Wolfbeis)
06/2010	Allgemeine Hochschulreife , Regental-Gymnasium (RTG), Nittenau

Weiterbildungen

Mai 2018	Endspurt für Horizon 2020, EU-Forschungsförderung (Universität Regensburg, Regensburg)
April 2018	2 nd Spring School on Properties, Design and Applications of Upconversion Nanoparticles (Universität Valencia, Valencia, Spanien)
Juli 2017	10 th Advanced Study Course on Optical Chemical Sensors (Institut für Photonik und Elektronik, Tschechische Akademie der Wissenschaft, Třešť, Tschechien)
Februar 2017	COST ACTION TRAINING SCHOOL – Upconverting nanoparticles in bioaffinity assay, (Universität von Turku, Turku, Finnland)
Juli 2015	Qualitätsmanagement in der Analytischen Chemie (Universität Regensburg, Regensburg)
Februar 2015	Frühjahrsschule Industrielle Analytische Chemie (Fachgruppe Analytische Chemie der Gesellschaft Deutscher Chemiker, Regensburg)

Stipendien / Auszeichnungen

04/2016 – 03/2018	Stipendium des Fonds der Chemischen Industrie (FCI)
04/2016	Preis der „Fachgruppe Analytische Chemie der GDCH“ für den besten Master-Abschluss in Analytischer Chemie im Jahr 2015
04/2014	Preis der „Fachgruppe Analytische Chemie der GDCH“ besten Bachelor-Abschluss in Analytischer Chemie im Jahr 2013
04/2012 – 09/2013	Stipendium der August-Wilhelm-von-Hofmann Stiftung

LIST OF PUBLICATIONS

- [8] **Himmelstoß SF**, Wiesholler LM, Märkl S, Hirsch T, Duerkop A, Bäumner AJ. Luminescence-based self-referenced enzymatic L-lactate sensing by tandem-sensitized NIR to UV NaYF₄(Yb,Tm) upconversion nanoparticles. Manuscript in Preparation.
- [7] **Himmelstoß SF**, Hirsch T (2019) Aqueous dispersions of NaYF₄-type upconversion nanoparticles: Influence of surface chemistry on colloidal and chemical stability, Part. Part. Sys. Char. (accepted July 2019)
- [6] Tsai ES, **Himmelstoß SF**, Wiesholler LM, Hirsch T, Hall EAH (2019) Upconversion Nanoparticles for Sensing pH. Submitted to Analyst.
- [5] **Himmelstoß SF**, Hirsch T (2019) A critical comparison of lanthanide based upconversion nanoparticles to fluorescent proteins, semiconductor quantum dots, and carbon dots for use in optical sensing and imaging. *Methods Appl. Fluoresc.* 7(2):22002.
- [4] Schwanzer P, Rabl HP, Loders S, Seifert P, **Himmelstoß S**, Gaderer M (2019) Difference in the Tailpipe Particle Number by Consideration of Sub-23-nm Particles for Different Injection Settings of a GDI Engine. *Emission Control Science and Technology.* 1-6.
- [3] **Himmelstoß SF**, Wiesholler LM, Buchner M, Muhr V, Märkl S, Bäumner AJ, Hirsch T (2017) 980 nm and 808 nm excitable upconversion nanoparticles for the detection of enzyme related reactions. *SPIE BIOS* 10077:100770L1-100770L6.
- [2] Buchner M, Muhr V, **Himmelstoß SF**, Hirsch T (2016) Functionalization Aspects of Water Dispersible Upconversion Nanoparticles. In *Upconverting Nanomaterials* (pp 69-100). CRC Press, Boca Raton.
- [1] Wilhelm S, del Barrio M, Heiland J, **Himmelstoß SF**, Galbán J, Wolfbeis OS, Hirsch T (2014) Spectrally matched upconverting luminescent nanoparticles for monitoring enzymatic reactions. *ACS Appl. Mater. Interfaces* 6(17):15427-33.

CONFERENCE CONTRIBUTIONS

Oral Presentations

- 2018 Europt(r)ode XIV, Naples, Italy
Luminescence sensing of lactate and glucose in serum based on 808 nm NIR excitation.
- 2017 SPIE West Photonics BIOS, San Francisco, USA
Enzymatic sensor for online monitoring of L-lactate using upconversion nanoparticles.

Poster Presentations

- 2018 2nd Concerence and Spring School on Properties, Design and Applications of Upconversion Nanoparticles, Valencia, Spain
Luminescence Sensing of L-Lactate and D-Glucose in Human Serum based on 808 nm NIR Excitation.
- 2017 15th Concerence on Methods and Applications in Fluorescence, Brugge, Belgium
Upconversion nanoparticles with tandem sensitisation for online monitoring of enzymatic reactions in human serum.
- 2016 Europt@ode XIII, Graz, Austria
Protein-reactive Upconverting Luminescence Liposomes.
- 2015 11th BBMEC 2015, Regensburg, Germany
Protein-reactive Liposomes with Upconverting Luminescence Properties.
- 2015 Anakon, Graz, Austria
Upconverting Luminescent Nanoparticles for Monitoring FAD and NADH-related Enzymatic Reactions.
- 2015 Deutsches BioSensor Symposium, Munich, Germany
Spectrally Matched Upconverting Luminescent Nanoparticles for Monitoring FAD- and NADH related Enzymatic Reactions.

DANKSAGUNG

Zuallererst möchte ich mich bei **Prof. Dr. Antje J. Baeumner** und **Dr. Thomas Hirsch** für die Möglichkeit bedanken, meine Promotion über dieses spannende und umfangreiche Thema anfertigen zu können. Vielen Dank für die stete Betreuung, Unterstützung und Hilfe bei Problemen aller Art.

Vielen Dank auch an **Prof. Dr. Hubert Motschmann** für die Übernahme des Zweitgutachtens.

Ebenfalls ein herzliches Dankeschön an **Prof. Dr. Reinhard Rachel** – einerseits für die exzellente Unterstützung bei TEM Fragestellung, sowie für die Übernahme der Aufgabe des Dritprüfers.

Prof. Dr. Frank-Michael Matsyk danke ich für das Ausüben der Funktion des Prüfungsvorsitzenden.

Beim **Fond der Chemischen Industrie** möchte ich mich für die finanzielle Unterstützung meiner Doktorarbeit bedanken.

Weiterhin möchte ich mich bei **Prof. Dr. Stefan Wilhelm** bedanken, der mich in die Welt der UCNPs eingeführt hat und meine Faszination für dieses Thema geweckt hat.

Ich möchte mich ebenso bei **Susanne Märkl** bedanken, die im Rahmen Ihrer Bachelorarbeit an einem Teil der Studien beteiligt war, sowie bei allen Kollegen, die zum Gelingen dieser Arbeit beigetragen haben.

Bei **Dr. Christoph Fenzl** bedanke ich mich für seine unendliche Geduld beim TEM. Danke auch an **Joachim Rewitzer** für die Unterstützung bei den ICP-OES und ICP-MS Messungen sowie für den einen oder anderen Kaffee.

Beim **Upcon-Team**, bedanke ich mich für die unzähligen hilfreichen wissenschaftlichen und auch nichtwissenschaftlichen Diskussionen, Hilfestellungen und Denkanstöße. Allen voran danke ich hier **Dr. Thomas Hirsch** für seine schier endlose Unterstützung und Ermutigung.

Vielen Dank ebenso an die gute Seele **Rosi Walter** für ihre unermüdliche Hilfe und aufmunternden Worte.

Für die wunderbare Arbeitsatmosphäre sowie auch Freizeitaktivitäten möchte ich mich bei der gesamten aktuellen und ehemaligen Arbeitsgruppe „**4. Stock**“, sowie **allen Kollegen und Mitarbeitern am Institut** bedanken.

Zu guter Letzt möchte ich mich bei meinen Eltern **Sonya und Rudolf Himmelstoß** und meinem Freund **Markus Bodensteiner** bedanken. Für ihre Liebe, ihr Vertrauen und ihre fortwährende Unterstützung, in jeglicher Hinsicht. Durch euren stetigen Rückhalt und verrückten Aktionen wurde diese Arbeit erst machbar.

Danke

EIDESSTATTLICHE ERKLÄRUNG

Ich erkläre hiermit an Eides statt, dass ich die vorliegende Arbeit ohne unzulässige Hilfe Dritter und ohne Benutzung anderer als der angegebenen Hilfsmittel angefertigt habe; die aus anderen Quellen direkt oder indirekt übernommenen Daten und Konzepte sind unter Angabe des Literaturzitats gekennzeichnet.

Weitere Personen waren an der inhaltlich-materiellen Herstellung der vorliegenden Arbeit nicht beteiligt. Insbesondere habe ich hierfür nicht die entgeltliche Hilfe eines Promotionsberaters oder anderer Personen in Anspruch genommen. Niemand hat von mir weder unmittelbar noch mittelbar geldwerte Leistungen für Arbeiten erhalten, die im Zusammenhang mit dem Inhalt der vorgelegten Dissertation stehen.

Die Arbeit wurde bisher weder im In- noch im Ausland in gleicher oder ähnlicher Form einer anderen Prüfungsbehörde vorgelegt.

Ort, Datum

Unterschrift